UNIVERSITY OF OTTAWA

Design, Synthesis, and Evaluation of Fluorogenic, BODIPY-based Probes for Specific Protein Labelling in Live Cells

Sydney Acton

A THESIS

SUBMITTED

IN PARTIAL FULFILMENT OF THE REQUIREMENTS FOR THE

MASTER OF SCIENCE DEGREE IN CHEMISTRY

Department of Chemistry and Biomolecular Sciences

Faculty of Science

University of Ottawa

Abstract

Visualizing proteins in living cells without perturbing biological function remains a key challenge in chemical biology. A chemical approach to this problem is the synthesis of small molecule fluorophores that react specifically with a protein of interest (POI). We have developed a site-specific labelling method based on a Fluorogenic Addition Reaction (FlARe). The FlARe probe's fluorescence is quenched until it undergoes thiol addition with a small, genetically encoded dicysteine peptide tag fused to the POI. Recent blue coumarin probes were shown to be highly selective for target proteins over other cellular thiols; however, fluorogens that can label in the red and green channels of the fluorescence microscope are more desirable for cellular imaging, as red light is lower in energy and therefore less photo-toxic. In the work presented herein, we use DFT calculations to guide the design of red-shifted, PeT-quenched BODIPY based dimaleimide fluorogens. Driven by the preliminary results of a FlARe probe (**YC29**) that emitted in the red channel, we attempted to prepare the hit compound through a new synthetic approach to further evaluate kinetics and *in cellulo* labelling. Given the time available, this compound was unable to be synthesized through an S_NAr or Pd-catalyzed approach. Alternatives probes lacking the red-shifting substituent were synthesized and evaluated *in vitro* and *in cellulo*. The fluorescent enhancement and reaction kinetics of these probes were evaluated in detail, in order to determine the suitability of their application to cellular labelling. A green-BODIPY fluorogen was synthesized that exhibits suitable kinetics for labelling and a dramatic fluorescent enhancement of ~800-fold upon tagging. This probe was successfully applied to the specific, fluorescent labelling of a nuclear histone protein *in cellulo.*

Keywords: fluorogenic probes, protein labelling, BODIPY, maleimide, peptide tag

Acknowledgements

I've said it before and I'll say it again, I can't imagine a better supervisor than Jeff. Not only is he brilliant but he's also caring, thoughtful, kind, and supportive. Jeff's persistent optimism was a driving force for me throughout this experience. I can't thank you enough, Jeff.

I would like to thank all members of the Keillor group, both past and present. Our group has a way of attracting wonderful people, and I really value the connections we made over the past few years. Thank you all for the support.

A special thanks to two special Keillors, Kelvin Tsao and Dr. Yingche Chen. Without Yingche's hard work, the BODIPY FlARe project might have never gotten off the ground. Kelvin, thank you for your patience in taking the time to help me learn the biology side of things.

I'd also like to thank my committee members Dr. Boddy and Dr. Shuhendler, and the Centre for Chemical and Synthetic Biology. Being immersed in such a collaborative atmosphere and surrounded by excellent scientists was motivating and inspiring for me.

And of course, a final shout out to my amazing friends and family. I am so lucky to have a group of wonderful people who were there for me every step of the way and I could always count on. Love you guys!

Dedication

This Thesis is dedicated to my family: my mom, dad, and sister. Even though you were 4000 km away you were always there for me: you were so excited about my presentations and publication, proofread papers even though they might as well have been in a different language, and liked every single Facebook post I've ever made.

Table of Contents

Abstract ii
Acknowledgements iii
Dedication iv
Table of Contents v
List of Tables ix
List of Figures x
List of Schemes xv

LIST OF SYMBOLS AND ABBREVIATIONS XVI

CHAPTER ONE: INTRODUCTION 1
1.1 Fluorescent Protein Labelling 1
1.1.1 Mechanism of Fluorescence 2
1.1.2 Fluorescence Microscopy 5
1.1.3 Advantages of Fluorescent Methods 7
1.2 Labelling Techniques 7
1.2.1 Genetic Fusion to a Fluorescent Protein 8
1.2.2 Enzymatic Labelling 9
1.2.2.1 Enzyme Tags 9
1.2.2.2 Substrate Tags 10
1.2.3 Labelling with Small Molecules 10
1.2.3.1 Unnatural Amino Acid Incorporation 11
1.2.3.2 Peptide Tag Incorporation 12
1.3 Small Molecule Fluorophores for Cellular Imaging 13
1.3.1 Fluorogenic Probes 15
1.4 FlARe Labelling Method 16
1.4.1 General Design 17
1.4.2 PeT Quenching 18
1.4.3 Di-cysteine Tag Development 21
1.4.4 Optimization of FlARe Fluorogens 23
1.4.4.1 Linker 23
1.4.4.2 Maleimide 25
1.4.4.3 Fluorophore 26
1.4.5 BODIPY as a New Fluorogen Scaffold 27
1.5 Objectives 29
1.5.1 Towards a Red-Shifted BODIPY FlARe Probe (Chapter Two) 29
1.5.2 Design, Synthesis, and Evaluation of a Green BODIPY FlARe Probe (Chapter Three) 30
1.5.3 Conclusions and Future Perspectives (Chapter Four) 30

CHAPTER TWO: TOWARDS A RED-SHIFTED BODIPY FLARE PROBE 31
2.1 Introduction 31
2.2 Design of a Red FlARe Probe 32

2.2.1 Synthetic Strategy....32
2.2.1.1 Functionalization Strategies for BODIPY....32
2.2.1.2 S_NAr Approach....34
2.2.2 Molecular Modelling of YC29....36
2.3 First synthetic approach....39
2.3.1 Preliminary Results....40
2.4 Towards a New Synthetic Approach....43
2.4.1 Synthesis of the dimaleimide scaffold....44
2.4.2 Synthesis of methoxymaleic anhydride....45
2.4.3 Synthesis of 3,5-dichloroBODIPY....46
2.4.4 Synthesis....48
2.4.4.1 S_NAr Steps....48
2.4.4.2 Nitro Reduction....49
2.4.4.3 Addition of Methoxymaleic Anhydride....49
2.4.4.4 TFA Removal of BF_2 from BODIPY....51
2.5 A New Convergent Strategy....51
2.5.1 Dimaleimide Aniline Synthesis....53
2.5.2 α-N-MePh BODIPY S_NAr....54
Final S_NAr....55
2.5.3 S_NAr Analysis....57
2.5.4 Pd-Catalyzed Aryl-Amination....58
2.5.5 Comments on Pd-catalyzed Coupling....61
2.6 Towards a Simplified BODIPY FlARe Probe....62
2.6.1 Molecular Modelling....62
2.6.2 In Vitro Evaluation....64
2.6.2.1 Target protein....64
2.6.2.2 Kinetic evaluation....66
2.6.3 Synthesis....69
2.6.4 In Vitro Evaluation....71
2.6.5 Cellular Imaging Experiments....74
2.7 Future Perspectives & Conclusion....80
2.8 Experimental....81
2.8.1 Molecular Modelling....81
2.8.2 General Synthetic Procedures and Characterization....81
2.8.3 Tert-butyl (3,5-dinitrophenyl)carbamate (2.1) preparation....82
2.8.4 Methoxymaleic acid anhydride preparation....84
2.8.4.1 2-Bromo-*N*-phenylmaleimide (**2.10**)....84
2.8.4.2 2-Methoxy-*N*-phenylmaleimide (**2.11**)....85
2.8.4.3 N-Phenyl-2-methoxymaleamic Acid (**2.12**)....86
2.8.4.4 Methoxy-maleic acid anhydride (**2.13**)....87
2.8.4.5 2,2'-(phenylmethylene)bis(1*H*-pyrrole) (**2.14**)....88
2.8.5 Original Route to YC29....91
2.8.5.1 *Tert*-butyl(7-chloro-5,5-difluoro-10-phenyl-5H-5λ^4,6λ^4-dipyrrolo[1,2-*c*:2',1'-*f*][1,3,2]diazaborinin-3-yl)(3,5-dinitrophenyl)carbamate (**2.3**)....91

2.8.5.2 *Tert*-butyl (5,5-difluoro-7-(methyl(phenyl)amino)-10-phenyl-5H-5λ^4,6λ^4-dipyrrolo[1,2-*c*:2',1'-*f*][1,3,2]diazaborinin-3-yl)(3,5-dinitrophenyl)carbamate (**2.4**) 92
2.8.5.3 *Tert*-butyl (3,5-bis(3-methoxy-2,5-dioxo-2,5-dihydro-1H-pyrrol-1-yl)phenyl)(5,5 difluoro-7-(methyl(phenyl)amino)-10-phenyl-5H-5λ4,6λ4-dipyrrolo[1,2-*c*:2',1'-*f*][1,3,2]diazaborinin-3-yl)carbamate (**2.18**) 94
2.8.6 Preparation of YC29 intermediates by convergent strategy 95
2.8.6.2 *Tert*-butyl (3,5-bis(3-methoxy-2,5-dioxo-2,5-dihydro-1H-pyrrol-1-yl)phenyl)carbamate (**2.20**) 96
2.8.6.3 1,1'-(5-amino-1,3-phenylene)bis(3-methoxy-1H-pyrrole-2,5-dione) (**2.21**) 97
2.8.6.4 1,1'-(5-((7-chloro-5,5-difluoro-10-phenyl-5H-5λ^4,6λ^4-dipyrrolo[1,2-*c*:2',1'-*f*][1,3,2]diazaborinin-3-yl)amino)-1,3-phenylene)bis(3-methoxy-1H-pyrrole-2,5-dione) aka **Ph-BODIPY-NHdM10-Cl** (**2.23**) 98
2.8.6.5 5,5'-(phenylmethylene)bis(2-chloro-1H-pyrrole) (**2.15**) & 2-chloro-5-(phenyl(1H-pyrrol-2-yl)methyl)-1H-pyrrole (**2.24**) 99
2.8.6.6 3-chloro-5,5-difluoro-10-phenyl-5H-5λ^4,6λ^4-dipyrrolo[1,2-*c*:2',1'-*f*][1,3,2]diazaborinine (**2.25**) 100
2.8.6.7 1,1'-(5-((5,5-difluoro-10-phenyl-5H-5λ^4,6λ^4-dipyrrolo[1,2-*c*:2',1'-*f*][1,3,2]diazaborinin-3-yl)amino)-1,3-phenylene)bis(3-methoxy-1*H*-pyrrole-2,5-dione) (**2.26**) 101
2.8.7 MBP-dC10α Expression and Purification 102
2.8.8 Kinetic Measurements 103
2.8.9 Cell Culture 103
2.8.10 Cellular Labelling 104

CHAPTER THREE: GREEN BODIPY-BASED FLARE PROBE 106
3.1 Contributions 106
3.2 Introduction 106
3.3 BODIPY-FlARe Probe Design 107
3.4 Synthesis of YC23 113
3.5 In Vitro Evaluation 115
3.5.1 Kinetics 117
3.5.2 Background Reaction with Thiols 119
3.5.3 Quantum Yield 120
3.5.4 SDS-PAGE Gel Analysis and YC23 Stability Under Denaturing Conditions 125
3.6 Cellular Evaluation and Imaging 126
3.6.1 Cytotoxicity 126
3.6.2 Cellular Labelling of H2B-dC10α with YC23 and DAPI 129
3.6.3 Cellular Labelling of H2B-dC10α with YC23 and Hoechst 131
3.7 Conclusion 133
3.8 Experimental 134
3.8.1 Molecular Modelling 134
3.8.2 Synthesis 134

3.8.2.1 (Z)-2-((3,5-Dimethyl-2H-pyrrol-2-ylidene)(2,4-dinitrophenyl)methyl)-3,5-dimethyl-1H-pyrrole (**3.1**)....136
3.8.2.2 10-(2,4-Dinitrophenyl)-5,5-difluoro-1,3,7,9-tetramethyl-5H-dipyrrolo[1,2-c:2',1'-f][1,3,2]diazaborinin-4-ium-5-uide (**3.2**)....137
3.8.2.3 10-(2,4-Diaminophenyl)-5,5-difluoro-1,3,7,9-tetramethyl-5H-dipyrrolo[1,2-c:2',1'-f][1,3,2]diazaborinin-4-ium-5-uide (**3.3**)....138
3.8.2.4 10-(2,4-Bis(3-methoxy-2,5-dioxo-2,5-dihydro-1H-pyrrol-1-yl)phenyl)-5,5-difluoro-1,3,7,9-tetramethyl-5H-dipyrrolo[1,2-c:2',1'-f][1,3,2]diazaborinin-4-ium-5-uide (**3.4** aka **YC23**)....139
3.8.3 Fluorescent Enhancement Ratios....140
3.8.4 Kinetic Measurements....141
3.8.5 Quantum Yield Measurements....142
3.8.6 Cell Viability....143
3.8.7 Cellular Labelling....143

CHAPTER FOUR: CONCLUSIONS AND FUTURE PERSPECTIVES....145
4.1 A Red-Shifted BODIPY FlARe Probe....145
4.1.1 Goal....145
4.1.2 Results Achieved and Conclusions....145
4.1.3 Future Perspectives....146
4.2 A Green BODIPY FlARe Probe....147
4.2.1 Goal....147
4.2.2 Results Achieved and Conclusions....147
4.2.3 Future Perspectives....148
4.3 A New dC10 Tag for Improved Selectivity and Labelling....148
4.3.1 Future work with dC10*....149
4.4 Potential New Red Flare Probes....150
4.5 Conclusion....151

APPENDIX: NMR SPECTRA....152

REFERENCES....173

List of Tables

Table 2.1 Summary of HOMO/LUMO energies for **YC29** determined by molecular modelling. 37

Table 2.2 Experimental conditions for the S_NAr between compound **2.21** and **2.22.**..... 55

Table 2.3 Conditions a -c for the Pd-catalyzed aryl amination between compound **2.22** and **2.21.** All reactions were carried out under anhydrous conditions at a 40 mg scale of compound **2.22** with 1.5 eq of aniline **2.21**. Reactions were run overnight under nitrogen/argon. Conversion determined by TLC analysis. Catalyst and ligand structures shown in Figure **2.9** below. 60

Table 2.4 Summary of HOMO/LUMO energies for **Ph-BODIPY-NHdM10-H/Cl** determined by molecular modelling 64

Table 3.1 Summary of HOMO/LUMO energies and D-A distances for Nagano's probes determined by molecular modelling. 109

Table 3.2 Summary of HOMO/LUMO energies for **YC23** determined by molecular modelling. 112

List of Figures

Figure 1.1 (Top) Jablonski diagram for fluorescence. Absorption of a photon excites an electron (electronically and vibrationally) to a higher energy singlet state, which then relaxes non-radiatively through vibrational levels before radiative relaxation to the ground state. (Bottom) Simulated excitation and emission spectra for a fluorophore. 3

Figure 1.2 Diagram of an epifluorescent microscope (excitation light shown in green, emission shown in red).[1] 5

Figure 1.3 Comparison of genetic methods of fluorescent labelling of a POI (β-actin) highlighting the relative size of the encoded gene.[4] 8

Figure 1.4 Example UAAs, from left to right: fluorescent coumarin, azide, alkyne, ketone, and tetrazine. [13] 11

Figure 1.5 FlAsH (left) and ReAsH (right) fluorogenic probes developed by the Tsien group. . 12

Figure 1.6 General FlARe labelling strategy. 17

Figure 1.7 Jablonski diagrams for the d-PeT quenching mechanism between maleimides (A) and the fluorophore (D). Quenching is abolished when the maleimide is transformed to a succinimide as the LUMO energy level is increased, disfavouring electron transfer. 19

Figure 1.8 Changes to the amino acid sequence to form the dC10α-helical peptide tag. 22

Figure 1.9 (Left) Dansyl and coumarin FlARe probes with first generation linker. (Right) Comparison of dimaleimide scaffold and second generation linker.[42] 24

Figure 1.10 Hydrolysis rates (k_{OH}) and thiol addition rates (k_2) for R substituted *N*-phenyl maleimide. 26

Figure 1.11 IUPAC numbering (red) and naming (blue) for BODIPY scaffold. 28

Figure 2.1 Summary of the synthetic strategies for postfunctionalization of the BODIPY core. 33

Figure 2.2 Double S_NAR design of a wavelength-tunable BODIPY FlARe probe. 35

Figure 2.3 FlARe scheme for red BODIPY fluorogen **YC29**. 36

Figure 2.4 DFT-minimized geometry of fluorogen **YC29,** showing: A) the relevant distance between the maleimide and BODIPY group, B) the BODIPY excited state (LUMO +1), and C) the maleimide LUMO. 37

Figure 2.5 Molecular orbital diagram for YC29 before addition reaction (left), after one thiol addition (middle), and after two thiol additions (right). 38

Figure 2.6 Excitation and emission spectra of 25 μM MBP-dC10α labelled with **YC29.** 41

Figure 2.7 (Left) Fluorescence enhancement (λ_{ex}= 580 nm) of 25 μM **YC29**, incubated in the absence (black) and presence of MBP-dC10α (red) overnight. (Right) Time-dependent fluorescence increase of 25 μM **YC29** reacting with one equivalent of test protein MBP-dC10α (red) and excess thiols. λ_{ex} = 580 nm, λ_{em} = 630 nm..... 42

Figure 2.8 Retrosynthetic analysis for convergent S_NAr strategy to **YC29**..... 52

Figure 2.9 Palladium catalysts and ligands referenced in Table 2.3.[65,66] 60

Figure 2.10 Ph-BODIPY-NHdM10-H (Left) and **Ph-BODIPY-NHdM10-Cl** (right) orbital localization. 63

Figure 2.11 Excitation/emission spectra for 25 μM **Ph-BODIPY-NHdM10-Cl** (max excitation at 535 nm and max emission at 585 nm, normalized to 100 %) after reaction with 25 μM MBP-dC10α in 50 mM HEPES buffer (pH 7.4, 250 μM TCEP, 10% DMSO) at 37 °C overnight. 66

Figure 2.12 Time-dependent fluorescence (λ_{ex}= 535 nm, λ_{ex}= 585 nm, gain = 65) increase of 25 μM **Ph-BODIPY-NHdM10-Cl** reacting with 25 μM MBP-dC10α in 50 mM HEPES buffer (pH 7.4, 250 μM TCEP, 10% DMSO) at 37 °C. The solid line through the data was obtained by fitting to a second order equation. (Blank corrected)..... 67

Figure 2.13 Time-dependent fluorescence increase (λ_{ex} = 535 nm, λ_{em} = 585 nm, gain = 65) of 25 μM **Ph-BODIPY-NHdM10-Cl** reacting with one equivalent of test protein MBP-dC10α (black), and excess thiols (grey) in 50 mM HEPES buffer (pH 7.4, 250 μM TCEP, 10% DMSO) at 37 °C. 69

Figure 2.14 Excitation/emission spectra for 25 μM **Ph-BODIPY-NHdM10-H** (max excitation at 525 nm and max emission at 575 nm, normalized to 100 %) after reaction with 25 μM MBP-dC10α in 50 mM HEPES buffer (pH 7.4, 250 μM TCEP, 10% DMSO) at 37 °C overnight. 71

Figure 2.15 Time-dependent fluorescence (λ_{ex}= 520 nm, λ_{em}= 572 nm, gain = 80) increase of 25 μM **Ph-BODIPY-NHdM10-H** reacting with 25 μM MBP-dC10α in 50 mM HEPES buffer (pH 7.4, 250 μM TCEP, 10% DMSO) at 37 °C. The solid line through the (blank corrected) data was obtained by fitting to a second order equation. 72

Figure 2.16 Time-dependent fluorescence increase (λ_{ex} = 520 nm, λ_{em} = 572 nm, gain = 80) of 25 μM **Ph-BODIPY-NHdM10-H** reacting with one equivalent of test protein MBP-dC10α (black), and excess thiols (grey) reacting with 25 μM MBP-dC10α in 50 mM HEPES buffer (pH 7.4, 250 μM TCEP, 10% DMSO) at 37 °C. 73

Figure 2.17 HeLa cells transfected with histone H2B-dC10α (top) or pcDNA 3.1 (+) (bottom) before labelling with **Ph-BODIPY-NHdM10-H** (10 μM) for 1 h followed by Hoechst (8 μM) for 15 min. The Hoechst channel was excited at 390 nm and observed in the 460-510 nm channel. **Ph-BODIPY-NHdM10-H** was excited at 513 nm and observed in the 588-618 nm channel. Scale bars: 20 μm. 75

Figure 2.18 Zoom in of Figure 2.16 (top). Scale bars: 20 μm. 76

Figure 2.19 HeLa cells transfected with histone H2B-dC10α (top) or pcDNA 3.1 (+) (bottom) before labelling with **Ph-BODIPY-NHdM10-Cl** (10 μM) for 1 h followed by Hoechst (8 μM) for 15 min. The Hoechst channel was excited at 390 nm and observed in the 460-510 nm channel. **Ph-BODIPY-NHdM10-Cl** was excited at 513 nm and observed in the 588-618 nm channel. Scale bars: 20 μm. 77

Figure 2.20 Zoom in of Figure 2.18 (top), scale bars = 20 μm. 78

Figure 2.21 HeLa cells transfected with histone H2B-dC10α (top) or pcDNA 3.1 (+) (bottom) before labelling with **Ph-BODIPY-NHdM10-Cl** (10 μM) for 3 h followed by Hoechst (8 μM) for 15 min. The Hoechst channel was excited at 390 nm and observed in the 460-510 nm channel. **Ph-BODIPY-NHdM10-Cl** was excited at 513 nm and observed in the 588-618 nm channel. Scale bars: 20 μm. 79

Figure 2.22 Synthetic route for the preparation of methoxymaleic acid anhydride. 84

Figure 2.23 Synthetic route for the preparation of 3,5-dichloroBODIPY. 88

Figure 3.1 Nagano's thiol-reactive BODIPY-maleimide probes.[51] 108

Figure 3.2 Protein labelling with the BODIPY dimaleimide FlARe fluorogen **YC23**. 110

Figure 3.3. DFT-minimized geometry of green fluorogen **YC23**, showing: A) the relevant distance between the *ortho*-maleimide and BODIPY group, B) the *ortho* maleimide LUMO (LUMO +2), and C) the BODIPY excited state. 111

Figure 3.4 Excitation (red) and emission (black) spectra for 25 μM **YC23**+MBP-dC10α. 116

Figure 3.5 (Left) Fluorescence enhancement (λ_{ex}=480 nm) of 25 μM fluorogen **YC23,** incubated in the absence (black) and presence of varied concentrations of MBP-dC10α (coloured). (Right) Linear fit of fluorescence intensity of **YC23** vs. [MBP-dC10α]. 117

Figure 3.6 Time-dependent fluorescence (λ_{ex}=495 nm, λ_{ex}=525 nm, gain =65) increase of 25 μM **YC23** reacting with 25 μM MBP-dC10α in 50 mM HEPES buffer (pH 7.4, 250 μM TCEP, 10% DMSO) at 37°C. The solid line through the data was obtained by fitting to a second order equation. 118

Figure 3.7 Fluorescence emission spectra after 16 h of incubation of 25 µM **YC23** with 1 eq test protein MBP-dC10α, 10 eq of cysteine (Cys), 10 eq of homocysteine (hcy) and 40 eq (1 mM) of glutathione (GSH). 120

Figure 3.8 Plot of absorbance vs. fluorescein concentration, determined at 498 nm, 0.1 M NaOH, 22 °C. 122

Figure 3.9 Plot of absorbance vs. [addition product of MBP-dC10 and **YC23**] (25 µM of each incubated overnight in the dark at pH 7.4 in the presence of 250 µM TCEP and 10 % DMSO) determined at 498 nm, pH 7.4 (50 mM HEPES buffer), 22 °C. 123

Figure 3.10 Plot of integrated fluorescence intensity vs. absorbance for fluorescein standard in 0.1 M NaOH at 22 °C. Absorbance values were determined at 498 nm and λ_{exc} = 498 nm. 123

Figure 3.11 Plot of integrated fluorescence intensity vs. absorbance for the addition product of MBP-dC10 and **YC23** (25 µM of each incubated overnight in the dark at pH 7.4 in the presence of 250 µM TCEP and 10 % DMSO) determined at pH 7.4 (50 mM HEPES buffer), 22 °C. 124

Figure 3.12 SDS-PAGE gel developed by (A) Commassie blue staining and (B) fluorescence (λ_{ex} = 491 nm, (λ_{em} = 408 nm). Lane 1: molecular weight markers. Lane 2 and 3: Soluble lysate of bacteria expressing MBP-dC10α, treated with 10 or 50 µM **YC23** respectively, and 0.5 mM TCEP overnight. 125

Figure 3.13. Cytotoxicity of **YC23** in cultured HEK293T cells. Cells were incubated with the corresponding concentrations of fluorogen for 20 h. Cell viability was measured by MTT assay and the results are reported as percentage relative to untreated cells (mean ± SD). 127

Figure 3.14 Overlaid excitation and emission spectra for the nuclear dyes DAPI and Hoechst (Thermofisher – Fluorescence SpectraViewer). 129

Figure 3.15 HeLa cells transfected with histone H2B-dC10α (top) or pcDNA 3.1 (+) (bottom) before labelling with **YC23** (10 µM) for 45 min followed by DAPI (1 µM) for 15 min. The DAPI channel was excited at 390 nm and observed in the 460-510 nm channel. **YC23** was excited at 485 nm and observed in the 535/45 nm channel. Scale bars: 20 µm. 130

Figure 3.16 HeLa cells transfected with histone H2B-dC10α (top) or pcDNA 3.1 (+) (bottom) before labelling with **YC23** (10 µM) for 45 min followed by Hoechst (8 µM) for 15 min. The Hoechst channel was excited at 390 nm and observed in the 460-510 nm channel. **YC23** was excited at 485 nm and observed in the 535/45 nm channel. Scale bars: 20 µm. 131

Figure 3.17 HeLa cells transfected with histone H2B-dC10α (top) or pcDNA 3.1 (+) (bottom) before labelling with **YC23** (10 μM) *without surfactant* for 45 min followed by Hoechst (8 μM) for 15 min. The Hoechst channel was excited at 390 nm and observed in the 460-510 nm channel. **YC23** was excited at 485 nm and observed in the 535/45 nm channel. Scale bars: 20 μm. 133

Figure 3.18 Overall synthesis of green BODIPY fluorogen **YC23**. 136

Figure 4.1 Potential red fluorophore, indazole BODIPY (λ_{em}=634 nm). 151

List of Schemes

Scheme 2.1 Linear synthesis for preparation of **YC29** with reported yields achieved by Dr. Yingche Chen. 40

Scheme 2.2 Synthesis of the NHdM10 scaffold. 44

Scheme 2.3 Synthetic route for the preparation of methoxymaleic anhydride. 45

Scheme 2.4 Synthesis of 3.5-dichloroBODIPY. 46

Scheme 2.5 Synthetic route to **YC29** with improved yields. 48

Scheme 2.6 Test reaction for maleimide addition. 50

Scheme 2.7 Convergent synthetic route to **YC29.** 53

Scheme 2.8 S_NAr coupling of NHdM10 to 3,5-dichloroBODIPY. 56

Scheme 2.9 Catalytic cycle for palladium catalyzed aryl-amination. 58

Scheme 2.10 Pd-catalyzed aryl-amination (Buchwald-Hartwig amination) strategy to form **YC29**. Conditions a-c are summarized in **Table 2.3**. 59

Scheme 2.11 Parallel synthesis of **Ph-BODIPY-NHdM10-Cl** and **Ph-BODIPY-NHdM10-H**. 70

Scheme 3.1 Synthetic route for preparation of methoxymaleic anhydride. [62] 113

Scheme 3.2 Synthesis of compound **YC23**. 114

List of Symbols and Abbreviations

The following is a list of abbreviations and symbols employed in this Thesis, most of which are in common use in the chemical literature.

% m/m	percent by mol
% v/v	percent by volume
% w/w	percent by weight
Å	Ångstrom, 10^{-10} m
aaRS	aminoacyl tRNA synthetase
ACN	acetonitrile
a-Pet	acceptor photo-induced electron transfer
Ar	aryl
atm	atmosphere
Boc	*tert*-butyloxycarbonyl
BODIPY	boron-dipyrromethene
br	broad
*t*Bu	*tert*-butyl, Me_3C-
^{13}C	carbon-13
°C	degree Celsius
calcd	calculated
cm^{-1}	wavenumber, $1.877 \cdot 10^{-23}$ J
compd	compound
CI	chemical ionization
δ	chemical shift
d	days, or doublet (in a spectrum)
D	deuterium, ^2H
DAPI	4′,6-diamidino-2-phenylindole
dC10α	dicysteine alpha helical peptide tag, cysteine residues 10 Å apart
DCM	dichloromethane
dd	doublet of doublets
DDQ	2,3-dichloro-5,6-dicyano-1,4-benzoquinone
DFT	Density Functional Theory
DMF	dimethylformamide
DMSO	dimethylsulfoxide
D_2O	deuterium oxide
d-Pet	donor photo-induced electron transfer
E^+	electrophile
E. coli	Escherichia coli

eq.	equation, or equivalents
ESI	electrospray ionization
Et	ethyl, CH_3CH_2-
eV	electron volt, $1.602 \cdot 10^{-19}$ J
FlARe	Fluorogenic Addition Reaction
FlAsH	Fluorescein Arsenical Hairpin binder
FE	fluorescent enhancement
FP	fluorescent protein
FRET	Forster resonance energy transfer
g	grams
GFP	green fluorescent protein
GSH	glutathione
H2B	histone 2B
^{1}H	proton
h	hours
HEPES	4-(2-hydroxyethyl)-1-piperazineethanesulfonic acid
His	histidine
HMDS	hexamethyldisilazane
HOMO	highest occupied molecular orbital
HRMS	high resolution mass spectrometry
Hz	hertz, s^{-1}
*i*Pr	isopropyl, $(CH_3)_2CH$-
IPTG	isopropyl β-D-1-thiogalactopyranoside
IR	infrared
J	joule, kg m^2 s^{-2}
J	coupling constant (in spectroscopy)
K	degree Kelvin
k	rate constant
kDa	kilo Dalton
L	neutral, 2-electron-donor ligand; or litre, 10^{-3} m^3
LRMS	low resolution mass spectrometry
LUMO	lowest unoccupied molecular orbital
M	metal; or molar, mol L^{-1}
m	multiplet (in a spectrum)
m/z	mass-to-charge ratio (in mass spectrometry)
MBP	maltose-binding protein
Me	methyl, CH_3-
min	minutes
mmol	millimole, 10^{-3} mole

mM	millimole per litre
MO	molecular orbital
mol	mole, $6.022 \cdot 10^{23}$ particles
mL	millilitre, 10^{-3} L
µL	microlitre, 10^{-6} L
µM	micromole per litre, 10^{-6} mol/L
MTT	3-(4,5-dimethylthiazol-2-yl)-2,5- diphenyl tetrazolium bromide
MS	mass spectrum, mass spectrometry
$^{n}J_{AB}$	n-bond coupling between atoms A and B
Nu^-	nucleophile
NCS	*N*-chlorosuccinimide
NIR	Near IR
NMR	nuclear magnetic resonance
OMe	methoxy, CH_3O-
PeT	photoinduced electron transfer
Ph	phenyl, C_6H_5-
POI	protein of interest
ppm	parts per million
R	alkyl
Rf	retention factor
RFU	relative fluorescence units
RT	room temperature
s	singlet (in a spectrum)
SDS-PAGE	sodium dodecyl sulfate – polyacrylamide gel electrophoresis
S_EAr	electrophilic aromatic substitution
S_NAr	nucleophilic aromatic substitution
S_0	ground state
S_1	singlet excited state
t	triplet (in a spectrum)
TBET	through-bond energy transfer
TCEP	tris(2-carboxyethyl)phosphine
THF	tetrahydrofuran, C_4H_8O
TFA	trifluoroacetic acid
TLC	thin layer chromatography
UAA	unnatural amino acid
UV	ultra-violet
X	halide or other anionic 1-electron-donor ligand
λ	wavelength
c	speed of light, 3.0×10^8 m/s

ν	frequency, s^{-1}
Φ	quantum yield
ε	molar extinction coefficient, M^{-1}

Chapter One: Introduction

1.1 Fluorescent Protein Labelling

Cells are exquisitely complex systems, driven by intricately intertwined, dynamic biological events. Deconvoluting how the cell functions at the molecular and macromolecular level, in both healthy and disease states, is arguably one of the greatest challenges in chemical biology. Our understanding of the cell at this level is tied to our ability to visualize how key components (e.g. proteins, nucleic acids, lipids, and metabolites) localize and interact with one another.

For chemists and biologists seeking to gain greater insight into the mysteries of the cell, molecular tools are needed to visualize biomolecules with high spatiotemporal resolution. Many imaging modalities are currently available, most of which can be broadly categorized into either optical imaging, using visible or near-IR light, or radiological imaging. Common radiological techniques include X-ray computed tomography (CT), magnetic resonance imaging (MRI), positron emission tomography (PET), and single-photon emission computed tomography (SPECT).[1] These are powerful tools, particularly in terms of *in situ* imaging in living organisms. However, optical imaging remains a powerful and broadly accessible tool for visualizing biomolecules in living cells, and light microscopy has been a major driving force in biological research.

Fluorescence microscopy enables imaging with high sensitivity in living cells, in real time. Chemical and synthetic biologists are uniquely equipped to create fluorescent tools to visualize cellular processes and phenomena, such as dynamic protein trafficking and protein-protein interactions.

1.1.1 Mechanism of Fluorescence

A fluorophore is a species that emits light upon relaxation of an excited state electron to the stable ground state electronic configuration. Emission of light by a compound is broadly referred to as luminescence and further divided into two categories based on mode of radiative relaxation: phosphorescence and fluorescence. Phosphorescence occurs on a significantly slower timescale (microseconds) compared to fluorescence due to relaxation through a quantum 'spin-forbidden' transition from a triplet excited state to the ground state. Alternatively, fluorescence emission is extremely fast, occurring on the nanosecond time scale.[2]

Emission of light via fluorescence can be separated into three stages: excitation by absorption of energy, partial relaxation, followed by complete relaxation and emission of a photon. These stages are depicted in Figure 1.1 on the following page.

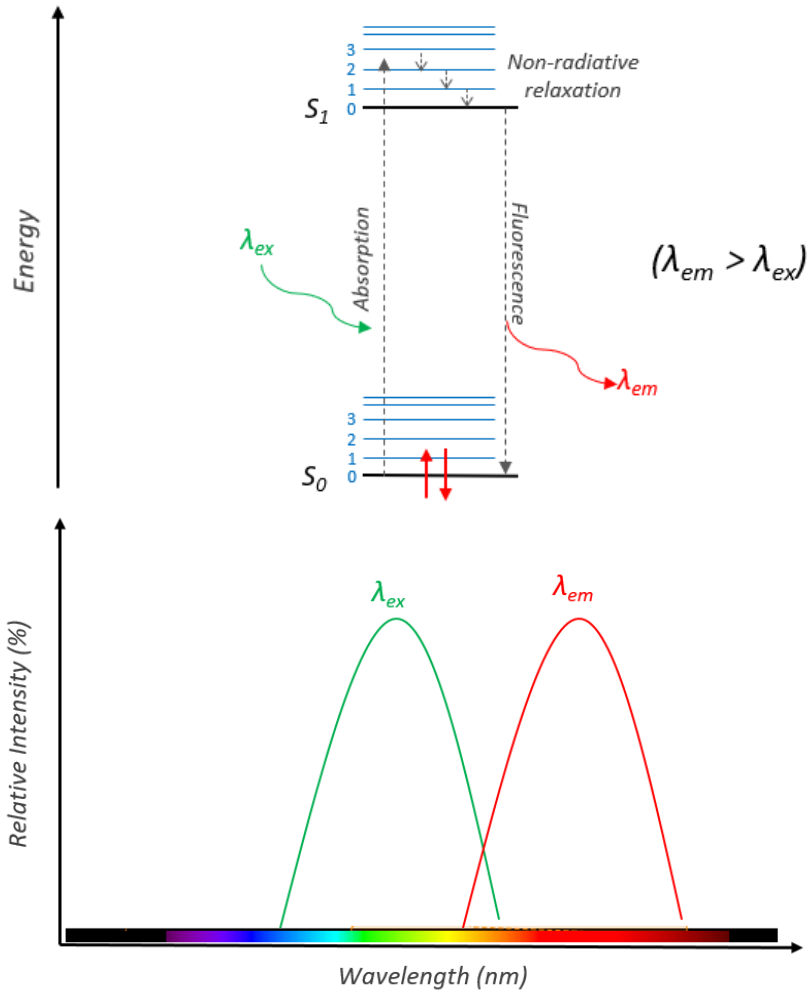

Figure 1.1 (Top) Jablonski diagram for fluorescence. Absorption of a photon excites an electron (electronically and vibrationally) to a higher energy singlet state, which then relaxes non-radiatively through vibrational levels before radiative relaxation to the ground state. **(Bottom)** Simulated excitation and emission spectra for a fluorophore.

First, when a fluorophore is irradiated with a wavelength of light (λ_1) equal to the energy difference (or *band gap*) between the ground state (S_0) highest occupied molecular orbital (HOMO) and the excited state (S_1) lowest unoccupied molecular orbital (LUMO), an electron in

S_0 is promoted to a higher electronic and vibrational level singlet excited state, S_1'. This electron undergoes rapid modes of non-radiative relaxation at the picosecond timescale, including vibrational, rotational, or collisional, to the lowest vibrational energy level, S_1.[2] The singlet electron can then relax to the ground state S_0 radiatively by emission of a photon of light, λ_2.

Since $\lambda = c/\nu$, where c is the speed of light and ν is frequency, and frequency is directly proportional to energy by the equation $E = h\nu$, the relationship between energy and wavelength of light can be shown to be $E = hc/\lambda$. Energy is inversely proportional to wavelength. The photon emitted at λ_2 is always lower in energy than the light absorbed at λ_1 due to the partial relaxation to a lower vibrational energy level and therefore $\lambda_2 > \lambda_1$. For a fluorophore, λ_1 is referred to as the excitation wavelength (λ_{ex}) and λ_2 the emission wavelength (λ_{em}). The inherent energy difference between the two manifests itself on a spectrum of overlaid excitation and emission curves as a shift to longer wavelength, referred to as a red-shift or Stokes' shift (shown in Figure 1.1, bottom).[2] The shape, width, relative intensity, and degree of Stokes' shift depends on the fluorophore itself as well as environmental factors.

Predicting if a compound will be fluorescent is not simple, even when computational molecular modelling is used. However, fluorophores typically share general commonalities, such as polyaromaticity and extended pi-conjugation. In addition, they often bear electron-donating groups that 'push' electron density into the pi-system and electron-withdrawing groups that 'pull' electron density, creating a "push-pull" system and greater charge separation.

1.1.2 Fluorescence Microscopy

Fluorescent cellular imaging has been enabled by recent advances in fluorescence microscopy technology. In 2014, the Nobel Prize in chemistry was awarded for "the development of super-resolved fluorescence microscopy" to Eric Betzig, William Moerner, and Stefan Hell.

A fluorescence microscope must contain three essential elements: an excitation light source, wavelength filters to separate excitation and emission photons, and a detector that measures the fluorescence signal output. The most widely used fluorescent microscopes are epifluorescent (or epi-illumination). These microscopes use the objective lens to both illuminate and image the sample.[2] The design of this category of microscope is shown below.

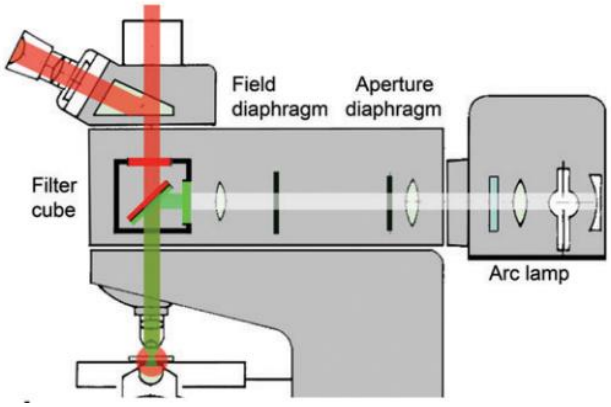

Figure 1.2 Diagram of an epifluorescent microscope (excitation light shown in green, emission shown in red).[2]

In this instrumental arrangement, the objective functions to image and magnify the specimen, and serves as the condenser that illuminates the sample from above. In the above figure, excitation light is shown in green, originating from the light source (in this case an arc lamp) and emission from the sample is shown in red. The filter cube functions to prevent excitation light

from reaching the detector. In addition to a dichroic beam splitter mirror to separate excitation from emission, two additional filters are used: an excitation filter that pre-selects excitation wavelength and a barrier filter that only allows longer wavelength light to hit the detector. Multiple cubes (aka filter sets) can be present and computer automated to rapidly switch between filter sets to image different wavelength in one sample. Typical light sources are arc lamps (such as mercury and xenon) and lasers.[2]

To fluorescently image live cells, several factors and limitations of the microscope must be considered. Firstly, UV radiation is known to damage DNA and fluorescence excitation can result in phototoxicity of cells and tissues, mainly through formation of reactive oxygen species and free radicals.[3] Photobleaching of fluorophores can also result from prolonged excitation, causing the fluorescent signal to fade permanently. Estimates of 10,000-40,000 cycles between ground state and excited states are cited as the limit for good fluorophores before bleaching occurs.[2] As a result, it is critical to expose the cells to as little light as possible, and therefore detectors must be highly sensitive and collect as much light as possible. Spectral bleeding (or "cross-talk") refers to overlap of emission/excitation spectra and is a serious concern when imaging multiple fluorophores in a single sample. Filter sets and fluorophores must be chosen carefully to minimize this effect. Lastly, cells are not flat and differences in thickness can affect fluorescence signal unless a confocal microscope is used. For example, vertical membranes will always appear brighter than membranes in the horizontal (parallel) plane since there can be many more fluorescent molecules 'stacked' and contributing to a pixel.

1.1.3 Advantages of Fluorescent Methods

Fluorescence microscopy aims to detect a fluorescent signal in an otherwise black background. As a result, this technique is highly sensitive. Fluorescent methods can also provide high spatio-temporal resolution, allowing living systems to be monitored *in real time.* There are many examples in the literature of single molecule detection using super-resolution fluorescence microscopy methods, such as STORM and PALM, which provide resolution between 10-55 nm.[4]

Perhaps the greatest advantage of fluorescence microscopy is the ability to perform multicolour experiments, such as tracking multiple cellular species and visualizing colocalization. Wavelength ranges across the visible spectrum (300 nm to 700 nm), as well as the NIR-I and NIR-II window (700-950 nm and 1000-1700 nm, respectively) can be observed, allowing the potential combined use of fluorophores across the visible spectrum limited only by available fluorophores, spectral overlap, and available filter sets.

1.2 Labelling Techniques

One of the most widely used methods of studying protein localization, expression, trafficking, and interactions is to fluorescent label a specific protein of interest (POI). While early applications were rather limited in scope and mainly tackled monitoring protein dynamics, more recent fluorescent techniques have investigated enzymatic activity and global changes in cellular state, such as membrane potential, cell division, and tissue differentiation.[5]

The most common genetic methods of fluorescent protein labelling can be broadly categorized into four classes: 1) fusion of the POI to a fluorescent protein, 2) fusion of the POI to an enzyme that can be subsequently labelled using functionalized irreversible inhibitors, 3) fusion of the POI to a "substrate tag" that can be labelled with a co-expressed enzyme, and lastly, 4) incorporation

of an unnatural amino acid or minimal peptide tag to the POI that reacts with a small molecule fluorophore.

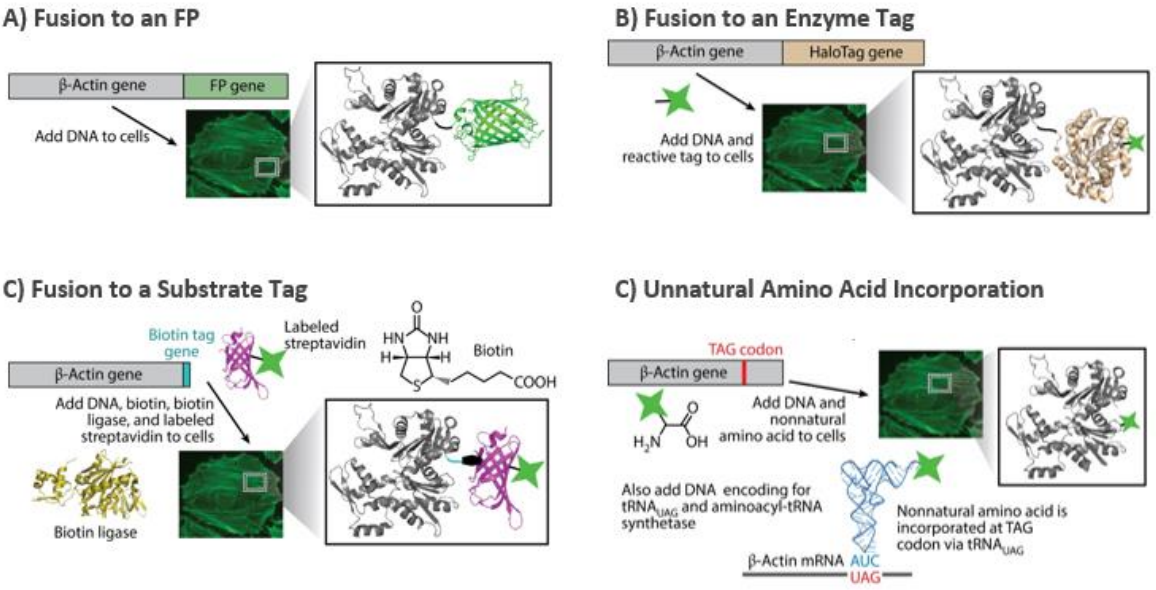

Figure 1.3 Comparison of genetic methods of fluorescent labelling of a POI (β-actin) highlighting the relative size of the encoded gene.[5]

1.2.1 Genetic Fusion to a Fluorescent Protein

Over the past two decades since the method was first published by Tsien,[6] fluorescent labelling of a POI by genetic fusion to a fluorescent protein (FP) has remained the most widely applied method for live cell imaging. As shown in Figure 1.3 above, FPs are composed of beta-strands which form a characteristic 27 kDa beta-barrel tertiary structure.[6] Inside the hollow beta-barrel, a small number of amino acid residues form the chromophore autocatalytically. Since the first discovery of Green Fluorescent Protein (GFP), additional discovery and extensive protein engineering efforts have been undertaken to create FPs whose emission wavelengths span most

of the visible spectrum. Additional optical properties such as brightness and photostability have been tuned, as well as biochemical properties including chromophore maturation.[5]

FP-POI fusions can be expressed ectopically, virally, or more recently, endogenously using TALENS and CRISPR.[7,8] Due to genetic fusion directly to the fluorescent reporter tag, the intrinsic specificity of the labelling method is unparalleled. However, as shown in Figure 1.3 (A), the large size of the FP is a major drawback, as it may perturb the native function or trafficking of the POI, particularly for proteins that assemble into larger complexes or protein-protein interactions. Other limitations of FPs include large bandwidths and their tendency to aggregate, despite years of engineering to create soluble monomers, increasing the potential negative steric effects of the method drastically.[9]

1.2.2 Enzymatic Labelling

Enzymatic labelling tags are an alternative method of fluorescently labelling proteins, which exploit enzymes exquisite selectivity for their substrates. In addition, enzymes' rapid reaction rates and suitability to mild reaction conditions make them very attractive for protein labelling applications. Enzymatic labelling methods are distinguished into two categories depending on which component (either the enzyme or the substrate) is fused to the POI as a 'tag': 1) enzyme tags and 2) substrate tags.

1.2.2.1 Enzyme Tags

In this method, an enzyme tag genetically fused to the POI reacts specifically with a small molecule (typically an analog of a specific, irreversible inhibitor of the enzyme) which may be modified to be fluorescent or contain a reactive handle to subsequently append a fluorophore.

Some examples of enzyme tags include haloalkane dehalogenase (HALOtag),[10] O^6-alkylguanine-DNA-alkyltransferase (SNAPtag),[11] CLIPtag,[12] and *E-coli* dihydrofolate reductase (TMPtag).[13]

As shown in Figure 1.3 (B), the size of these enzyme tags is comparable to GFP, ranging from 18 kDa to 33 kDa.[10,13] In the example shown, the HaloTag is nearly the same size as the POI. This method therefore suffers the same steric downfalls as described for FPs.

1.2.2.2 Substrate Tags

Alternatively, substrate tags are small 13-15 amino acid peptide sequences introduced into the POI, which are then modified by an enzyme that shows affinity and selectivity for the tag. Some widely used substrate tags include Q-tag (transglutaminase), LPXTG-tag (sortase), and acyl carrier protein (ACP)tag (PPTase).[14]

While the genetic modification to the POI is considerably smaller than fusion to the enzyme, a major disadvantage is that the enzyme that accomplishes the labelling must be co-expressed.

Additionally, for both enzymatic approaches the endogenous enzyme may be present in the system being investigated, which can cause off-target labelling and decrease labelling efficiency.

1.2.3 Labelling with Small Molecules

Labelling strategies that rely on specific chemical reactivity (as opposed to enzymatic specificity) typically exploit either the incorporation of an unnatural amino acid (UAA) into the POI or a genetically encoded, short sequence of amino acids that react selectively to append a fluorophore.

1.2.3.1 Unnatural Amino Acid Incorporation

UAAs may in some cases be fluorescent themselves (such as the coumarin fluorophore shown in Figure 1.4) or more commonly function as a biorthogonal chemical handle to incorporate a fluorophore. The modified residues often have biorthogonal functional groups to allow for specific conjugations to occur, such as azide/alkyne click reactions, aldehyde/ketone condensations, and tetrazine ligations.[14] Some example UAAs containing these handles are shown below, with conjugation moieties highlighted in blue.

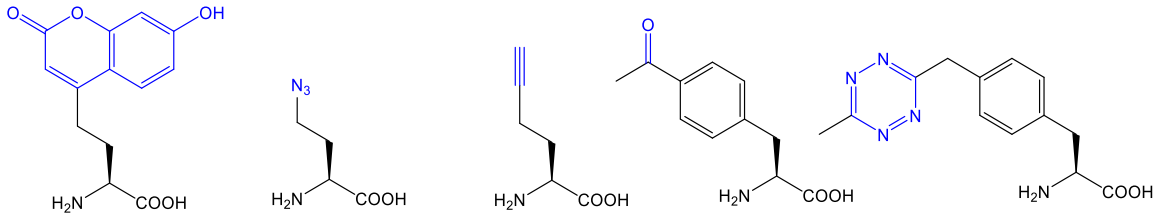

Figure 1.4 Example UAAs, from left to right: fluorescent coumarin, azide, alkyne, ketone, and tetrazine. [14]

Two incorporation methods have been described to date. The first uses existing aminoacyl tRNA synthetases (aaRS) to recognize and incorporate UAAs; however, competition with the endogenous amino acid substrate for the aaRS is an issue, resulting in a mixture of protein-conjugates after labelling. [14] The second method is more selective (shown in Figure 1.3 (D)). The amber stop codon UAG is reassigned to insert a UAA using suppressor tRNAs commonly obtained from bacteria (e.g. *E. coli*) or protozoa (e.g. *Tetrahymena thremophilia)* that introduce an amino acid at the UAG stop codon instead of stopping translation.[15,16] An aaRS and orthogonal tRNA pair must then be evolved and introduced into a host, such as *E. coli,* along with the amber stop codon. Experimentally, this method is time-intensive and complex. Some

limitations include decreased expression of the desired full length POI, truncated protein by-products, and incompatibility of the orthogonal aaRS-tRNA pair. [14]

1.2.3.2 Peptide Tag Incorporation

Alternatively, a small peptide tag that reacts selectively with a fluorophore probe can be fused to the terminus of a POI by common protein engineering strategies. One of the most classic examples is the His-tag. The strong coordination of six histidine residues in the tag to transition metals such as Ni^{2+} can be used for protein-purification by pull-down, as well as to attach a fluorophore. In most cases the tag is very small (0.84 kDa) and does not affect native folding or function of the POI.[17]

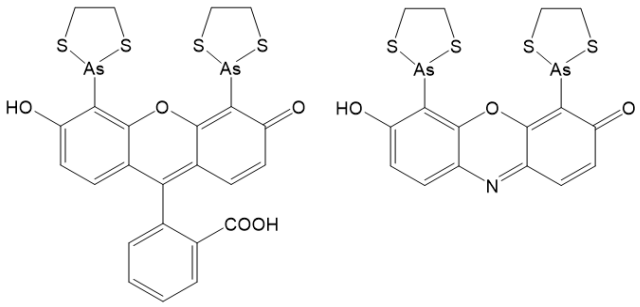

Figure 1.5 FlAsH (left) and ReAsH (right) fluorogenic probes developed by the Tsien group.

Another widely applied and commercialized method is the Tsien group's peptide tag. They use a tetra-cysteine tag with biarsenical ligands, termed FlAsH and ReAsH.[18] These probes are small, highly permeable, and fluoresce more brightly (green and red respectively) upon binding the four cysteine residues of their short encoded peptide tag, exploiting the affinity of arsenic toward thiols. However, the FlAsH/ReAsH method presents major limitations. It suffers from background signal, which requires washing steps to limit background fluorescence when labelling cells. This is particularly problematic since the probe's binding is also reversible and

washing runs the risk of removing the fluorescent probe entirely. The probes are also known to be highly toxic, limiting their application *in vivo*, and the tetra-cysteine motif is sensitive to oxidizing environments, making extra-cellular labelling difficult.[19]

Peptide tag-molecule probe labelling systems can overcome the greatest drawbacks of the other fluorescent labelling methods discussed. This method utilizes small molecule fluorophores as opposed to bulky fluorescent proteins and enzyme tags, avoiding the potential steric limitations. In addition, synthetic chemistry allows for fine tuning of probes in terms of reactivity, stability, solubility, permeability, and spectral properties such as wavelength, bandwidth, and brightness. Small molecule probes can be tailored to specific needs. For example, fluorophores can be designed to be membrane permeable or impermeable to report on intracellular vs. extracellular events.

Typically, small molecule fluorophores have narrow excitation/emission bands compared to FPs and can therefore be used to circumvent spectral bleeding and overlap issues when imaging multiple fluorescent species.

1.3 Small Molecule Fluorophores for Cellular Imaging

There are now hundreds of commercially available organic dyes spanning the visible and NIR wavelength range.[5] Many of these fluorophores result from synthetic modification of a smaller number of core scaffolds. Some of the most widely used classes of fluorophores include fluorescein, rhodamine, coumarin, cyanine, and BODIPY.

Currently, there is a heavy focus in the field to create fluorophores that move out of the visible spectrum for traditional fluorescence imaging (400 – 700 nm) toward the near IR regions (700 –

1700 nm).[20] Near-IR (NIR) dyes are especially in demand for *in vivo* imaging due to increased tissue penetration of longer wavelength light and decreased photo-toxicity of lower radiation. Existing fluorophore structures have been modified to increase conjugation, add heteroatoms to shift their emission into the NIR region. For example, silicon-rhodamine (SiR) dyes have recently emerged as a new class of promising fluorophores and have been used to create NIR substrates for SNAP-tag, CLIP-tag, and Halo-Tag.[21]

Several design criteria must be considered to apply small molecule fluorophores for *in cellulo* and *in vivo* imaging. Firstly, the fluorophore must be non-toxic. For optimal sensitivity, the fluorophore should be bright and photostable. The brightness of a fluorophore is proportional to the product of its quantum yield (Φ) and molar extinction coefficient (ε). Quantum yield is a measure of fluorescence efficiency, whereas molar extinction coefficient measures how strongly a compound absorbs light at a given concentration. High extinction coefficients are useful when light intensity needs to be minimized, such as in live cell fluorescence imaging. Useful small organic fluorophores are cited to have ε between 25,000 to 200,000. In comparison, enhanced GFP has a ε of 60,000.[2] Similarly, a high quantum yield increases fluorescence intensity, reducing the amount of excitation photons that need to be applied. Quantum yields near 100% are not unheard of for small molecules. Fluorescein, for example, has a quantum yield of 95%, compared to 60% for EGFP. [2,22]

The fluorophore must also be aqueous soluble, cell permeable and stable under the cellular conditions. In terms of labelling, the chemistry must be bio-orthogonal and compatible with the cellular matrix.[19] As mentioned above, imaging in tissue and *in vivo* bring the added

requirements of fluorophores whose emission/excitation spectra are red-shifted (ideally NIR) for better tissue penetration and decreased toxicity.

Designing and synthesizing small molecule fluorophores that meet these requirements is challenging. The two most frequently cited limitations of organic fluorophores for live cell-imaging are lack of specificity and poor cell permeability.[23] Specificity of the fluorescent probe is critical, as non-specific labelling can result in background fluorescence, and decrease sensitivity. To label proteins inside the cell, the small molecule must be able to cross the lipid bilayer membrane of the cell. Factors that contribute to cell permeability of a small molecule can be incorporated into its design using medical chemistry drug design concepts such as Lipinski's Rule of Five, which consider hydrogen bonding ability, size, conformational flexibility, and partitioning between phases. However, cell permeability can only be determined experimentally, and compounds which appear to be promising on paper may still have permeability issues in the complex milieu of cells.

1.3.1 Fluorogenic Probes

For any fluorescent imaging method, high resolution and low background signal are critical. A fluorophore label is always fluorescent when illuminated, both in its 'free' state and its bound or reacted state. This means that the fluorophore is indistinguishable from its free and bound state by fluorescence microscopy. As a result, undesired background signal is a major concern and is typically mediated by post-labelling washing steps to remove unbound/unreacted fluorescent probe.

To limit non-specific background signal, small molecule probes should ideally be non-fluorescent until labelling has occurred. A *fluorogenic* labelling agent is a molecule which

undergoes a significant fluorescent enhancement upon labelling or is completely non-fluorescent before reaction. In other words, the fluorogen's fluorescence is *quenched* until it undergoes a reaction which restores fluorescence. Fluorogens are attractive for cellular imaging due to their low background signal, allowing a "no wash" labelling method. Ideally, the fluorogen would exhibit completely efficient quenching (and therefore no background fluorescence) and become brightly fluorescent upon labelling.

One illustrative example of fluorogenic labelling tools are the Tsien group's FlAsH and ReAsH organoarsenic probes, mentioned previously.[24] The biarsenical dyes incorporate the fluorescein fluorophore and exhibit increased fluorescence upon binding to a tetra-cysteine peptide tag, making their labelling method fluorogenic. These fluorogens have been commercialized and marketed for live cell imaging and have been applied widely in areas such as protein localization and trafficking, affinity-purification of proteins, and SDS-page protein-detection.[25,26] FlaSh/ReAsH probes exhibit a relatively low fluorescent enhancement (FE) of approximately 20-fold.[18] This enhancement has proven to provide sufficient contrast for cellular fluorescence imaging, although it limits the sensitivity of the technology.

Other groups have recently developed fluorogenic versions of more traditional biorthogonal labelling agents, including azidofluoresceins,[27] BODIPY-tetrazines,[28] and fluorogenic inhibitors of the SNAP-tag, Halo-tag, and BI-tag.[21,29]

1.4 FlARe Labelling Method

The Keillor group has developed a protein labelling method using small molecule fluorogenic labelling agents and a short genetically encoded terminal peptide tag. This method has been termed FlARe, due to the Fluorogenic Addition Reaction upon which it is based.

1.4.1 General Design

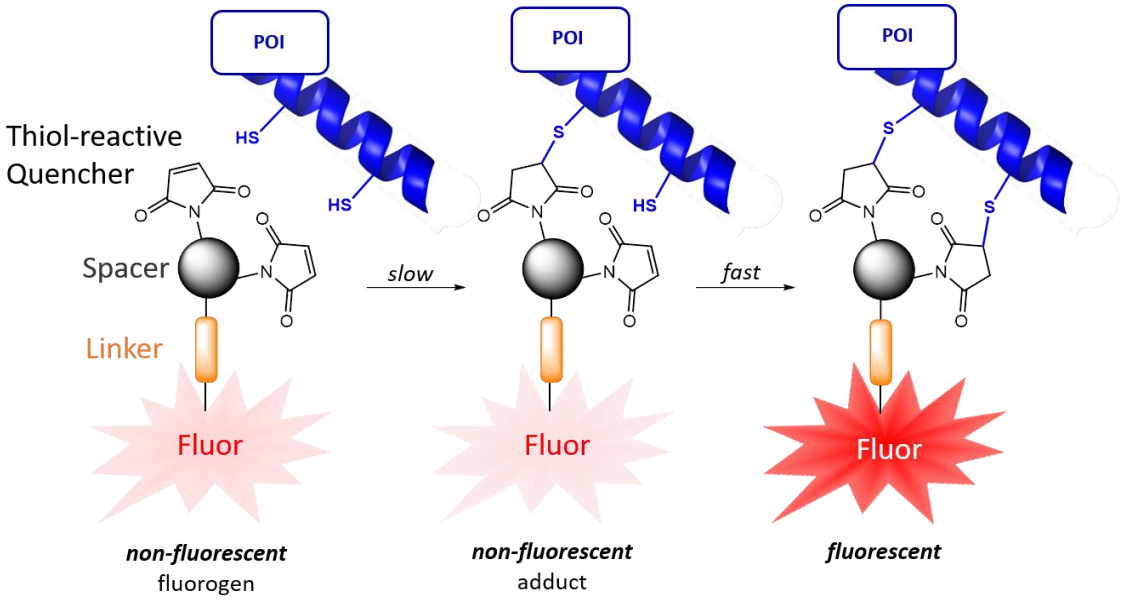

Figure 1.6 General FlARe labelling strategy.

The FlARe method relies on two complementary components: the reactive fluorogenic labelling agent and the peptide tag. The peptide tag, shown in blue above, can be genetically fused to the terminus of a POI and contains two nucleophilic cysteine residues. The FlARe fluorogen is comprised of four segments, each of which serves an important function and will be discussed separately in more detail in the following sections: 1) thiol-reactive quencher, 2) spacer, 3) linker, and 4) the fluorophore.

As shown above, the thiol-reactive quencher is a dimaleimide group. The maleimides are separated by the same distance as the cysteine residues by the spacer group (grey). The linker (orange) attaches the di-maleimide scaffold to the fluorophore (red), which is quenched in the unreacted state of the probe. The first addition reaction between the maleimide and a thiol is

intermolecular and the rate-limiting step. The mono-succinimide adduct formed still bears one maleimide group, which can quench fluorescence. The reaction of the second maleimide with the tag is very fast, as it is intramolecular, and therefore its effective concentration is greatly increased. Both addition steps are essentially irreversible, forming a strong covalent bond to the tag. Fluorescence is produced only after both maleimides react with the di-cysteine peptide tag. The rarity of the specific discysteine motif of the tag in biological systems confers selectivity for the labelling reaction over other native biological thiols.

1.4.2 PeT Quenching

As shown above, the FlARe method relies on a fluorophore linked to a quencher moiety.

There are three broad categories of fluorescence quenching: 1) environmental, 2) energy transfer mechanisms, such as Forster resonance energy transfer (FRET) and through-bond energy transfer (TBET), or 3) electron transfer mechanisms.

Some well-established moieties capable of quenching through electron transfer in the literature include: azides, tetrazines, alkynes, and maleimides.[30] Maleimides have been known to quench fluorescence in their conjugated form for quite some time; however, after the conjugated double bond undergoes an addition reaction to form a succinimide, they no longer exhibit a quenching effect.[31] Despite their widespread use over the years, very little work was done to elucidate their quenching mechanism.

The mechanism by which maleimides quench fluorescence in FlARe probes was determined to be through Photo-induced electron Transfer (PeT) in a previous study by Keillor.[31] PeT refers to electron transfer from an electron rich donor (D) and electron deficient acceptor (A). Quenching

can either be dynamic, occurring via collisions between two molecules, or static, where a stable complex contains both D and A.[32] There are two different types of PeT, distinguished by the direction of electron transfer between D and A. In donor pet (d-PeT), electron transfer occurs from the excited state of the fluorophore to the quencher, whereas in acceptor PeT, (a-PeT), the electron is transferred from the quencher to the fluorophore.[33] In FlARe, D and A exist in the same molecule and electron transfer occurs to the maleimides, therefore PeT quenching is intramolecular and d-PeT. A simplified Jablonski diagram for the d-PeT quenching mechanism by maleimides is depicted below.

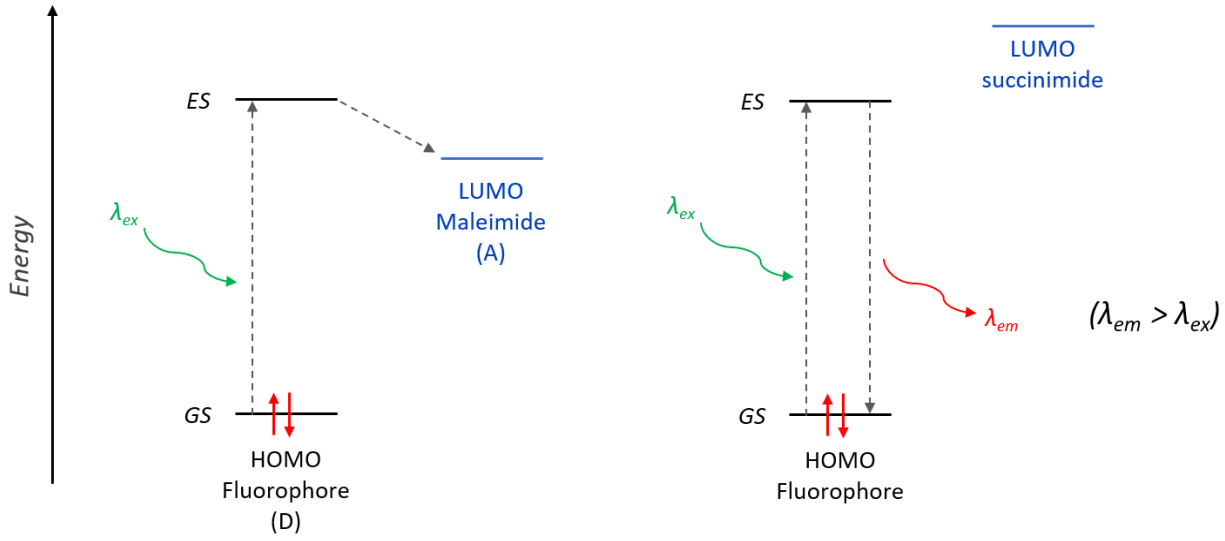

Figure 1.7 Jablonski diagrams for the d-PeT quenching mechanism between maleimides (A) and the fluorophore (D). Quenching is abolished when the maleimide is transformed to a succinimide as the LUMO energy level is increased, disfavouring electron transfer.

As described previously, fluorescence occurs when a ground state electron is promoted to an excited state, followed by relaxation by emission of a photon. However, d-PeT quenching can occur by maleimides if the energy (redox potential) of the LUMO is sufficiently low in

comparison to the excited state fluorophore orbital such that electron transfer from the ES to the maleimide LUMO is favourable. In this case, the excited electron is transferred to the maleimide LUMO and relaxes to the ground state through non-radiative processes, abolishing the native fluorescence of the fluorophore.

Fluorogenicity results when the reduction potential of the quencher maleimide changes upon reaction with the target tag such that ΔG of electron transfer becomes disfavoured. Specifically, the LUMO of the succinimide formed after reaction with the di-cysteine tag becomes higher energy, and therefore electron transfer and quenching does not occur and fluorescence is restored.

$$\Delta G_{eT}^{0} = E\left(\frac{D^{+}}{D} - \frac{A}{A^{-}}\right) - \Delta E(0,0) - wp$$

The probability of PeT can be predicted partially using the Rehm-Weller equation (providing the Gibbs energy of PeT) shown above.[34,35] This relationship takes into account the oxidation potential of fluorophore donor and the reduction potential of the maleimide acceptor, the energy gap between the ground and excited singlet state of the fluorophore ($\Delta E_{0,0}$), and the reorganizational energy (*wp*). Non-experimentally, molecular modelling and DFT calculations can be used to predict the relative energy levels of the fluorophore and maleimide and subsequent likelihood of d-PeT quenching, providing a basis for the rational design of complementary donor-acceptor pairs for our FlARe probes.

1.4.3 Di-cysteine Tag Development

The peptide tag component of the FlARe system is a short alpha-helical amino acid sequence containing two nucleophilic cysteine residues separated by two turns of the helix (*i*, *i* + 7). This configuration places the two cysteine residues approximately 10 Å apart, the complementary distance to our dimaleimide motif. In addition, this distance positions the cysteine residues far enough apart to disfavour disulphide bond formation, allowing the tag to be used in oxidizing environments as demonstrated by successful labelling of cell surface proteins. [36]

The first proof of principle for the FlARe labelling method used a mutant of the helical transcription factor Fos, a 380 amino acid protein.[37] Site-directed mutagenesis introduced a lysine to cysteine mutation at position 56, two turns of the alpha helix away from a native cysteine residue. The Keillor group was interested in a much smaller peptide tag that could be encoded onto the terminus of a POI with minimal perturbation of the POIs structure and function. Toward that goal, a synthetic peptide designed to fold into a short monomeric alpha helix with four complete turns was discovered in the literature. [38,39] The N-terminal acetyl and C-terminal carboxamide groups were then replaced with known N-cap and C-cap sequences to give the sequence **2** in Figure 1.8.

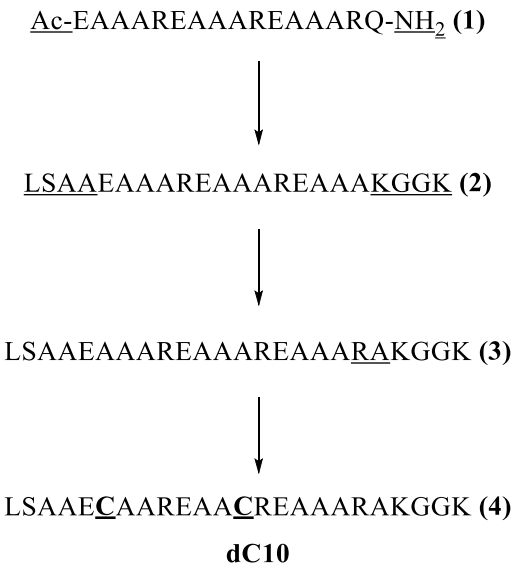

Figure 1.8 Changes to the amino acid sequence to form the dC10α-helical peptide tag.

Next, the sequence was extended by two residues to form a complete number of turns to further stabilize the helix, forming the parent sequence **3**. Finally, two cysteine residues were introduced *i, i* + 7 to give the final tag, named dC10α (describing the di-Cysteines, 10 Å apart in the α-helix). The helical secondary structure of the tag was confirmed by CD spectroscopy via fusion of the tag to a test protein (Maltose Binding Protein, MBP), both before and after reaction with a dimaleimide fluorogen.[36]

More recent efforts have altered the reactivity of the tag by site-directed mutagenesis of residues within hydrogen bond distance of the cysteines to decrease the pK_a of the thiols. Results on a new dC10α* tag were published in 2018.[40] This tag was not used within the scope of this thesis; however, it will be discussed in more detail in Chapter Four: Future Perspectives.

1.4.4 Optimization of FlARe Fluorogens

1.4.4.1 Linker

Maleimides quench fluorescence by acting as an electron acceptor in donor-PeT.[41] Electron transfer in PeT can occur through-space or through-bond, though previous studies have shown through-space to be more efficient within shorter distances.[42] To obtain good contrast for cellular imaging using fluorogens, efficient quenching to reduce background fluorescence is equally as important as bright fluorescence after labelling.

The first proof of principle FlARe probes in 2005 for *in vitro* application with the Fos protein were naphthalene and coumarin derivatives that had maleimide groups attached directly to the fluorophore core.[37] As expected, bringing the quencher and fluorophore into as close of proximity as possible showed excellent quenching efficiency; however, their difficult linear synthesis and low quantum yields made them poorly suited for practical applications.

Next, a more convergent synthetic route was developed that linked the dimaleimide moiety to the fluorophore though a phenyl spacer to give an approximate 10-Å distance. Dansyl and fluorescein based FlARe probes (shown below) were coupled to the dimaleimide through a five atom linker chain and showed promising preliminary results with the dC10α tag. [43] These compounds were synthesized by reacting the benzoic acid maleimide core to a free amine linker by typical peptide coupling conditions.

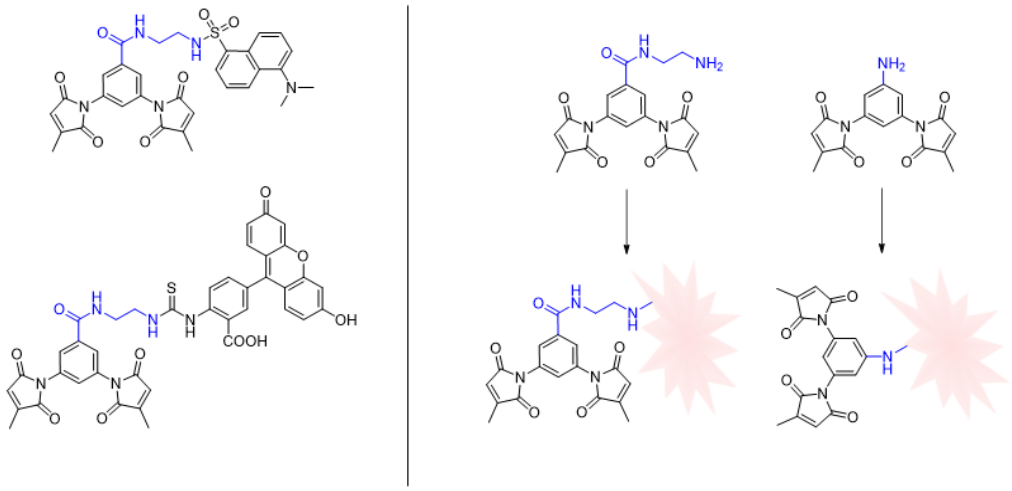

Figure 1.9 (Left) Dansyl and coumarin FlARe probes with first generation linker. (Right) Comparison of dimaleimide scaffold and second generation linker.[43]

In a subsequent 2011 study, "spacer-less" fluorogens were developed by synthesizing a series of coumarin probes where linker length and rigidity were systematically varied. [43] Fluorescent enhancements for these compounds ranged from 2-fold to 6-fold, correlating roughly linearly with decreased distance through-space, not through-bond.

This work confirmed an increase in quench efficiency by decreasing space between fluorophore and quencher and led to a new convergent synthetic strategy to decrease linker length.[43] The reactivity of the coupling was reversed, using a nucleophilic aniline spacer as opposed to the electrophilic acid. This allowed amine-reactive fluorophores to be coupled more directly to the spacer. For example, when the linker length was decreased from five atoms to two in the dansyl FlARe probe, the result was an increase in FE from 2-fold to an estimated 300-fold. This aniline scaffold, which separates the dimaleimides by ~10 Å, will sometimes be referred to as NHdM10 for short.

1.4.4.2 Maleimide

Maleimides are among the most common functional groups used for bioconjugation reactions with thiols, as they react rapidly in a Michael fashion under physiological conditions.[44] Their popularity can be attributed to many factors including reaction rate, selectivity, high yield, and good stability to heat and water.[45] The specificity of this reaction is associated with Hard-Soft Acid-Base theory, as thiols are a soft nucleophile and maleimides a soft electrophile, as well as the pka of thiols (~8).[45]

Although the rarity of the discysteine motif of the dC10α tag in biological systems creates selectivity for the labelling reaction, other biological thiols are present in the cellular milieu that present potential problematic off-targets. Of particular concern is glutathione (GSH) is a thiol-containing tripeptide that is present inside the cell in concentrations of 10 mM. Susceptibility of the reactive handle to hydrolysis is also major consideration for application in the aqueous cellular environment.

In a 2015 study, the Keillor group investigated maleimide C=C substituent effects on the reaction rates with thiols as well as hydrolysis rates to consider stability in aqueous solution.[44] For substrates with R = H, Me, Et, ^{i}Pr, and OMe, thiol addition reaction was >100-fold faster than background hydrolysis. R=Et and ^{i}Pr had hydrolysis rates an order of magnitude smaller than the other substituents, suggesting that increasing steric bulk at C=C bond mitigates hydrolysis. In terms of thiol addition, the unsubstituted maleimide had the highest rate constant as expected, as there is no steric hinderance. While substituent effects on the rate of thiol addition were also observed and correlate roughly with steric bulk, they were less pronounced than the effect on hydrolysis rates.

substrate	R	k_{OH} (M^{-1} s^{-1})	k_2 (M^{-1} s^{-1})	k_{OH}/k_2 ratio
S1	H	67 ± 17	8.9 ± 0.7	7.6
S2	Me	24 ± 4	4.4 ± 0.2	5.6
S3	Et	2.5 ± 0.5	2.2 ± 0.2	1.1
S4	^{i}Pr	1.1 ± 0.3	1.3 ± 0.1	0.8
S5	OMe	45 ± 5	1.3 ± 0.1	40.5
S6	OEt	41 ± 7	N.D.[a]	
S7	O^{i}Pr	15 ± 1	N.D.[b]	

Figure 1.10 Hydrolysis rate constants (k_{OH}) and thiol addition rate constants (k_2) for R-substituted *N*-phenyl maleimide.

For biorthogonal labelling, a maleimide should be chosen that minimizes background hydrolysis rate and background reaction with biological thiols like GSH, while maximizing rate of reaction with the dC10α tag. As shown in Figure 1.10, substrates S4 and S5 had the smallest rate constant for reaction with small molecule thiols (k_2). Despite having a relatively high rate of hydrolysis under basic conditions in comparison with unsubstituted maleimides, the methoxy substituted maleimide (highlighted in Figure. 1.10 above) has been shown to react very slowly with small molecule thiols *in vitro* in comparison to the dc10α tag and is stable to hydrolysis at physiological pH.[46]

1.4.4.3 Fluorophore

Early generation FlARe probes incorporated fluorophores such as dansyl, coumarin and FITC, which were synthetically convenient as they could be coupled to the dimaleimide-aniline moiety directly.[43] Preliminary success with these probes included both intracellular and extracellular labelling of target proteins such as cytosolic actin, nuclear histone,[46] and the cell-surface receptor protein epidermal growth factor receptor (EGFR).[36]

These fluorophores all have relativity high energy excitation wavelengths in the UV, blue, and green range, respectively. Their high energy excited states make these fluorophores easily amenable to PeT quenching by the maleimide groups. However, high energy excitation is problematic for *in vivo* and *in cellulo* applications due to photobleaching and phototoxicity.

1.4.5 BODIPY as a New Fluorogen Scaffold

An ideal fluorophore candidate would have a high quantum yield and molar extinction coefficient, low photobleaching, red-shifted excitation/emission, and efficient quenching by PeT. Although its preparation was first published in 1968,[47] popularity of the BODIPY (difluoroboron dipyrromethene) class of fluorophores for cellular applications has risen dramatically in recent years due to several promising features including robustness, brightness, narrow emission bandwidth, and good aqueous solubility. [48]

BODIPYs exhibit a wide range of emission/excitation wavelengths with examples across the visible range and even NIR based on modification around the core structure.[49,50] Recently, NIR and red BODIPYs such as Aza-BODIPYs and dimeric structures have been synthesized.[50,51] Many synthetic approaches to diversifying the BODIPY core have emerged, broadly categorized into pre-functionalization or post-functionalization strategies depending on if modifications to the core structure occur before installing the difluoro boron moiety. The BODIPY core including the IUPAC numbering system for functionalization is shown below.

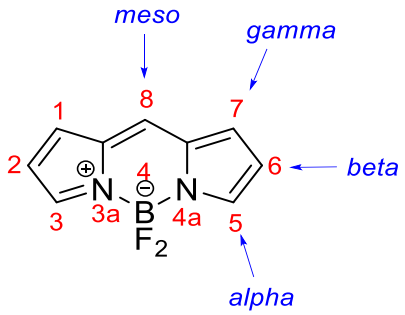

Figure 1.11 IUPAC numbering (red) and naming (blue) for BODIPY scaffold.

Longer wavelength emission fluorophores are predicted to have smaller HOMO-LUMO gaps from DFT calculations, and this decreased band-gap typically results from a lower energy LUMO, as opposed to a higher energy HOMO. As a result, red-shifted fluorophores are much more problematic in terms of PeT quenching compatibility than previous blue, cyan and green fluorophores. The structure of such a fluorogen would have to be changed either to lower the LUMO of the maleimide below that of the fluorophore, or to raise both the HOMO and LUMO energies of the fluorophore.

A recent computational study by the Cosa group investigated a library of 100 BODIPY structures and showed that the probability of PeT can be predicted by using the Hammett constant to correlate BODIPY excited state redox potentials.[35] DFT calculations suggest that PeT quenching should be possible using the BODIPY scaffold.[32] Additionally, Nagano and coworkers' fluorogenic probe provided further evidence that maleimides can quench BODIPY fluorescence.[52] DFT modelling can therefore provide a means of rational design of BODIPY-based FlARe fluorgens to create a new generation of FlARe probes with improved optical properties for *in cellulo* protein labelling.

1.5 Objectives

Visualizing and monitoring proteins in live cells without disturbing their biological function is a key challenge in chemical biology. Despite recent advances in labelling tags with small molecule fluorophores, the available toolkit of labelling agents is still limited in terms of toxicity, background signal and washing steps, and multicolour imaging of multiple target proteins in living cells. To address these limitations in the field, we set out to create a new generation of FlARe fluorogenic labelling agents for no wash protein labelling in living cells based on the BODIPY scaffold. Our synthetic design focuses on green and red dyes, as red shifted dyes are advantageous for live cell labelling and most fluorescence microscopes used to investigate biological systems are equipped with green and red filters. The research towards these probes will be presented herein in the following Chapters.

1.5.1 Towards a Red-Shifted BODIPY FlARe Probe (Chapter Two)

First, we aimed to develop the first red FlARe probe by exploiting the versatile BODIPY fluorophore. To do this we built off promising preliminary work done by the Keillor group on a lead compound, referred to as **YC29** herein, which exhibited good kinetic and fluorogenic properties and emission in the red range of the visible spectrum. In this chapter we will discuss: 1) the design and computational modelling of **YC29**, 2) synthetic efforts towards improving the preparation of **YC29**, 3) the synthesis of two alternative red-shifted, potential FlARe probes based on **YC29**, and 4) *in vitro* kinetic evaluation and glutathione reactivity of these potential probes and *in cellulo* labelling of a dC10α-tagged POI.

1.5.2 Design, Synthesis, and Evaluation of a Green BODIPY FlARe Probe (Chapter Three)

Next, we aimed to develop a green BODIPY FlARe probe that would be red-shifted in comparison to previous dansyl (UV) and coumarin (blue) FlARe probes,[41,46] and provide a useful green channel fluorescent protein labelling agent. In this chapter we will discuss: 1) the design and computational modelling of **YC23**, 2) the synthesis of the green BODIPY probe, 3) *in vitro* determination of kinetic profile, quantum yield, and off-target thiol reactivity and 4) *in cellulo* toxicity and cellular labelling of a dC10α-tagged POI. Much of the work included in this chapter was recently published as a communication in *Angewandte Chemie International Edition* (2018).[53]

1.5.3 Conclusions and Future Perspectives (Chapter Four)

The final chapter of this thesis will summarize the results achieved in Chapters Two and Three in terms of synthetic preparation, spectral properties, kinetic profiles, fluorogenicity, and cellular labelling. This chapter will also briefly discuss recent improvements made to our dC10α tag that should be incorporated in future investigations and propose new red-shifted FlARe probes for future work.

Chapter Two: Towards a Red-Shifted BODIPY FlARe Probe

2.1 Introduction

As introduced in Chapter One, the FlARe labelling method exploits the selective reaction between a genetically encodable α-helical peptide containing two cysteine residues separated by ~10Å (dC10α) and a complementarily sized dimaleimide fluorogen. The first nucleophilic addition reaction of the thiol group to the electrophilic carbonyl of the maleimide is intermolecular and rate limiting, whereas the second intramolecular addition that restores fluorescence is very rapid. The addition reaction of the FlARe probe is kinetically favoured over reaction with small molecule thiols due to its constrained geometry and lowered cysteine pK_a values, resulting in high selectivity and low background signal.

Although there has been considerable success with early generation FlARe probes, their application has been limited by the high energy light required for excitation of the fluorophore. In terms of *in cellulo* and *in vivo* applications, fluorophores with red-shifted excitation and emission spectra are advantageous. To create FlARe probes that are better suited for live cell imaging, red-shifted dyes that are amenable to efficient quenching by maleimides through d-PeT are required. This can be challenging, as the smaller band-gaps of longer wavelength emission fluorophores are typically due to a lower energy LUMO, as opposed to a higher energy HOMO, which can disfavour d-PeT. The BODIPY fluorophore has emerged as a potential new fluorophore for FlARe that could circumvent these challenges. In particular, the recent work of the Cosa group was instructive, as it demonstrated a large library of BODIPY compounds that should be amenable to d-PeT.[54]

2.2 Design of a Red FlARe Probe

BODIPY-based fluorescent dyes have grown in popularity immensely in recent years, particularly as fluorescent indicators,[48] biological labels,[55] and fluorescent probes for bioimaging.[56] As discussed in Chapter One, the success of BODIPY for these applications can be attributed to several intrinsic properties including bright fluorescence (due to both high quantum yields and large molar absorption coefficients), narrow emission bandwidths within the range of the visible spectrum, good solubilities, and robustness. Perhaps most strikingly, the spectroscopic and photophysical properties of the dye can be tuned by functionalization of the BODIPY core at different positions with a wide variety of functional groups.[57] Modification to the simplest BODIPY structure can occur either by *pre*functionalization or *post*functionalization. In prefunctionalization, the desired functional group(s) are installed before the boradiaza-*s*-indacene core is formed by using functionalized versions of the pyrrole precursors. Alternately with postfunctionalization, modification occurs on the already formed core structure later in the synthetic route.

2.2.1 Synthetic Strategy

2.2.1.1 Functionalization Strategies for BODIPY

To design a wavelength-tunable FlARe probe, a synthetic route that incorporates late-stage modification is preferable, as this enables a more divergent strategy for the installation of different functional groups to achieve red-shifted emissions and even create small libraries of potential probes. To this end, our BODIPY scaffold was designed to be modified using a postfunctionalization strategy.

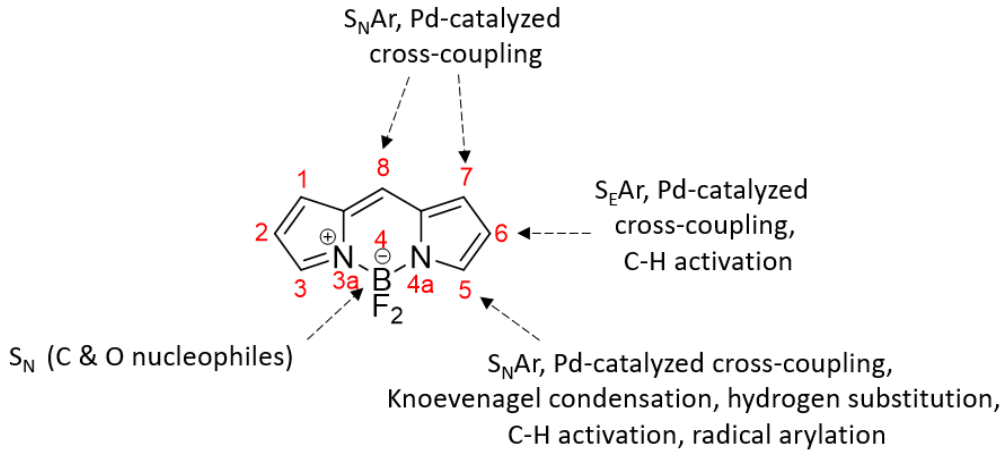

Figure 2.1 Summary of the synthetic strategies for postfunctionalization of the BODIPY core.

The current methods of postfunctionalization, based on position around the core, are summarized in

Figure **2.1**. For clarity, only one half of the symmetrical core is labelled, although the strategies shown are mirrored for positions 1-3. Preferential position(s) of functionalization based on the synthetic strategy used can impart regioselectivity; however, disubstitution is often possible at the mirrored position on the second pyrrole. Broadly, these strategies include substitution, aromatic substitution, Pd-catalyzed couplings, Knoevenagel-type condensation, C-H activation, and radical arylation.[57] Among the many available methods for derivatization, nucleophilic aromatic substitution (S_NAr) can be used for BODIPYs that are halogenated at the 1, 3, 5, 7, or 8 positions, whereas electrophilic aromatic substitution (S_EAr) is selective for position 2 and 6 (beta). S_NAr is electronically restricted to the 1, 3, 5, 7, and 8 positions because attack allows the resulting intermediate carbanion to be delocalized onto one of the nitrogen atoms.

2.2.1.2 S_NAr Approach

We were intrigued by the potential to append our nucleophilic aniline dimaleimide building block (aka NHdM10) to a halogenated BODIPY core directly through an S_NAr approach, as well as a functional group to red-shift the fluorophore's emission. A red-shift is often achieved by increasing the length of the pi conjugated system, lowering the LUMO energy and therefore decreasing the energy gap between HOMO and LUMO (band gap).[58] Amino substituents have been shown to affect the size of the band gap and this effect is dependent on position. 3- and 5-amino substitution has been shown to red-shift due to increased pi conjugation.[59] The work by Dehaen *et al*. on functionalization of halogenated BODIPYs via nucleophilic aromatic substitution was highly instructive in providing potential substituents to shift the emission wavelength.[60] This paper presented successful incorporation of a series of O, N, S, and C nucleophiles to a 3,5-chlorinated BODIPY via substitution and showed their effect on the spectral properties of BODIPY. Notably, they showed that aniline substituents shifted the emission towards 600 nm, with a di-aniline substituted BODIPY exhibiting the most red-shifted wavelength of 613 nm (in methanol).

Encouraged by these results, a 3,5-dichloro substituted BODIPY was chosen to functionalize. This overall approach is shown in Figure 2.2 below, where the dimaleimide scaffold is first installed by an S_NAr reaction followed by a wavelength-tuning substituent (R) by a second S_NAr reaction. The dimaleimides can then be installed using the nitro groups as synthetic handles.

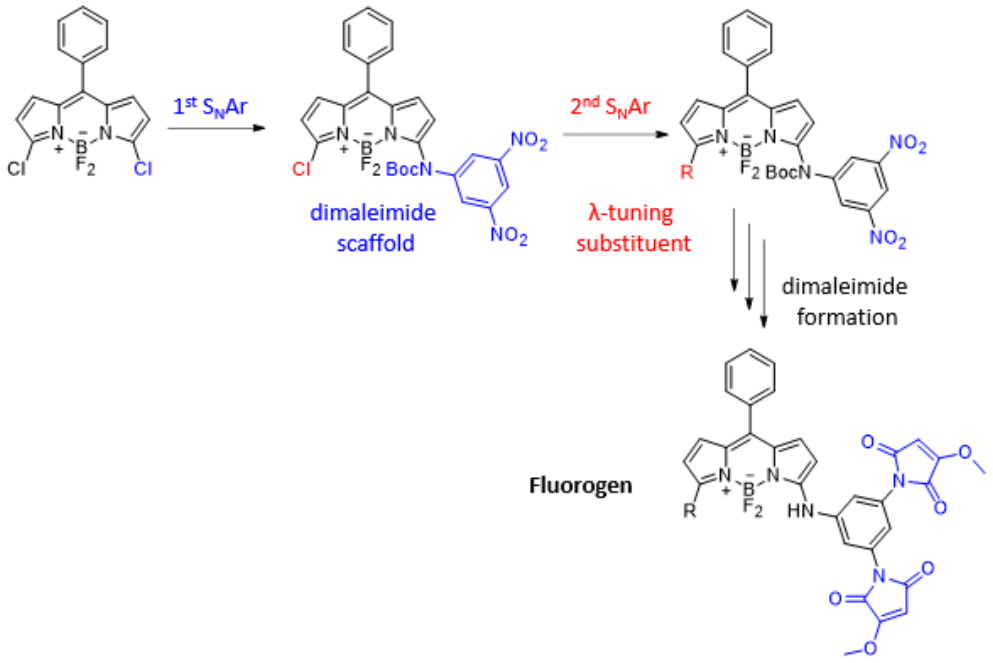

Figure 2.2 Double S_NAR design of a wavelength-tunable BODIPY FlARe probe.

Dr. Yingche Chen, a former post-doctoral fellow in the Keillor group, devised a series of compounds through this double S_NAR strategy to red-shift the emission wavelength of BODIPY, while maintaining the BODIPY ES at a higher energy than the maleimide-based LUMO to favour quenching by d-PeT. This endeavour involved computational modelling and analysis of energy levels for several potential compounds.

Based on the computational results obtained by Dr. Chen, the compound with R = *N*-methylaniline stood out as having the smallest band gap and therefore most red-shifted emission, while still able to quench by d-PeT. The target compound, referred to as **YC29**, is shown below in the overall FlARe scheme, where addition reaction with our di-thiol dC10α tag ultimately results in a fluorogenic response.

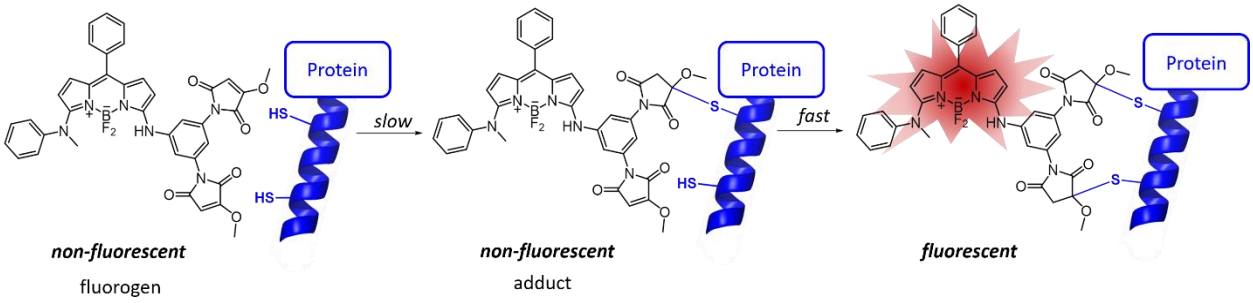

Figure 2.3 FlARe scheme for red BODIPY fluorogen **YC29**.

2.2.2 Molecular Modelling of YC29

The potential FlARe compound, **Ph-BODIPY-NHdM10-*N*-MePh** (aka **YC29**), was modelled herein by TD-DFT calculations (B3LYP functional and 6-31G(d) set) to determine if quenching by d-PeT should be possible, as well as to predict emission wavelength. As shown in Figure 2.4 below, the BODIPY excited state (B) and the maleimide LUMO (C) are separated by approximately 5.4 Å (A), which is within the distance range for d-PeT.

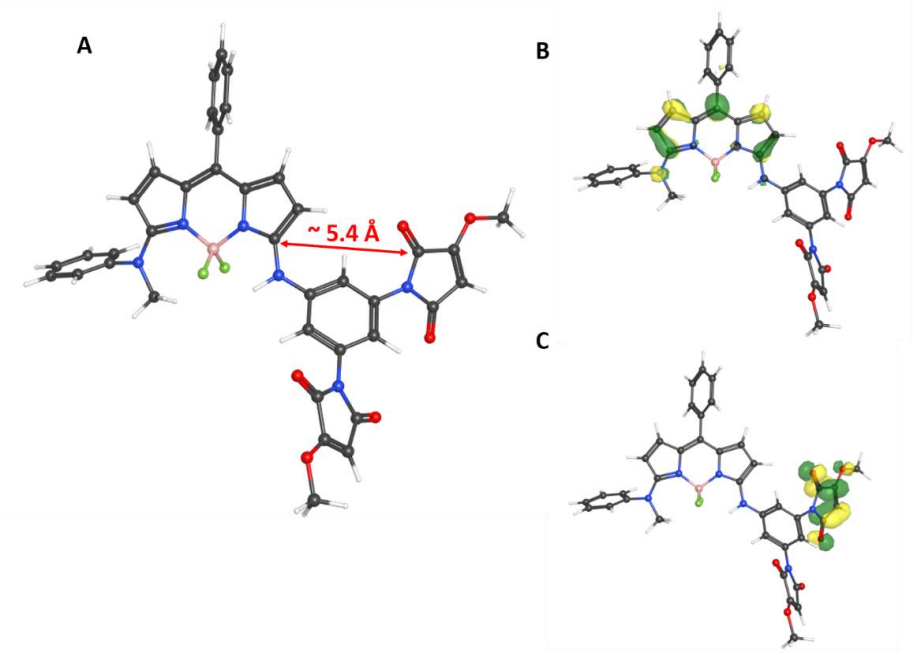

Figure 2.4 DFT-minimized geometry of fluorogen **YC29**, showing: A) the relevant distance between the maleimide and BODIPY group, B) the BODIPY excited state (LUMO +1), and C) the maleimide LUMO.

The energies of the relevant orbitals are summarized in Table 2.1 below. These modelling results show that the LUMO energies of the maleimides are slightly lower than that of the excited state BODIPY LUMO, and therefore quenching by d-PeT should be thermodynamically favourable.

Table 2.1 Summary of HOMO/LUMO energies for **YC29** determined by molecular modelling.

	Energy (Hartree)			
	HOMO (BODIPY GS)	**LUMO + 2 (BODIPY ES)**	**LUMO (maleimide)**	**LUMO + 1 (maleimide)**
Fluorogen YC29	-0.175	-0.082	-0.088	-0.087

The molecular orbital diagram below illustrates the changes in orbital energies after reaction with one equivalent model thiol, MeSH (middle), and the dithiol adduct (right).

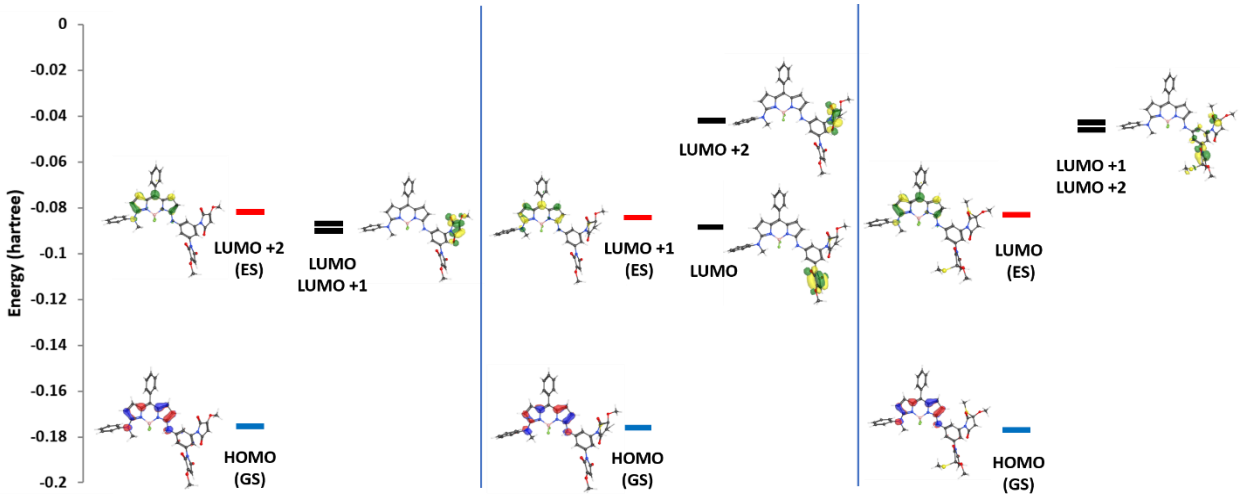

Figure 2.5 Molecular orbital diagram for **YC29** before addition reaction (left), after one thiol addition (middle), and after two thiol additions (right).

Before addition reaction, the LUMO and LUMO +1 are lower in energy than the BODIPY ES, meaning d-PeT should be favoured and the native fluorescence of the compound should be quenched. After the first rate-limiting intermolecular addition reaction between a maleimide and thiol, the energy of the resulting succinimide (LUMO +2) is raised higher than the BODIPY ES; however, the second unreacted maleimide orbital is still able to accept the excited state electron. After the disuccinimide adduct is formed, the ES of the BODIPY becomes the LUMO, restoring the native fluorescence.

After reaction with two equivalents of model thiol (MeSH), the excitation energy of **YC29** was calculated to be 2.45 eV, corresponding to an excitation band with λ_{max} = 505 nm. Considering typical Stokes' shifts are rather small for BODIPYs, the maximum emission wavelength of this

compound would be predicted to be >520 nm, in the green range of the visible spectrum. However, the maximum emission wavelength and bandwidth must be determined experimentally, and the structural similarity of **YC29** to Dehaen's dianiline compound[60] would suggest the emission wavelength of **YC29** should be closer to 600 nm (orange/red).

2.3 First synthetic approach

The first approach to the synthesis of the BODIPY fluorogen was devised by Dr. Yingche Chen and is shown below in Scheme 2.1. This route incorporated previous FlARe probe building blocks, the dinitro compound **2.1** as well as methoxymaleic anhydride, whose preparations will be discussed in the following section. From the compound **2.1** and the 3,5-dichloroBODIPY **2.2**, preparation of **YC29** followed a linear route that began with subsequent S_NAr steps to install the dimaleimide scaffold, followed by the wavelength-tuning *N*-methylaniline group to give compound **2.4**. Next, both nitro groups were reduced by hydrogen over palladium on carbon (10% w/w). The resulting diamine was then reacted with excess methoxymaleic anhydride to form the acyl intermediate, which immediately underwent ring closure overnight in a mixture of sodium acetate and acetic anhydride. Under these conditions, Dr. Chen found that the boron core was removed resulting in compound **2.6**, and so it was subsequently reinstalled. The conditions for boron complexation serendipitously removed the Boc group, which gave the final desired compound without employing an additional Boc deprotection step.

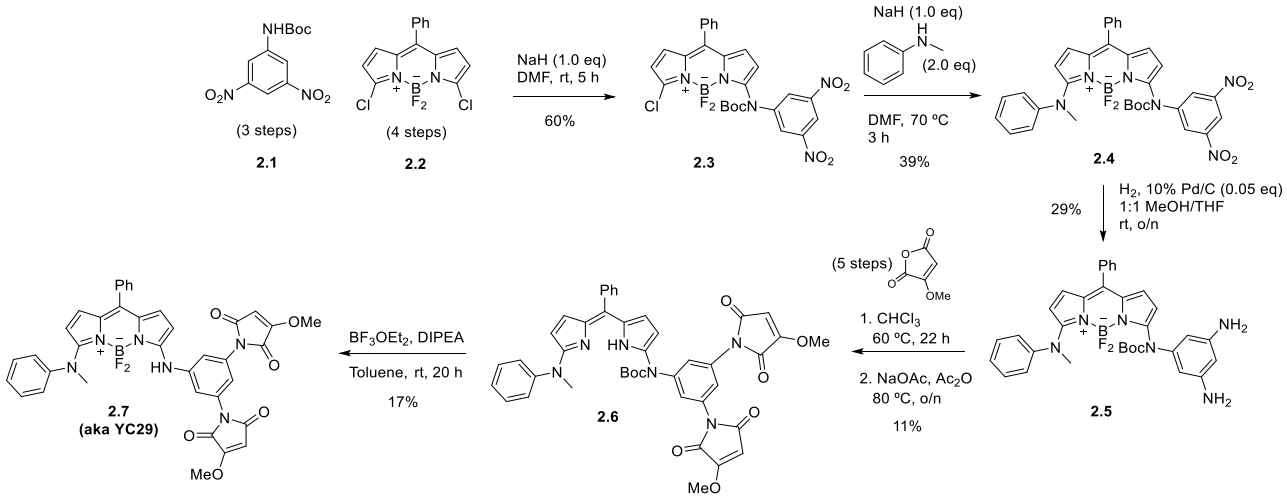

Scheme 2.1 Linear synthesis for preparation of YC29 with reported yields achieved by Dr. Yingche Chen.

This synthesis has a total of 18 steps and is highly linear. 3,5-dichloroBODIPY and dinitro compound **2.1** were prepared on the gram scale; however, due to compounding low yielding steps, only 7 mg of the final FlARe probe was isolated.

2.3.1 Preliminary Results

The characterization of **YC29** reported below was completed by former post doctoral fellow, Dr. Chen. These results were highly promising for a red FlARe probe. Briefly, the excitation and emission spectra of **YC29** after reaction with a dC10α-tagged test protein showed that the compound was more red shifted than computational modelling predicted, giving a maximum excitation at 580 nm and emission at 630 nm, with considerable emission up to ~650 nm as the emission band was rather broad. This brought the emission of the compound well into the red channel of most fluorescence microscopes.

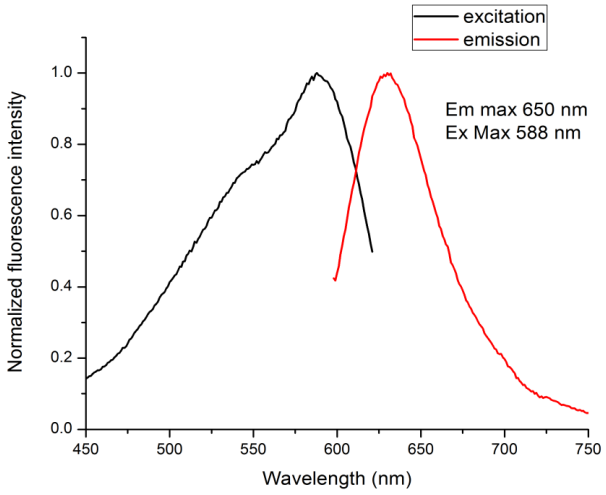

Figure 2.6 Excitation and emission spectra of 25 µM MBP-dC10α labelled with **YC29**.

Further, the compound was shown to be efficiently quenched in the absence of tagged test protein (black link, Figure 2.7 (left)) and undergo a 300-fold fluorescence enhancement after reaction. The fluorescence increase was also measured as a function of time for the labelling reaction with dC10α-tagged test protein (right). Nearly maximum fluorescence was reached after 2 hours of reaction. No fluorescence increase was measured when **YC29** was incubated with excess GSH, showing the compound's selectivity for the tag over other small molecule thiols.

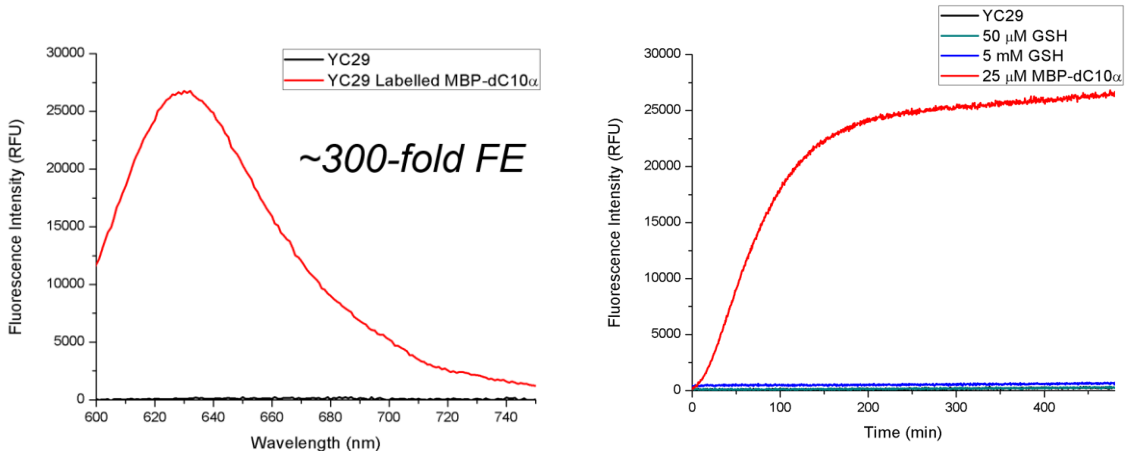

Figure 2.7 (Left) Fluorescence enhancement (λ_{ex}= 580 nm) of 25 μM **YC29**, incubated in the absence (black) and presence of MBP-dC10α (red) overnight. **(Right)** Time-dependent fluorescence increase of 25 μM **YC29** reacting with one equivalent of test protein MBP-dC10α (red) and excess thiols. λ_{ex} = 580 nm, λ_{em} = 630 nm.

Although these results are highly preliminary, they are promising for a potential *in cellulo* labelling agent. Unfortunately, the compound's original preparation was deemed to be synthetically impractical. The small amount of product obtained from the synthesis outlined in Scheme 2.1 was sufficient for some initial analyses, such that the stock of **YC29** was quickly depleted and some results were unable to be replicated by subsequent Keillor lab members. In particular, a rate constant, quantum yield, and publication level cellular images were not obtained. To determine the feasibility of **YC29** as a probe, the compound needed to be resynthesized in higher yields and further evaluated *in vitro*.

2.4 Towards a New Synthetic Approach

In analyzing the first synthetic preparation of the compound (Scheme 2.1), several issues became apparent. Firstly, the first S_NAr step is not regioselective; both α positions can be attacked by the aniline without preference. S_NAr proceeds through a stepwise mechanism: nucleophilic attack and re-hybridization of the ipso carbon (sp^2 to sp^3) followed by leaving group departure to reform the sp^2 centre.[61] S_NAr reactions are typically pushed towards completion by using excess nucleophile since the rate limiting step depends on intermolecular nucleophilic attack. However, in this case, there is a trade-off between yield of desired product and side product. To achieve the 60% yield of compound **2.3** in Scheme 2.1, 1.5 eq of aniline was used, which resulted in a 20% yield of undesired α,α-bis coupled compound.

Nitro reduction by hydrogen over palladium has been used extensively in the Keillor group and typically is much higher yielding (>80%), therefore, the 29% yield shown in Scheme 2.1 was cause for concern. Additionally, the low yield paired with the removal of the boron group upon addition of the maleimides is very problematic. The chemistry for maleimide addition to the dianiline scaffold has been well developed in the Keillor group over the last several years, and typical yields for this reaction (over two steps) with the methoxymaleic anhydride range between ~ 40 -80 %, therefore an 11% yield was suprising.[62] Although Dr. Chen was able to reform the BODIPY core after BF_2 was unintentionally removed, this unexpected step was much lower yielding than a TFA deprotection is expected to be, and much lower yielding than expected for a typical boron complexation.

After identification of these concerns, the original synthetic route was repeated with modifications to improve the overall yield and thereby the feasibility of preparation of **YC29** for

application as a labelling agent. First, the preparation of the three key intermediates (compounds **2.1**, **2.2**, and methoxymaleic anhydride) shown in Scheme 2.1 will be described in the following section.

2.4.1 Synthesis of the dimaleimide scaffold

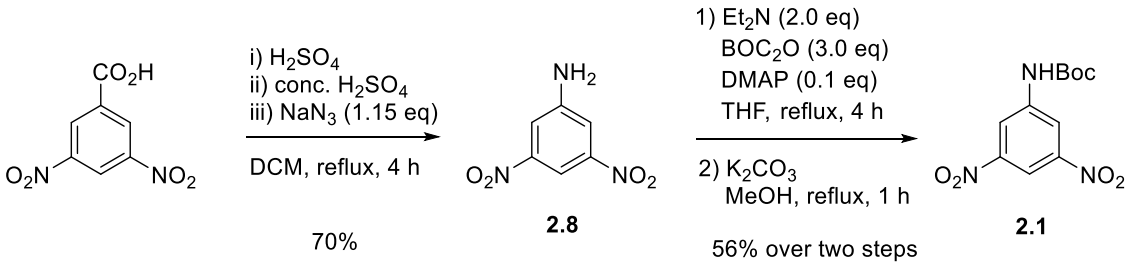

Scheme 2.2 Synthesis of the NHdM10 scaffold.

As described in Chapter One, the dimaleimide scaffold has been developed and optimized for FlARe probes to be a rigid linker between the fluorophore and the maleimides that separates the two maleimides by approximately 10 Å. The Boc protected dinitro compound was synthesized according to procedure previously published by the Keillor group.[43,62] A Schmidt rearrangement of 3,5-benzoic acid produced the corresponding aniline in 70% yield as a bright yellow solid that is easily isolated by filtration. Next, a mono Boc protection of dinitroaniline was achieved by first making a mixture of mono and bis protected aniline that was then subjected to mild deprotection conditions using K_2CO_3 that is chemoselective for removal of the one Boc group only.

2.4.2 Synthesis of methoxymaleic anhydride

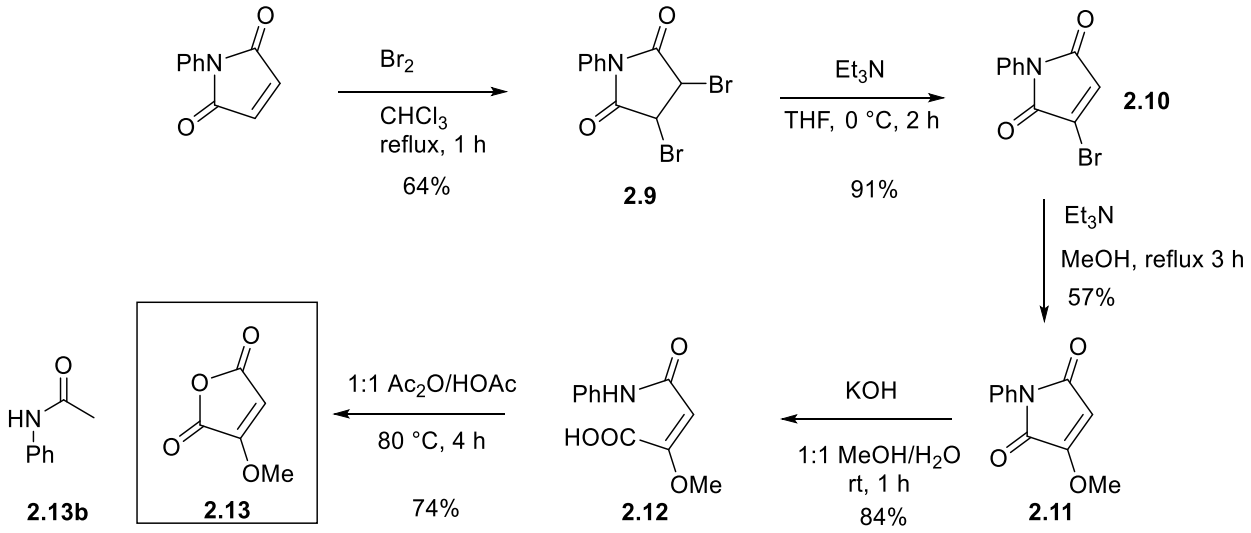

Scheme 2.3 Synthetic route for the preparation of methoxymaleic anhydride.

Methoxymaleic anhydride was then prepared according to literature procedure.[63] First, the unsubstituted *N*-phenyl maleimide was reacted with bromine in chloroform under reflux conditions for 1 h and the resulting dibromosuccinimide **2.9** was isolated in 64% yield by precipitation at 0°C. Dehydrobromination with triethylamine at 0 °C gave the bromomaleimide **2.10** in 91% yield. Base-catalyzed vinylic substitution with methanol gave the methoxymaleimide **2.11** in 57% yield after purification by flash chromatography. Next, a regioselective base-catalyzed hydrolysis gave the maleamic acid **2.12** as a crystalline solid in 84% yield. Finally, a 1:1 mixture of acetic anhydride and acetic acid gave the methoxymaleic acid anhydride **2.13** and the major acetic-anilide side product **2.13b**, which were separated by flash chromatography to give the maleic anhydride in 74% yield.

2.4.3 Synthesis of 3,5-dichloroBODIPY

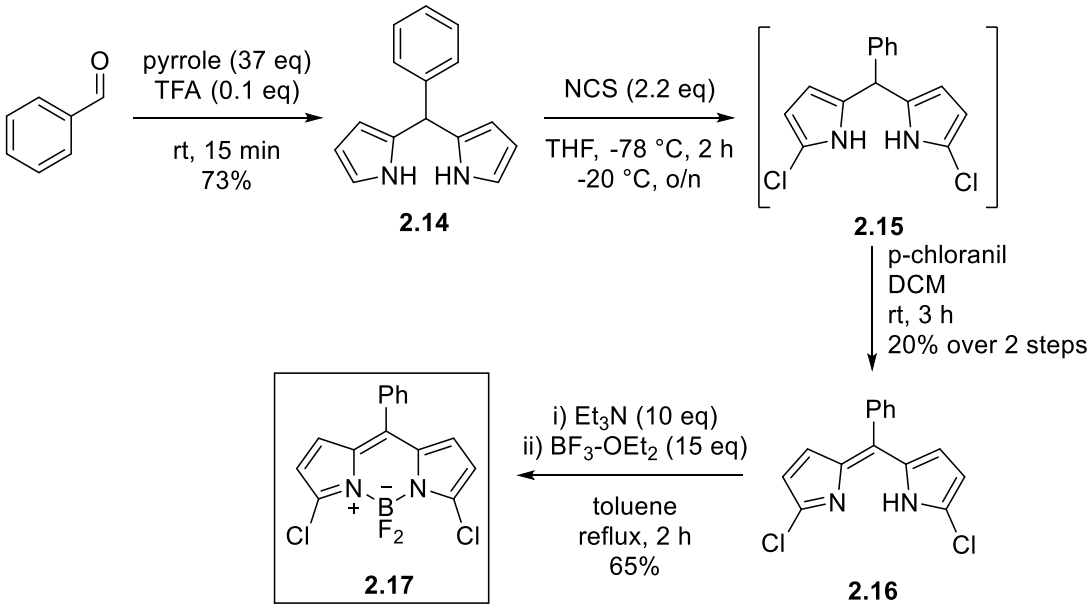

Scheme 2.4 Synthesis of 3.5-dichloroBODIPY.

BODIPY **2.17** was prepared following a literature procedure for the *para* hydroxylated analogue of our desired compound.[64] To our knowledge, this BODIPY derivative has not been previously reported in the literature. We found that in many preparations of similar compounds, characterization data of the common precursors is limited or missing entirely. As a result, we attempted to fully isolate and characterize the intermediates and optimize purification procedures to assist future syntheses.

This preparation is challenging due to the inherent instability of the pyrrole precursors. In many cases in the literature, crude material is pushed forward through several steps without characterization due to the difficulty of purification.

First, the dipyrromethane **2.14** was prepared by condensation of benzaldehyde with excess pyrrole as the solvent using a catalytic amount of TFA. To limit possible degradation and side

products, fresh and degassed pyrrole was used and the reaction was run in the dark under nitrogen for only 15 minutes. Excess pyrrole was then removed by distillation under vacuum as quickly as possible after the reaction. Although after much effort the dipyrrin was able to be isolated for characterization, in subsequent preparations the non-purified product was pushed forward in the next step immediately to limit degradation.

Next, regioselective chlorination at the alpha positions was achieved following a literature procedure to give compound **2.15**.[60] Maintaining the reaction at -78 °C is critical for regioselectivity for the 3,5 position. As Garcia-Moreno and coworkers showed for a *meso* aryl substituted BODIPY core, chlorination using NCS at room temperature installs the chlorides preferentially at the 2,6 positions. This work also suggested up to 3 eq NCS could be used without significant yields of trichlorinated product formed; however, a more conservative excess of 2.2 eq was used following the route described by Dehaen and Boens.[60] In all repetitions of this reaction, the mono chlorinated compound was formed as a side-product that was inseparable from the desired product by column chromatography despite several attempts due to similarity in RF values. As a result, the crude mixture was oxidized without purification, giving the desired 2,5-dichlorodipyrromethene **2.16** in 20% yield over two steps.

Finally, complexation with BF_3-Et_2O gave the desired 3,5-dichloroBODIPY in a 14 % overall yield, as compared to the 20% overall yield reported by Dahaen and Boens.[60]

2.4.4 Synthesis

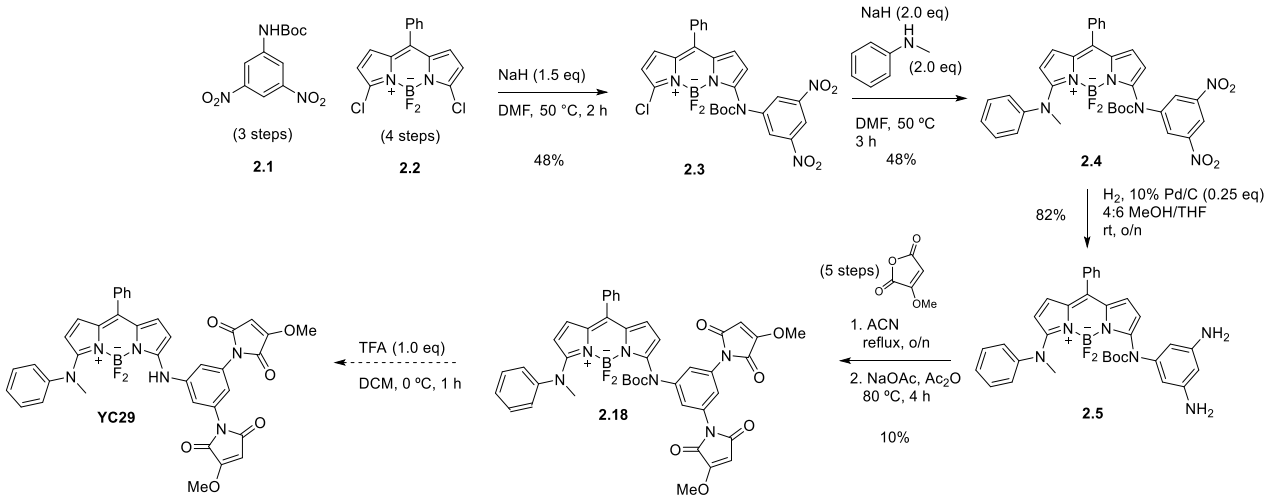

Scheme 2.5 Synthetic route to **YC29** with improved yields.

2.4.4.1 S_NAr Steps

With the key building blocks in hand, we attempted to optimize the selectivity of the first S_NAr reaction, in terms of maximizing yield of the desired mono coupled product over the bis coupled side product. Firstly, the equivalents of aniline nucleophile **2.1** was reduced from 1.5 to 1.0 eq. 1.5 eq of NaH was used as strong, non-nucleophilic base to ensure all Boc-protected aniline nucleophile was deprotonated. Using 1.5 eq of nucleophile (Scheme 2.1) gave mixtures of 48 - 60% mono and ~ 20% bis coupled product, with 20% recovered BODIPY starting material. A comparable 48 % yield was obtained under the modified conditions, with a noteworthy difference of an increase in recovered starting material (36%) and negligible amount of bis-coupled side product. We expect that the decreased reaction time (from 5 h to 2 h) with increased temperature may also optimize the ratio of mono to bis coupled product. Increasing the reaction time may improve the yield of desired compound, but at the expense of recovered starting

material. A shorter reaction is preferable, as the BODIPY precursor is very valuable and in this case, can be recovered and reused.

The subsequent S_NAr with 2 eq *N*-methylaniline using NaH as a non-nucleophilic base gave a 48% yield after 3 h at 50 °C, resulting in a 10 % increase in yield compared to Dr. Chen's original synthesis. This is comparable to the 60% yield obtained by Rohand and Dehaen for the same substitution on an alpha chlorinated BODIPY.[60]

2.4.4.2 Nitro Reduction

The following reduction of both nitro groups by hydrogen over palladium on carbon was a step where we hoped to achieve a significant yield increase from the original 29%. The Pd/C (10% w/w) catalyst loading was increased from 5% m/m to 25% m/m, and the product was obtained in an 82% yield after filtration through celite. It is possible that the catalyst used in the first synthesis may have been poisoned, or that the reaction requires longer than 18 hours at 5% m/m.

2.4.4.3 Addition of Methoxymaleic Anhydride

Addition of the maleimides was the most problematic step in the original synthesis, as the boron group was removed under the reaction conditions and only an 11% yield of the corresponding dipyrromethene product (compound **2.6**) was isolated. At this point in the synthesis, both the dianiline **2.5** (prepared in 10 steps) and the methoxymaleic anhydride (prepared in 5 steps) starting materials are extremely valuable. This is arguably the most critical reaction in the synthesis.

As we were concerned about stability of the methoxymaleimide to hydrolysis, we opted to change the solvent from chloroform to a similar boiling point solvent that was available on our solvent purification system, acetonitrile, to ensure that the reaction was anhydrous. Next, a

model reaction between citraconic anhydride and the dianiline scaffold, shown below, was run in acetonitrile at reflux to test reaction conditions and intermediate isolation.

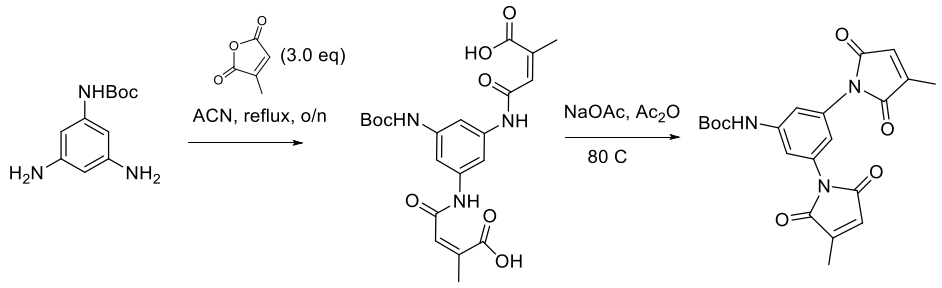

Scheme 2.6 Test reaction for maleimide addition.

After reaction at reflux overnight, TLC analysis (5% MeOH/EtOAc eluent system) showed full consumption of dianiline starting material, remaining excess maleic anhydride, and a single new spot. This new spot was successfully isolated from the excess starting material by a series of triturations with Et_2O. As expected, ^{1}HNMR analysis of the isolated solid showed pure dimaleamic acid. This result suggested that the dramatically low yield of the original synthetic route was likely due to the ring closing step. Additionally, it was also predicted that the boron was removed during the ring closing step, since BODIPY should be stable under the relatively mild heating conditions of the first step. The given ring closure conditions shown overnight gave mainly desired product without purification. The reaction mixture appeared the same by TLC after 3 h and after overnight reaction, and therefore we opted for a shorter reaction time to maintain BF_2 complexation.

The methoxymaleic anhydride addition was run under the described test reaction conditions at the same scale (see Experimental). Again, the aniline starting material **2.5** was completely consumed by TLC and the intermediate was isolated as a deep purple precipitate from excess

maleic anhydride by trituration with diethyl ether, appearing as a single spot by TLC. The subsequent ring closure using NaOAc/Ac_2O to form the mixed anhydride was given 4 h to react. The mixture was purified by column chromatography to give ~10 mg of desired compound **2.18** and ~4 mg of compound **2.6**, originally isolated by Dr. Chen.

The small amount of isolated compound **2.18** was subjected to deprotection conditions using TFA; however, no desired final fluorogen was detected by MS or NMR analysis.

2.4.4.4 TFA Removal of BF_2 from BODIPY

Upon review of the literature for conditions that might be responsible for decomposition of the BODIPY compound in the final steps of the synthesis, we discovered that Brønsted acids (including TFA) have been recently published as deprotecting reagents for *F*-BODIPY derivatives and are effective in near quantitative yields for the corresponding dipyrrins.[65] As a result, even if the problems with the maleic anhydride addition step could be solved, the compound could likely not be deprotected without removing the BF_2 group and subsequently needing to reinstall it. This flaw in the synthetic design would need to be overcome in order to create a higher yielding, reproducible pathway for the red fluorogen.

2.5 A New Convergent Strategy

Due to the synthetic incompatibility of the BODIPY fragment and Boc-deprotection conditions, as well as the dramatic loss of yield at the maleic anhydride addition step, the original synthetic approach needed to be redesigned.

Starting from the same 3,5-dichloroBODIPY precursor, we envisioned a more modular convergent strategy involving two late stage S_NAr reactions to combine the fluorophore, with the NHdM10 maleimide fragment, and a wavelength tuning substituent. This strategy would not

only be useful for the synthesis of **YC29** but could also be used to incorporate any nucleophilic wavelength tuning substituent, thereby allowing the creation of a library of compounds relatively quickly. The retrosynthetic approach for the convergent strategy is shown below. The order of substitution of the two substituents at the alpha positions is interchangeable, providing two possible routes.

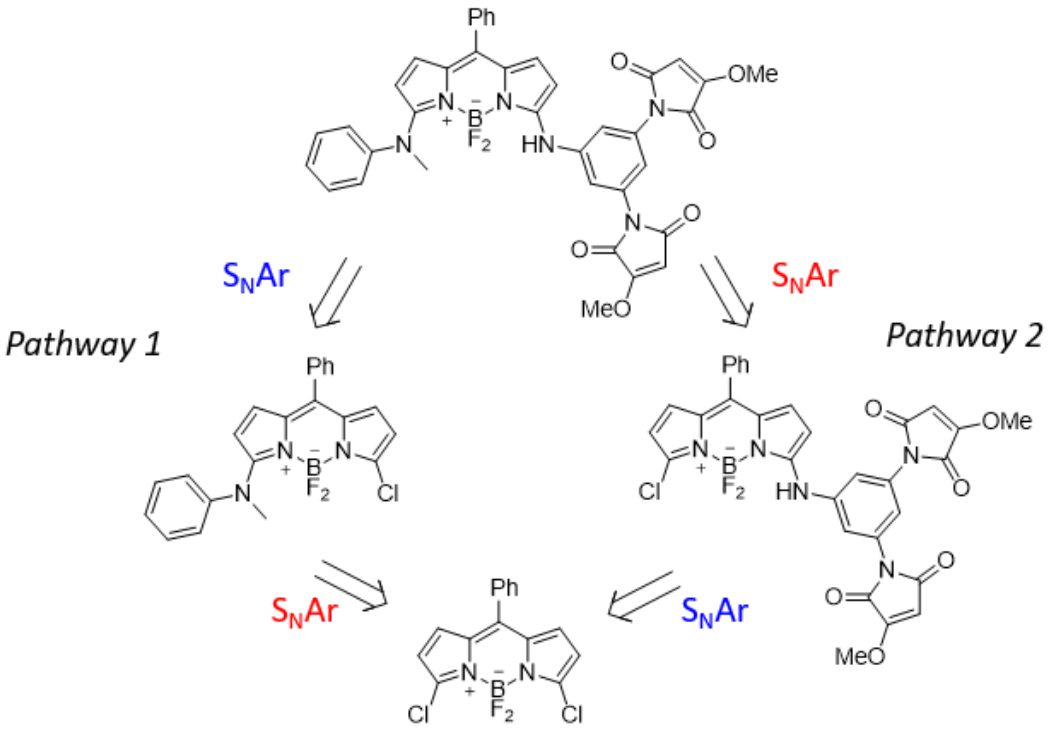

Figure 2.8 Retrosynthetic analysis for convergent S_NAr strategy to **YC29**.

Pathway 1 in Figure 2.8 was chosen as the preferred route, as it incorporates the most synthetically valuable half of the compound, the dimaleimide portion, which is prepared in 12 steps, at the end. The synthetic scheme chosen for pathway 1 is shown below.

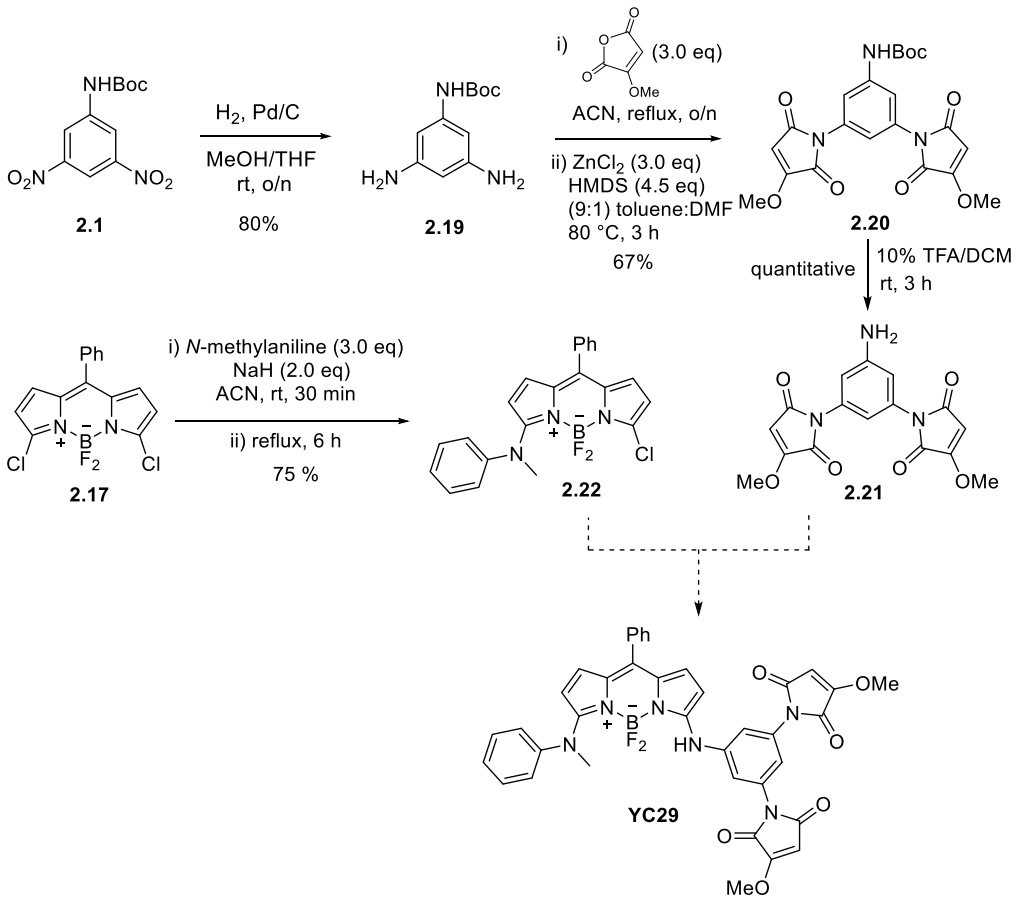

Scheme 2.7 Convergent synthetic route to **YC29** (Pathway 1).

2.5.1 Dimaleimide Aniline Synthesis

In this scheme, the dimaleimide NHdM10 is formed independently, as opposed to attaching the maleimide scaffold to the BODIPY core initially and functionalising the nitro groups. In this design, the BODIPY core is incorporated after the TFA deprotection step. Beginning from dinitro compound **2.1**, both nitro groups were reduced under hydrogen using the same conditions as described previously to give compound **2.19** in 80 % yield. Next, the same conditions for maleic anhydride addition were used as in the previous synthesis. The isolated maleamic acid intermediate was then subjected to alternative ring closing conditions, according to a literature

procedure.[46] $ZnCl_2$ and hexamethyldisilazane (HMDS) were used to activate the diacid towards intramolecular nucleophilic attack by the amide nitrogen. The desired Boc protected compound **2.20** was isolated in 67% yield over 2 steps and subsequently deprotected using a 10% TFA/DCM solution to give the dimaleimide **2.21** in quantitative yields. This was a significant improvement compared to the 54% yield obtained in the literature procedure published in the Keillor group.[46] The increase in yield was attributed to optimized work up conditions (see Experimental). Briefly, the aniline was observed to be partially soluble in the aqueous phase and therefore a large amount of product was likely lost during aqueous workup in the original procedure.

2.5.2 α-N-MePh BODIPY S_NAr

The *N*-methylaniline mono substitution procedure to form compound **2.22** was optimized over several reactions, starting from a literature procedure for the substitution of aniline to a 3,5-dichloro aryl BODIPY.[60]

3,5-Disubstitution was a problem for substitution with dinitro compound **2.1** in the linear synthesis, and thus we expected a similar selectivity issue for this compound. However, the authors reported a 70% yield of the mono-substituted product using 2 eq of nucleophile at room temperature in only 30 minutes, and disubstitution after 8 hours reflux with 4 eq of nucleophile. We found that refluxing overnight with 1.0 eq of *N*-MePh resulted in a 25% yield, whereas 2.0 eq gave a 50% yield. In both cases, a mixture of starting material and desired product was obtained; however, no bis coupled by-product was detected by ^{1}H NMR analysis. 3,5-dichloroBODIPY and compound **2.22** were inseparable by column chromatography, therefore pushing the reaction towards completion was crucial not only for characterization but also for the

subsequent S_NAr coupling. The amount of *N*-MePh was increased to 3.0 eq, resulting in a 75% yield of compound **2.22** with traces of unreacted starting material detected by NMR.

Final S_NAr

The experimental conditions used to couple compound **2.22** and **2.21** are summarized in Table 2.2 below. All reactions were run overnight under anhydrous conditions and a nitrogen atmosphere using NaH (60% dispersion in mineral oil) as a base. NaH was stirred with the nucleophile for ~20 min to preform the anionic aniline, which was then added to a solution of the electrophile (0.05 M). Each reaction was run on a 20-mg scale. Only a slight excess (1.2 eq) of NHdM10 nucleophile was used, as this material was highly valuable.

Table 2.2 Experimental conditions for the S_NAr between compound **2.21** and **2.22**.

ENTRY	***E^+***	***NU^-***	***EQ NU^-***	***SOLVENT/TEMP***	***RESULT***
1	**Ph-BODIPY-*N*-MePh-Cl (2.22)**	NHdM10 (**2.21)**	1.2	ACN/40°C	No conversion by TLC
2	**Ph-BODIPY-*N*-MePh-Cl**	NHdM10	1.2	ACN/ 82°C	No conversion by TLC
3	**Ph-BODIPY-*N*-MePh-Cl**	NHdM10	1.2	DMF/100-120°C	No product detected by NMR
4	**Ph-BODIPY-NHdM10-Cl (2.23)**	*N*-MePh	2.0	ACN/40°C	No product detected by NMR

We first attempted the substitution under relatively mild conditions (Entry 1 above) with minimal heating to achieve solubility of compound **2.21**. No conversion of starting materials was observed by TLC, even when the reaction was heated to reflux overnight (Entry 2). The temperature was further increased to 120 °C in DMF (Entry 3). In this case, both starting materials were consumed, resulting in a dark baseline spot (25% EtOAc/hexanes) and a red fluorescent spot at Rf = 0.25. 6 mg of the red fluorescent compound was isolated by column chromatography and subsequently analyzed by ^{1}H NMR; however, no desired product was detected. As no desired product was detected from Entries 1-3, we tried reversing the order of the S_NAr reactions, following Pathway 2 in Figure 2.8 to prepare the **Ph-BODIPY-NHdM10-Cl** in 33% yield (shown below).

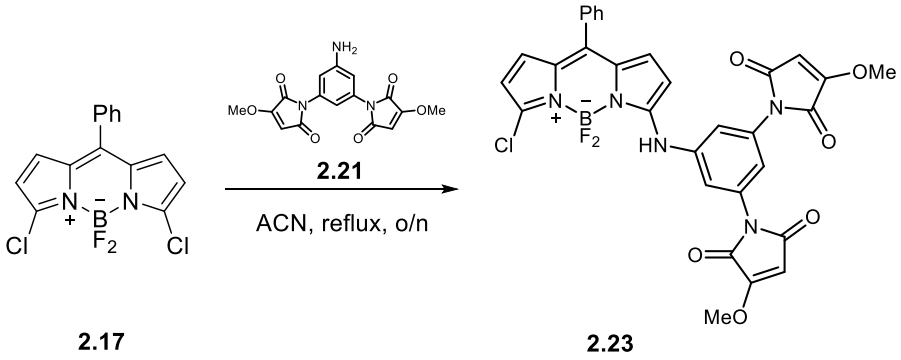

Scheme 2.8 S_NAr coupling of NHdM10 to 3,5-dichloroBODIPY.

This alternative approach allowed for greater excess of nucleophile to be used in order to push the reaction further to completion, since *N*-methylaniline is commercially available. As shown in Table 2.2 Entry 4, compound **2.23** was refluxed in acetonitrile with 2.0 eq of *N*-MePh nucleophile overnight. TLC analysis showed that compound **2.23** was completely consumed and

a deep red spot appeared on the baseline that did not migrate in 100% EtOAc. The crude mixture was analyzed by NMR after aqueous work-up, but no product was detected.

2.5.3 S_NAr Analysis

Despite the efforts outlined in Table 2.2, we were unable to synthesize **YC29** by the S_NAr-based strategies. Both potential precursors **2.22** and **2.23** were successfully prepared; however, the second S_NAr step appears to be particularly challenging. There are several possible reasons for the difficulty of the second substitution. The first reason is simply a statistical argument. The 3,5-dichloroBODIPY precursor is a symmetrical compound with two potential reactive sites, therefore the mono substitution is more probable.

We also considered both electronic and steric factors. The electronic environment of both potential aniline nucleophiles and electrophilic aryl reaction sites were compared. In terms of the nucleophilicity of the aniline, a large difference between the *N*-methyl aniline and the maleimide bearing aniline NHdM10 is not predicted, particularly since a full negative charge is formed on the nitrogen (upon deprotonation with NaH), which is strongly nucleophilic. Alternatively, we considered that perhaps after one aniline substitution (regardless of the aniline), the remaining α-chlorinated position becomes less reactive towards S_NAr. However, if this were the case, there must be a fundamental difference between the electronic effects of *N*-methylaniline and 3,5-dintroaniline, as the mono dinitro substituted BODIPY undergoes the second S_NAr with both *N*-methylaniline and 3,5-dintroaniline rather easily.

Steric hindrance may also be a factor in the second S_NAr reaction. Steric hindrance is increased substantially after the first substitution. The NHdM10 group is larger than the BODIPY fluorophore itself, so it is not surprising that substitution onto the more hindered Ph-BODIPY-*N*-

MePh-Cl would be more difficult than with the unsubstituted dichloroBODIPY, and vice versa for *N*-MePh substitution. While it is possible that substitution could be achieved under harsher reaction conditions (i.e. higher temperature, longer reaction times, greater excess of aniline) we were concerned about the stability of our compounds and turned to another alternative approach.

2.5.4 Pd-Catalyzed Aryl-Amination

As introduced in Section 2.2, other methods have been used to functionalize the BODIPY core at the α positions, including palladium-catalyzed cross couplings. Without needing to alter our 3,5-dichloroBODIPY fluorophore, we saw the opportunity for a Buchwald-Hartwig aryl-amination between our aryl chloride and the aniline NHdM10. The catalytic cycle is depicted below and is comprised of 4 steps: 1) oxidative addition of the aryl-chloride to the palladium (0) source, 2) coordination of the amine to the electron deficient palladium (II) centre, 3) deprotonation of the coordinated amine, and 4) reductive elimination of the aryl-amine.

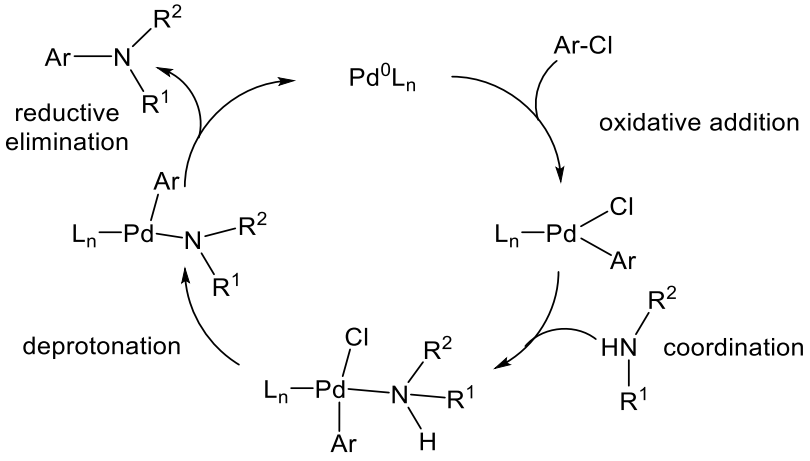

Scheme 2.9 Catalytic cycle for palladium catalyzed aryl-amination.

Recent catalyst systems have been developed to increase the rate of oxidative addition by increasing electron density on the metal and improve the rate of reductive elimination by

increasing steric bulk of the ligands (L_n).[66] Aniline coordination is more challenging than alkyl amine coordination, as anilines are less electron rich. However, there are several examples in the literature of catalytic systems that can mediate this amination with anilines. Typically, these reactions are heated to temperatures >100 °C due to the difficulties encountered in the middle steps of the cycle.[66]

We first attempted a coupling based on a 2017 literature example of a catalyst used in the amination of a 2-iodoBODIPY with a range of simple anilines, including electron deficient anilines.[67] No conversion was observed after overnight reaction. This reaction is summarized in Table 2.3 (Entry a).

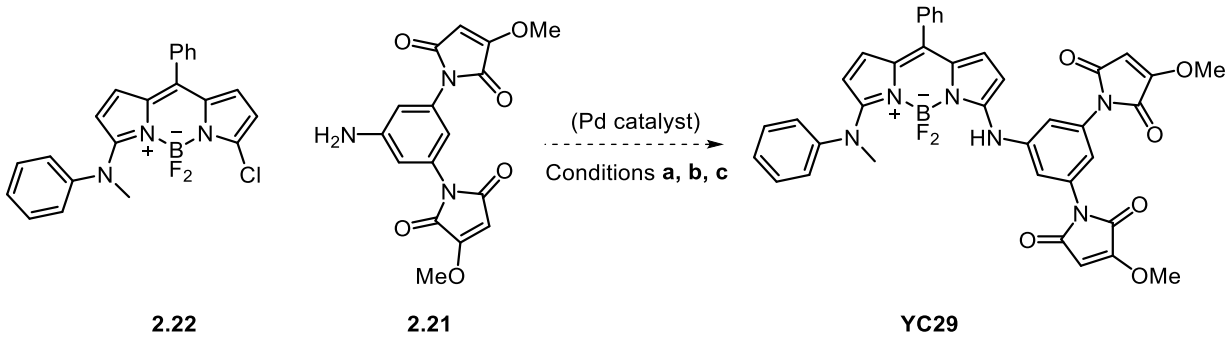

Scheme 2.10 Pd-catalyzed aryl-amination (Buchwald-Hartwig amination) strategy to form **YC29**. Conditions a-c are summarized in Table 2.3.

Table 2.3 Conditions a -c for the Pd-catalyzed aryl amination between compound **2.22** and **2.21**. All reactions were carried out under anhydrous conditions at a 40 mg scale of compound **2.22** with 1.5 eq of aniline **2.21**. Reactions were run overnight under nitrogen/argon. Conversion determined by TLC analysis. Catalyst and ligand structures shown in Figure 2.9 below.

Entry	***Pd Catalyst***	***Base***	***Solvent/Temp***	***Result***	***Reference***
a	$Pd(dba)_2$/SPhos (10 mol %)	Cs_2CO_3 (1.5 eq)	Dioxane/95°C	No conversion	[67]
b	Pd-PEPPSI-IPent^{Cl}-*o*-Picoline (3 mol %)	Cs_2CO_3 (3.0 eq)	DME/50°C	No conversion	[66]
c	Pd-PEPPSI-IPent^{Cl}-*o*-Picoline (3 mol %)	Cs_2CO_3 (3.0 eq)	Toluene/110°C	No conversion	[66]

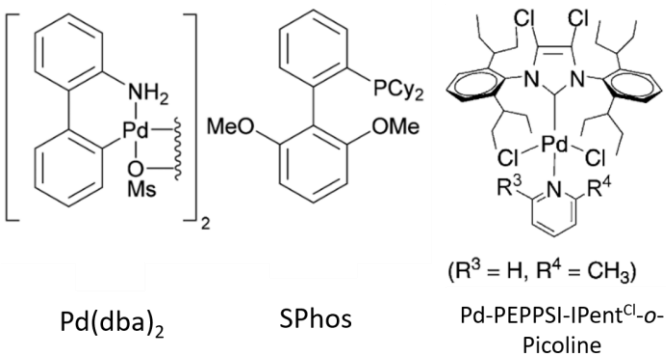

Figure 2.9 Palladium catalysts and ligands referenced in Table 2.3.[66,67]

The Organ group recently developed a pre-catalyst Pd-PEPPSI that was able to couple anilines with electron-rich, deactivated aryl chlorides using Cs_2CO_3. In rate studies, they showed that amination with anilines is first order with respect to both the aniline and the base.[66] This suggests that aniline coordination and deprotonation are rate-determining. The most recent catalyst, Pd-PEPPSI-IPent^{Cl}-*o*-Picoline was shown to perform strongly against other available amination catalysts and catalyze the coupling of strongly deactivated aryl chlorides at room temperature in very high yields. Further, they also showed successful coupling to highly deactivated anilines. In demonstrating the substrate scope of their catalyst, an *ortho* methoxy substituted aryl chloride was used as the most sterically hindered substrate.

Although the PEPPSI catalyst was shown in the original publication to be effective at room temperature, in our application the reaction was heated gently to solubilize NHdM10 (Entry b). Unfortunately, no conversion of starting materials was observed using the PEPPSI catalyst, even at higher temperature (Entry c).

We speculate that the steric bulk of our compounds may prevent coordination to the metal centre. After deprotonation, both the aryl chloride and aniline must be bound to the metal centre and oriented in such a way that bond formation is possible. The large size of both starting materials, in addition to the considerable steric bulk of the IPent ligand, may prevent the necessary coordination.

2.5.5 Comments on Pd-catalyzed Coupling

Due to time restrictions, we decided not to pursue additional catalytic systems and conditions. A more comprehensive catalyst screening may reveal a successful system for this coupling; however, this is beyond the scope of this project. Both our BODIPY-chloride and NHdM10

aniline are very synthetically valuable and much more material would be required for a method development project.

2.6 Towards a Simplified BODIPY FlARe Probe

While the computational and preliminary experimental results obtained for **YC29** were very promising for it to become the first red FlARe probe developed by the Keillor group, we became aware over the course of this project of the many synthetic challenges that needed to be overcome.

Although a red probe is alluring for *in vivo* applications, improved fluorogens for all common microscope channels (i.e. blue, green, red) are also very valuable to us and we were still excited about the potential for new generation FlARe probes using the BODIPY fluorphore with enhanced fluorogenic and spectral properties.

Since amino substitution at the 3,5 position has been shown to red-shift the BODIPY emission due to increased pi conjugation, we were curious whether substitution of our NHdM10 group alone would result in a red-shift, perhaps the most red-shifted FlARe probe to date. We had successfully substituted a single aniline onto the 3,5-dichloroBODIPY several times in previous syntheses. Based on the previous synthetic work described above, we knew that we had rapid synthetic access to two other potential BODIPY FlARe probes that we could evaluate as fluorogens: **Ph-BODIPY-NHdM10-H** and **Ph-BODIPY-NHdM10-Cl** (Figure 2.10).

2.6.1 Molecular Modelling

Pursuing this line of research, the probes shown in Figure 2.10 were first investigated computationally to determine their relevant orbital energies.

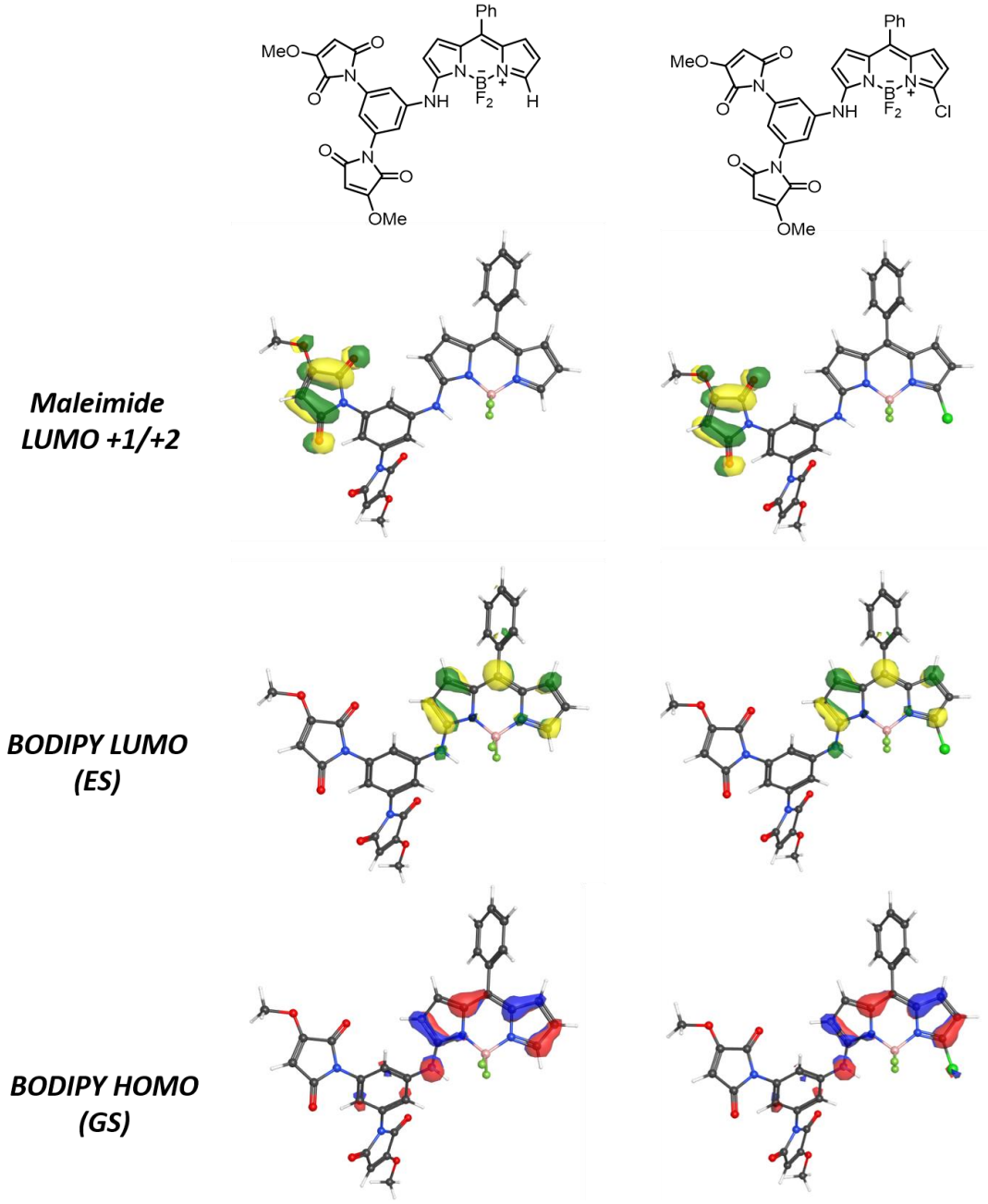

Figure 2.10 Ph-BODIPY-NHdM10-H (Left) and **Ph-BODIPY-NHdM10-Cl** (right) orbital localization.

The compounds were modelled as described previously. As opposed to Ph-BODIPY-NHdM10-*N*-MePh (orbital energies summarized in Table 2.1), both compounds have a lower energy

ground state and BODIPY excited state, making the BODIPY ES lower in energy than the maleimide orbitals (LUMO+1/+2). This suggests that d-PeT between the BODIPY excited state and maleimide would be disfavoured and, therefore, the fluorophore may not be efficiently quenched.

Table 2.4 Summary of HOMO/LUMO energies for **Ph-BODIPY-NHdM10-H/Cl** determined by molecular modelling

	Energy (Hartree)			
	HOMO (BODIPY GS)	**LUMO (BODIPY ES)**	**LUMO + 1 (maleimide)**	**LUMO + 2 (maleimide)**
Ph-BODIPY-NHdM10-H	-0.198	-0.096	-0.089	-0.088
Ph-BODIPY-NHdM10-Cl	-0.199	-0.099	-0.089	-0.088

Since the LUMO and LUMO +1/+2 are so close in energy, the computational results should be interpreted cautiously, as quenching may still occur. With the chloro compound **2.23** already in hand from the convergent route discussed in section 2.5, we opted to move forward with *in vitro* analysis to determine experimentally if it would be fluorogenic.

2.6.2 In Vitro Evaluation

2.6.2.1 Target protein

First, we determined the fluorogenicity of **Ph-BODIPY-NHdM10-Cl** by measuring its fluorescence before and after addition reaction with the di-thiol dC10α tag. The reactivity of the

methoxymaleimide moiety has been tuned to be so slow with small molecule thiols such as GSH that these thiols cannot be used to measure fluorescent enhancement. The FlARe probe must be reacted with a dC10α-tagged target protein to measure the maximum increase in fluorescence.

While there are several factors to consider when choosing a target protein for cellular labelling, *in vitro* evaluation is less complex. The target protein should be highly soluble, monomeric, and be expressed easily in high yields. Maltose binding protein (MBP) has been the test protein of choice for the structural and kinetic characterization of FlARe probes, as it meets all these requirements. MBP is a commonly used protein expression tag, as fusion of a target protein to MBP allows for single step purification using an amylose resin. Our dC10α sequence was genetically fused to the C-terminus of MBP to give the fusion protein, MBP-dC10α. In a preliminary proof-of-principle study, it was confirmed that no reaction between the dimaleimide FlARe probes occurred with unmodified MBP as a negative control.[36]

MBP-dC10α was expressed and purified in *E-coli* as described in detail in the Experimental section. Briefly, LB media was inoculated with an MBP preculture and protein expression was induced with IPTG (Isopropyl ß-D-1-thiogalactopyranoside). IPTG is a mimic of a lactose metabolite, allolactose, a compound that initiates transcription of the *lac* operon in *E-coli* thereby inducing protein expression. Cells were subsequently isolated by centrifugation and lysed by sonication. MBP was purified from the cell lysate by gravity chromatography using an amylose resin. The protein was purified to apparent homogeneity as determined by SDS-PAGE using Coomassie staining. MBP concentration was determined to be 1.16 mM using a standard Bradford protein assay.

2.6.2.2 Kinetic evaluation

The excitation and emission spectra for **Ph-BODIPY-NHdM10-Cl** after equimolar reaction with MBP-dC10α were measured (Figure 2.11). These data provided a maximum λ_{ex}=535 nm (green) and maximum λ_{em}=585 nm (orange).

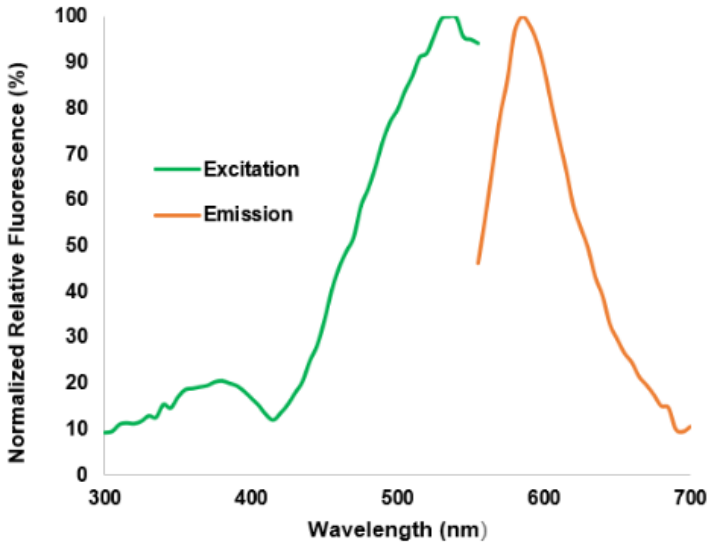

Figure 2.11 Excitation/emission spectra for 25 µM **Ph-BODIPY-NHdM10-Cl** (max excitation at 535 nm and max emission at 585 nm, normalized to 100 %) after reaction with 25 µM MBP-dC10α in 50 mM HEPES buffer (pH 7.4**,** 250 µM TCEP, 10% DMSO) at 37 °C overnight.

The addition reaction between the dimaleimide motif of a FlARe probe and the two nucleophilic cysteines of the dC10α tag occurs in two sequential steps: the first slow *inter*molecular addition followed by a rapid *intra*molecular addition. The second addition reaction can be assumed to be very fast, as the effective concentration of intramolecular nucleophilic additions can reach up to 10^8 M.[46] This assumption allows us to approximate a second order model, as the intermolecular nucleophilic addition is rate-limiting. The time-dependent increase in fluorescence for the equimolar reaction between 25 µM probe and dC10α-tagged target protein was measured

overnight in triplicate. The data approximately follows a second order increase curve, leading towards a plateau near 9,000 RFU. The data were fitted to a second order model (black line) as shown below in Figure 2.12.

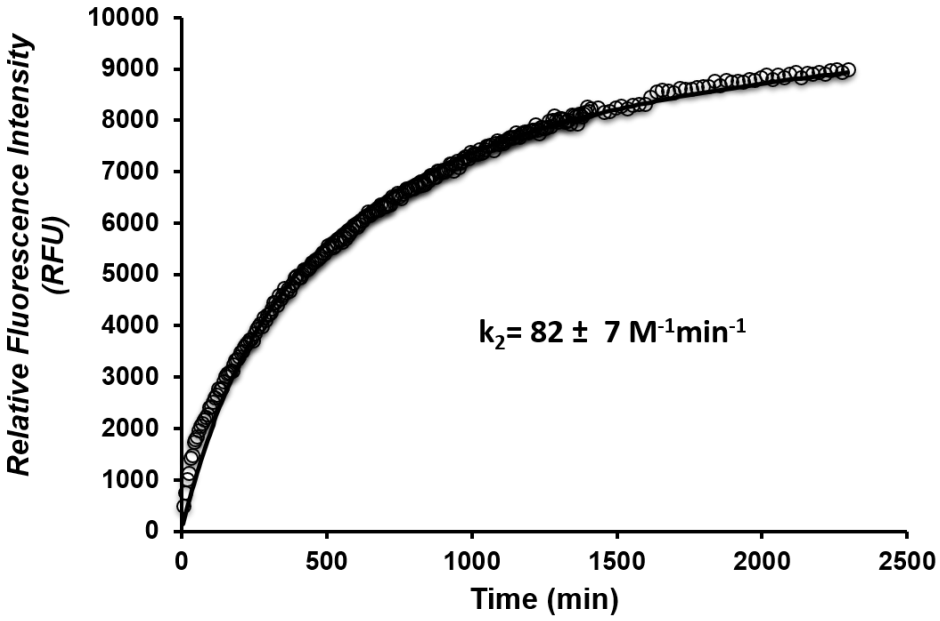

Figure 2.12 Time-dependent fluorescence (λ_{ex}= 535 nm, λ_{ex}= 585 nm, gain = 65) increase of 25 µM **Ph-BODIPY-NHdM10-Cl** reacting with 25 µM MBP-dC10α in 50 mM HEPES buffer (pH 7.4, 250 µM TCEP, 10% DMSO) at 37 °C. The solid line through the data was obtained by fitting to a second order equation. (Blank corrected)

The second order rate constant obtained by fitting to a second order equation by non-linear regression (see Experimental) was 82 ± 7 $M^{-1}min^{-1}$. The reaction was surprisingly slow, with fluorescence appearing to plateau after nearly 2 days of reaction at 37 °C. This maximum fluorescence corresponds to an ~18-fold increase. However, on the timescale relevant to a live cell imaging experiment, a large FE should be evident ideally in under the first hour, although, in

our experience, labelling times may go as high as 3 hours before significant cell death is observed. From the kinetic trace, there is an ~4-fold enhancement after 1 h, and ~6.5-fold increase after 3 h of labelling reaction. This could potentially provide enough contrast for cellular imaging, particularly since the rate of reaction with the tag may differ *in cellulo* than *in vitro* to our benefit.

The stability of the compound in buffer in the absence of the target protein was assessed as well as stability in the presence of excess concentrations of GSH (250 μM and 1 mM), as shown in Figure 2.13. The negative control showed a negligible increase in fluorescence after 2 days and the data overlaid nearly perfectly with those obtained when the probe was incubated with GSH, which suggests there was no measurable reaction with GSH. This suggests that the slight increase in fluorescence observed in both traces may be due to slow evaporation over such a long timescale. Alternatively, the increase could be due to background hydrolysis of the probe. As a result, the fluorescence increase data obtained for the compound with MBP-dC10α was blank corrected for the kinetic fit shown in Figure 2.12.

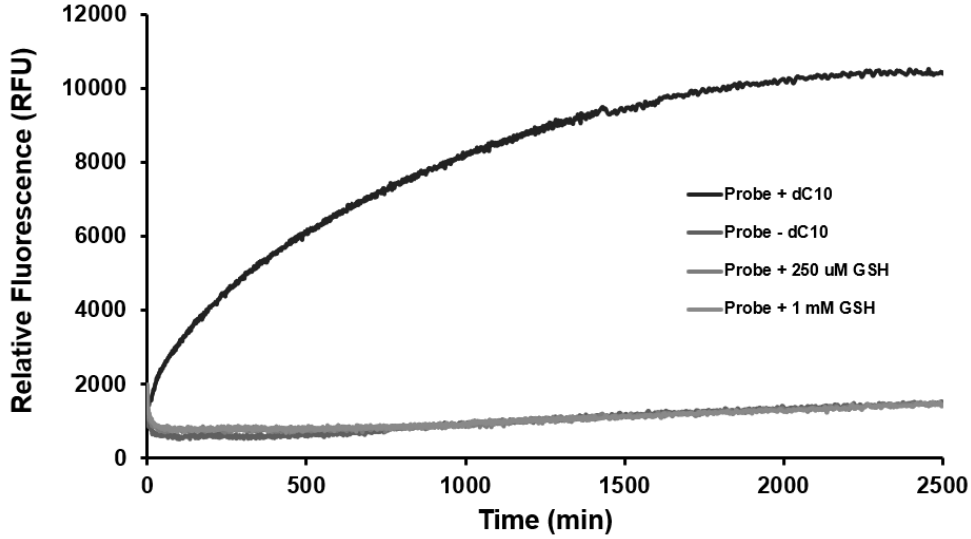

Figure 2.13 Time-dependent fluorescence increase (λ_{ex} = 535 nm, λ_{em} = 585 nm, gain = 65) of 25 μM **Ph-BODIPY-NHdM10-Cl** reacting with one equivalent of test protein MBP-dC10α (black), and excess thiols (grey) in 50 mM HEPES buffer (pH 7.4, 250 μM TCEP, 10% DMSO) at 37 °C.

2.6.3 Synthesis

Ph-BODIPY-NHdM10-Cl (**2.23**) was prepared as a precursor from the convergent synthesis of **YC29**, therefore it was available for preliminary evaluation as a potential probe. We also saw the opportunity to push forward the unavoidable monochloro by-product of the previous syntheses to easily have access to both the dichloro and monochloro BODIPY fluorophores (Scheme 2.11). In this way, **Ph-BODIPY-NHdM10-H** could be synthesized along side the chloro analogue. We were interested in seeing if the kinetics and fluorescence enhancement would be improved compared to compound **Ph-BODIPY-NHdM10-H**. The overall synthesis to prepare the **Ph-BODIPY-NHdM10-Cl** and **Ph-BODIPY-NHdM10-H** shown below follows that of Scheme 2.4 for **YC29** with a few modifications. First, the initial dipyrrin formed was immediately subjected

to chlorination conditions. The monochloro and dichloro products were separable by column chromatography in 5 and 17% yields over two steps, respectively.

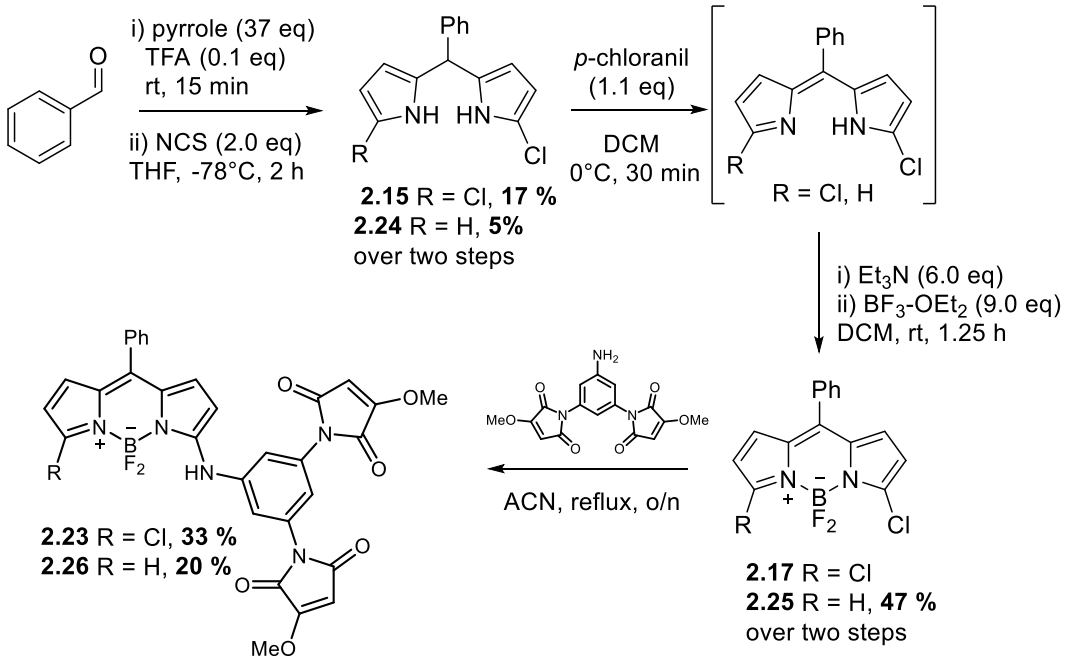

Scheme 2.11 Parallel synthesis of **Ph-BODIPY-NHdM10-Cl** and **Ph-BODIPY-NHdM10-H**.

Next, compounds **2.15** and **2.24** were subjected to one-pot oxidation and boron complexation, following a recent literature procedure for the high-yielding synthesis of *F*-BODIPYs from the Thompson group.[68] This publication showed that a 6:9 ratio of Et_3N and BF_3-OEt_2 is critical to the success of the reaction. Boron complexation conditions were much milder (room temperature, 1.25 h) than those used previously, and showed full conversion by TLC analysis. The one-pot reaction gave the mono chloro BODIPY **2.25** in a 47% yield over two steps, which subsequently underwent the S_NAR with the NHdM10 to give compound **2.26** in a 20 % yield.

2.6.4 In Vitro Evaluation

The excitation and emission spectra for **Ph-BODIPY-NHdM10-H** are shown below. The maximum excitation falls in the green range (525 nm) while emission is red-shifted ~50 nm into the yellow/orange range (575 nm).

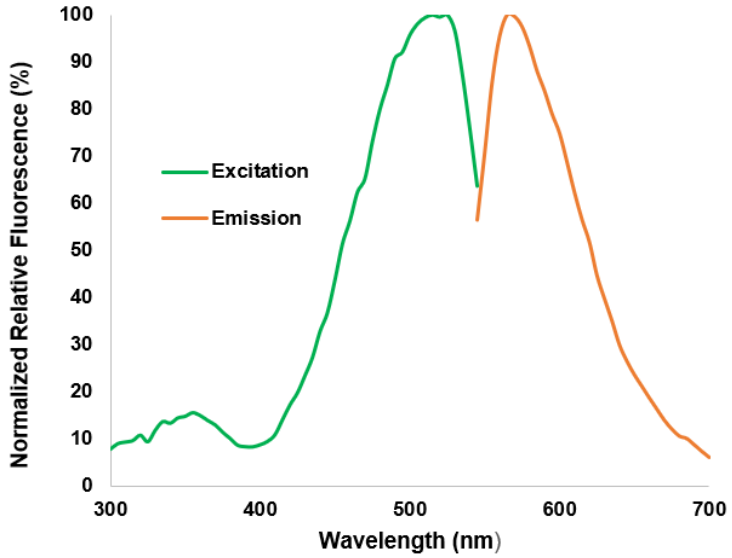

Figure 2.14 Excitation/emission spectra for 25 µM **Ph-BODIPY-NHdM10-H** (max excitation at 525 nm and max emission at 575 nm, normalized to 100 %) after reaction with 25 µM MBP-dC10α in 50 mM HEPES buffer (pH 7.4**,** 250 µM TCEP, 10% DMSO) at 37 °C overnight.

The fluorescence increase over time for the equimolar reaction between 25 µM **BODIPY-NHdM10-H** and dC10α-tagged target protein was measured overnight in triplicate under the same conditions as **Ph-BODIPY-NHdM10-Cl**. The data were fit to a second order increase equation (see Experimental) with a y-axis offset.

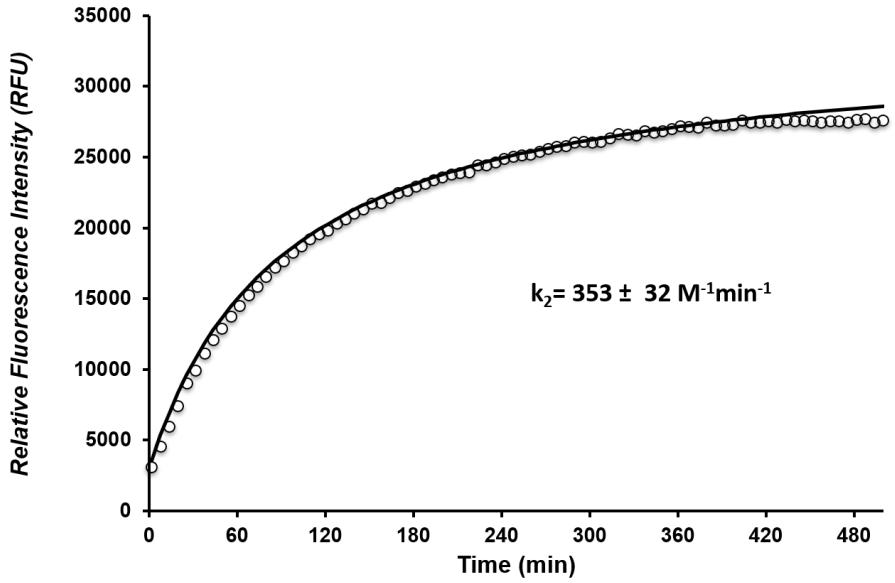

Figure 2.15 Time-dependent fluorescence (λ_{ex}= 520 nm, λ_{em}= 572 nm, gain = 80) increase of 25 µM **Ph-BODIPY-NHdM10-H** reacting with 25 µM MBP-dC10α in 50 mM HEPES buffer (pH 7.4**,** 250 µM TCEP, 10% DMSO) at 37 °C. The solid line through the (blank corrected) data was obtained by fitting to a second order equation.

Compared to the chloro substituted analog, a larger second order rate constant of 353 ± 32 $M^{-1}min^{-1}$ was measured, and the fluorescence reached a maximum plateau at ~ 6 h. As a result, the fluorescence enhancement after 1 h of labelling reaction corresponds to a minimum 5-fold increase. Further, a longer labelling time upwards of 3 h would provide nearly the full fluorescence increase, an ~ 8-fold increase.

As with the chloro analogue, the compound showed no reaction with excess concentrations of GSH (250 µM and 1 mM) compared to the negative control which showed a negligible increase in fluorescence over 16 hours in the absence of target protein.

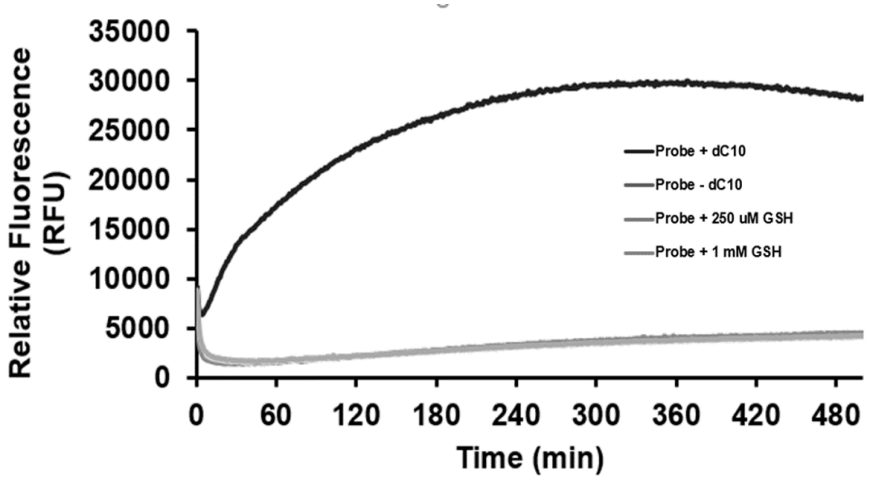

Figure 2.16 Time-dependent fluorescence increase (λ_{ex} = 520 nm, λ_{em} = 572 nm, gain = 80) of 25 μM **Ph-BODIPY-NHdM10-H** reacting with one equivalent of test protein MBP-dC10α (black), and excess thiols (grey) reacting with 25 μM MBP-dC10α in 50 mM HEPES buffer (pH 7.4, 250 μM TCEP, 10% DMSO) at 37 °C.

The chloro analogue exhibited a slightly greater fluorescence enhancement as well as a larger second order rate constant, corresponding to a faster reaction with our dC10α tag. In the case of the hydro analogue, there appears to be a loss in fluorescence after the maximum is reached, which may be the result of photobleaching. In either case, these enhancements are much smaller than the ~300-fold enhancement measured for **YC29**. We were surprised to see that changing the alpha substituent from N-MePh to Cl/H had such a dramatic effect on FE. Encouraged by the red-shifted emission of these compounds, we moved to testing the labelling reaction in a mammalian cell line to determine if the fluorescence enhancement would translate to enough contrast for cellular imaging.

2.6.5 Cellular Imaging Experiments

The choice of an appropriate target protein for *in cellulo* labelling has additional layers of complexity in comparison with *in vitro* applications; one must consider transfection efficiency as well as cellular localization and trafficking. While extracellular labelling methods can provide useful insights, there are more applications and need for intracellular protein labelling. While MBP-dC10α was useful for *in vitro* characterization, we were interested in choosing a protein with a very clear localization that we could use a second cellular dye for colocalization studies to unambiguously confirm the selectivity of our labelling method. To this end, we chose to label histone H2B, given its localization in the nucleus.[69] This would allow us to also co-stain with a standard nuclear dye. We chose Hoechst as a commonly used nuclear stain for live cell imaging. In colocalization studies, the most important factor to consider when choosing dyes is that they have complementary, well separated fluorescence spectra to avoid spectral bleeding. Hoechst is excited in UV region and emits in the blue region, therefore its excitation spectrum is ideally separated from that of our fluorogens.

The dC10α tag was genetically fused to the C-terminus of histone H2B as described previously.[62] Mammalian HeLa cells were chosen as this immortal cell line has well defined nuclei, is robust to transfection and is simple to culture. HeLa cells were cultured and transfected with the H2B-dC10α gene transiently using lipid-mediated gene delivery with lipofectamine.

For an intracellular protein to be labelled, the fluorogenic probe must be cell permeable, moving from the labelling media across the lipid bilayer of the cell. As discussed in Chapter 1, this is one of the greatest challenges that small molecule fluorophores face in cellular labelling. A nonionic surfactant (F127) was used to help our compounds cross the cell membrane.

First, HeLa cells transfected with H2B-dC10α, as well as mock cells transfected with pcDNA, were labelled with 10 µM **Ph-BODIPY-NHdM10-H** for 1 h, followed by 8 µM Hoechst for 15 minutes. The cells were then immediately imaged using a Nikon Ni-U Ratiometric fluorescence microscope without washing (see Experimental). The Hoechst channel was excited at 390 nm and observed in the 460-510 nm channel and the probes were excited at 513 nm and observed in the 588-618 nm channel. The resulting images are shown in Figure 2.17 below.

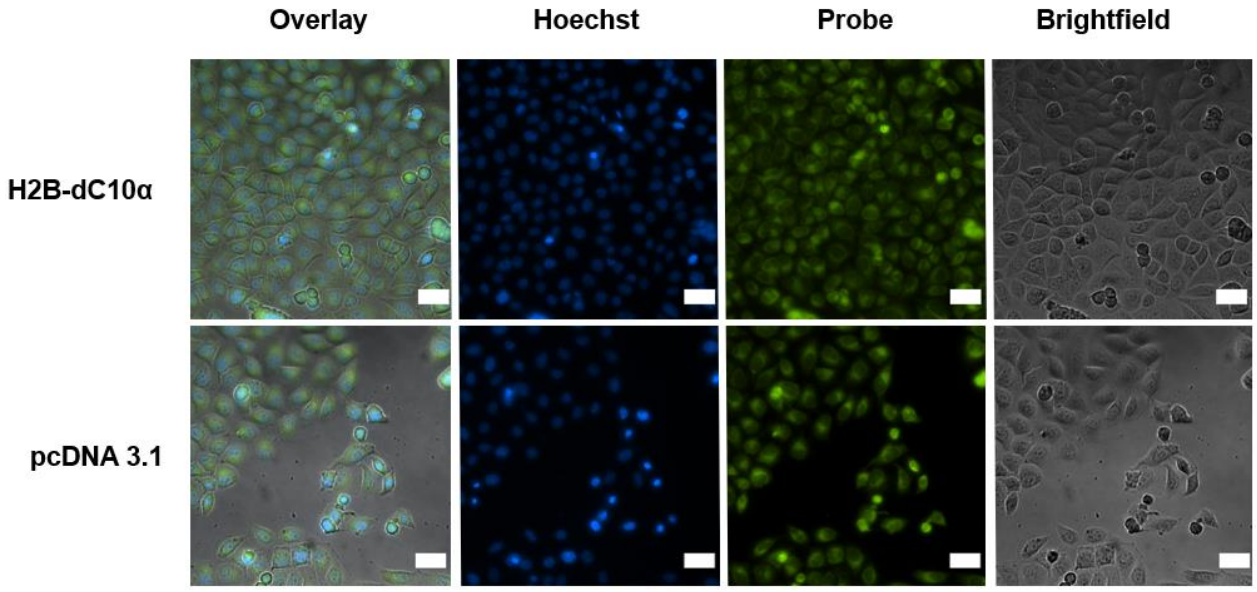

Figure 2.17 HeLa cells transfected with histone H2B-dC10α (top) or pcDNA 3.1 (+) (bottom) before labelling with **Ph-BODIPY-NHdM10-H** (10 µM) for 1 h followed by Hoechst (8 µM) for 15 min. The Hoechst channel was excited at 390 nm and observed in the 460-510 nm channel. **Ph-BODIPY-NHdM10-H** was excited at 513 nm and observed in the 588-618 nm channel. Scale bars: 20 µm.

If labelling was successful and selective, we would expect to see perfect overlay of the blue and 588-618 nm channel (shown in green) in the transfected cells corresponding to fluorescence only

in the nucleus, and no fluorescence in the green channel of the mock pcDNA cells, which do not express the dC10α-tagged POI. While the Hoechst stain successfully labelled all nuclei blue, the fluorescence imaged in the 588-618 nm channel did not overlay with the nuclei and was not selective for cells expressing our tagged protein. Fluorescence appeared to be present in the cyotosol and brighter around the nuclei, with possible dim fluorescence in the nuclei. There was no difference between the mock cells and cells expressing H2B-dC10α, therefore any fluorescence observed can only be attributed to background fluorescence of the unreacted probe or off-target fluorescence due to reaction with biological thiols. No distinguishable protein labelling occurred. We also noted that every cell imaged had taken up the probe, suggesting that the **BODIPY-NHdM10** is highly cell permeable.

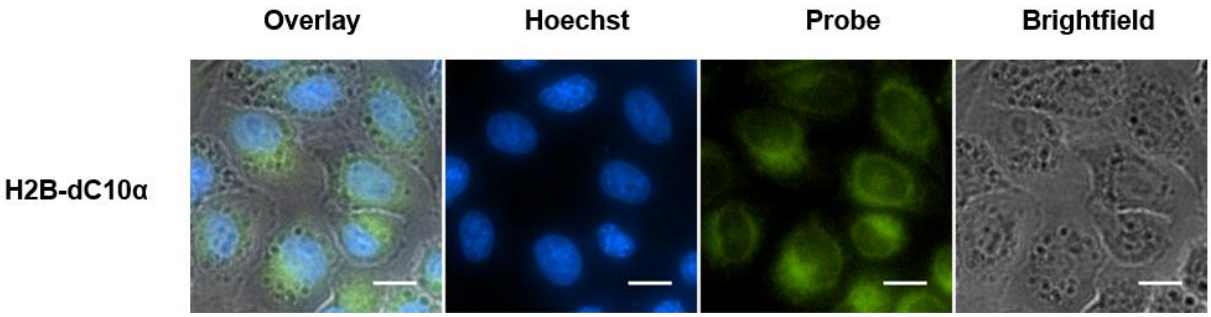

Figure 2.18 Zoom in of Figure 2.16 (top). Scale bars: 20 µm.

Looking at these cells more closely (Figure 2.18), it is clear that they exhibit non-ideal morphology; they have many vacuoles, which can be indicative of imminent cell-death. We had observed slow growth rates with these cells after several passages, suggesting in retrospect that they may not have been robust enough for a labelling experiment.

Next, HeLa cells cultured from a new stock were transfected with H2B-dC10α and labelled with **Ph-BODIPY-NHdM10-Cl** for 1 h under the same conditions, and the resulting images appeared identical to those previously obtained. Ruling out a problem with cell health, we speculated that the fluorescence observed was the result of inefficient quenching and slow reaction. If the probe was taken up by all cells and exhibited the same fluorescence in mock cells as in cells expressing tagged protein, then perhaps we were seeing background fluorescence and a significant amount of the labelling reaction with the dC10α tag had not occurred within 1 h. Our computational modelling suggests that d-PeT quenching may not be efficient with these probes, and a low FE was measured *in vitro*.

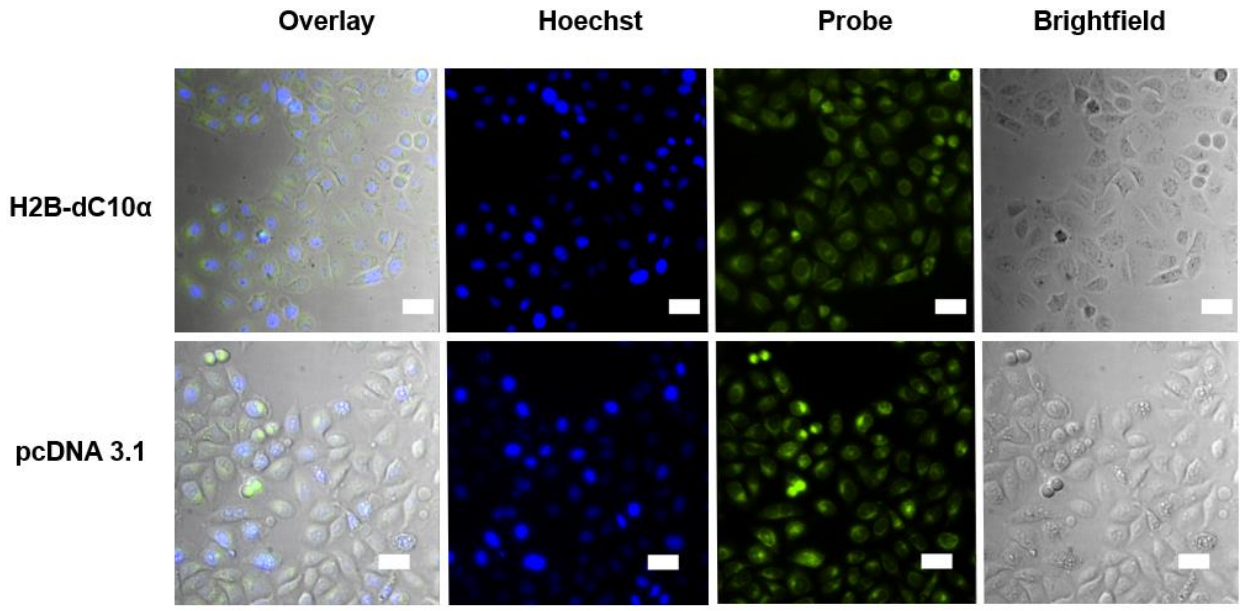

Figure 2.19 HeLa cells transfected with histone H2B-dC10α (top) or pcDNA 3.1 (+) (bottom) before labelling with **Ph-BODIPY-NHdM10-Cl** (10 μM) for 1 h followed by Hoechst (8 μM) for 15 min. The Hoechst channel was excited at 390 nm and observed in the 460-510 nm

channel. **Ph-BODIPY-NHdM10-Cl** was excited at 513 nm and observed in the 588-618 nm channel. Scale bars: 20 µm.

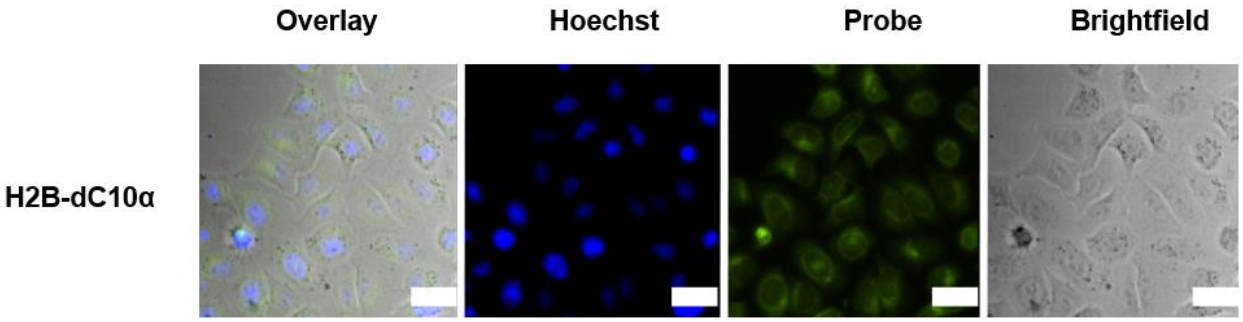

Figure 2.20 Zoom in of Figure 2.18 (top), scale bars = 20 µm.

We then labelled the cells with **Ph-BODIPY-NHdM10-Cl** for 3 h to determine if more time was necessary for the addition reaction to occur. Unfortunately, there was no discernible difference in the images obtained after 3 h of labelling compared to 1 h (Figure 2.21).

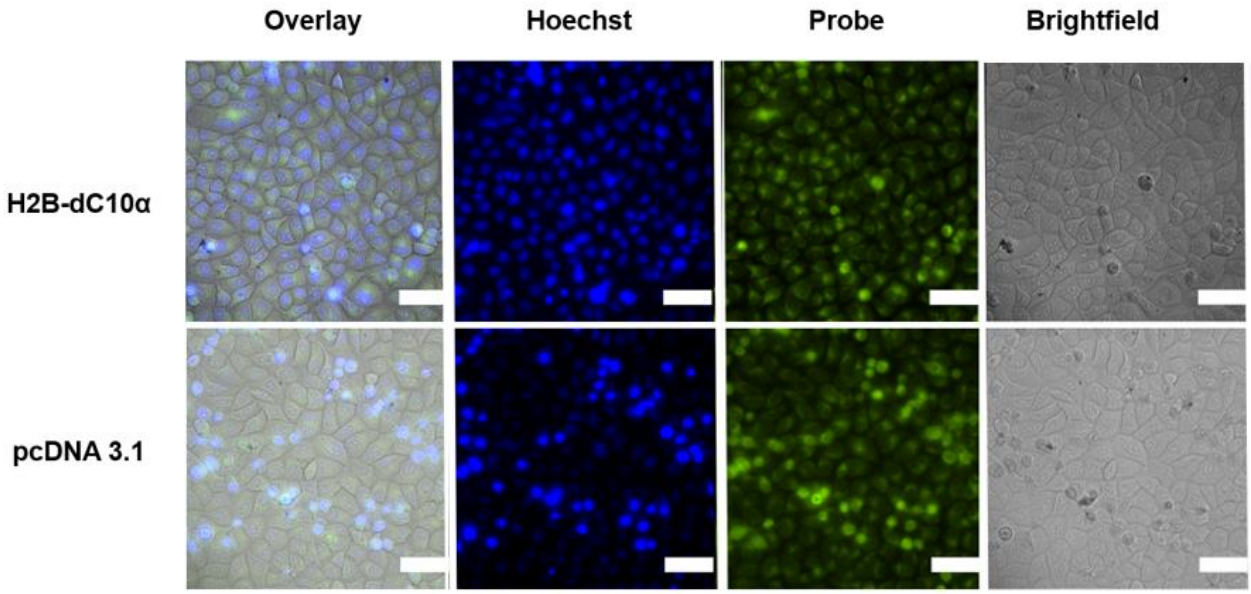

Figure 2.21 HeLa cells transfected with histone H2B-dC10α (top) or pcDNA 3.1 (+) (bottom) before labelling with **Ph-BODIPY-NHdM10-Cl** (10 μM) for 3 h followed by Hoechst (8 μM) for 15 min. The Hoechst channel was excited at 390 nm and observed in the 460-510 nm channel. **Ph-BODIPY-NHdM10-Cl** was excited at 513 nm and observed in the 588-618 nm channel. Scale bars: 20 μm.

While we considered there might be a possible issue with transfection, resulting in no protein expression and therefore no selective labelling, the same H2B gene, transfection agents, and cell line were used in other experiments and functioned as expected, as will be demonstrated in Chapter Three.

Taken together, this led us to reason that if labelling did not occur within 3 h, these probes were not strong candidates to push forward as labelling agents.

2.7 Future Perspectives & Conclusion

While compound **YC29** was very alluring as a potential red FlARe probe with an impressive fluorescence enhancement (300-fold), its preparation proved to be too challenging for the time available to us, and therefore impractical. Red-shifting the emission of our probes by functionalization means that we are trying to make inherently complex, densely functionalized small molecules. As demonstrated, this can lead to added complications of steric problems, protection strategy incompatibility, and long synthetic routes. It may be possible to overcome the challenges in the preparation of **YC29** that were presented in this chapter through the investigation of additional catalyst systems and conditions for a late-stage Buchwald-Hartwig coupling strategy, or by applying a protecting group strategy that is compatible with the BODIPY core. However, it is obvious that a more practical, robust, higher yielding synthesis would be absolutely necessary to move forward with this compound as an imaging tool that could be widely applied by other researchers.

Although compounds **Ph-BODIPY-NHdM10-Cl** and **Ph-BODIPY-NHdM10-H** were simpler synthetically and exhibited red-shifted emission spectra into the orange range of the visible spectrum, we conclude that a combination of poor quenching and slow rate of addition reaction made them not viable as practical labelling agents.

2.8 Experimental

2.8.1 Molecular Modelling

All calculations were performed using Gaussian 09. Density functional theory (DFT) was used to optimize the geometry of ground state structures (B3LYP functional and 6-31G(d) basis set). Time-dependent DFT (TD-DFT) calculations were then performed at the B3LYP/6-31G(d) level with water as a solvent based on the optimized structure of the ground state.

2.8.2 General Synthetic Procedures and Characterization

All reagents and solvents were used as received unless otherwise stated. Dichloromethane, acetonitrile, methanol, and tetrahydrofuran were dried with a solvent purification system from LC Technology Solution Inc. All reactions were performed under inert atmosphere (e.g. N_2) in flame-dried apparatus unless otherwise stated.

Reactions were monitored by thin layer chromatography (TLC) using E. Merck silica gel 60F254 pre-coated aluminum plates. Components were visualized by illumination with a short-wavelength or long-wavelength ultra-violet followed by staining in $KMnO_4$ or ninhydrin solution with heating. Flash column chromatography was performed on ZEOCHEM® silica gel 60 (ECO 40-63 μm) using eluting solvents described in the following procedures.

Nuclear magnetic resonance (NMR) spectra were recorded in deuterochloroform at ambient temperature unless otherwise stated. Residual chloroform solvent peak was used as an internal standard: 7.26 ppm for ^{1}H and 77.16 for ^{13}C spectra.[70] The experiments were performed mainly on a Bruker Avance 400 Fourier Transform Spectrometer operating at 400 MHz for ^{1}H and at 100.6 MHz for ^{13}C.

EI-MS spectra were recorded on a Kratos concept mass spectrometer for both low-resolution and high-resolution mass spectra. ESI-MS spectra were recorded on a Waters Micromass Q-Tof mass spectrometer.

2.8.3 Tert-butyl (3,5-dinitrophenyl)carbamate (2.1) preparation

2.8.3.1.1 3,5-dinitroaniline **(2.8**)

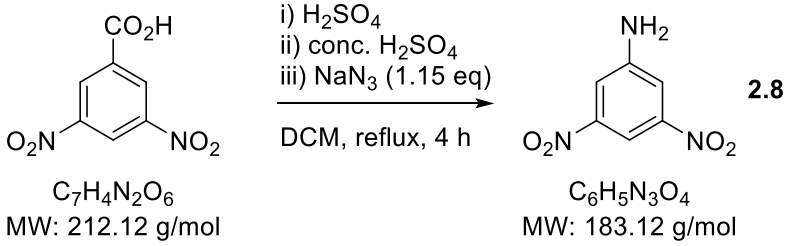

4.004 g (18.88 mmol, 1.0 eq) 3,5-dinitrobenzoic acid was dissolved in 50 mL DCM. 18 mL fuming sulfuric acid was added slowly in portions by pipette, followed by 6 mL conc. H_2SO_4 at room temperature. 1.4002 g NaN_3 (28.32 mmol, 1.15 eq) was added in small portions, allowing gas formation to decrease between additions. The reaction mixture was refluxed for 4 h with vigorous stirring. The mixture was allowed to cool to room temperature before it was poured over a mixture of water and ice. The precipitate formed was isolated by vacuum filtration and dried overnight. The aniline product was obtained as 2.413g (13.18 mmol, 70% yield) of a bright yellow precipitate. ^{1}H NMR (400 MHz, $CDCl_3$): δ = 8.38 (s, 1H), 7.78 (s, 2H), 4.43 (s (br), 2H). ^{13}C NMR (101 MHz, $CDCl_3$): δ = 149.4, 148.4, 113.7, 107.8.

2.8.3.1.2 *Tert*-butyl (3,5-dinitrophenyl)carbamate (**2.1**)

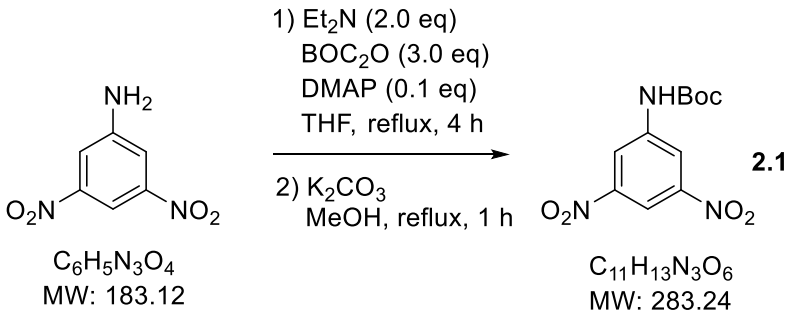

9.1915 g of Boc_2O (42.7 mmol, 3.1 eq) was added to a solution of 2.5433 g dinitroaniline (13.9 mmol, 1.0 eq) in 50 mL THF. 0.1776 g dimethylaminopyridine (1.45 mmol, 0.1 eq) was then added, followed by 3.80 mL Et_3N (27.3 mmol, 2.0 eq), neat. The reaction flask was then purged with nitrogen and the mixture was refluxed for 4 h. The solvent was removed *in vacuo* and the resulting brown residue was dissolved in 60 mL EtOAc and washed with 1 M HCl (50 mL), followed by saturated $NaHCO_3$ (50 mL), and brine (3 x 50 mL). The organic layer was dried over $MgSO_4$, filtered to remove $MgSO_4$, and solvent was removed *in vacuo*. The light brown oil obtained was dissolved in 60 mL methanol and 5.7091 g of K_2CO_3 (41.3 mmol, 3.0 eq) was added. After refluxing the mixture for 1 h, solvent was evaporated, and the residue was dissolved in 30 mL EtOAc. The organic solution was partitioned with 60 mL water and extracted with EtOAc (3 x 30mL). The organic layers were washed with 1 M HCl (30 mL), followed by brine (30 mL), dried over $MgSO_4$, filtered to remove $MgSO_4$, and solvent was removed *in vacuo*. Crude residue was purified by flash column chromatography using a gradient elution (5-25% EtOAc/hexanes) to obtain 2.2047 g (7.78 mmol, 56% yield over two steps) of compound **2.1** as a fluffy, tan coloured solid. ^1H NMR (400 MHz, $CDCl_3$): δ = 8.67 (t, J = 2.0 Hz, 1H), 8.63 (d, J =

1.9 Hz, 2H), 7.06 (br s, 1 H) 1.56 (s, 9 H). ^{13}C NMR (101 MHz, $CDCl_3$): δ = 152.0, 149.0, 141.2, 117.9, 112.5, 83.1, 28.3.

2.8.4 Methoxymaleic acid anhydride preparation

Methoxymaleic acid anhydride was prepared according to literature procedures as shown below.[63]

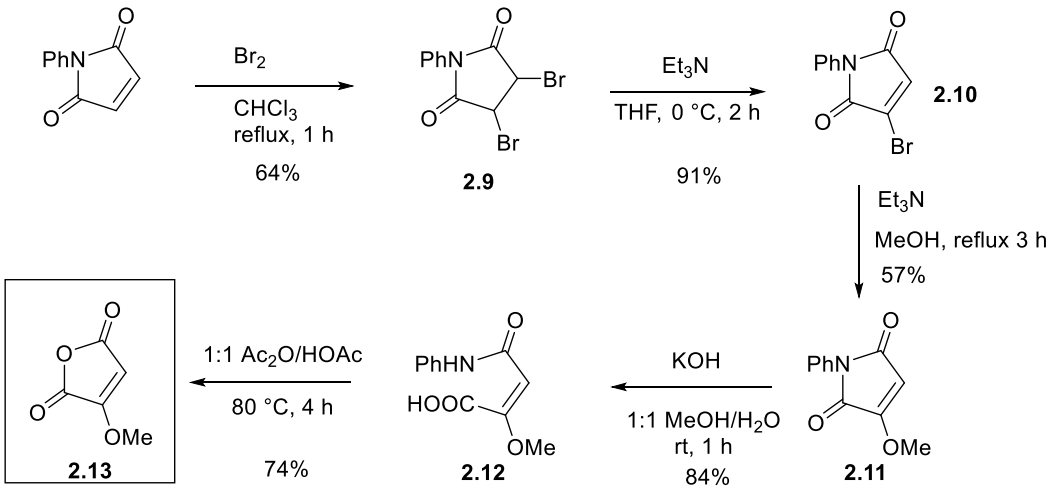

Figure 2.22 Synthetic route for the preparation of methoxymaleic acid anhydride.

2.8.4.1 2-Bromo-*N*-phenylmaleimide (**2.10**)

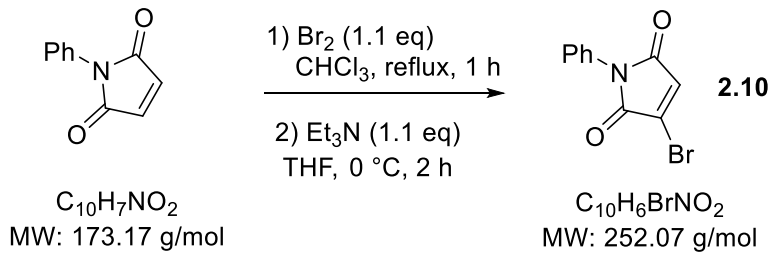

A solution of Br_2 (3.3 mL, 63.5 mmol, 1.1 eq) in 60 mL chloroform was added dropwise to a solution of *N*-phenylmaleimide (10.00 g, 57.7 mmol) in 90 mL chloroform using a cannula under nitrogen at room temperature. The reaction mixture was refluxed for 1 h. The solution was then

allowed to cool slowly to 0°C and the resulting precipitate was isolated by vacuum filtration and allowed to dry overnight. The product was obtained as 11.6463 g (35.0 mmol, 61%) of light peach coloured, fluffy solid. This dibromo intermediate was pushed forward without further characterization. The dibromo succinimide was dissolved in 125 mL THF and cooled to 0°C. Et_3N (5.37 mL, 38.5 mmol, 1.1 eq.) was diluted in 100 mL THF and added dropwise as a solution using a cannula. The reaction mixture was stirred at 0°C for 2 hours. Solvent was removed *in vacuo* and the residue was dissolved in EtOAc. This organic layer was washed once with water, followed by brine. It was then dried with $MgSO_4$ and filtered to remove $MgSO_4$. The solvent was removed *in vacuo* to yield 7.8664 g (31.2 mmol, 89% yield) of 2-bromo-*N*-phenylmaleimide as a white, fluffy solid. ^{1}H NMR (400 MHz, $CDCl_3$): δ = 7.33-7.50 (m, 5H), 7.03 (s, 1H). ^{13}C NMR (101 MHz, $CDCl_3$): δ =167.4, 164.2, 131.9, 131.9, 131.1, 129.3, 128.4, 126.1.

2.8.4.2 2-Methoxy-*N*-phenylmaleimide (**2.11**)

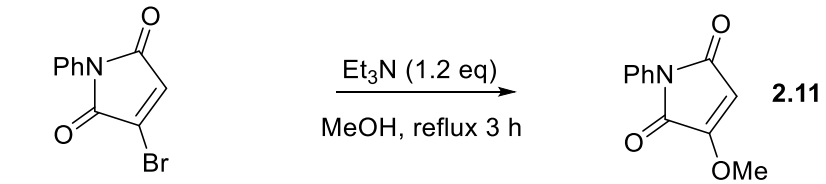

$C_{10}H_6BrNO_2$
MW: 252.07 g/mol

$C_{11}H_9NO_3$
MW: 203.20 g/mol

0.4361 g (1.73 mmol, 1.0 eq) of *N*-phenyl 3-bromomaleimide was dissolved in 25 mL of anhydrous methanol under anhydrous conditions. 0.23 mL of Et_3N (2.08 mmol, 1.2 eq) was then added dropwise via syringe at room temperature. The reaction mixture was refluxed for 3 h, after which time solvent was removed *in vacuo*. The crude residue was purified by flash column chromatography using a gradient elution system (25-50% EtOAc/hexane) to obtain 0.1997 g

(0.98 mmol, 57% yield) of 2-methoxy-N-phenylmaleimide as an off-white solid. ^{1}H NMR (400 MHz, $CDCl_3$): δ 7.41 (m, 5H), 5.57 (s, 1H), 4.01 (s, 3H).^{13}C NMR (101 MHz, $CDCl_3$): δ 169.0, 164.5, 160.9, 131.2, 129.2, 127.9, 126.2, 96.6, 59.2.

2.8.4.3 N-Phenyl-2-methoxymaleamic Acid (**2.12**)

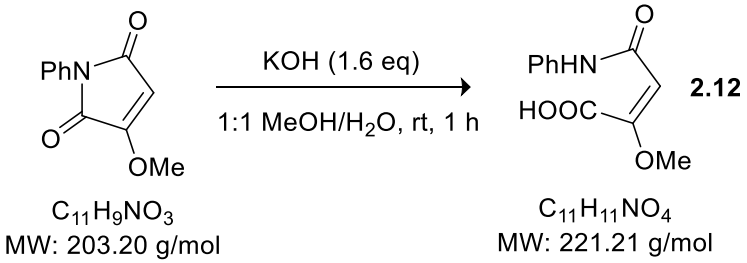

$C_{11}H_9NO_3$
MW: 203.20 g/mol

$C_{11}H_{11}NO_4$
MW: 221.21 g/mol

0.2580 g (1.270 mmol, 1.0 eq) of 2-methoxy-*N*-phenylmaleimide was dissolved in 5 mL of methanol. A solution of 0.1122 g KOH (2.00 mmol, 1.6 eq) in 5 mL water was added slowly. The reaction mixture was then stirred at room temperature for 1 h. The mixture was then concentrated to ~ 2 mL solvent *in vacuo*. 10-M HCl was then added dropwise to the solution at 0°C. The resulting precipitate was isolated by vacuum filtration and rinsed with minimal cold water before it was allowed to dry under vacuum overnight to give 0.1914 g of 2-methoxymaleanic acid (0.0865 mmol, 84% yield) as a flakey, white solid. ^{1}H NMR (400 MHz, CD_3OD): δ = 7.55 (d, J = 7.67 Hz, 2H), 7.31 (m, 2 H), 7.10 (m, 1 H), 5.72 (s, 1H), 3.77 (s, 3H). ^{13}C NMR (101 MHz, CD_3OD): δ = 128.9, 128.5, 128.4, 124.3, 120.1, 98.6, 92.7, 56.3, 55.6. LRMS (ESI+) *m/z* (%): 244.1 (M+Na); HRMS (ESI): calcd for $C_{11}H_{11}N_4O_4Na$: 244.0586, found: 244.0590.

2.8.4.4 Methoxy-maleic acid anhydride (**2.13**)

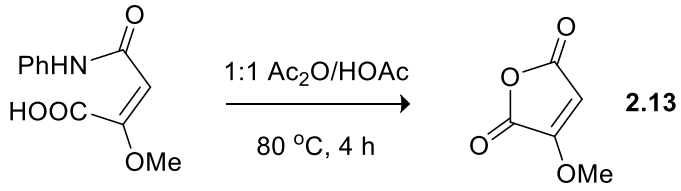

$C_{11}H_{11}NO_4$
MW: 221.21 g/mol

$C_5H_4O_4$
MW: 128.08 g/mol

3.4329 g (15.5 mmol, 1.0 eq) of N-phenyl-2-methoxymaleamic acid was dissolved in 100 mL of a 1:1 mixture of Ac_2O/HOAc under a nitrogen atmosphere in a flame-dried flask. The suspension was heated to 80 °C for 4 h. The resulting solution was allowed to cool to room temperature and the solvent was removed *in vacuo* as a toluene azeotrope several times. The crude residue was purified by short gravity column chromatography using a gradient elution system (20-50 % EtOAc/hexanes). R_f (25 % EtOAc/hexanes) ~ 0.2. 1.4762 g of methoxy-maleic acid-anhydride (11.5 mmol, 74 % yield) was obtained as a viscous, colourless oil. ^{1}H NMR (400 MHz, $CDCl_3$): δ (ppm) 5.77 (s, 1 H), 4.01 (s, 3 H). ^{13}C NMR (101 MHz, $CDCl_3$): δ (ppm): 162.7, 161.7, 160.5, 98.8, 60.4.

3,5-dichloro BODIPY (**2.17**)

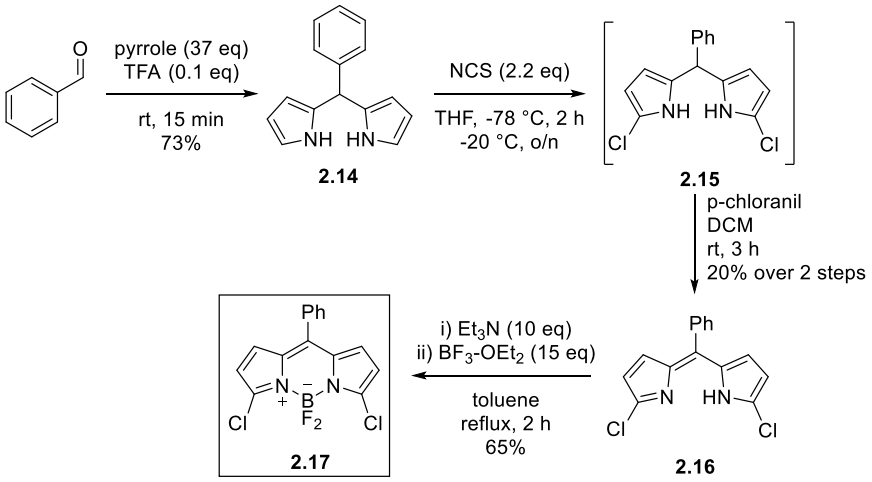

Figure 2.23 Synthetic route for the preparation of 3,5-dichloroBODIPY.

2.8.4.5 2,2'-(phenylmethylene)bis(1*H*-pyrrole) (**2.14**)

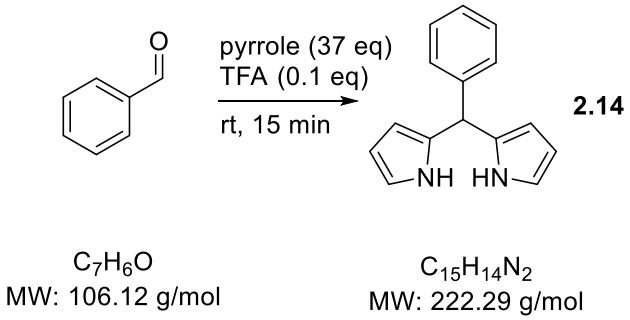

100 mL pyrrole (1.44 mol, 37 eq) and 4.0 mL benzaldehyde (39.2 mmol, 1.0 eq) were combined under a nitrogen atmosphere and the mixture was degassed by bubbling nitrogen through the solution for 15 minutes. 0.34 mL trifluoroacetic acid (4.4 mmol, 0.1 eq) was added neat via syringe and the reaction was stirred for 15 minutes at room temperature in the dark. Excess pyrrole was then removed by short path vacuum distillation. The resulting crude oil was purified by flash column chromatography (15% EtOAc/hexanes) to obtain 6.3785 g (28.7 mmol, 73%

yield) of 5-phenyldipyrromethane as a light brown solid. ^{1}H NMR (400 MHz, $CDCl_3$): δ: 7.80 (s, 2H), 7.35 – 7.10 (m, 7H), 6.63 (s, 2H), 6.13 (dt, *J* = 9.1, 4.7 Hz, 2H), 5.89 (s, 2H), 5.41 (s, 1H). ^{13}C NMR (101 MHz, $CDCl_3$): 142.2, 132.6, 128.7, 128.4, 127.0, 117.3, 108.5, 107.3, 44.0.

2.8.4.5.1 (*Z*)-2-chloro-5-((5-chloro-2H-pyrrol-2-ylidene)(phenyl)methyl)-1H-pyrrole (**2.16**)

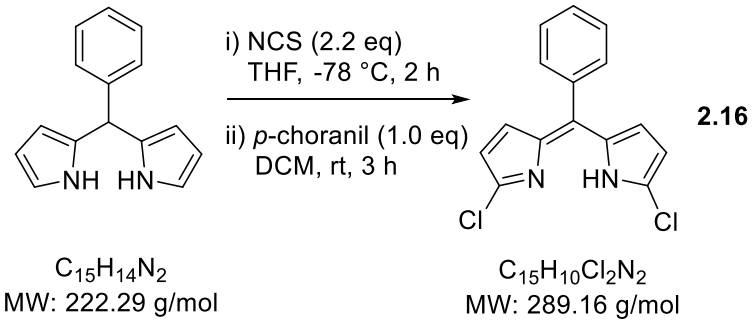

3.2858 g of 5-phenyldipyrromethane (14.8 mmol, 1.0 eq) was dissolved in 150 mL THF and the reaction flask was purged with nitrogen. The solution was cooled to -78 °C in an acetone/CO_2 bath. 4.3441 g of *N*-chlorosuccinimide (32.5 mmol, 2.2 eq) was suspended in 40 mL THF in a separate flask and stirred rapidly. An 18 G syringe was used to transfer the suspension to the cooled solution of 5-phenyldipyrromethane in portions over 10 min. The reaction mixture was then stirred for 2 h at -78 °C. The mixture was stored at -20 °C overnight. The cold mixture was then added to 150 mL water and extracted with DCM (3 x 30 mL). The black residue showed no remaining starting material by TLC and was used immediately in the next step without further purification. 4.3036 g of crude intermediate (14.8 mmol assuming 100% yield, 1.0 eq) was dissolved in 75 mL anhydrous DCM at room temperature under nitrogen. 3.6357 g *p*-chloranil (14.8 mmol, 1.0 eq) was dissolved in 25 mL anhydrous DCM in a separate flask. The *p*-chloranil solution was added to the reaction mixture in portions over 5 minutes, after which the reaction was stirred at rt for 3 h. Solvent was then removed under vacuum and the resulting black residue

was purified by flash column chromatography using gradient elution (2 – 3 % EtOAc/hexanes). 816 mg of desired product was obtained as a red solid (2.8 mmol, 20% isolated yield over two steps). ^{1}H NMR (400 MHz, $CDCl_3$): δ 12.38 (br s, 1H), 7.47 (m, 5 H), 6.52 (d, J =4.24 Hz, 2 H), 6.26 (d, J =4.23 Hz, 2 H).^{13}C NMR (101 MHz, $CDCl_3$): δ 141.9, 140.0, 138.7, 135.6, 130.9, 130.2, 129.5, 128.0, 117.1. LRMS (ESI+) *m/z* (%): 289.0976 (M+H, 100 %); HRMS (ESI+): calcd for $C_{15}H_{10}Cl_2N_2$: 289.0299, found: 289.0271.

2.8.4.5.2 3,7-dichloro-5,5-difluoro-10-phenyl-5H-4λ^4,5λ^4-dipyrrolo[1,2-*c*:2',1'-*f*][1,3,2]diazaborinine **aka 3,5-dichloroBODIPY** (**2.17**)

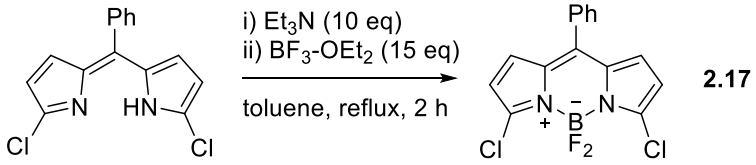

$C_{15}H_{10}Cl_2N_2$
MW: 289.16 g/mol

$C_{15}H_9BCl_2F_2N_2$
MW: 336.96 g/mol

213 mg of compound **2.17** (0.74 mmol, 1.0 eq) was dissolved in 30 mL toluene under a nitrogen atmosphere. 0.80 mL Et_3N (7.4 mmol, 10 eq) was added neat via syringe and the solution was heated to 70 °C for 30 minutes. 1.4 mL BF_3-OEt_2 (11 mmol, 15 eq) was added via syringe and the solution was refluxed for 2 h under nitrogen. The reaction mixture was cooled to rt and 20 mL 1 M NaOH was added. The resulting mixture was extracted with DCM (3 x 20 mL) and washed with water, followed by brine. The organic layer was dried over $MgSO_4$, filtered to remove $MgSO_4$, and solvent was removed *in vacuo*. Crude residue was purified by flash column chromatography using a gradient elution (10 – 25 % EtOAc/hexanes). R_f (25 % EtOAc/hexanes) ~ 0.58. 166 mg (0.49 mmol, 65 % yield) of desired BODIPY was obtained as iridescent green

crystals. ^{1}H NMR (400 MHz, $CDCl_3$): δ 7.62 – 7.47 (m, 5H), 6.85 (d, J = 4.1 Hz, 2H), 6.44 (d, J = 4.1 Hz, 2H). ^{13}C NMR (126 MHz, $CDCl_3$) δ 145.1, 144.1, 134.0, 133.9, 131.8, 131.1, 130.6, 128.7, 119.1. HRMS (EI): calcd for $C_{15}H_9BCl_2F_2N_4$: 336.0204, found: 336.02273.

2.8.5 Original Route to YC29

2.8.5.1 *Tert*-butyl(7-chloro-5,5-difluoro-10-phenyl-5H-5λ^4,6λ^4-dipyrrolo[1,2-*c*:2',1'-*f*][1,3,2]diazaborinin-3-yl)(3,5-dinitrophenyl)carbamate (**2.3**)

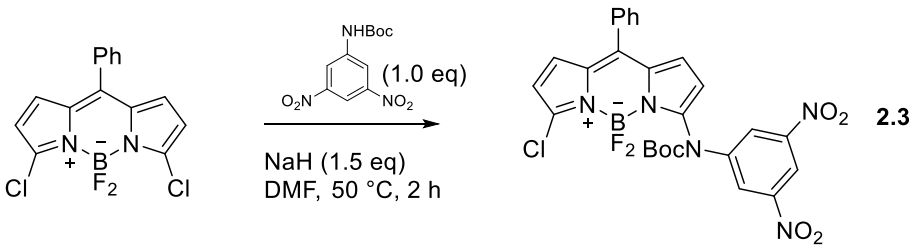

$C_{15}H_9BCl_2F_2N_2$
MW: 336.96 g/mol

$C_{26}H_{21}BClF_2N_5O_6$
MW: 583.74 g/mol

200 mg (0.59 mmol. 1.0 eq) BODIPY **2.17** was dissolved in 60 mL DMF under a nitrogen atmosphere. In a separate flask, 36 mg NaH (60 % in mineral oil, 0.89 mmol, 1.5 eq) was added to a solution of 170 mg compound **2.1** (0.59 mmol. 1.0 eq) in 2.5 mL DMF and the mixture was stirred for 20 min at rt. The NaH solution was taken up in a gas-tight syringe and slowly added to the flask containing 3,5-dichloroBODIPY over two hours at 50 °C using a syringe pump. The reaction mixture was quenched with saturated NH_4Cl and extracted with EtOAc three times. The organic layer was washed with 0.1 M HCl, water, and brine. The organic layer was dried over $MgSO_4$, filtered to remove $MgSO_4$, and solvent was removed *in vacuo*. The crude residue was purified by flash column chromatography using a gradient elution system (10-25% EtOAc/Hexanes). R_f (25 % EtOAc/hexanes) ~ 0.2. 164 mg of the desired compound was obtained as a red solid (0.28 mmol, 48 % yield). 73 mg of BODIPY starting material was recovered (36 %). ^{1}H NMR (400 MHz, $CDCl_3$): δ (ppm) 8.81 (s, 1 H), 8.61 (s, 2 H), 7.72-7.74

(m, 5 H), 6.96 (dd, J = 12.8, 4.3 Hz, 1 H), 6.49 (d, J = 29.7, 4.3 Hz, 1 H), 1.54 (s, 9 H). (Matches data obtained by Dr. Yingche Chen).

^{13}C NMR (101 MHz, $CDCl_3$): δ (ppm) 151.53, 148.23, 147.14, 146.24, 143.94, 134.57, 133.30, 132.34, 131.24, 130.82, 130.66, 128.70, 123.88, 119.98, 117.34, 114.56, 84.76, 27.97. ^{19}F NMR (376.7 MHz, $CDCl_3$): δ (ppm) –146.82 (s); LRMS (ESI) *m/z* : 606.1([M+Na]$^+$); HRMS (ESI): calcd for $C_{26}H_{21}BClF_2N_5NaO_6$: 606.1144, found: 606.1135.[1]

2.8.5.2 *Tert*-butyl (5,5-difluoro-7-(methyl(phenyl)amino)-10-phenyl-5H-5λ^4,6λ^4-dipyrrolo[1,2-*c*:2',1'-*f*][1,3,2]diazaborinin-3-yl)(3,5-dinitrophenyl)carbamate (**2.4**)

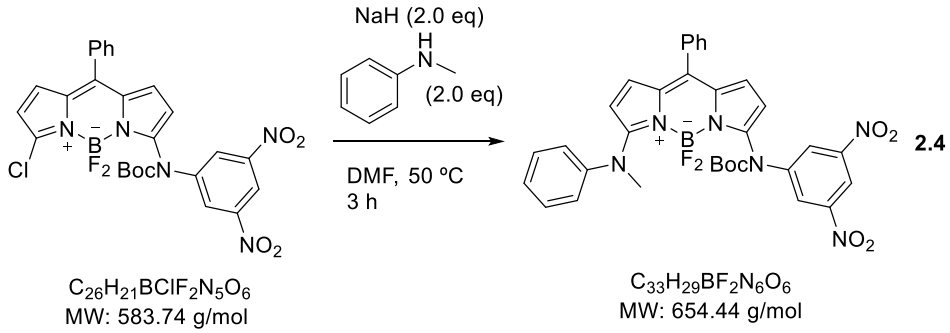

180 mg of chloro-BODIPY **2.3** (0.31 mmol, 1.0 eq) was dissolved in 15 mL DMF under a nitrogen atmosphere. 0.67 mL of 10% *N*-methylaniline in DMF (0.62 mmol, 2.0 eq) was added at 0 °C. 27 mg of NaH (60 % in mineral oil, 0.62 mmol, 2.0 eq) was added to the cooled solution in small portions. The reaction mixture was heated to 50 °C and stirred for 3 h before it was allowed to cool to rt and quenched with saturated NH_4Cl (1 x 25 mL). The mixture was then extracted with EtOAc (3 x 10 mL), washed with 0.1 M HCl (1 x 10 mL), washed with water (1 x 10 mL), and washed with brine (1 x 10 mL). The organic layer was dried over $MgSO_4$, filtered to remove $MgSO_4$, and solvent was removed *in vacuo*. Crude residue was purified by flash column chromatography using a gradient elution system (12-15% EtOAc/Hexanes). R_f (25 % EtOAc/hexanes) ~ 0.4. 95 mg of desired compound **2.4** was obtained as a deep red solid (0.15

[1] Additional characterization data obtained by Dr. Yingche Chen (former Keillor Post-Doctoral Fellow)

mmol, 48 % yield). ^{1}H NMR (400 MHz, $CDCl_3$) δ 8.74 (dd, *J* = 5.0, 3.0 Hz, 1H), 8.70 (d, *J* = 2.0 Hz, 2H), 7.53 – 7.42 (m, 9H), 7.24 (s, 1H), 6.69 (d, *J* = 5.2 Hz, 1H), 6.39 (d, *J* = 3.8 Hz, 1H), 6.30 (d, *J* = 3.9 Hz, 1H), 5.64 (d, *J* = 5.2 Hz, 1H), 3.82 (s, 3H), 1.53 (s, 9H). ^{13}C NMR (101 MHz, $CDCl_3$): δ (ppm) 151.9, 148.0, 146.6, 145.6, 137.6, 136.2, 134.4, 134.4, 133.30, 132.34, 131.8, 130.6, 130.2 129.1, 128.5, 128.3, 126.6, 123.6, 117.8, 117.6, 113.5, 112.2, 83.2, 28.0. LRMS (ESI) *m/z*: 677.4 ([M+Na]$^+$); HRMS (ESI): calcd for $C_{33}H_{29}BF_2N_6NaO_6$: 677.2128, found: 677.2107.

2.8.5.2.1 *Tert*-butyl (3,5-diaminophenyl)(5,5-difluoro-7-(methyl(phenyl)amino)-10-phenyl-5H-5λ^4,6λ^4-dipyrrolo[1,2-*c*:2',1'-*f*][1,3,2]diazaborinin-3-yl)carbamate (**2.5**)

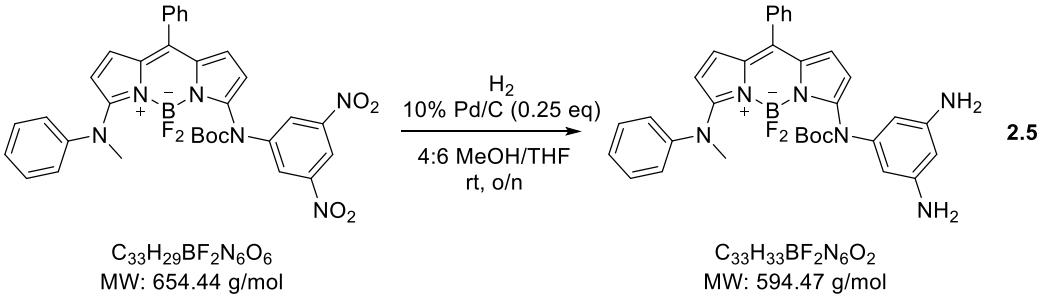

165 mg of dinitro-BODIPY **2.4** (0.25 mmol, 1.0 eq) was dissolved in 5 mL of 4:6 MeOH:THF and the reaction flash was purged with nitrogen. 67 mg of 10 % Pd/C (0.06 mmol, 0.25 eq) was added. The reaction flask was purged once with H_2 gas under vacuum before stirring under balloon pressure H_2 overnight at rt. The reaction mixture was filtered over celite to yield 123 mg of the desired aniline-BODIPY **2.5** (0.21 mmol, 82 % yield). R_f (100 % EtOAc) ~ 0.5.

^{1}H NMR (400 MHz, $CDCl_3$) δ 7.49 – 7.29 (m, 10H), 6.61 (d, *J* = 5.1 Hz, 1H), 6.34 (d, *J* = 1.9 Hz, 1H), 6.13 (d, *J* = 3.9 Hz, 1H), 5.84 (t, *J* = 1.9 Hz, 1H), 5.59 (d, *J* = 5.1 Hz, 1H), 3.92 (s, 3H), 1.49 (s, 9H).

^{13}C NMR (101 MHz, $CDCl_3$): δ (ppm) 163.5, 154.1, 147.2, 147.0, 144.7, 142.3, 135.3, 134.9, 133.3, 132.5, 130.6, 130.1, 129.6, 128.8, 128.0, 127.9, 126.6, 118.9, 116.4, 111.9, 103.4, 99.3, 84.2, 60.4, 51.3, 43.5, 43.4, 43.4, 43.3, 43.3, 28.2, 21.4, 17.3, 14.2; ^{19}F NMR (376.7 MHz, $CDCl_3$): δ (ppm) –125.42, –131.43; LRMS (ESI) *m/z:* 617.4 ([M+Na]$^+$); HRMS (ESI): calcd for $C_{33}H_{33}BF_2N_6NaO_2$: 617.2639, found: 617.2624.[2]

2.8.5.3 *Tert*-butyl (3,5-bis(3-methoxy-2,5-dioxo-2,5-dihydro-1H-pyrrol-1-yl)phenyl)(5,5 difluoro-7-(methyl(phenyl)amino)-10-phenyl-5H-5λ4,6λ4-dipyrrolo[1,2-*c*:2',1'-*f*][1,3,2]diazaborinin-3-yl)carbamate (**2.18**)

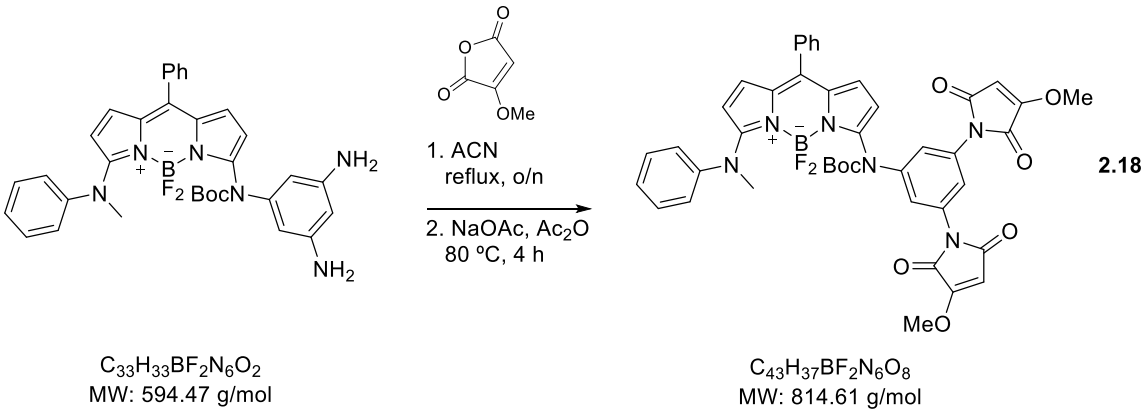

47 mg of methoxymaleic anhydride (0.33 mmol, 3.0 eq) and 60 mg of aniline compound **2.5** (0.11 mmol, 1.0 eq) were dissolved in 1.3 mL acetonitrile under a nitrogen atmosphere. The mixture was heated to reflux overnight under nitrogen. The solvent was evaporated, and the resulting purple oil was triturated with minimal ether several times to yield a deep purple solid. The isolated intermediate was dissolved in 5 mL Ac_2O and 28 mg NaOAc (0.27 mmol, 2.5 eq) was added. The reaction was purged with nitrogen and heated to 80 °C for 4 h. The solvent was removed *in vacuo* and the resulting residue was purified by flash column chromatography using a gradient elution system (10-25 % ACN/DCM). The first red band collected was determined to

[2] Additional characterization data obtained by Dr. Yingche Chen (former Keillor Post-Doctoral Fellow)

be the desired product by mass spec and NMR analysis. 11 mg of compound **2.18** was obtained (0.007 mmol, 10% yield).

^{1}H NMR (400 MHz, $CDCl_3$) δ 7.55 (d, *J* = 1.9 Hz, 2H), 7.48 – 7.33 (m, 11H), 6.61 (d, *J* = 5.1 Hz, 1H), 6.34 (d, *J* = 3.9 Hz, 1H), 6.20 (d, *J* = 3.9 Hz, 1H), 5.58 (d, *J* = 5.1 Hz, 1H), 5.52 (s, 2H), 3.97 (s, 6H), 3.93 (s, 3H), 1.53 (s, 9H). LRMS (ESI) *m/z:* 837.3 ([M+Na]$^+$).

Insufficient amount obtained for ^{13}C NMR analysis.

2.8.6 Preparation of YC29 intermediates by convergent strategy

2.8.6.1.1 7-chloro-5,5-difluoro-*N*-methyl-*N*,10-diphenyl-5H-4λ^4,5λ^4-dipyrrolo[1,2-*c*:2',1'-*f*][1,3,2]diazaborinin-3-amine (**2.22**)

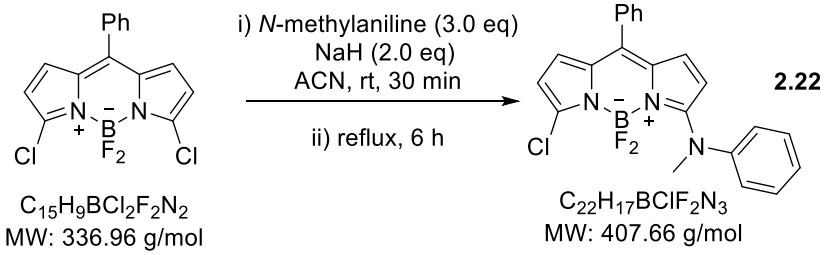

24 mg NaH (60 % in mineral oil, 0.60 mmol, 2.5 eq) was added to a solution of 97 µL *N*-methylaniline (0.89 mmol, 3.0 eq) in 1 mL acetonitrile and the mixture was stirred at rt for 30 min under a nitrogen atmosphere. The mixture was then added to a solution of 100 mg 3,5-dichloroBODIPY (0.30 mmol, 1.0 eq) in 5 mL acetonitrile. The reaction was heated to reflux for 6 h. The solvent was evaporated, and the residue was dissolved in 25 mL EtOAc and quenched with 25 mL saturated ammonium chloride. The mixture was washed with 1:1 1 M HCl/Brine (2 x 50 mL). The organic layer was dried with $MgSO_4$, filtered, and the solvent was removed *in vacuo*. The resulting residue was purified by flash column chromatography using a gradient

elution system (2 - 4 % EtOAc/hexanes). 89 mg of desired product was obtained as a red solid (0.22 mmol, 74 % yield). ^{1}H NMR (400 MHz, $CDCl_3$) δ 7.52 – 7.29 (m, 10H), 6.65 (d, *J* = 5.1 Hz, 1H), 6.26 (dd, *J* = 26.2, 3.8 Hz, 2H), 5.65 (d, *J* = 5.1 Hz, 1H), 3.98 (t, *J* = 2.1 Hz, 3H). ^{13}C NMR (101 MHz, CDCl3) δ 163.3, 146.8, 135.5, 134.4, 133.8, 131.3, 131.2, 130.4, 130.3, 130.2, 129.8, 129.2, 129.0, 128.4, 128.3, 128.2, 126.7, 122.6, 118.8, 117.1, 112.9, 43.41. (Additional signals due to traces of starting material **2.17**, visible in ^{1}H NMR. See Appendix.) LRMS (ESI) *m/z:* 430.2 ($[M+Na]^+$); HRMS (ESI): calcd for $C_{22}H_{17}BClF_2N_3Na$: 430.1059, found: 430.1070.

2.8.6.2 *Tert*-butyl (3,5-bis(3-methoxy-2,5-dioxo-2,5-dihydro-1H-pyrrol-1-yl)phenyl)carbamate (**2.20**)

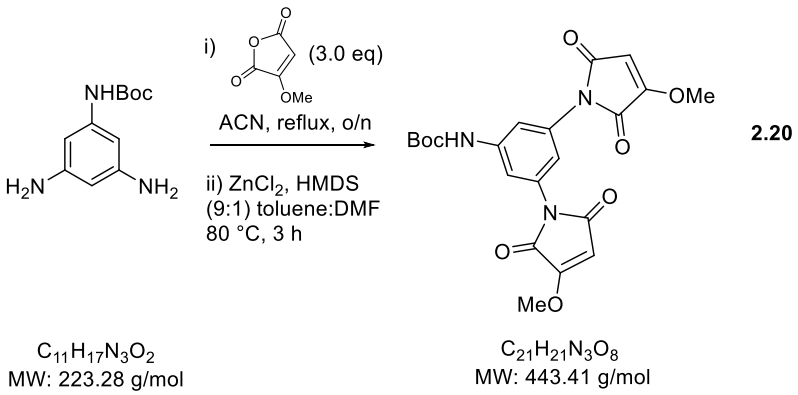

500 mg of methoxymaleic anhydride (4.56 mmol, 3.0 eq) and 333 mg of aniline compound **2.19** (1.49 mmol, 1.0 eq)[3] were dissolved in 3 mL acetonitrile under a nitrogen atmosphere. The mixture was heated to reflux overnight under nitrogen. The solvent was evaporated, and the resulting red oil was triturated with minimal ether 5 times to yield a solid. The isolated intermediate was dissolved in 55 mL of 9:1 toluene:DMF. 604 mg $ZnCl_2$ (4.46, 3.0 eq) was added as a solid. In a separate flask under nitrogen, 1.41 mL HMDS (6.71 mmol, 4.5 eq) was

[3] Prepared by graduate student Kelvin Tsao (Keillor lab) according to literature procedure.[45]

dissolved in 25 mL toluene. The HMDS solution was added to the reaction flask over 20 minutes at rt using a cannula. The mixture was then heated to 80 °C for 3 h before it was cooled to rt. The solvent was evaporated, and the residue was dissolved in 100 mL EtOAc and washed with 0.1 M HCl (3 x 100 mL), followed by $NaHCO_3$ (1 x 100 mL) and brine (1 x 100 mL). The organic layer was dried with $MgSO_4$, filtered, and the solvent was removed *in vacuo*. The resulting residue was purified by flash column chromatography using a gradient elution system (40 - 50 % EtOAc/hexanes). 442 mg of desired product was obtained as a tan coloured solid (1.0 mmol, 67 % yield). ^{1}H NMR (400 MHz, $CDCl_3$) δ 7.45 (d, *J* = 1.4 Hz, 2H), 7.16 (t, *J* = 1.8 Hz, 1H), 6.60 (s, 1H), 5.56 (s, 2H), 4.00 (s, 6H), 1.50 (s, 9H). ^{13}C NMR (101 MHz, $CDCl_3$) δ 168.3, 163.8, 160.7, 139.5, 132.1, 117.1, 114.6, 96.6, 59.1, 28.3.

2.8.6.3 1,1'-(5-amino-1,3-phenylene)bis(3-methoxy-1H-pyrrole-2,5-dione) (**2.21**)

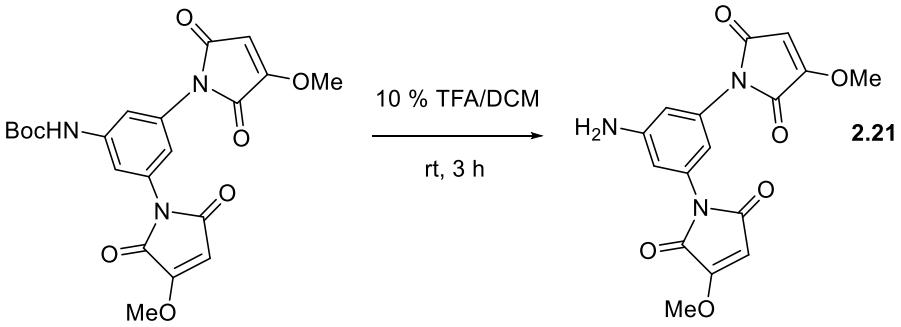

$C_{21}H_{21}N_3O_8$
MW: 443.41 g/mol

$C_{16}H_{13}N_3O_6$
MW: 343.30 g/mol

424 mg of compound **2.20** (0.96 mmol, 1.0 eq) was dissolved in 5 mL DCM. A solution of 1mL TFA in 4 mL DCM was added to the reaction flask dropwise at 0 °C. The reaction was warmed to rt and stirred for 3 h. Saturated Na_2CO_3 solution was added slowly to the reaction flask at 0 °C until the aqueous layer was pH~7 using pH paper. The mixture was then extracted with DCM (3 x 10 mL) and washed with brine. The aqueous phase was then extracted several times with

EtOAc until the aqueous layer was colourless. The organic layers were combined and dried with $MgSO_4$, filtered, and the solvent was removed *in vacuo*. 330 mg of pure aniline **2.21** was obtained as a tan coloured solid (0.96 mmol, 100 % yield). ^{1}H NMR (400 MHz, $CDCl_3$) δ 6.84 (t, *J* = 1.8 Hz, 1H), 6.66 (d, *J* = 1.8 Hz, 2H), 5.52 (s, 2H), 3.97 (s, 6H).

2.8.6.4 1,1'-(5-((7-chloro-5,5-difluoro-10-phenyl-5H-5λ^4,6λ^4-dipyrrolo[1,2-*c*:2',1'-*f*][1,3,2]diazaborinin-3-yl)amino)-1,3-phenylene)bis(3-methoxy-1H-pyrrole-2,5-dione) aka **Ph-BODIPY-NHdM10-Cl** (**2.23**)

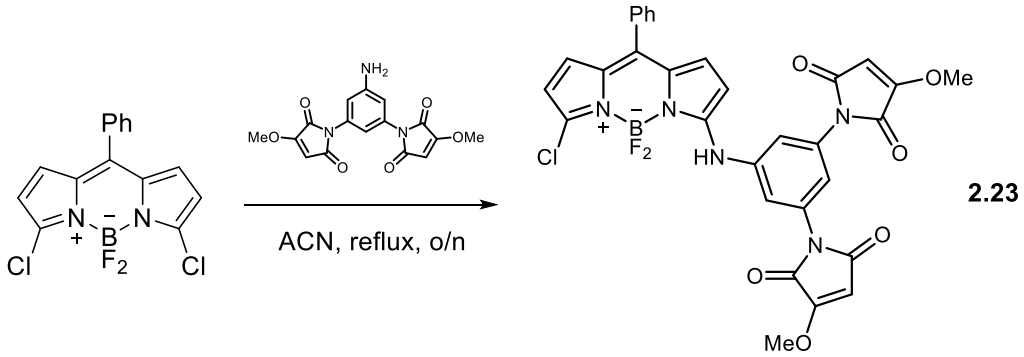

$C_{15}H_9BCl_2F_2N_2$
MW: 336.96 g/mol

$C_{31}H_{21}BClF_2N_5O_6$
MW: 643.79 g/mol

20 mg BODIPY **2.17** (0.06 mmol, 1.0 eq) and 20 mg aniline **2.21** (0.06 mmol, 1.0 eq) were dissolved in 1.2 mL acetonitrile under a nitrogen atmosphere. The reaction mixture was heated to reflux overnight. The solvent was evaporated and the residue was purified by flash column chromatography using a gradient elution system (25 - 50 % EtOAc/hexanes). R_f (100 % EtOAc) ~ 0.7. The desired product was obtained as 15 mg of a red solid as well as a grease contaminant (0.02 mmol, 33 % yield). ^{1}H NMR (400 MHz, $CDCl_3$) δ 8.20 (br s, 1H), 7.54 – 7.43 (m, 7H), 7.31 (d, *J* = 1.8 Hz, 2H), 6.95 (d, *J* = 5.0 Hz, 1H), 6.73 (d, *J* = 5.0 Hz, 1H), 6.46 (d, *J* = 4.0 Hz, 1H), 6.24 (d, *J* = 4.0 Hz, 1H), 5.60 (s, 2H), 4.01 (s, 6H). ^{13}C NMR (101 MHz, $CDCl_3$) δ 168.2, 163.8, 160.9, 158.2, 138.4, 136.0, 135.0, 133.7, 133.0, 132.5, 132.2, 130.5, 129.8, 128.5, 122.7,

118.7, 117.6, 113.9, 111.9, 96.9, 59.4, 29.8 (grease). LRMS (ESI) *m/z:* 666.3375 ($[M+Na]^+$); HRMS (ESI): calcd for $C_{31}H_{21}BClF_2N_5NaO_6$: 666.1146, found: 666.1139.

2.8.6.5 5,5'-(phenylmethylene)bis(2-chloro-1H-pyrrole) (**2.15**) & 2-chloro-5-(phenyl(1H-pyrrol-2-yl)methyl)-1H-pyrrole (**2.24**)

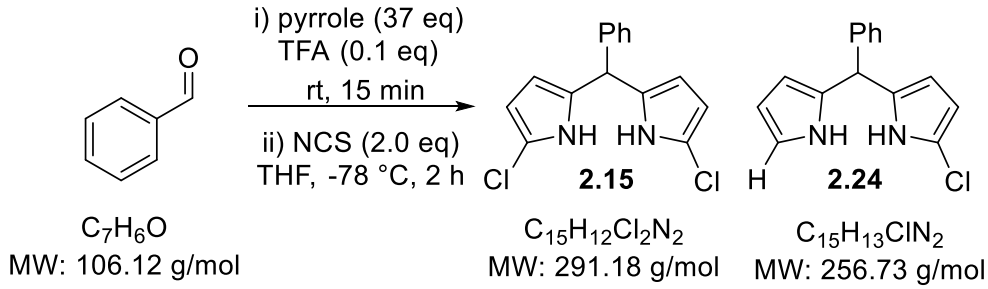

C_7H_6O
MW: 106.12 g/mol

$C_{15}H_{12}Cl_2N_2$
MW: 291.18 g/mol

$C_{15}H_{13}ClN_2$
MW: 256.73 g/mol

100 mL pyrrole (1.44 mol, 37 eq) and 4.0 mL benzaldehyde (39.2 mmol, 1.0 eq) were combined under a nitrogen atmosphere and the mixture was degassed by bubbling nitrogen through the solution for 15 minutes. 0.34 mL trifluoroacetic acid (4.4 mmol, 0.1 eq) was added neat via syringe and the reaction was stirred for 15 minutes at room temperature in the dark. Excess pyrrole was then removed by short path vacuum distillation. The resulting oil was pushed forward in the next step immediately without further purification. The residue was dissolved in 400 mL THF and the reaction flask was purged with nitrogen. The solution was cooled to -78 °C in an acetone/CO_2 bath. 11.55 g of *N*-chlorosuccinimide (88.6 mmol, 2.2 eq) was suspended in 100 mL THF in a separate flask and stirred rapidly. The suspension was added to the cooled solution of 5-phenyldipyrromethane slowly via an addition funnel. The reaction mixture was then stirred for 2 h at -78 °C. The mixture was stored at -20 °C overnight. The cold mixture was then added to 150 mL water and extracted with DCM (3 x 100 mL). The organic layer was dried with $MgSO_4$, filtered, and the solvent was removed *in vacuo*. The resulting black residue was purified by flash column chromatography using gradient elution (5 – 20 % EtOAc/hexanes). 1.90

g of the dichloro **2.15** was isolated as the major product (6.5 mmol, 17 % yield over two steps) as well as 498 mg of the monochloro by-product **2.24** (1.9 mmol, 5 % yield over two steps).

Minor: ^{1}H NMR (400 MHz, $CDCl_3$) δ 7.89 (br s, 2H), 7.37 – 7.19 (m, 5H), 6.71 (td, *J* = 2.7, 1.6 Hz, 1H), 6.16 (dd, *J* = 6.0, 2.7 Hz, 1H), 5.97 – 5.94 (m, 1H), 5.94 – 5.92 (m, 1H), 5.83 – 5.79 (m, 1H), 5.39 (s, 1H).

Major: Crude pushed forward immediately in the following reaction without further characterization. 3,5-DichloroBODIPY **2.17** fully characterized and shown in previous procedure.

2.8.6.6 3-chloro-5,5-difluoro-10-phenyl-5H-5λ^4,6λ^4-dipyrrolo[1,2-*c*:2',1'-*f*][1,3,2]diazaborinine (**2.25**)

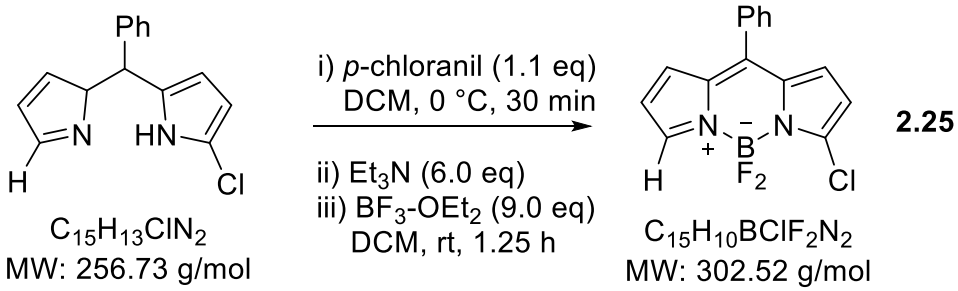

498 mg of dipyrromethane **2.24** (1.98 mmol, 1.0 eq) was dissolved in 6 mL DCM under a nitrogen atmosphere. A suspension of 562 mg of *p*-chloranil (2.3 mmol, 1.1 eq) in 2 mL DCM was added slowly at 0 °C and the reaction was stirred for 30 min at 0 °C. 1.25 mL Et_3N (11.4 mmol, 6.0 eq) was then added at 0 °C and the mixture was stirred for 20 minutes. 2.02 mL BF_3-OEt_2 was added (17.1 mmol, 9.0 eq), the reaction was warmed to rt and let sir for 1.25 h. The solvent was evaporated, and the residue was dissolved in 100 mL EtOAc and washed with 1 M HCl (3 x 100 mL), followed by 5 M HCl (1 x 100 mL) and brine (3 x 100 mL). The organic

layer was dried with $MgSO_4$, filtered, and the solvent was removed *in vacuo*. The resulting residue was purified by flash column chromatography (10 % EtOAc/hexanes). 269 mg of desired BODIPY **2.25** (0.89 mmol, 47 % yield over two steps). ^{1}H NMR (400 MHz, $CDCl_3$) δ 7.94 (s, 1H), 7.63 – 7.50 (m, 5H), 6.91 (d, *J* = 4.2 Hz, 1H), 6.89 (d, *J* = 4.4 Hz, 1H), 6.56 (dd, *J* = 4.2, 1.1 Hz, 1H), 6.43 (d, *J* = 4.3 Hz, 1H). ^{3}C NMR (101 MHz, $CDCl_3$) δ 145.7, 144.5, 134.7, 134.0, 133.1, 131.9, 131.5, 130.8, 130.5, 128.6, 128.5, 118.9, 118.4. HRMS (EI): calcd for $C_{15}H_{10}BClF_2N_2$: 302.05936, found: 302.05667.

2.8.6.7 1,1'-(5-((5,5-difluoro-10-phenyl-5H-5λ^4,6λ^4-dipyrrolo[1,2-*c*:2',1'-*f*][1,3,2]diazaborinin-3-yl)amino)-1,3-phenylene)bis(3-methoxy-1*H*-pyrrole-2,5-dione) (**2.26**)

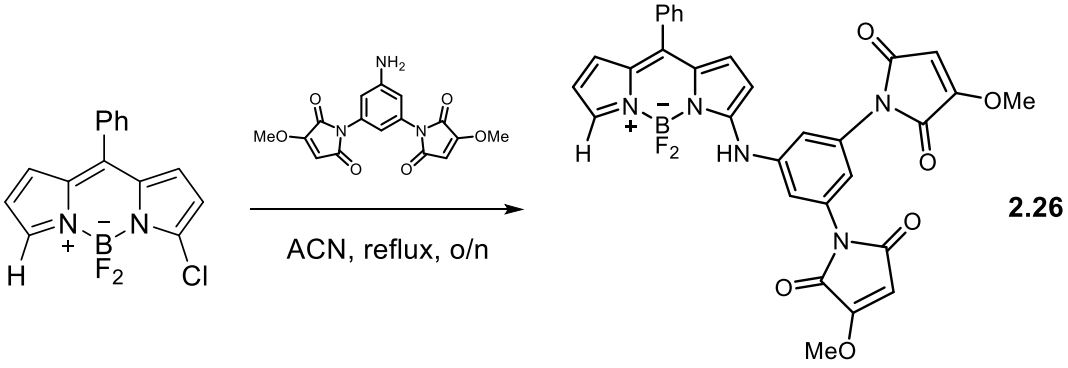

$C_{15}H_{10}BClF_2N_2$
MW: 302.52 g/mol

$C_{31}H_{22}BF_2N_5O_6$
MW: 609.35 g/mol

50 mg of BODIPY **2.25** (0.17 mmol, 1.0 eq) and 68 mg aniline **2.21** (0.20 mmol, 1.2 eq) were dissolved in 2 mL acetonitrile and the mixture was refluxed under a nitrogen atmosphere overnight, after which time the solvent was removed *in vacuo*. The resulting residue was purified by flash column chromatography using a gradient elution system (50 - 70 % EtOAc/hexanes). R_f (100 % EtOAc) ~ 0.8. 20 mg of desired product was obtained as a deep red solid (0.033 mmol, 20 % yield). ^{1}H NMR (300 MHz, DMSO-D_6, 80 °C) δ 9.75 (br s, 1 H), 7.64 – 7.31 (m, 9H), 7.12 – 7.01 (m, 1H), 6.62 (dd, *J* = 10.6, 4.2 Hz, 1H), 6.49 – 6.30 (m, 2H), 6.02 (s, 2H), 4.00 (s,

6H). ^{13}C NMR (101 MHz, $CDCl_3$) δ 145.8, 144.6, 134.9, 134.1, 133.3, 132.5, 132.0, 131.8, 131.7, 131.0, 130.6, 129.6, 128.9, 128.7, 128.7, 119.1, 118.5, 53.6 (spectra complicated by the presence of rotomers).

LRMS (ESI) *m/z:* 632.2 ($[M+Na]^+$); HRMS (ESI): calcd for $C_{31}H_{22}BF_2N_5NaO_6$: 632.1530, found: 666.1529.

2.8.7 MBP-dC10α Expression and Purification

Maltose binding protein (MBP) purification has been well established, and the protocol is summarized as followed. 500 mL LB medium (2% glucose) was inoculated with 3 mL MBP pre-culture (3L21 cells). Culture was incubated at 37 °C until an OD600 of 0.4-0.6 was obtained. 150 µL IPTG was then added to a final concentration of 0.3 mM and the culture was incubated at 37 °C for an additional 3 h. Cells were isolated by centrifugation (4000 g for 20 min), after which cells were resuspended in binding buffer (20 mM Tris-HCl, 200 mM NaCl, 1 mM EDTA, pH 7.4). The suspended cells were lysed by sonication on ice (3 cycles of 1 min pulses, at a 100% intensity/1 min pause between cycles) using a Branson sonicator equipped with a 3M probe. 2 mL amylose resin was added to the column, followed by binding buffer (5 column volumes wash). Insolubles were removed from lysate by centrifugation, after which cell lysate was added to the conditioned column and incubated at 4 °C for 2 h with shaking. Using gravity chromatography, the flow-through was collected, followed by 3 washes of 2 column volumes of elution buffer (20 mM Tris-HCl, 200 mM NaCl, 1 mM EDTA, 10 mM Maltose, pH 7.4). MBP-dC10α was eluted with 1 column volume elution buffer. Protein concentration was quantified using a Bradford protein assay and purity was assessed via SDS page gel.

2.8.8 Kinetic Measurements

Protein labelling kinetics were studied by following the time-dependent fluorescence increase at 37 ºC using a Synergy H4 Hybrid Multi-Mode Microplate Reader with excitation and emission monochromators set at a 9-nm bandpass. The reaction was prepared in 50 mM HEPES buffer (pH 7.4) with 10 % DMSO. Solutions of MBP-dC10α were prepared in a 96-well plate and **SA1** or **SA2** in DMSO was added immediately before recording. The final concentrations of **SA1/SA2** and MBP–dC10α were both 25 µM in 50 mM HEPES buffer (pH 7.4) with 10 % DMSO and 250 µM TCEP. **SA1** and **SA2** samples were excited at 520 nm and 505 nm, respectively, and fluorescence intensity was followed at 572 nm or 585 nm, respectively, as a function of time. The time-dependent fluorescent data shown in Figure 2.15 and Figure 2.12 were fitted by non-linear regression to the following second order equation:

$$[P] = [dM]_0 - \frac{1}{k_2 t + \frac{1}{[dM]_0}}$$

where P is the fluorescent product, dM is the dimaleimide fluorogen **SA1** or **SA2**, k_2 is the second order rate constant and t is time. Kinetic reactions were performed in triplicate and reported as mean ± standard deviation. (k_2 = 353 ± 32 $M^{-1}min^{-1}$ for **SA1** and k_2 = 82 ± 7 $M^{-1}min^{-1}$ for **SA2**).

2.8.9 Cell Culture

9 mL DMEM (1% P/S, 10% FBS) was seeded with 1 mL frozen culture of HeLa Cells (thawed for 4 minutes) in a 50 mL falcon tube. Cells were pelleted by centrifugation (750 rpm, 5 min) and media containing DMSO was subsequently removed. Pelleted cells were resuspended in 10 mL DMEM and incubated at 37 °C in a 75 cm^2 culture flask until 85-95% confluency. Cells

were then passaged as follows: old media was removed, and adhered cells were washed with DPBS (no calcium or magnesium) 2 x 5 mL. 2 mL trypsin was added to cover the surface of cells and incubated at 37 °C for 7 min. 8 mL DMEM was added and suspended cells were transferred to a 50 mL Falcon tube and resuspended 10 times. 1.0-1.5 mL of suspended cells were taken back into the culture flask and diluted to 10 mL with DMEM and incubated at 37 °C until the desired confluency was reached. This passaging protocol was repeated as necessary to maintain cell cultures.

To maintain a stock of HeLa cells, cells were frozen as needed according to the following protocol. Confluent cells were trypsinized and suspended in DMEM as described above. Cells were then counted used trypan blue staining and bright line counting chamber. Cells were pelleted by centrifugation (100 g, 3 min) to remove passaging media and diluted to a final concentration of $2.1x10^6$ cells/mL in freezing medium (DMEM containing 5% DMSO, 10% FBS, and 1% P/S). Cells were resuspended and aliquoted into cryogenic vials. Vials were cooled slowly at 1 °C/min before storing in liquid nitrogen.

2.8.10 Cellular Labelling

HeLa cells (5.25 × 105 cells) were plated onto 60-mm dishes and grown in Opti-MEM supplemented with 5 % FBS for 16 h before transfection. Cells were transiently transfected with histone H2B–dC10 or pcDNA3.1(+) (mock) by first incubating lipofectamine 2000 (10 μg) in Opti-MEM medium (300 μL) for 20 min. The lipofectamine 2000 solution was then incubated for 30 min with a solution of the plasmid (10 μg) in Opti-MEM medium (300 μL) for a final liopfectamine 2000 to DNA ratio of 1:1. Lastly, the HeLa cells were incubated in this lipofectamine 2000:DNA mixture for 24 h.

After transfection, the medium was removed and replaced with 10 μM **SA1/SA2** in Live Cell Imaging Solution (Invitrogen) supplemented with F127 surfactant (0.1 % v/v) and DMSO (final concentration of 0.4 % v/v). Cells were incubated at 37 °C for 1 hour. Afterwards, the imaging solution containing the probe was removed, cells were quickly rinsed with clear imaging solution (3 x 2 mL) and then incubated with 8 μM Hoechst 33342 (Life TechnologiesTM) in the imaging solution for 15 min at room temperature. Hoechst solution was removed and cells were quickly rinsed with clear imaging solution (3x2 mL) and then observed on a Nikon Ni-U Ratiometric Fluorescence Microscope with a 40X/0.8 NA objective. The recorded images were subsequently analyzed with NIS-Elements software.

Chapter Three: Green BODIPY-Based FlARe Probe

3.1 Contributions

Much of the work encompassed in the following chapter was recently published as a communication in Angewandte Chemie International Edition (2018).[53] Significant contributions were made by my co-authors, Dr. Yingche Chen and Kelvin Tsao (PhD Candidate). Dr. Yingche Chen is credited with initial design and synthesis of the green-BODIPY probe, named **YC23** in her honour, as well as preliminary evaluation. Kelvin Tsao guided cell culture and labelling experiments and was crucial in obtaining the cellular images that were included in the publication.

3.2 Introduction

For biological applications of a fluorogenic labelling agent *in cellulo* and *in vivo*, fluorophores with lower energy, red-shifted excitation and emission wavelengths are advantageous. As discussed in Chapter Two, creating FlARe probes that incorporate red-shifted dyes that are still efficiently quenched by maleimides through d-PeT is challenging. The smaller band-gaps of longer wavelength emission fluorophores are typically due to a lower energy LUMO, as opposed to a higher energy HOMO, which can disfavour d-PeT. The BODIPY fluorophore has emerged as a potential new fluorophore for FlARe that could circumvent these challenges. The preliminary results for the red FlARe probe substituted at the alpha positions designed by Dr. Chen (Chapter Two) were very promising, showing a red-shifted BODIPY fluorogen that exhibited efficient quenching and a large fluorescent enhancement after reaction with the dC10α tag. However, I was unable to reproduce these results in the time available to me, and the synthetic route originally employed was not feasible for preparation of high enough yields of the

compounds to be applied as a labelling agent and biological tool. Compounds **2.23** and **2.26** (Chapter Two) were designed and synthesized as potential alternative BODIPY labelling agents in the yellow/orange range; however, these compounds suffered from slow kinetics and a low fluorescent enhancement and their labelling *in cellulo* was not successful. In this Chapter, the design, synthesis, and evaluation of a *meso* substituted BODIPY fluorogen for labelling in the green channel of fluorescence microscopes will be discussed.

3.3 BODIPY-FlARe Probe Design

The computational study by Cosa on a large library of BODIPY compounds suggested that electron transfer may be possible from the excited state of BODIPY to an adjacent maleimide group; therefore, the BODIPY fluorophore could be amenable to PeT quenching in a FlARe probe. Additionally, a thiol-reactive probe published by the Nagano group in 2007 provided strong experimental evidence and was highly instructive for the design of our first BODIPY-based FlARe probe. Nagano and coworkers synthesized a series of *meso* substituted phenyl BODIPYs incorporating a maleimide group at the *ortho*, *meta*, and *para* positions, as shown below. These probes were designed to be thiol-reactive fluorogenic reporters. The maleimide group functions as both a d-PeT quenching moiety and an orthogonal handle to react selectively with thiols, which is mirrored in the FlARe probe design.

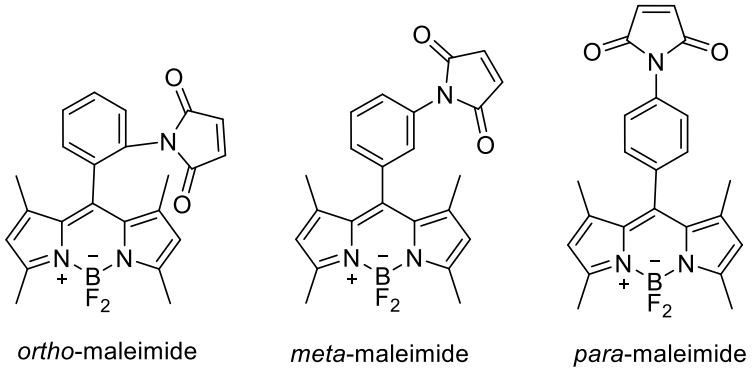

Figure 3.1 Nagano's thiol-reactive BODIPY-maleimide probes.[52]

Nagano predicted that the *ortho* substituted compound would be the most efficiently quenched due to the decreased distance between PeT donor and acceptor orbitals. Indeed, the fluorescence quantum yield of the ortho compound was 0.2 %, which is negligible in comparison to the *meta* and *para* derivatives (summarized in Table 3.1). Nagano measured a 350-fold fluorescence increase for the *ortho* probe upon reaction with a model small molecule thiol. This was the largest enhancement achieved for a thiol-reactive probe using visible light at the time. These probes were excited with green light (505 nm), which was also significantly red-shifted compared to previous thiol-reactive probes.

To further guide the design of our probe, we modelled Nagano's probes computationally to predict frontier orbital energies and D-A distances, which were not included in the original publication. These data are summarized in Table 3.1.

Table 3.1 Summary of HOMO/LUMO energies and D-A distances for Nagano's probes determined by molecular modelling.

	Energy (Hartree)				
BODIPY Fluorogen	**HOMO (BODIPY)**	**LUMO (maleimide)**	**LUMO + 1 (BODIPY)**	**D-A Distance (Å)**	**Quantum Yield (DMSO) (Φ_{fl})**
ortho	-0.1949	-0.1002	-0.0855	3.6	0.2 %
meta	-0.1954	-0.1097	-0.0856	5.7	37 %
para	-0.1965	-0.1095	-0.0864	7.1	54 %

There are very small differences in HOMO/LUMO energies based on the phenyl substitution pattern. For each probe, the HOMO is localized on BODIPY and the LUMO of the maleimide is lower energy than LUMO of the BODIPY, making d-PeT favourable. The distance between donor and acceptor was considerably shorter in the *ortho* probe as expected, corresponding to a quantum yield that was determined to be two orders of magnitude smaller. Although the authors did not report a quantum yield for the phenyl BODIPY compound without a maleimide, measurements in the literature range from ~70-86 % in different organic solvents, however a measurement in DMSO was not available for direct comparison.[71] Regardless, this shows that a single maleimide at the *meta* or *para* position still partially quenches the fluorescence of the BODIPY, resulting in quantum yields of 37 % and 54 %, respectively.

We saw the opportunity to exploit the powerful quenching ability of the *ortho* maleimide in our FlARe probes. The dimaleimide scaffold positions the maleimides *meta* with respect to each other, separating the reactive alkenes by approximately 10 Å. This spacing is complementary to the distance between the two cysteine residues of the dC10α tag. By placing our maleimides at the *ortho* and *para* positions relative to the fluorophore, as opposed to both *meta* positions as in previous FlARe probes, we would expect a much higher quenching efficiency and therefore a larger fluorescence enhancement. The envisioned reaction of the probe designed in this fashion is shown in Figure 3.2 below.

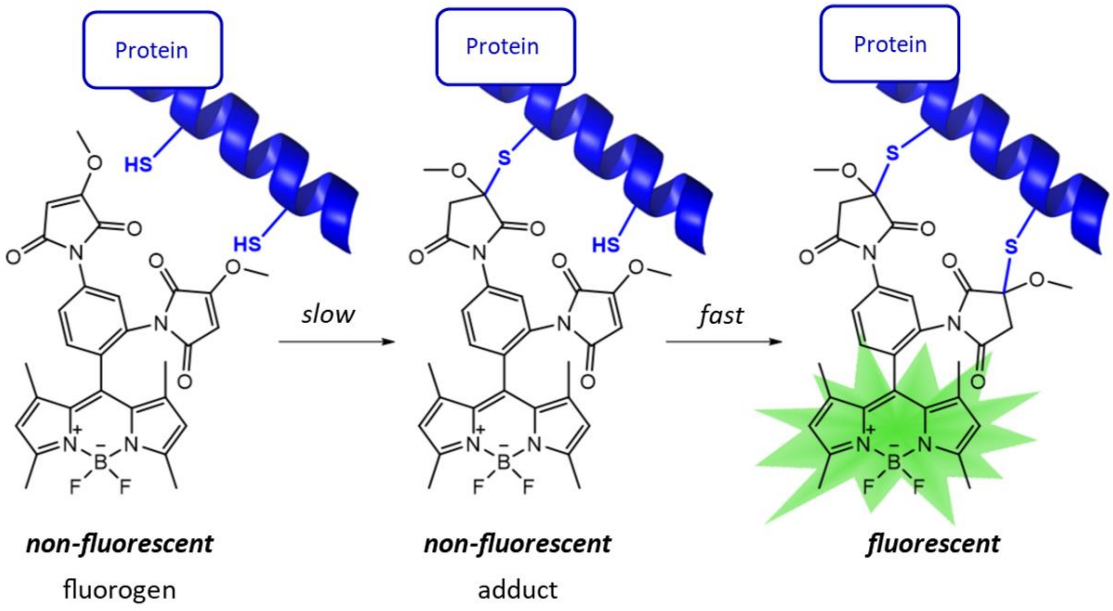

Figure 3.2 Protein labelling with the BODIPY dimaleimide FlARe fluorogen **YC23**.

First, the green FlARe probe (referred to as **YC23**) was modelled computationally using TD-DFT calculations (B3LYP functional and 6-31G(d) set) to determine the distance between the *ortho*-maleimide and the BODIPY fluorophore. As shown in Figure 3.3 below, the distance

between the BODIPY excited state and LUMO of the *ortho*-maleimide is approximately the same as in Nagano's probe, suggesting the BODIPY should be efficiently quenched.

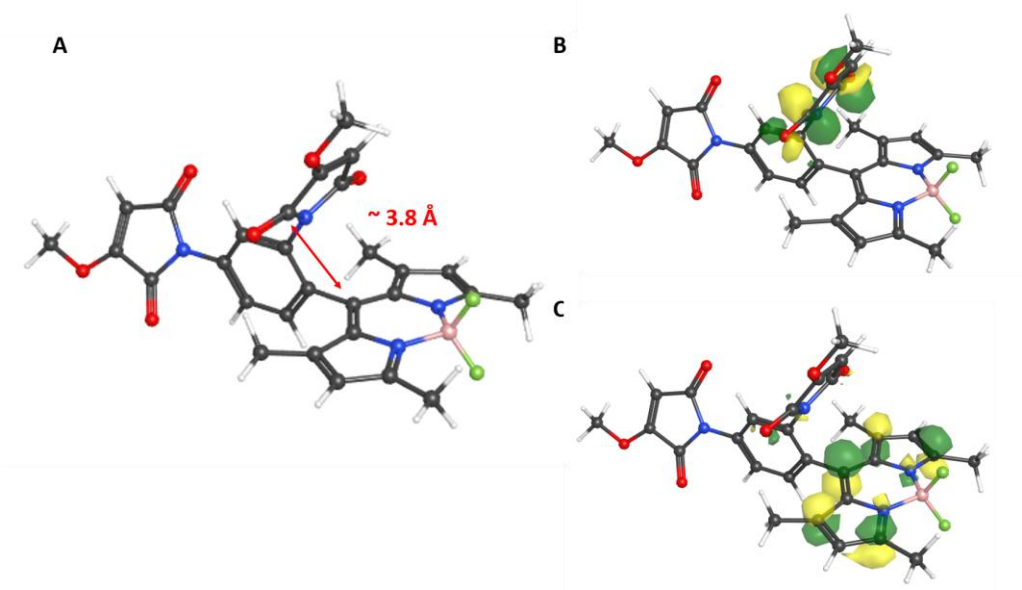

Figure 3.3. DFT-minimized geometry of green fluorogen **YC23**, showing: A) the relevant distance between the *ortho*-maleimide and BODIPY group, B) the *ortho* maleimide LUMO (LUMO +2), and C) the BODIPY excited state.

The TD-DFT calculations, summarized below in Table 3.2 show that the LUMO of the methoxymaleimide of fluorogen **YC23** is higher energy than that of an unsubstituted maleimide (-0.1002 au for Nagano's probes, Table 3.1). This increase in energy results in the unoccupied maleimide orbitals being higher energy than the excited state of the BODIPY, suggesting that d-PeT would not be favoured.

Table 3.2 Summary of HOMO/LUMO energies for **YC23** determined by molecular modelling.

	Energy (Hartree)			
BODIPY Fluorogen	**HOMO (BODIPY GS)**	**LUMO (BODIPY ES)**	**LUMO + 1 (*para*-maleimide)**	**LUMO + 2 (*ortho*-maleimide)**
YC23	-0.2038	-0.0952	-0.0895	-0.0869

Computational modelling provides valuable insights into the design of potential FlARe probes, as drastically incompatible orbital energy levels for d-PeT can be used to disregard a compound or, alternatively, compatible energy levels can lead us to move forward with a compound. However, the computational results must be interpreted cautiously. Since the energy levels of the BODIPY excited state and LUMO of the maleimides were very close to each other (within ~0.1 au) and there was strong experimental evidence that the probe would be quenched from Nagano's probe, **YC23** was synthesized to determine experimentally if it would in fact be quenched.

3.4 Synthesis of YC23

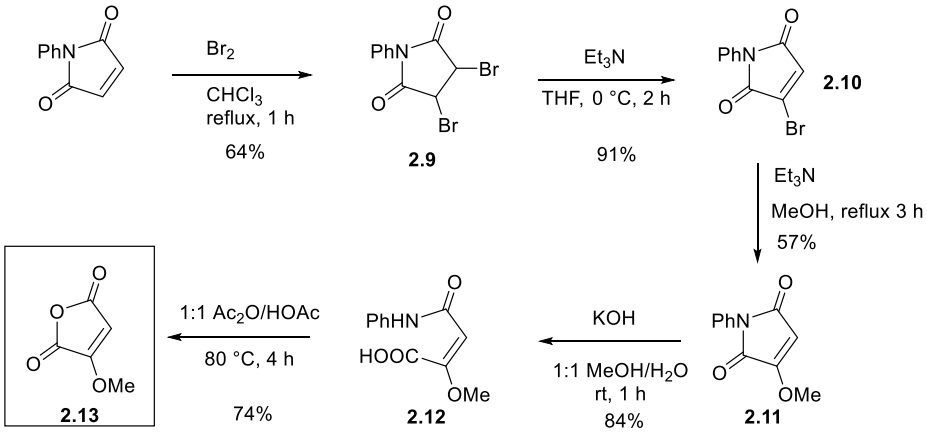

Scheme 3.1 Synthetic route for preparation of methoxymaleic anhydride. [63]

First, methoxymaleic anhydride was synthesized according to the route described previously in Chapter Two, summarized in Scheme 3.1.

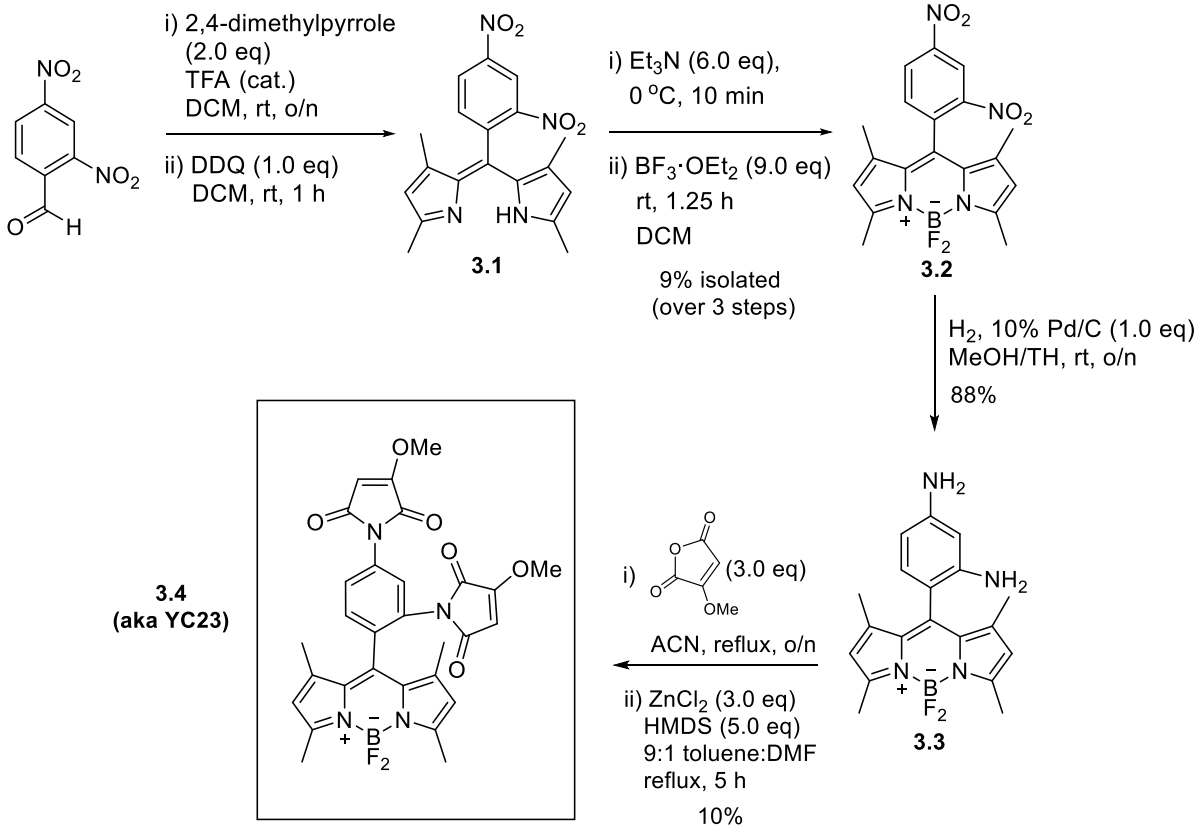

Scheme 3.2 Synthesis of compound **YC23**.

BODIPY fluorogen **YC23** was synthesized based on the route used by Nagano, starting with condensation between the commercially available 2,4-dinitrobenzaldehyde and 2,4-dimethyl pyrrole using a catalytic amount of TFA. As opposed to the postfunctionalization strategy exploited in Chapter Two, the BODIPY core is prefunctionalized using the *ortho-meta* dinitro substituted benzaldehyde precursor. This installs the synthetic handle at the *meso* position for the final dimaleimide (NHdM10) moiety immediately during dipyrrin formation. The dipyrromethane intermediate **3.1** formed was immediately oxidized using DDQ to give the dipyrromethene. Compound **3.2** was subsequently reacted with trifluoroboryl etherate to form the dinitro BODIPY derivative **3.3**. Next, both nitro groups were reduced by hydrogen over

palladium on carbon (10 % w/w) to give the corresponding diamine. The amines were then reacted with methoxymaleic anhydride to form the acyl intermediate **3.3**. This dicarboxylic acid intermediate has sufficiently low solubility in organic solvent so the excess methoxymaleic anhydride can be removed by trituration with ether. The isolated intermediate was immediately subjected to zinc- and HMDS-mediated ring closure to give **YC23** in sufficient yield for evaluation.

3.5 In Vitro Evaluation

To evaluate **YC23** as a selective protein labelling reagent, a target protein bearing the dC10α tag was first chosen. As discussed in Chapter Two, maltose binding protein (MBP) has been the test protein of choice for the structural and kinetic characterization of FlARe probes, as it is highly soluble, monomeric, and easily expressed. Our dC10α sequence was genetically fused to the C-terminus of MBP to give the fusion protein MBP-dC10α. MBP-dC10α was expressed and purified in *E-coli* as described previously in Chapter Two.[36]

Before reaction with dC10α, **YC23** is strongly quenched with barely detectable fluorescence at a concentration of 25 μM. The excitation and emission spectra for **YC23** after reaction with equimolar MBP-dC10α are shown in Figure 3.4. The intense maximum fluorescence at λ_{em}=535 nm is separated from the excitation maximum by a Stokes' shift of 40 nm, bringing the fluorescence into the green region of the visible spectrum.

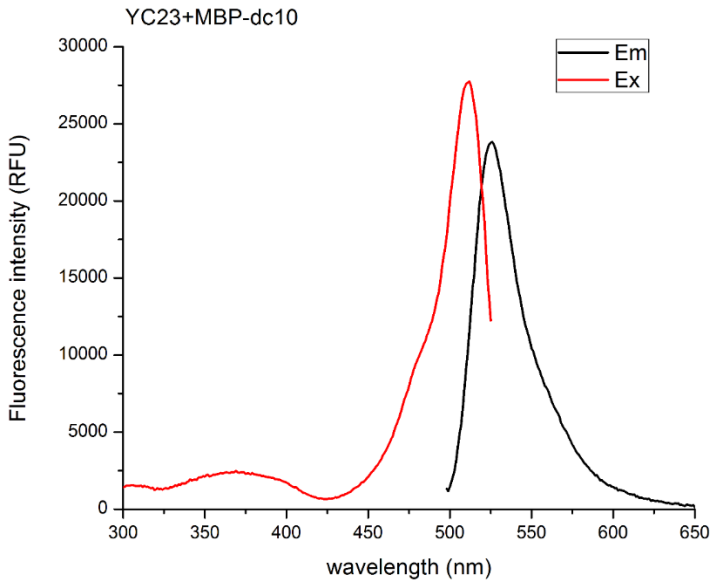

Figure 3.4 Excitation (red) and emission (black) spectra for 25 µM **YC23**+MBP-dC10α.

Next, the fluorescent enhancement was determined by measuring emission spectra of **YC23** after incubation with increasing concentrations of target protein after ~ 5 hours. Bright fluorescence (30,000 RFU) was obtained after reaction with 1 equivalent of MBP-dC10α. Additionally, the increase in fluorescence was found to be linearly dependent on MBP-dC10α concentration (Figure 3.5, right). The background fluorescence of unreacted **YC23** is shown in black in Figure 3.5 (left) and is so low that it is difficult to distinguish from the baseline. Although the LUMO of methoxymaleimide may be higher in energy than the BODIPY excited state, it is clear that **YC23** exhibits very efficient quenching, resulting in an ~800-fold fluorescence enhancement at the emission maximum (λ_{ex} = 480 nm).

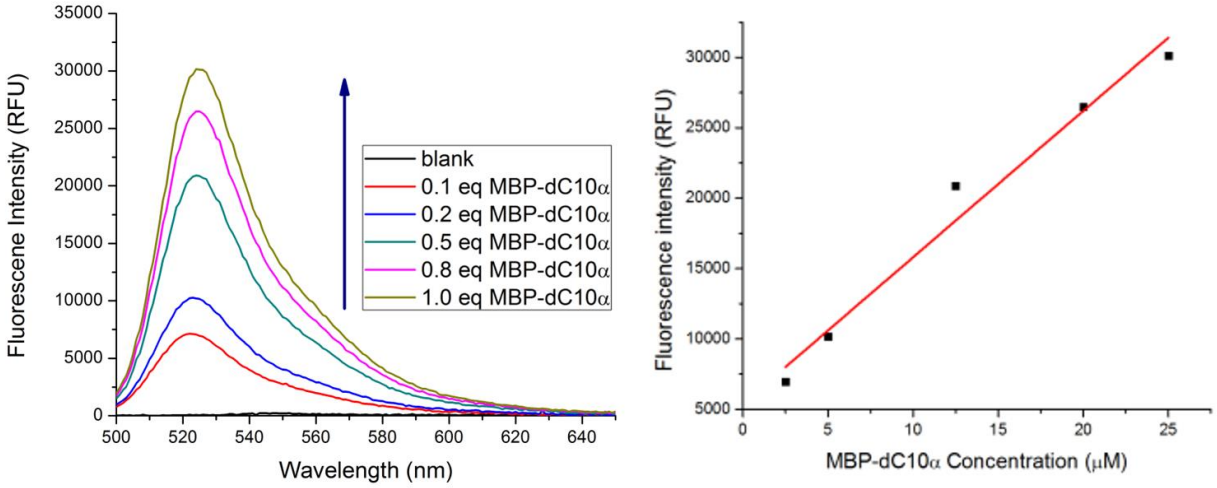

Figure 3.5 (Left) Fluorescence enhancement (λ_{ex}=480 nm) of 25 μM fluorogen **YC23**, incubated in the absence (black) and presence of varied concentrations of MBP-dC10α (coloured). (Right) Linear fit of fluorescence intensity of **YC23** vs. [MBP-dC10α].

3.5.1 Kinetics

The addition reaction between a FlARe probe and the dC10α tag occurs in two sequential steps: the first slow, intermolecular, addition followed by a rapid intramolecular addition. The second is assumed to be fast and rate-limiting, which allows us to approximate a second order model, as described in Chapter Two. The time-dependent increase in fluorescence for the equimolar reaction between probe and tag was measured overnight. The data leading up to the plateau at ~30,000 RFU were fitted to a second order model (black curve) as shown below.

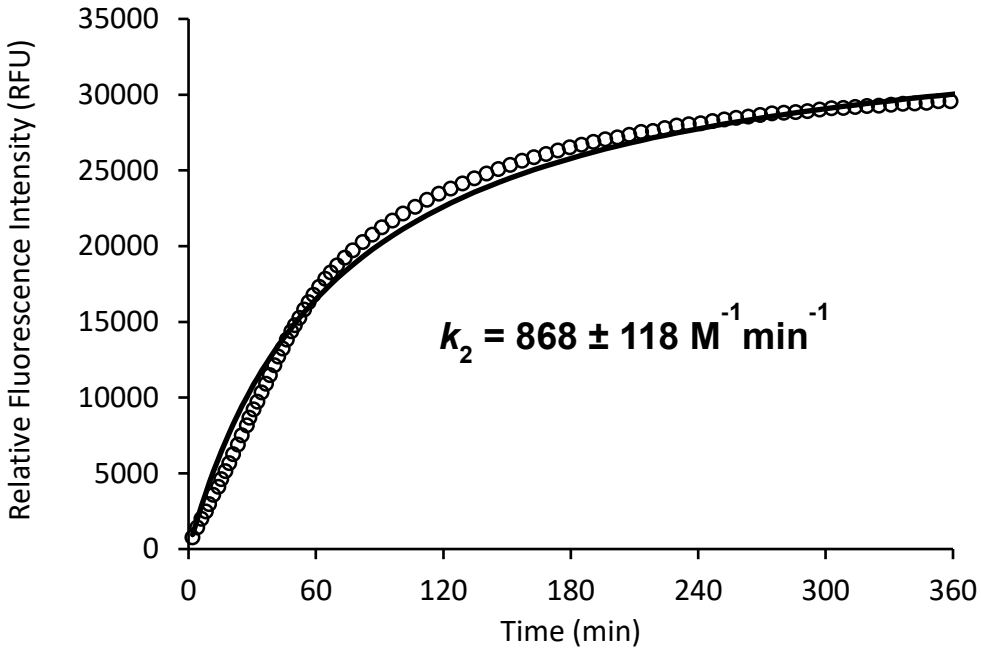

Figure 3.6 Time-dependent fluorescence (λ_{ex}=495 nm, λ_{ex}=525 nm, gain =65) increase of 25 μM **YC23** reacting with 25 μM MBP-dC10α in 50 mM HEPES buffer (pH 7.4, 250 μM TCEP, 10% DMSO) at 37°C. The solid line through the data was obtained by fitting to a second order equation.

The reaction curve obtained resembles that of a slightly biphasic curve expected for two sequential addition reactions, in which the second reaction produces the fluorescent signal. The second order rate constant calculated from the fitting was 868 ± 118 $M^{-1}min^{-1}$.

This rate constant is approximately three orders of magnitude lower than the comparable FlAsH organoarsenic probes.[18] The reaction is relatively slow, as maximum fluorescent signal takes approximately 4 hours to reach. However, for the desired application of our probes, it is important to consider fluorescence increase on a timescale relevant to an imaging experiment. Typically, cells are labelled between 45 min and 3-4 hours maximum. The labelling media used

lacks serum, and therefore cells are under nutrient deficient conditions. Subjecting cells to labelling solution for longer than this can often lead to cell death, decreasing the quality of the images obtained. Although the best labelling time is determined experimentally, if we estimate a 1 hour labelling, this would result in approximately half of the total fluorescence enhancement, a 400-fold increase. Even after only 15 minutes, a 10-fold increase was observed. We predicted that a minimum 10-fold enhancement would provide sufficient contrast for cellular imaging.

Additionally, the maximum fluorescence signal obtained in Figure 3.6 was stable over 16 hours during the kinetic experiment, which further supports the robustness of labelling as well as the fluorophore's resistance to photobleaching.

3.5.2 Background Reaction with Thiols

A major concern for any fluorogenic probe is its selectivity for the corresponding tag in the complex mixture of a cell. Although the peptide motif of two cysteine residues separated by 10 Å is rare in nature, there are many other biological thiols present in the cell. As mentioned previously, GSH is a particular concern as it is present in millimolar concentrations.[72]

YC23 was incubated with a large excess of biologically relevant thiols (10 eq cysteine, 10 eq homocysteine, 40 eq GSH). As shown in Figure 3.7, the fluorescent enhancement obtained after reaction with thiols was less than 10 % of that obtained by reaction with MBP-dC10α.

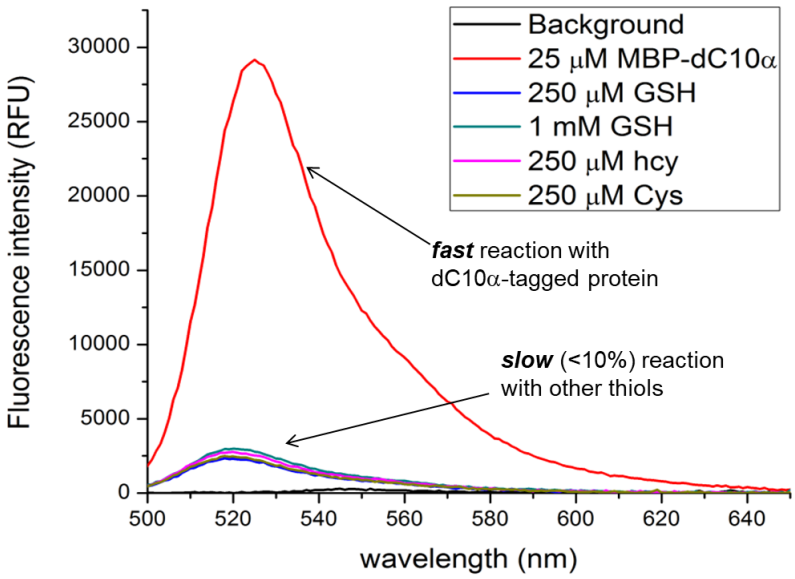

Figure 3.7 Fluorescence emission spectra after 16 h of incubation of 25 μM **YC23** with 1 eq test protein MBP-dC10α, 10 eq of cysteine (Cys), 10 eq of homocysteine (hcy) and 40 eq (1 mM) of glutathione (GSH).

Calculating a second order rate constant for the reaction with these thiols would give k_2 <0.417 M^1min^1. This dramatic difference in rate constants suggests that inside a cell the labelling agent would react with the desired dC10α tagged protein long before any background fluorescence would develop. This is particularly powerful on the short timescale of an imaging experiment.

3.5.3 Quantum Yield

Fluorescence quantum yield is a measure of the photons emitted divided by the number of photons absorbed by a fluorophore. Quantum yields are frequently reported as percentages in the literature. This value is therefore a measure of the efficiency of fluorescence and ranges between 0-100%, where 100% would be a theoretically perfect fluorophore that emits every absorbed

photon as fluorescence. In other words, no non-radiative pathways of relaxation from the excited state are possible. In reality, this is not possible, although some fluorophores come close. Quantum yields are also solvent and temperature dependent. It is not uncommon to see quantum yields for BODIPYs in the literature approaching 100% in water.[73] The quantum yield of **YC23** after conjugation to MBP-dC10α in HEPES buffer was calculated using a protocol adapted from several literature sources (see experimental) using fluorescein in 0.1 M NaOH at 22 °C as a standard, according to the following equation:

$$\varphi_{sample} = \varphi_{std}\left(\frac{m_{sample}}{m_{std}}\right)\left(\frac{\eta^2_{sample}}{\eta^2_{std}}\right)$$

This equation takes into consideration the different refractive indexes (η) of the two solvents and m, which is the slope from a plot of integrated fluorescence intensity vs absorbance.

First, the standard and reacted sample were diluted in their respective buffer until their longest wavelength band reached a maximum absorbance of 0.1 (7 µM and 12.5 µM, respectively) and the intersection between the two absorbance spectra was determined to be 498 nm. All fluorescence spectra were subsequently obtained using λ_{ex} = 499 nm. This absorbance value is commonly used in the literature for quantum yield determination, as the samples must be dilute to avoid aggregation effects of fluorophores and possible self quenching between molecules. Figure 3.8 and 3.9 below plot the extinction coefficients obtained for the standard fluorescein sample and the reacted **YC23** sample respectively, measured in duplicate. The reacted **YC23** sample was prepared by reaction with equimolar MBP-dC10α in HEPES buffer (pH 7.4, 10 % DMSO) by incubation at 37 °C overnight in the dark in the presence of 10 equivalents of TCEP.

The quantum yield was then calculated using the above equation, where Φ = quantum yield, m = gradient of integrated fluorescence intensity vs absorbance, and η = refractive index (1.33 for aqueous sample buffer and 1.33 for 0.1 M NaOH). The literature Φ_{std} for fluorescein is 95 % (at 22 ^{o} C in 0.1 M NaOH).[74] The values for m_{std} and m_{sample} correspond to the slopes obtained in Figure 3.10 and Figure 3.11 , respectively.

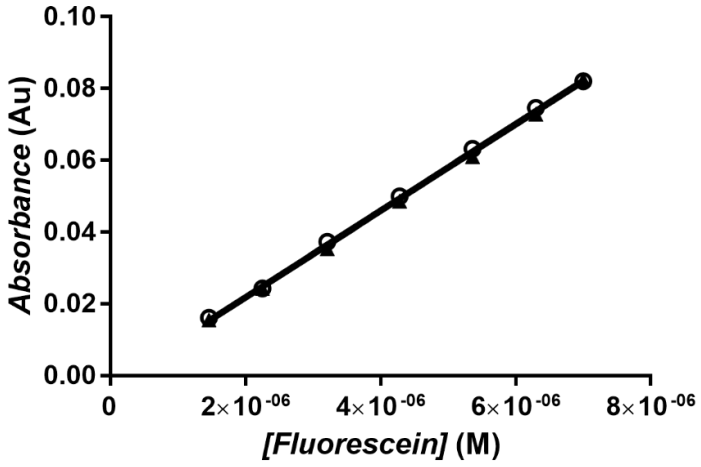

Figure 3.8 Plot of absorbance vs. fluorescein concentration, determined at 498 nm, 0.1 M NaOH, 22 °C.

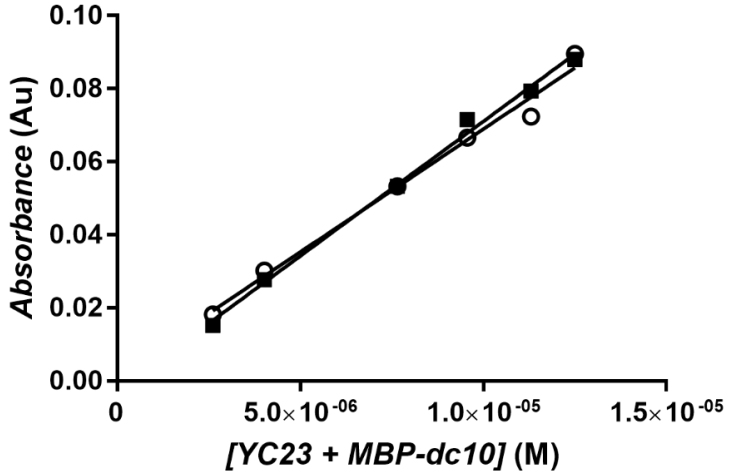

Figure 3.9 Plot of absorbance vs. [addition product of MBP-dC10 and **YC23**] (25 μM of each incubated overnight in the dark at pH 7.4 in the presence of 250 μM TCEP and 10 % DMSO) determined at 498 nm, pH 7.4 (50 mM HEPES buffer), 22 °C.

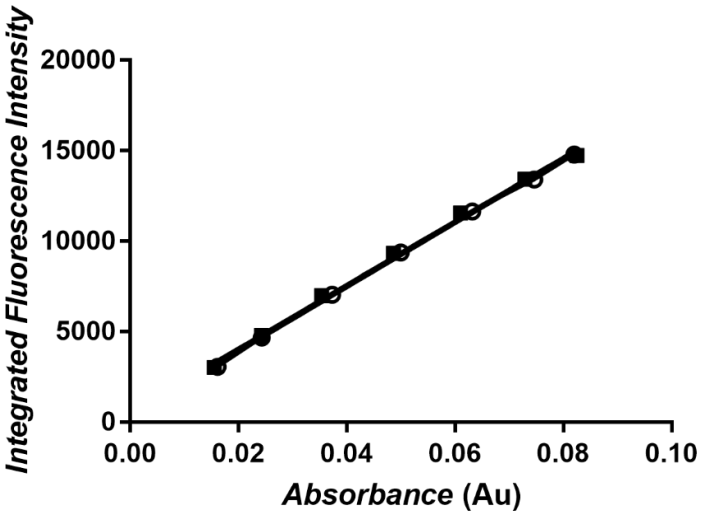

Figure 3.10 Plot of integrated fluorescence intensity vs. absorbance for fluorescein standard in 0.1 M NaOH at 22 °C. Absorbance values were determined at 498 nm and λ_{exc} = 498 nm.

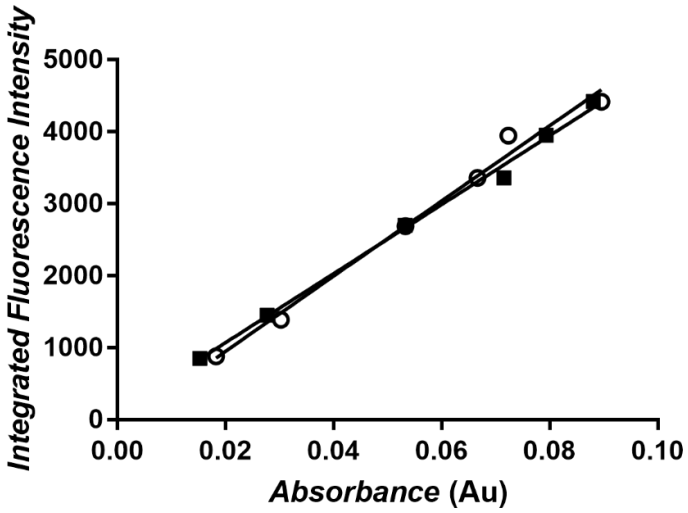

Figure 3.11 Plot of integrated fluorescence intensity vs. absorbance for the addition product of MBP-dC10 and **YC23** (25 μM of each incubated overnight in the dark at pH 7.4 in the presence of 250 μM TCEP and 10 % DMSO) determined at pH 7.4 (50 mM HEPES buffer), 22 °C.

Using this equation, the quantum yield of **YC23-**MBP-dC10α was determined to be 27%. This is comparable to other *meso* phenyl substituted BODIPYs in literature.[73] The quantum yield of the unreacted **YC23** was not determined, as quenching was so efficient that fluorescence was not detectable using the fluorimeter.

Since the extinction coefficient of **YC23**-MBP-dC10α was also obtained from Figure 3.9 (ε = 7048 M^{-1}), the brightness can be calculated. The brightness of a fluorophore is proportional to the product of its quantum yield (Φ) times its molar extinction coefficient (ε) and is therefore ~190,000 for **YC23**. This is impressively bright for a small molecule fluorophore. The high brightness and quantum yield suggested that this probe would be well suited for fluorescence imaging, which led us to further investigate the *in vitro* stability and selectivity.

3.5.4 SDS-PAGE Gel Analysis and YC23 Stability Under Denaturing Conditions

Next, we investigated the labelling in a more complex biological mixture, bacterial lysate, as opposed to purified target MBP-dC10α protein. MBP-dC10α was labelled with different concentrations of **YC23** overnight at 37 °C in bacterial lysate and the reaction was then quenched by heating to 95°C for 15 min. After denaturation, SDS-PAGE gel analysis (Figure 3.12) was performed. First, bright fluorescence was observed after denaturation, even with labelling concentrations as low as 10 μM **YC23** (Lane 2). This is highly promising for cellular labelling, as low concentrations of labelling reagent appear to be sufficient for bright contrast.

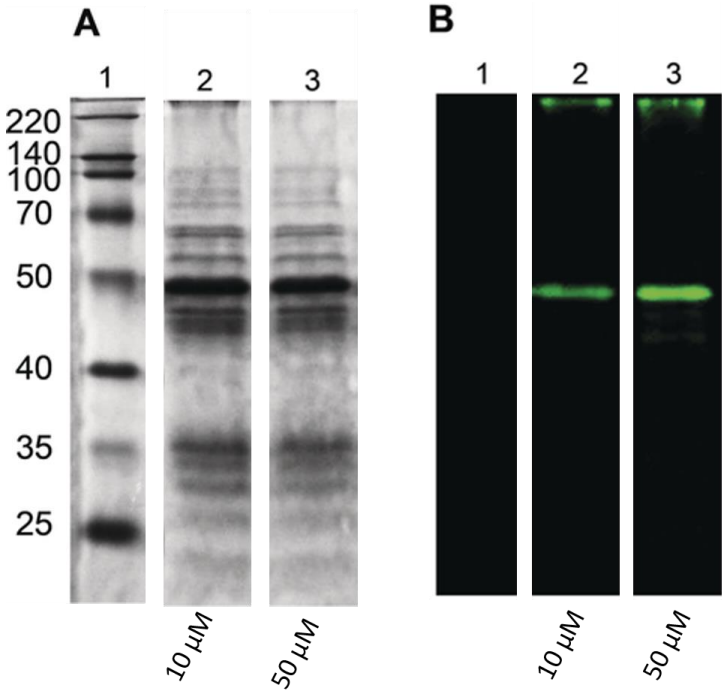

Figure 3.12 SDS-PAGE gel developed by (A) Commassie blue staining and (B) fluorescence (λ_{ex} = 491 nm, (λ_{em} = 408 nm). Lane 1: molecular weight markers. Lane 2 and 3: Soluble lysate of bacteria expressing MBP-dC10α, treated with 10 or 50 μM **YC23** respectively, and 0.5 mM TCEP overnight.

Second, the SDS-PAGE gel also supported the stability of the product formed. The addition reaction of a thiol to a maleimide results in formation of a highly stable thioether product.[44,45] The labelled protein at ~50 kDa remains fluorescently labelled (B) after denaturing conditions, showing that the covalent bonds formed between the maleimides and the di-cysteine tag are stable. Lastly, the gel was also promising in terms of selectivity of the labelling method, as only the band corresponding to the target protein was brightly labelled. We hypothesize that the bright band at the top of the gel is simply the result of insoluble labelled protein.

3.6 Cellular Evaluation and Imaging

3.6.1 Cytotoxicity

Prior to applying **YC23** for labelling in living cells, we investigated the cytotoxicity of the compound. A standard MTT-assay was used to determine if **YC23** showed any cytotoxicity in mammalian cells (HEK293T). MTT (3-(4,5-dimethylthiazol-2-yl)-2,5- diphenyl tetrazolium bromide) is a yellow tetrazolium salt that is reduced by mitochondria in living cells to a purple formazan. The resulting intracellular purple formazan is insoluble in aqueous solution, but it can be dissolved in Triton X100 and subsequently quantified by measuring the absorbance of the solution.

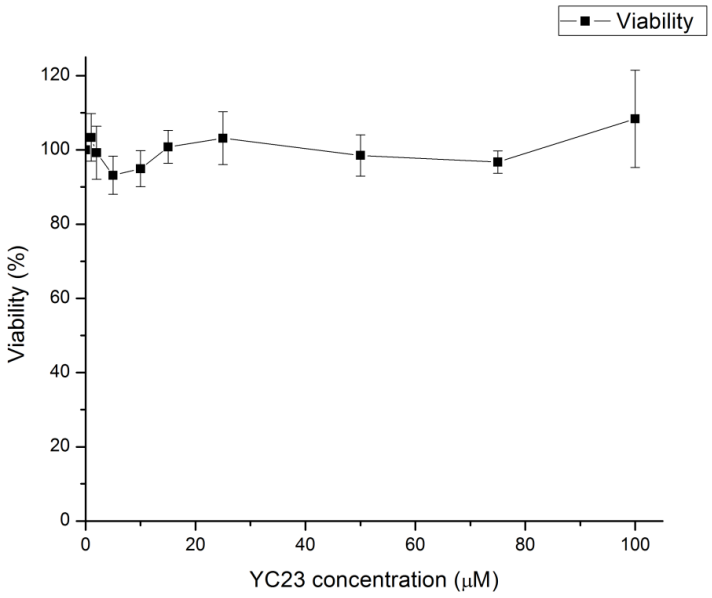

Figure 3.13. Cytotoxicity of **YC23** in cultured HEK293T cells. Cells were incubated with the corresponding concentrations of fluorogen for 20 h. Cell viability was measured by MTT assay and the results are reported as percentage relative to untreated cells (mean ± SD).

HEK293T cells were seeded in a multi-well plate and incubated with culture medium at increasing concentrations of the fluorogen **YC23** for 20 h. The absorbance of each well was measured after incubation with MTT solution for 4 hours, followed by solubilization solution overnight using a plate reader at λ=570 nm. The absorbance corresponding to the purple product can be monitored and compared to that of a positive and negative control cell sample, and therefore the cell viability was then calculated from the obtained absorbance values according to the following equation:

$$\text{Cell viability} = (A_{\text{with fluorogen}} - A_{\text{negative control}}) / (A_{\text{positive control}} - A_{\text{negative control}}) \times 100\ \%$$

As shown in Figure 3.13, **YC23** had negligible effects on cell viability within error when cells were incubated overnight with up to 100 µM of fluorogen.

The promising *in vitro* labelling results with **YC23**, paired with the compound's low cytotoxicity, prompted us to move forward with protein labelling in living cells. We are particularly interested in our FlARe probes' abilities to be applied for intracellular protein labelling, as there is a greater need for intracellular labeling agents. While MBP-dC10α was suitable for *in vitro* evaluation, we chose to label histone H2B in living cells, given its clear localization in the nucleus.[69] This would allow us to co-stain the labelled cells with a standard nuclear dye to confirm the selectivity of our labelling method. To this end, The dC10α tag was genetically fused to the C-terminus of histone H2B as described previously.[62] Mammalian HeLa cells were cultured and transfected with the H2B-dC10α gene transiently using lipid-mediated gene delivery with lipofectamine, as in Chapter 2. To aid in uptake of **YC23**, a nonionic surfactant (F127) was used, which has been found to improve membrane permeability.

Two of the most commonly used nuclear dyes are DAPI and Hoechst. DAPI has a lower membrane permeability and is therefore more commonly used for labelling fixed cells, whereas Hoechst is better suited to live cell imaging. Both dyes are non-fluorescent before they bind to the minor grove of DNA in the nucleus, which turns on their bright fluorescence.[75] The dyes have nearly identical spectral properties: their maximum excitation is in the UV region and they emit in the blue region. The fluorescence spectra are shown below. Although the emission bands show some overlap with that of **YC23** over 500 nm, the excitation spectra are well separated, therefore spectral bleeding is not a concern for colocalization studies.

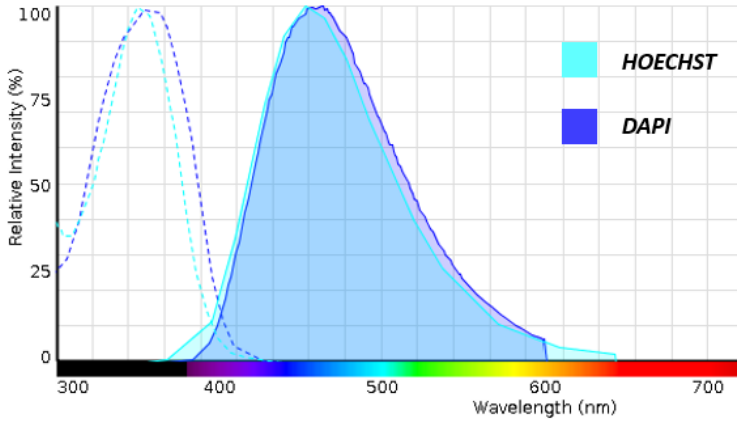

Figure 3.14 Overlaid excitation and emission spectra for the nuclear dyes DAPI and Hoechst (Thermofisher – Fluorescence SpectraViewer).

3.6.2 Cellular Labelling of H2B-dC10α with YC23 and DAPI

First, HeLa cells transfected with H2B-dC10α, as well as mock cells transfected with pcDNA, were labelled with 10 µM **YC23** for 45 minutes, followed by 1 µM DAPI for 15 minutes. The cells were then immediately imaged using a Nikon Ni-U Ratiometric fluorescence microscope without washing (see Experimental). The resulting images are shown in Figure 3.15.

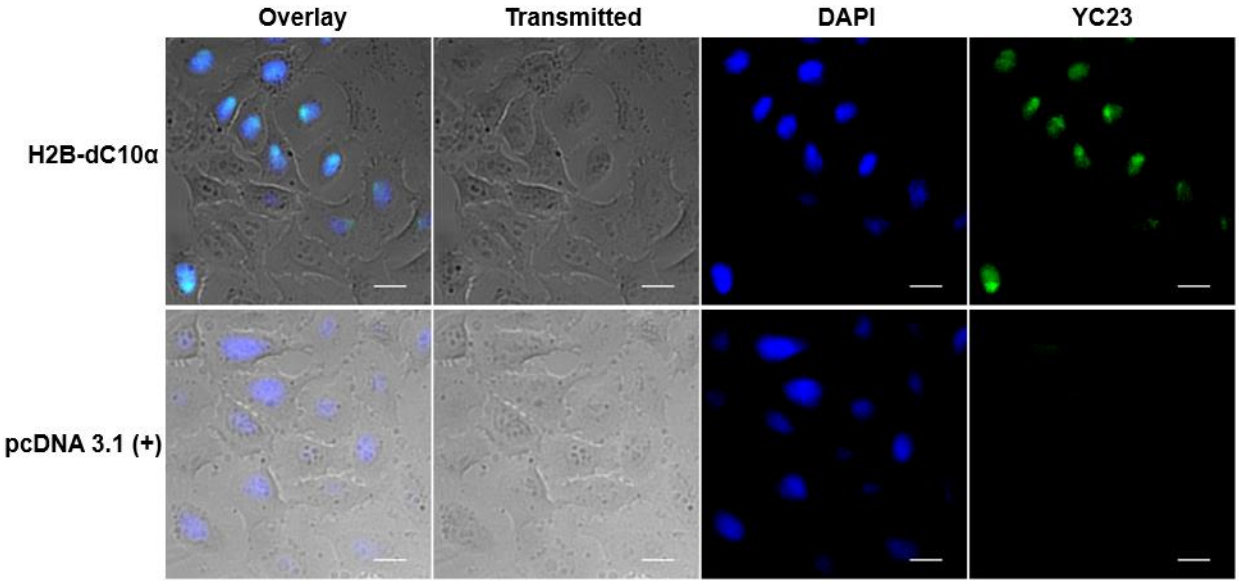

Figure 3.15 HeLa cells transfected with histone H2B-dC10α (top) or pcDNA 3.1 (+) (bottom) before labelling with **YC23** (10 μM) for 45 min followed by DAPI (1 μM) for 15 min. The DAPI channel was excited at 390 nm and observed in the 460-510 nm channel. **YC23** was excited at 485 nm and observed in the 535/45 nm channel. Scale bars: 20 μm.

The images obtained for cells transfected with H2B-dC10α are shown on the top row with cells transfected with pcDNA below. **YC23**, imaged in the green channel, was observed in several cells and appeared to be localized in the nucleus. Nuclear localization was confirmed by imaging DAPI in the blue channel and overlaying both images on the brightfield cell images. In the overlay image, it is clear that DAPI and **YC23** labelling overlay nearly perfectly; every cell that exhibits green fluorescence also shows co-localized blue fluorescence.

The most powerful conclusion drawn from these images comes from the mock cells. In these cells, which do not express the dC10α tagged POI, no green fluorescence is observed in the

YC23 channel after incubating with **YC23** labelling solution. This dark image shows that there is no background fluorescence on the timescale of the imaging experiment, even without washing.

3.6.3 Cellular Labelling of H2B-dC10α with YC23 and Hoechst

Although the cell images shown in Figure 2.10 provided strong evidence for our labelling method with **YC23**, they also showed that DAPI labelling was not as efficient as desired, as there are several cells whose nuclei were not labelled in the blue channel. As a result, the labelling experiment was redone under identical conditions, except the cells were stained with 8 µM Hoechst dye instead of DAPI. The images obtained are shown below in Figure 3.16.

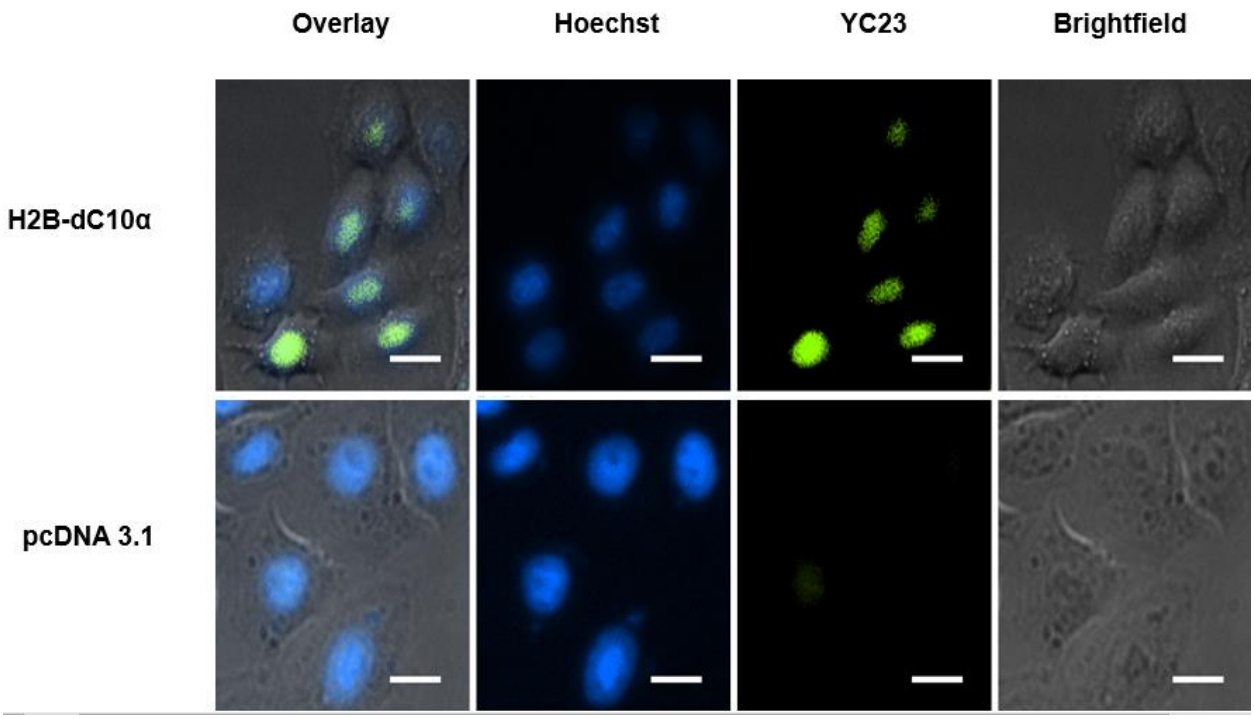

Figure 3.16 HeLa cells transfected with histone H2B-dC10α (top) or pcDNA 3.1 (+) (bottom) before labelling with **YC23** (10 µM) for 45 min followed by Hoechst (8 µM) for 15 min. The

Hoechst channel was excited at 390 nm and observed in the 460-510 nm channel. **YC23** was excited at 485 nm and observed in the 535/45 nm channel. Scale bars: 20 μm.

In this experiment, we observed much better nuclear labelling with Hoechst: nearly every cell imaged showed blue fluorescence in the nucleus. Of the 8 HeLa cells imaged in Figure 3.16(Top), 6 cells also showed green fluorescence in the nucleus. This clear colocalization, in addition to the lack of green fluorescence observed in the **YC23** channel of the mock cells (Figure 2.11, Bottom), shows the selectivity of labelling between **YC23** and our dC10α tag.

Although the surfactant F127 was used to assist in cellular uptake of our probe, ideally the method should perturb the native biology of the system as little as possible and this strong, ionic surfactant's effects on the cellular membrane and cell health could be detrimental. The cellular images shown below (Figure 3.17) were obtained *without* added surfactant. Although we observed weaker, less consistent labelling, these images show that selective labelling of our target protein is still possible without using a surfactant.

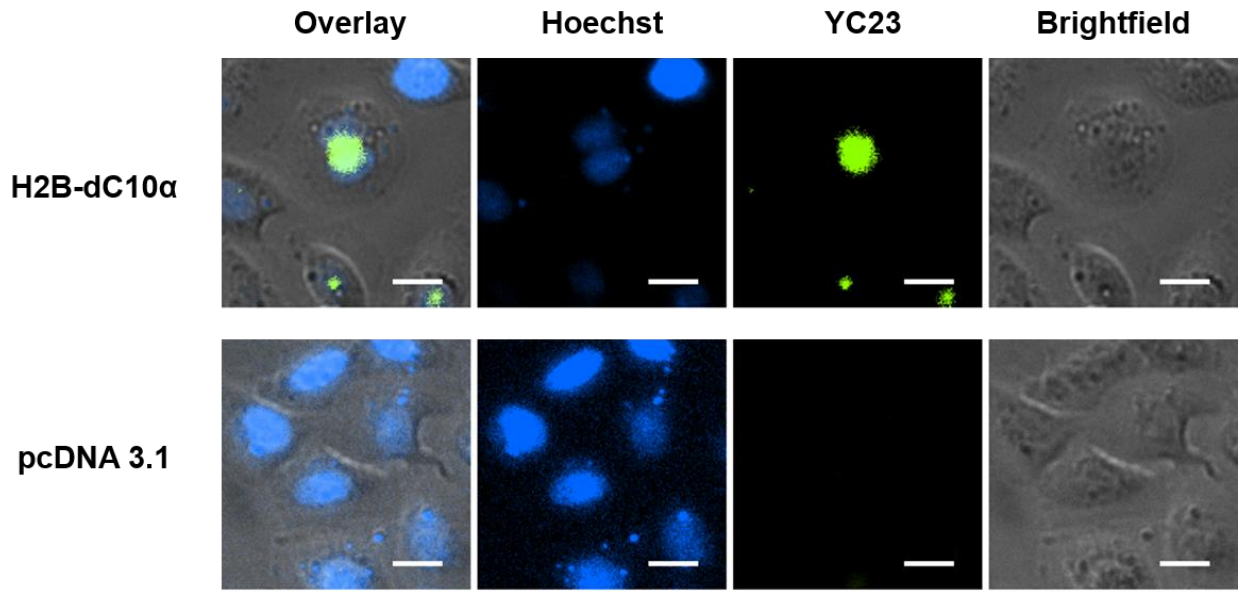

Figure 3.17 HeLa cells transfected with histone H2B-dC10α (top) or pcDNA 3.1 (+) (bottom) before labelling with **YC23** (10 μM) *without surfactant* for 45 min followed by Hoechst (8 μM) for 15 min. The Hoechst channel was excited at 390 nm and observed in the 460-510 nm channel. **YC23** was excited at 485 nm and observed in the 535/45 nm channel. Scale bars: 20 μm.

3.7 Conclusion

In conclusion, we have developed a new FlARe fluorogen based on the BODIPY fluorophore that exhibits efficient quenching by the pendant dimaleimide moiety and an ~800-fold fluorescent enhancement upon reaction with our dC10α tag. The reacted probe exhibits bright fluorescence and a quantum yield of nearly 30%. This probe shows high selectivity for our tag relative to other relevant intracellular thiols *in vitro*, and the strong covalent labelling is compatible with SDS-PAGE even under denaturing conditions. **YC23** shows negligible

cytotoxicity and was successfully applied to selectively label a nuclear histone H2B protein in living mammalian cells with no detectible background fluorescence.

FlARe probes have previously been used to label cell surface proteins as well as cytosolic proteins.[36,62] This green BODIPY-based FlARe probe adds to the diversity of application of the labelling method, showing selective protein labelling in living cells at the longest wavelength published by the Keillor group to date.

3.8 Experimental

3.8.1 Molecular Modelling

All calculations were performed using Gaussian 09. Density functional theory (DFT) was used to optimize the geometry of ground state structures (B3LYP functional and 6-31G(d) set. Time-dependent DFT (TD-DFT) calculations were then performed at the B3LYP/6-31G(d)/level with water as a solvent based on the optimized structure of the ground state.

3.8.2 Synthesis

All reagents and solvents were used as received unless otherwise stated. Dichloromethane, acetonitrile, methanol, and tetrahydrofuran were dried with a solvent purification system from LC Technology Solution Inc. All reactions were performed under inert atmosphere (e.g. N_2) in flame-dried apparatus unless otherwise stated.

Reactions were monitored by thin layer chromatography (TLC) using E. Merck silica gel 60F254 pre-coated aluminum plates. Components were visualized by illumination with a short-

wavelength or long-wavelength ultra-violet after which staining in $KMnO_4$, or ninhydrin solution followed by heating. Flash column chromatography was performed on ZEOCHEM® silica gel 60 (ECO 40-63 µm) using eluting solvents described in the following procedures.

Nuclear magnetic resonance (NMR) spectra were recorded in deuterochloroform at ambient temperature unless otherwise stated. Residual chloroform solvent peak was used as an internal standard: 7.26 ppm for ^{1}H and 77.16 for ^{13}C spectra.[70] The experiments were performed mainly on a Bruker Avance 400 Fourier Transform Spectrometer operating at 400 MHz for ^{1}H and at 100.6 MHz for ^{13}C.

EI-MS spectra were recorded on a Kratos concept mass spectrometer for both low-resolution and high-resolution mass spectra. ESI-MS spectra were recorded on a Waters Micromass Q-Tof mass spectrometer.

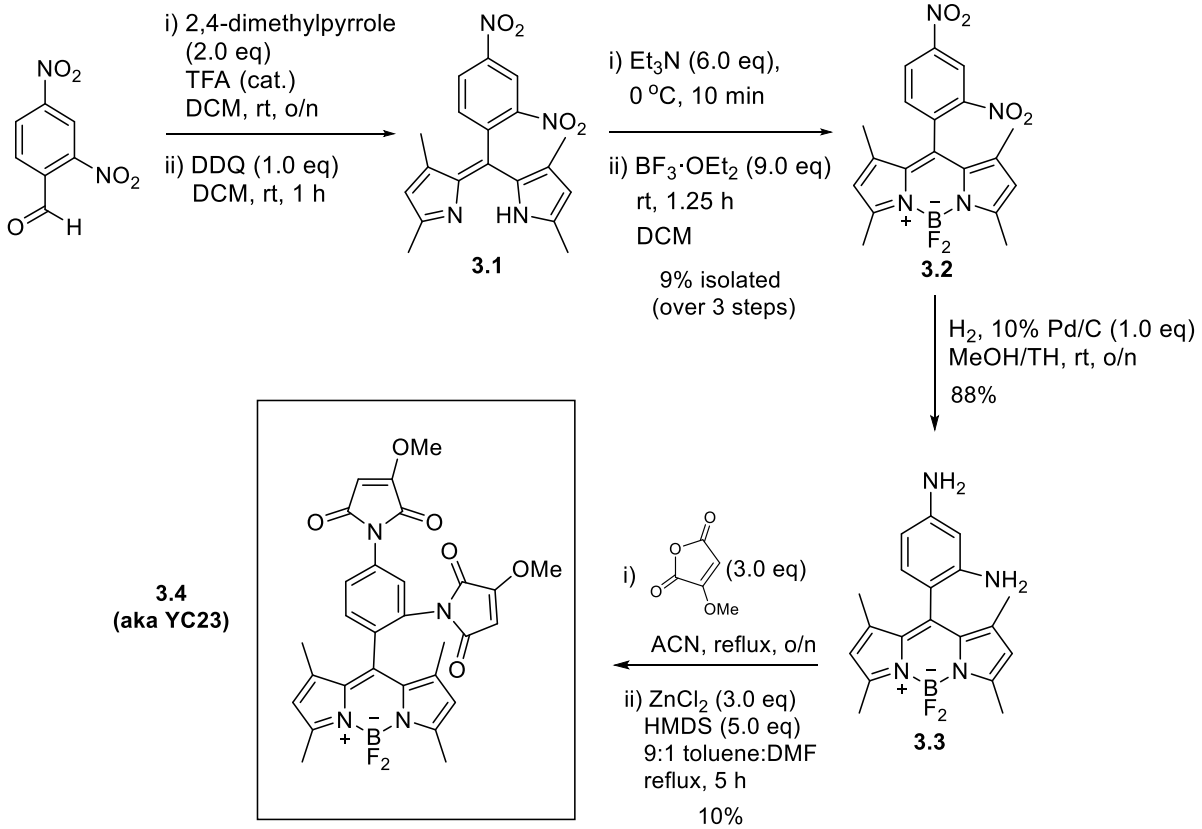

Figure 3.18 Overall synthesis of green BODIPY fluorogen **YC23**.

3.8.2.1 (Z)-2-((3,5-Dimethyl-2H-pyrrol-2-ylidene)(2,4-dinitrophenyl)methyl)-3,5-dimethyl-1H-pyrrole (**3.1**)

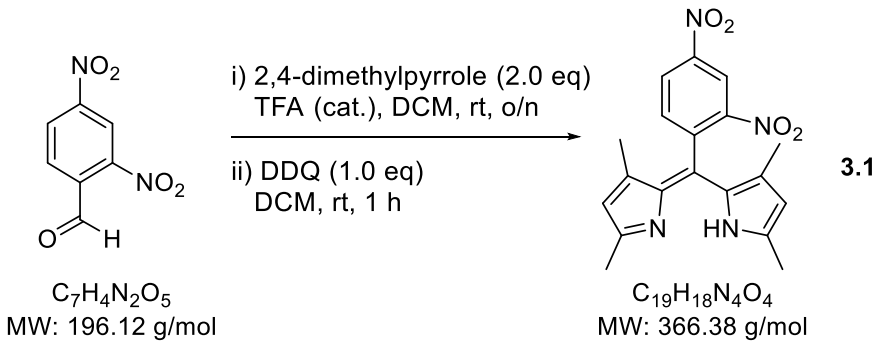

392 mg of 2,4-dinitrobenzaldehyde (2.0 mmol, 1.0 eq) and 412 µL of 2,4-dimethylpyrrole (4.0 mmol, 2.0 eq) were dissolved in 50 mL DCM under a N_2 atmosphere. One drop of TFA was

added and the solution was stirred at room temperature overnight in the dark. When monitoring by TLC showed complete consumption of aldehyde, a solution of 455 mg DDQ (2.0 mmol, 1.0 eq) in 10 mL DCM was added and stirring was continued for 1 h. The reaction mixture was washed with water, dried over $MgSO_4$, filtered to remove $MgSO_4$, and solvent was removed *in vacuo*. The crude residue was purified by short column chromatography (30 – 50 % EtOAc/hexanes) to give 850 mg of compound **3.1** as a brown solid (>100 % yield). ^{1}H NMR showed desired compound according to literature[53], as well as one major impurity, likely a triethylamine salt (see Appendix for spectra). The mixture was pushed forward in the next step without further characterization.

3.8.2.2 10-(2,4-Dinitrophenyl)-5,5-difluoro-1,3,7,9-tetramethyl-5H-dipyrrolo[1,2-c:2',1'-f][1,3,2]diazaborinin-4-ium-5-uide (**3.2**)

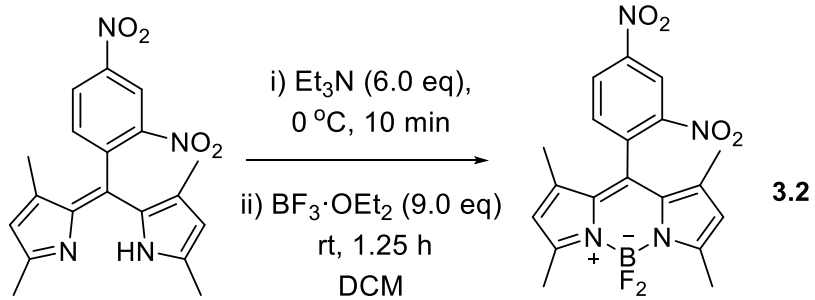

$C_{19}H_{18}N_4O_4$
MW: 366.38 g/mol

$C_{19}H_{17}BF_2N_4O_4$
MW: 414.18 g/mol

The dipyrrole mixture (734 mg, 2.0 mmol, assuming 100 % theoretical yield) was dissolved in anhydrous DCM and 1.7 mL of anhydrous Et_3N (12 mmol, 6.0 eq) was added under a N_2 atmosphere. The reaction mixture was cooled to 0 ºC and stirred for 10 minutes. To the cooled solution, 2.2 mL of boron trifluoride etherate (18 mmol, 9.0 eq) was added dropwise and the

solution was warmed to room temperature and stirred for another 1.25 h. DCM was removed *in vacuo* and the resulting residue was dissolved in ether and washed with 1:1 brine:1 M HCl. The organic layer was dried over $MgSO_4$, filtered and evaporated to dryness. The crude product obtained was purified by short column chromatography (30:70 EtOAc:hexanes) to yield 78 mg of dinitro BODIPY **3.2** as red crystals (0.19 mmol, 9 % yield over three steps). m.p. 216.9–218.6 ºC. ^{1}H NMR (400 MHz, $CDCl_3$): δ 8.99 (s, 1H), 8.62 (dd, *J* = 8.4, 2.3 Hz, 1H), 7.73 (dd, *J* = 8.4, 3.7 Hz, 1H), 6.03 (s, 2H), 2.57 (s, 6H), 1.37 (s, 6H). ^{13}C NMR (101 MHz, $CDCl_3$): δ 157.6, 149.2, 148.8, 141.5, 136.3, 133.2, 130.1, 128.2, 122.6, 120.4, 14.9, 14.3; LRMS (EI) *m/z* (%): 414.1 (M^+, 100 %); HRMS (EI): calcd for $C_{19}H_{17}BF_2N_4O_4$: 414.1311, found: 414.1333.

3.8.2.3 10-(2,4-Diaminophenyl)-5,5-difluoro-1,3,7,9-tetramethyl-5H-dipyrrolo[1,2-c:2',1'-f][1,3,2]diazaborinin-4-ium-5-uide (**3.3**)

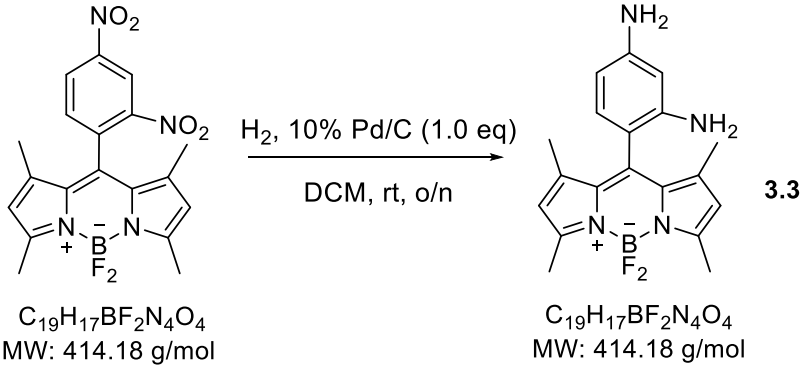

To a solution of the dinitro derivative 3.2 (78 mg, 0.19 mmol) in 4 mL 1:1 MeOH/THF was added 20 mg of Pd/C (10 % m/m, 0.19 mmol, 1.0 eq). The reaction mixture was stirred under balloon pressure H_2 at room temperature overnight. The reaction mixture was filtered through celite to remove the Pd/C. The filtrate was then evaporated to dryness to give 59 mg (0.14 mmol, 88 % yield) of compound **3.3**, which was used directly in the next step without further

purification. ^{1}H NMR (400 MHz, $CDCl_3$): δ 6.69 (d, *J* = 8.1 Hz, 1H), 6.20 (dd, *J* = 8.1, 2.0 Hz, 1H), 6.06 (d, *J* = 1.9 Hz, 1H), 5.96 (s, 2H), 3.73 (THF¸m, 12H), 2.54 (d, *J* = 12.5 Hz, 6H), 1.84 (THF, m, 12H), 1.63 (d, *J* = 16.9 Hz, 6H).^{13}C NMR (101 MHz, $CDCl_3$): δ 155.4, 148.5, 144.3, 143.5, 139.5, 132.0, 129.8, 121.0, 110.8, 107.0, 101.9, 77.5, 77.2, 76.8, 68.1 (THF), 45.8, 29.8, 25.7 (THF**)** 14.7, 14.0, 8.74; LRMS (EI) *m/z* (%): 354.2 ([M]$^{+}$, 100 %); HRMS (EI): calcd for $C_{19}H_{21}BF_2N_4$: 354.1827, found: 354.1831.

3.8.2.4 10-(2,4-Bis(3-methoxy-2,5-dioxo-2,5-dihydro-1H-pyrrol-1-yl)phenyl)-5,5-difluoro-1,3,7,9-tetramethyl-5H-dipyrrolo[1,2-c:2',1'-f][1,3,2]diazaborinin-4-ium-5-uide (**3.4** aka **YC23**)

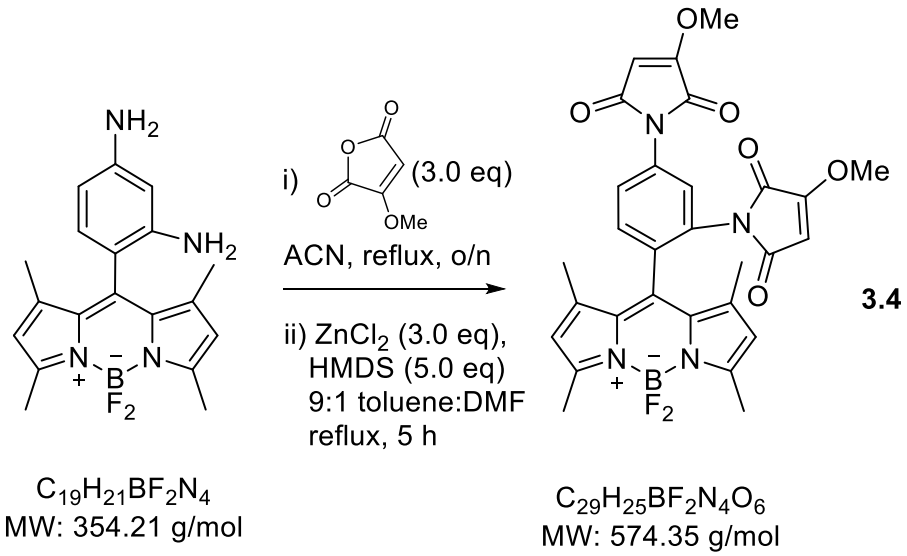

64 mg of 3-methoxymaleic anhydride (0.50 mmol, 3.0 eq) was added to a solution of 59 mg diamine **3.3** (0.17 mmol, 1.0 eq) in 1 mL anhydrous acetonitrile. The resulting mixture was heated to reflux overnight, after which the volatiles were evaporated under reduced pressure. The crude product was then triturated with minimal Et_2O three times, yielding the dimaleamic acid as an orange/red precipitate, which was used in the next step without further purification. The

dimaleamic acid and 68 mg of $ZnCl_2$ (0.50 mmol, 3.0 eq) were dissolved in 8 mL toluene–DMF (9:1). A dilute solution of 158 µL HMDS (0.75 mmol, 5.0 eq) in toluene was added over 20 min. The resulting mixture was then heated to reflux for 5 h, after which the volatiles were evaporated *in vacuo*. The resulting residue was dissolved in EtOAc and washed successively with 0.1 M HCl and saturated Na_2CO_3 (aq). This organic layer was dried over $MgSO_4$, filtered, and evaporated to dryness. The crude product was then purified by flash chromatography using a gradient elution system (2.5 - 5 % ACN/DCM) to give 8 mg of dimaleimide **3.4** (aka **YC23**) (0.013 mmol, 10 % yield). ^{1}H NMR (400 MHz, $CDCl_3$): δ (ppm) 7.76 (dd, J = 8.4, 2.0 Hz, 1 H), 7.58 (d, J = 2.1 Hz, 1 H), 7.49 (d, J = 8.4 Hz, 1 H), 5.94 (s, 2 H), 5.60 (s, 1 H), 5.36 (s, 1 H), 4.01 (s, 3 H), 3.88 (s, 3 H), 2.49 (s, 6 H), 1.58 (s, 6 H); ^{13}C NMR (100 MHz, $CDCl_3$): δ (ppm)168.4, 168.1, 164.2, 163.6, 160.8, 160.3, 156.0, 144.0, 135.8, 133.5, 133.3, 131.2, 131.2, 130.8, 126.6, 125.5, 121.6, 96.9, 96.8, 59.3, 59.0, 14.9, 14.7; LRMS (ESI) *m/z* (%): 575.0 ($[M+H]^+$), 597.0 ($[M+Na]^+$); HRMS (ESI): calcd for $C_{29}H_{25}BF_2N_4NaO_6$: 595.1735, found: 597.1738.

3.8.3 Fluorescent Enhancement Ratios

Emission spectra and fluorescence intensity measurements were recorded at 37 ºC with a Synergy H4 Hybrid Multi-Mode Microplate Reader with excitation and emission monochromators set at 9-nm bandpass. Fluorescence enhancement was measured for fluorogen **YC23** alone and for **YC23** after labelling with different concentrations of MBP-dC10α (Figure 2). Reaction mixtures of 25 µM **YC23** and 0, 2.5, 5, 12.5 20, or 25 µM MBP–dC10α in 50 mM HEPES buffer (pH 7.4) with 5 % DMSO were incubated at 37 ºC in the dark overnight, after which the fluorescence emission spectra were recorded (Figure 3.5). The ratio of fluorescence

intensity at maximum emission gave the fluorescence enhancement ratio. The excitation and emission spectra shown in Figure 3.4 were recorded for the reaction of 25 µM **YC23** with one equivalent of MBP–dC10α.

3.8.4 Kinetic Measurements

Protein labelling kinetics were studied by following the time-dependent fluorescence increase at 37 ºC using a Synergy H4 Hybrid Multi-Mode Microplate Reader with excitation and emission monochromators set at a 9-nm bandpass. The reaction was prepared in 50 mM HEPES buffer (pH 7.4) with 10 % DMSO. Solutions of MBP-dC10α were prepared in a 96-well plate and **YC23** in DMSO was added immediately before recording. The final concentrations of **YC23** and MBP–dC10α were both 25 µM in 50 mM HEPES buffer (pH 7.4) with 10 % DMSO and 250 µM TCEP. Samples were excited at 495 nm and fluorescence intensity was followed at 525 nm as a function of time. The time-dependent fluorescent data shown in Figure 3.6 were fitted by non-linear regression to the following second order equation:

$$[\mathrm{P}] = [\mathrm{dM}]_0 - \frac{1}{k_2 t + \frac{1}{[\mathrm{dM}]_0}}$$

where P is the fluorescent product, dM is the dimaleimide fluorogen **YC23**, k_2 is the second order rate constant and t is time. Kinetic reactions were performed in triplicate and reported as mean ± standard deviation. (868 ± 118 $M^{-1}min^{-1}$ for **YC23**).

3.8.5 Quantum Yield Measurements

Quantum yield experiments were performed based on protocol adapted from several literature sources.[4,5,6] Studies were conducted at 22 ^{o} C using a Cary Eclipse Fluorimeter and Cary 100 Bio UV-vis spectrometer. A standard solution of 0.1 mM fluorescein was prepared in 0.1 M NaOH. The sample of labelled protein was prepared by allowing a solution of **YC23** and MBP-dC10 (25 µM of each) to incubate overnight at 37 ºC in the dark in the presence of 250 µM TCEP and 10 % DMSO in 50 mM HEPES (pH 7.4). Unreacted **YC23** (25 µM in HEPES buffer with 250 µM TCEP, 10 % DMSO) gave no detectable fluorescence when excited at 498 nm.

The standard and reacted sample were diluted in buffer until their longest wavelength band reached a maximum absorbance of 0.1 (7 µM and 12.5 µM, respectively) and the intersection between the two absorbance spectra was found at 498 nm. All fluorescence spectra were subsequently obtained using λ_{ex} = 499 nm.

The linear equations obtained from Figure 3.8 – 3.11 are shown below:

3.8) Cell 1: $y = (12051 \pm 135\ M^{-1})x + (-0.0028 \pm 0.0006\ Au)$, $R^2 = 0.9994$

Cell 2: $y = (12072 \pm 127\ M^{-1})x + (-0.0018 \pm 0.0006\ Au)$, $R^2 = 0.9995$

3.9) Cell 1: $y = (7370 \pm 253\ M^{-1})x + (-0.0027 \pm 0.002\ Au)$, $R^2 = 0.9953$

Cell 2: $y = (6725 \pm 385\ M^{-1})x + (0.0016 \pm 0.0034\ Au)$, $R^2 = 0.9871$

3.10) Cell 1: $y = (175876 \pm 4281\ Au^{-1})x + (572 \pm 231)$, $R^2 = 0.9970$

Cell 2: $y = (176825 \pm 2275\ Au^{-1})x + (361 \pm 125)$, $R^2 = 0.9992$

---

[4] J. R. Lakowicz, *Principles of Fluorescence Spectroscopy*. 2nd ed.; Kluwer Academic/Plenum Press: New York, **1999**.
[5] C. Wurth, M. Grabolle, J. Pauli, M. Spieles, U. Resch-Genger, *Nat. Protoc.* **2013**, *8*, 1535.
[6] *A Guide to Recording Fluorescence Quantum Yields* by Jobin Yvon Ltd., Stanmore.

3.11) Cell 1: $y = (47943 \pm 1592\ Au^{-1})x + (112 \pm 99)$, $R^2=0.9956$

Cell 2: $y = (55247 \pm 2736\ Au^{-1})x + (-95 \pm 165)$, $R^2 =0.9892$.

3.8.6 Cell Viability

Cell viability was determined using the MTT assay previously described. HEK293T cells were seeded in a 96-well plate and incubated with 100 μL of culture medium with different amounts of the fluorogen **YC23** for 20 h. No fluorogen was added to the positive control and no cells were plated in the negative control. Portions of 25 μL of MTT solution (5 mg in 1 mL of Hanks' balanced salt solution) were added to the wells and the cells were further incubated at 37 ºC for 4 h. Solubilization solutions (100 μL) were then added, followed by incubation at room temperature in the dark overnight. The absorbance of each well was then measured using a plate reader at a wavelength of 570 nm with 690 nm as a reference.

3.8.7 Cellular Labelling

HeLa cells (5.25 × 105 cells) were plated onto 60-mm dishes and grown in Opti-MEM supplemented with 5 % FBS for 16 h before transfection. Cells were transiently transfected with histone H2B–dC10 or pcDNA3.1(+) (mock) by first incubating lipofectamine 2000 (10 μg) in Opti-MEM medium (300 μL) for 20 min. The lipofectamine 2000 solution was then incubated for 30 min with a solution of the plasmid (10 μg) in Opti-MEM medium (300 μL) for a final liopfectamine 2000 to DNA ratio of 1:1. Lastly, the HeLa cells were incubated in this lipofectamine 2000:DNA mixture for 24 h.

After transfection, the medium was removed and replaced with 8 μM Hoechst 33342 (Life TechnologiesTM) or 1 μM DAPI in the imaging solution for 15 min. Afterwards, the medium

was removed and replaced with 10 μM **YC23** in Live Cell Imaging Solution (Invitrogen) supplemented with F127 surfactant (0.1 % v/v) and DMSO (final concentration of 0.4 % v/v). Cells were incubated in this solution for 1 hour at 37 ºC. Afterwards, the medium was removed and replaced clear imaging solution and the cells were immediately observed on a Nikon Ni-U Ratiometric Fluorescence Microscope with a 40X/0.8 NA objective. The recorded images were subsequently analyzed with NIS-Elements software.

Chapter Four: Conclusions and Future Perspectives

4.1 A Red-Shifted BODIPY FlARe Probe

4.1.1 Goal

In Chapter Two we proposed to design, synthesize and evaluate a red-shifted BODIPY FlARe probe based on preliminary results obtained for Dr. Chen's compound **YC29**, which showed good kinetics, fluorescent enhancement, and red emission. We sought to achieve this by 1) improving the synthetic preparation of **YC29** to make enough material for thorough *in vitro* and *in cellulo* evaluation, 2) making synthetically accessible probes resembling **YC29** and 3) evaluating these probes *in vitro* and *in cellulo* to determine if they were comparable to **YC29**.

4.1.2 Results Achieved and Conclusions

Chapter Two presented several synthetic efforts towards improving the initial preparation of **YC29**. The original synthesis was very low yielding and was unable to be reproduced in the time available. The last precursor, compound **2.18**, was successfully synthesized; however, the final Boc deprotection step to yield **YC29** could not be achieved, due to TFA incompatibility with the BODIPY BF_2 core. An alternative, convergent synthetic route was discussed to potentially circumvent these synthetic issues by coupling the BODIPY derivative **2.22** with the NHdM10 moiety **2.21**. This coupling was attempted by S_NAr and palladium catalyzed Buchwald-Hartwig amination. Despite many efforts, no final compound was obtained. We propose that steric hindrance may prevent the final amination.

Due to the synthetic challenge of the second S_NAr coupling to 3,5-dichloroBODIPY, two simplified probes lacking the red-shifting *N*-methylaniline substituent were synthesized (**Ph-BODIPY-NHdM10-H** and **Ph-BODIPY-NHdM10-Cl**). Our kinetic evaluation confirmed the

negligible reactivity of these probes with glutathione, but also much lower fluorescent enhancements and second order rate constants of 82 and 353 $M^{-1}min^{-1}$ for the Cl and H analogue, respectively.

While these probes exhibited rather slow kinetics and low FEs compared to the 300-fold FE obtained for **YC29**, they were the most red-shifted of the Keillor FlARe probes to date (max λ_{em} = 585 nm) and therefore they were applied to the *in cellulo* labelling of a dC10α-tagged nuclear protein, histone H2B. No selective labelling was observed; fluorescence in the orange channel was observed equally in the cells transfected with target protein as the non-transfected mock cells. Further, this fluorescence was not localized in the nucleus, but rather appeared to be cytosolic. This suggested to us that while the probes are cell permeable, they exhibit background fluorescence due to poor quenching and their reaction with the dC10α-tagged POI is too slow for cellular imaging, even when labelling time was increased to 3 h.

4.1.3 Future Perspectives

Further alternative synthetic methods to prepare **YC29** should be considered. Firstly, there may be a palladium catalyst capable of coupling such bulky partners and if more time were available, more catalytic systems could be screened. The original linear preparation of **YC29** may also be feasible if a different protecting group strategy were employed and alternative maleamic acid ring closing conditions could be used, under which BODIPY would be stable. Notably, the Cbz protecting group likely could not be used as it would be removed during the nitro group reduction step. A protecting group such as acetyl, which is removed under basic conditions, may be a solution. Ring closure mediated by HMDS and $ZnCl_2$, as used to prepare NHdM10, should be attempted in the original **YC29** route, as the compound was unstable to $NaOAc/Ac_2O$.

4.2 A Green BODIPY FlARe Probe

4.2.1 Goal

The objective for Chapter Two was to 1) design, synthesize, and evaluate a green BODIPY FlARe probe, which would be red-shifted compared to previous dansyl (UV) and coumarin (blue) FlARe probes[41,46] and compatible with the green channel available on most fluorescence microscopes. And further, 2) to apply this probe to the selective labelling of a target protein *in cellulo*.

4.2.2 Results Achieved and Conclusions

Compound **YC23** was designed based on Nagano's maleimide probes and modelled computationally to predict PeT quenching,[52] and was shown to be efficiently quenched experimentally. After reaction with our dC10α tagged target protein (MBP) the compound underwent an impressive 800-fold fluorescence enhancement and a second order rate constant of 868 $M^{-1}min^{-1}$ was calculated for the addition reaction. Maximum excitation was determined to be 495 nm with an emission maximum at 525 nm, putting the fluorogen in the green range. Additionally, a quantum yield of 27% was determined for the reacted fluorogen. **YC23** showed negligible background reactivity with cellular thiols and exhibited selectivity for the POI by SDS page gel analysis.

YC23 showed no significant *in cellulo* toxicity and was successfully applied to the cellular labelling of a dC10α-tagged nuclear protein histone H2B in HeLA cells. **YC23** was shown to be cell permeable and exhibit bright, selective fluorescence for the target protein only in the nuceli, as determined by colocalization using a Hoecsht nuclear stain. In the absence of the target protein, in cells transfected with pcdna, no significant labelling was observed.

Much of the work included in this chapter was published as a communication in Angewandte Chemie International Edition (2018).[53]

4.2.3 Future Perspectives

While co-staining HeLa cells with a nuclear dye is useful in showing compartmentalization (i.e. showing that fluorescence is localized within the nuclei), this method does not prove that **YC23** is labelling our target protein in cells, and therefore does not show target validation. A more rigorous approach would be to co-stain using immunofluorescent methods, tagging our dC10-tagged POI with a specific antibody (both in cellular imaging experiments and SDS-PAGE gel analysis) to confirm our target. Future analysis should include this control.

Additionally, our most successful imaging shown used a strong surfactant, F127, to improve cell membrane permeability. The effect of this surfactant on cell viability should be analyzed further, or our method should be optimized without using a surfactant to perturb the native biology of the cell as little as possible. In terms of cellular health, cell viability should also be investigated in the presence of dC10-tagged target proteins. This control would show if the di-Cysteine tag itself has a negative impact on cell health and function.

Finally, driven by the initial success of this BODIPY fluorophore, it may be useful to demonstrate the broad scope of our labelling method, for example, by also showing labelling of a tagged cytosolic protein. We would also like to test **YC23** with a new, more reactive cysteine tag, as discussed in the following section.

4.3 A New dC10 Tag for Improved Selectivity and Labelling

The selectivity of the FlARe method relies on the kinetic advantage of reaction of the dimaleimide moiety with the dC10α tag over off-target reactions with other biological thiols.

Maleimide reactivity has been optimized in the Keillor group (as discussed in Chapter One), leading to the discovery of the methoxy substituted and isopropyl substituted maleimides as our lead compounds.[44] Alternatively, increasing the reactivity of the tag would also increase the selectivity of the labelling, as well as reduce cellular labelling times required. Keillor group members Dr. Miroslava Strmiskova and Kelvin Tsao very recently published a newly engineered dC10α sequence called dC10* that was shown to react nearly an order of magnitude faster than the dC10α parent sequence shown in this thesis.[40]

Through site-directed mutagenesis, 21 variants to the parent sequence 'LS**A**AE**C**AAREAA**C**RE**AA**ARAGGK' were expressed, bearing mutated residues in proximity of the two cysteine residues. The triple mutant 'LS**K**AE**C**AAREAA**C**RE**RK**ARAGGK' was found to be the most reactive. Introduction of positively charged residues was hypothesized to stabilize the thiolate form of the cysteine residues, thereby decreasing their pK_α and leading to a greater proportion of the reactive thiolate form. Typical peptide bound cysteine residue pK_α values range between 7.4 – 9.1;[76,77] however, this can be dramatically altered by the environment, as demonstrated by the low pK_α (3 - 4) of the active site thiol in cysteine proteases.[78]

*4.3.1 Future work with dC10**

This new tag could greatly improve the application of our **YC23** compound, either by improving the contrast obtained in cellular imaging or by allowing for much shorter labelling reaction times. Further, dC10* may help overcome the problems observed with the potential probes **Ph-BODIPY-NHdM10-H/Cl**, which suffered from slow kinetics with the dC10 tag and therefore were not viable for cellular imaging.

In future investigations, the FlARe probes discussed in this thesis should be re-evaluated kinetically for their reaction with dC10*. If a significant increase in second order rate constants is observed, the probes should be re-evaluated *in cellulo* as well. Further, in the future all FlARe probes should be evaluated with dC10*-tagged test proteins. While we currently have access to the H2B-dC10* fusion, a fusion to a cytosolic and extracellular POI would also be beneficial for demonstrating the scope of our labelling method.

4.4 Potential New Red Flare Probes

The Keillor group has made significant progress over the years toward creating a toolkit of FlARe probes whose emission spectra overlap with the three main channels of fluorescence microscopes: blue, green, and red. We currently have published a blue channel FlARe probe based on coumarin,[62] and now the green channel **YC23** probe. To complete this toolkit, we remain very eager to develop a successful red FlARe probe.

The initial success with incorporating the BODIPY fluorophore into our FlARe probe design showed us that new substituted BODIPYs should be investigated. In this Thesis, we have shown impressive fluorescent enhancements for **YC29** and **YC23**, and to a lesser extent **Ph-BODIPY-NHdM10-Cl/H.** Red fluorescent BODIPY compounds should be investigated in the literature and their orbital energies modelled computationally in order to predict the probability of PeT quenching. Specifically, we would like to look at new substitution patterns (such as 3,7) to prevent possible steric clashing between the wavelength-tuning substituent and the NHdM10 portion. For example, an indazole BODIPY was published very recently (shown below) with a maximum emission at 634 nm, high extinction coefficient (126,200 $M^{-1}cm^{-1}$) and quantum yield (62%).[79] Our NHdM10 portion could be added at the open 7 position.

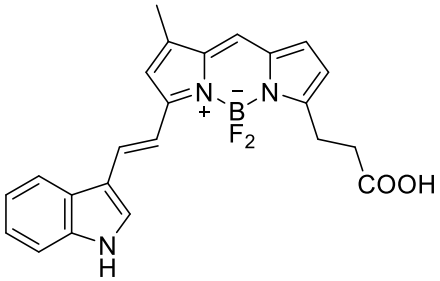

Figure 4.1 Potential red fluorophore, indazole BODIPY (λ_{em}=634 nm).

Additionally, Boron-azadipyrromethene (aza-BODIPYs), where C8 is replaced with N, have been shown to red-shift emission by ~100 nm.[80] This could provide a smaller scaffold without appending large, conjugated substituents. With the popularity of the BODIPY fluorophore only increasing and showing no sign of slowing down, particularly for NIR applications, the possibilities for red FlARe probes are nearly endless.

4.5 Conclusion

In the development of new small molecule labelling agents, every failed compound is as valuable as every successful probe created. Each compound helps to guide the design of future FlARe probes.

Appendix: NMR Spectra

Chapter Two NMR Spectra

Compound **2.1**

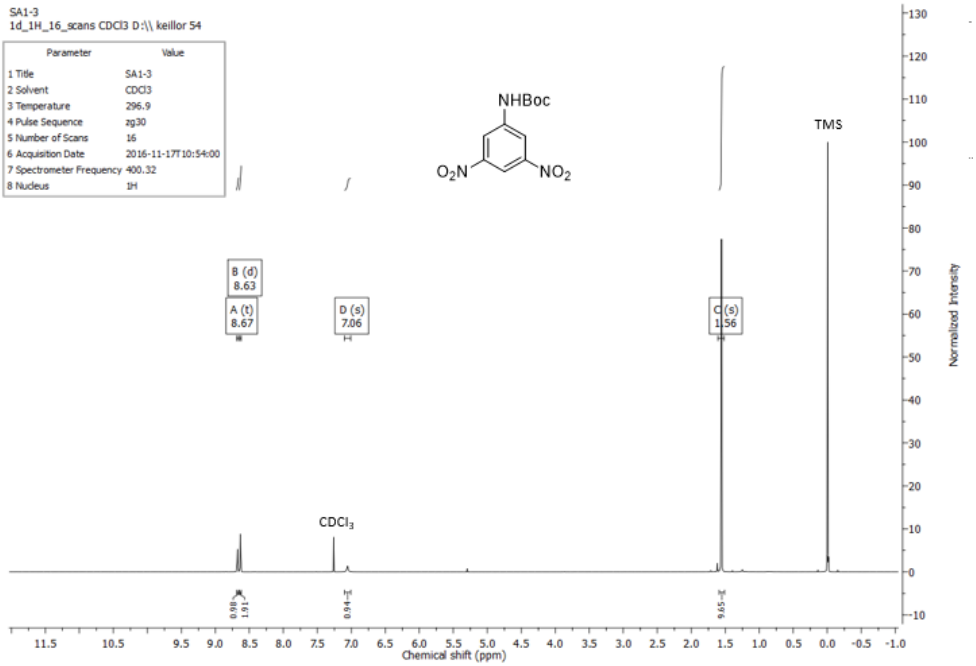

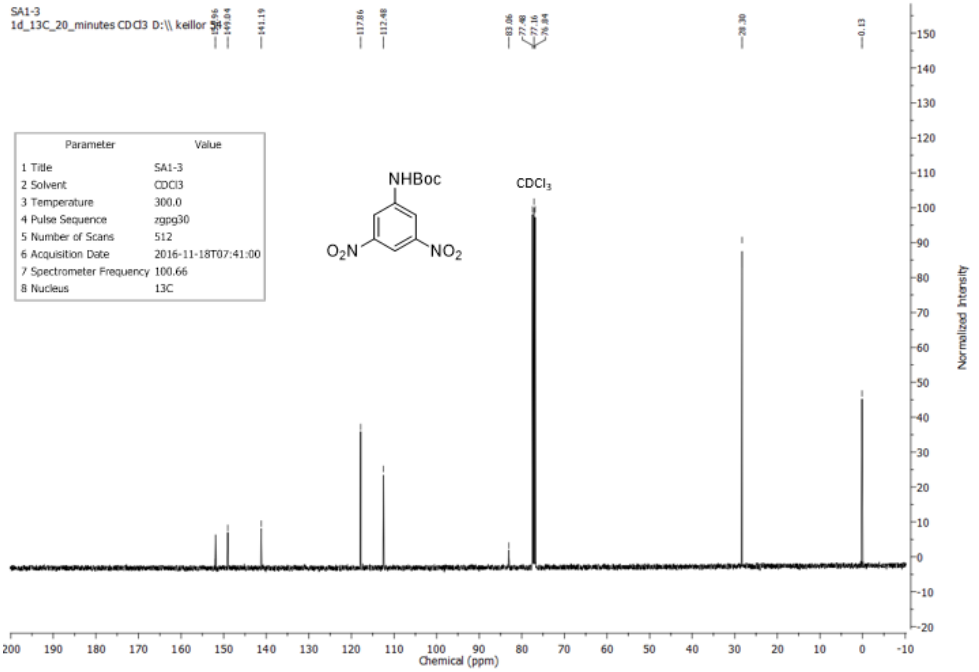

Compound **2.13**

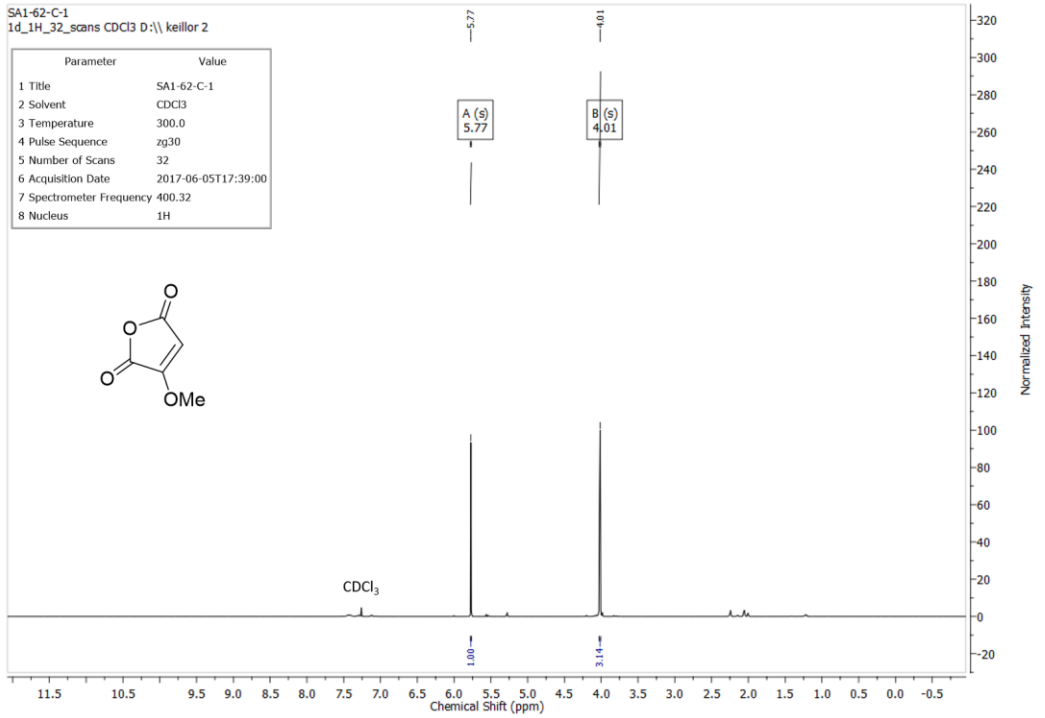

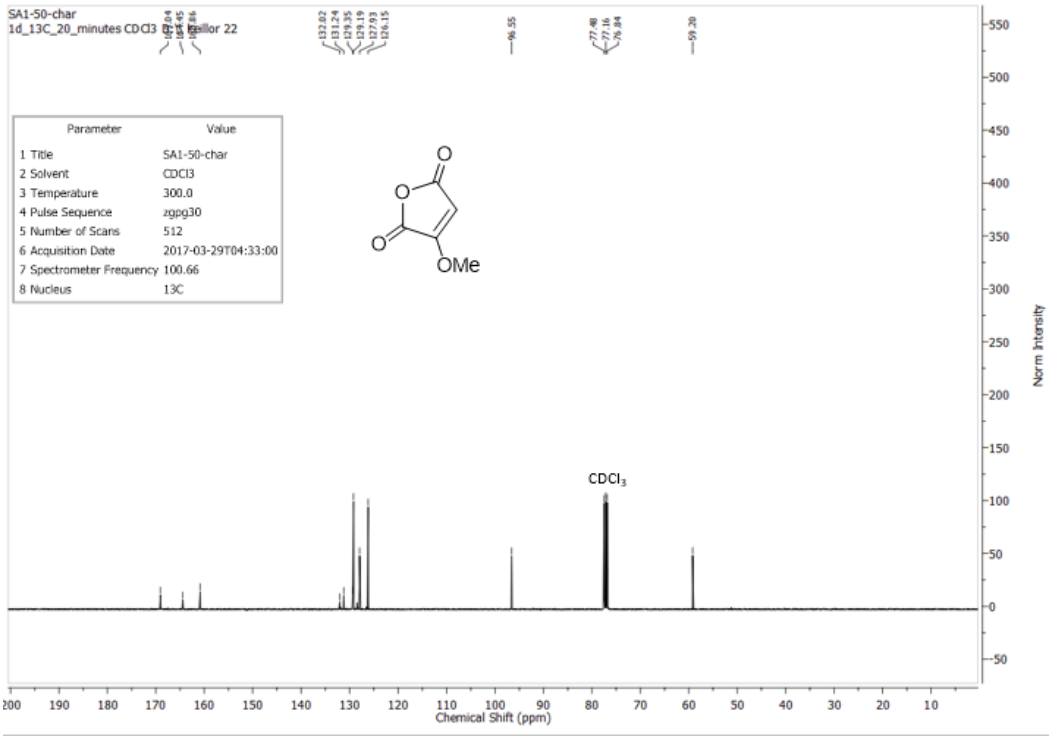

Compound **2.14**

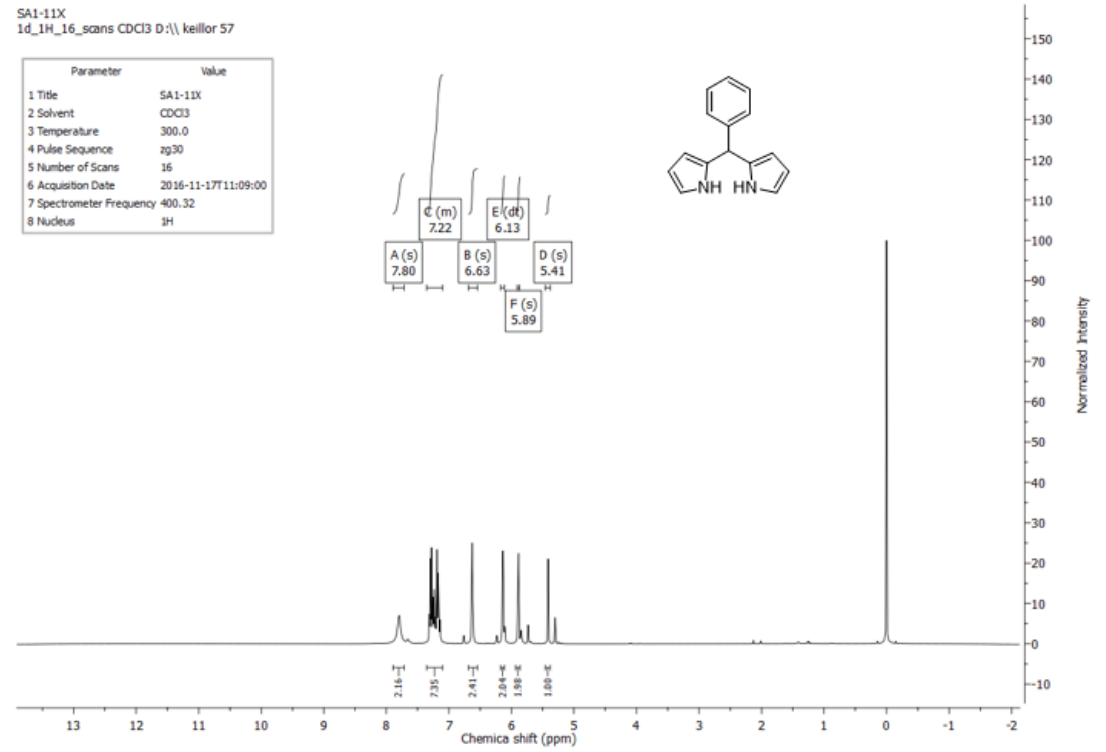

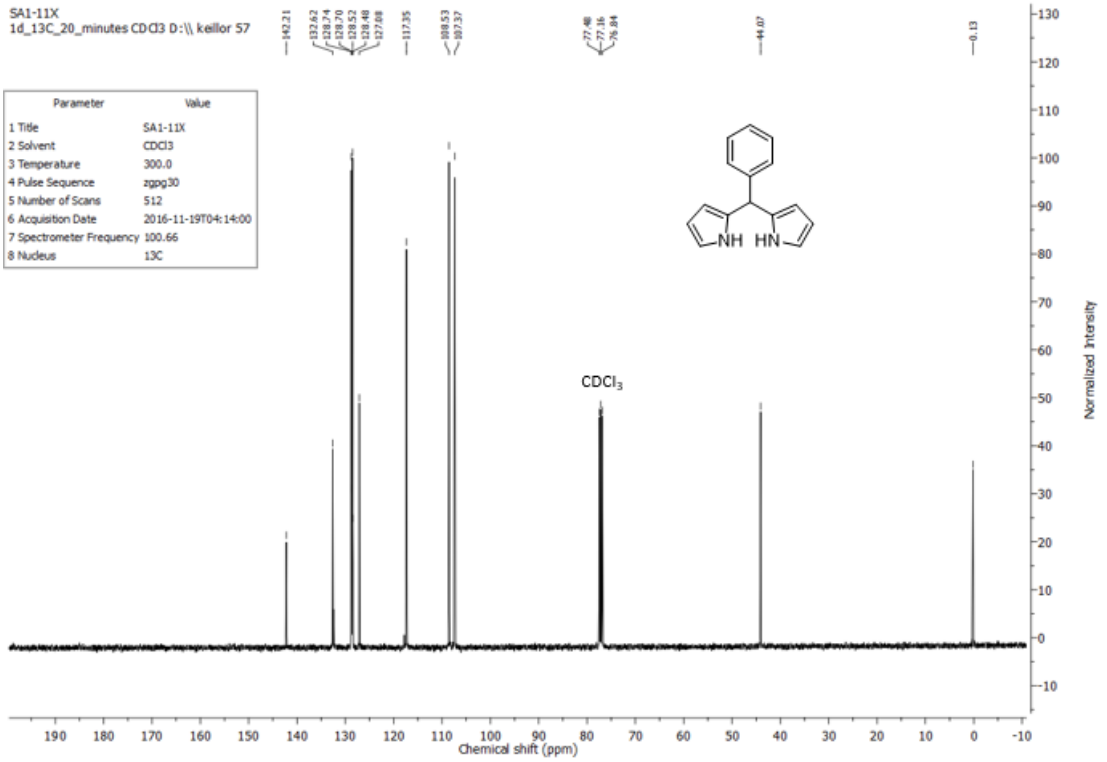

Compound **2.16**

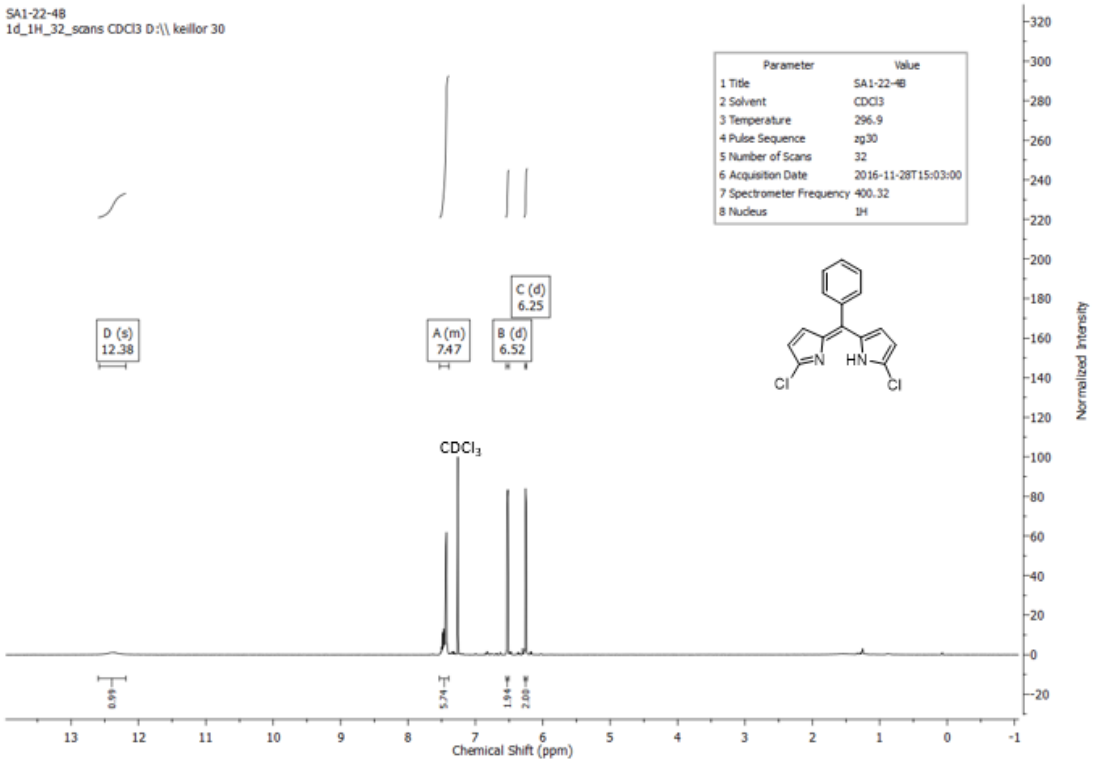

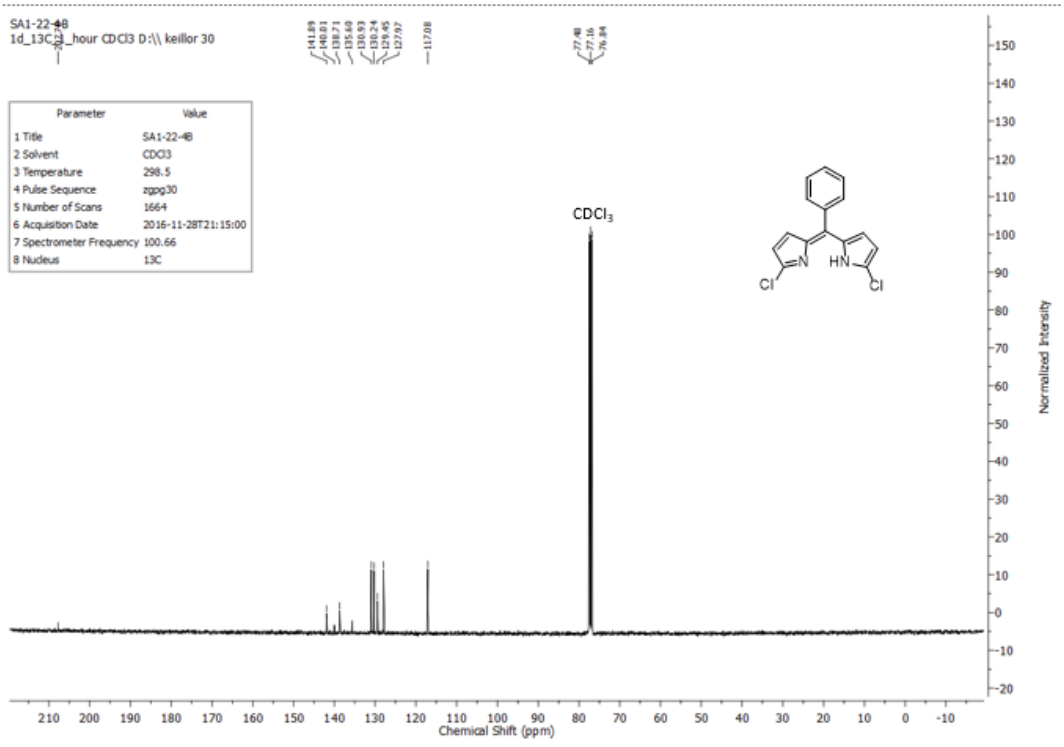

Compound **2.17**

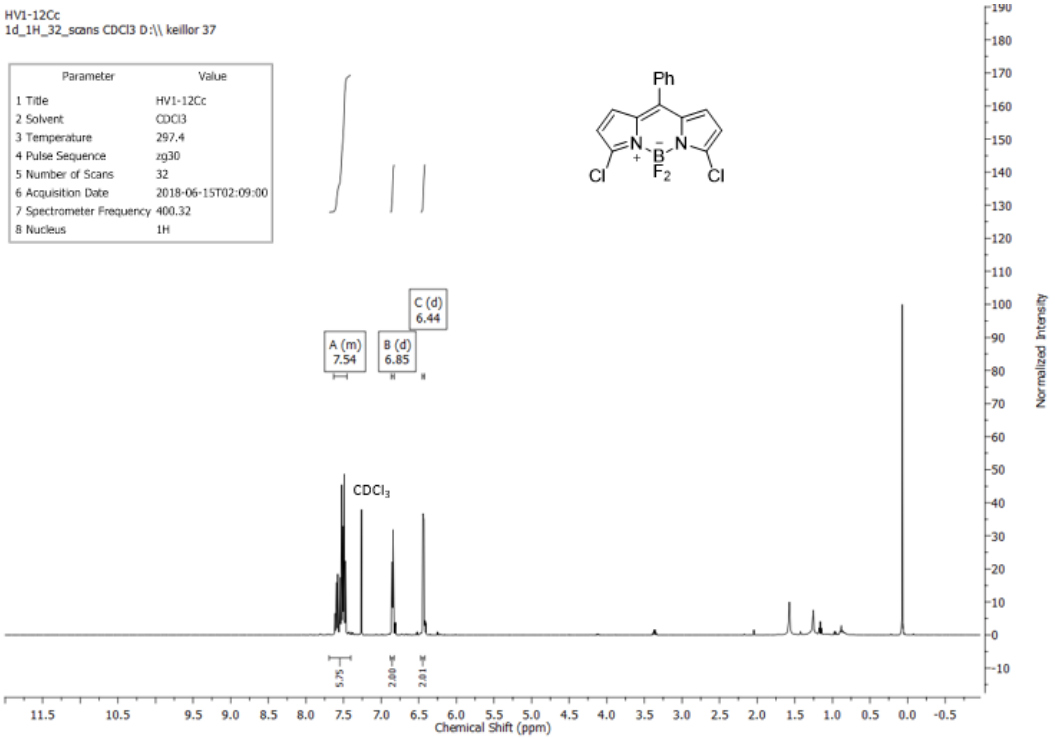

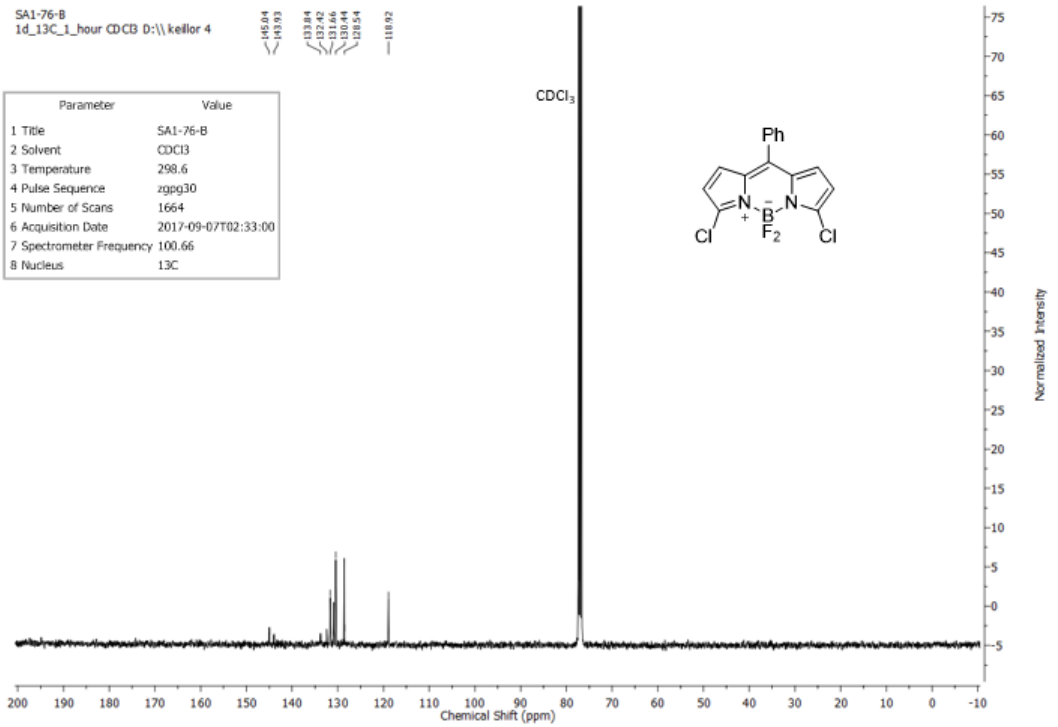

Compound **2.3**

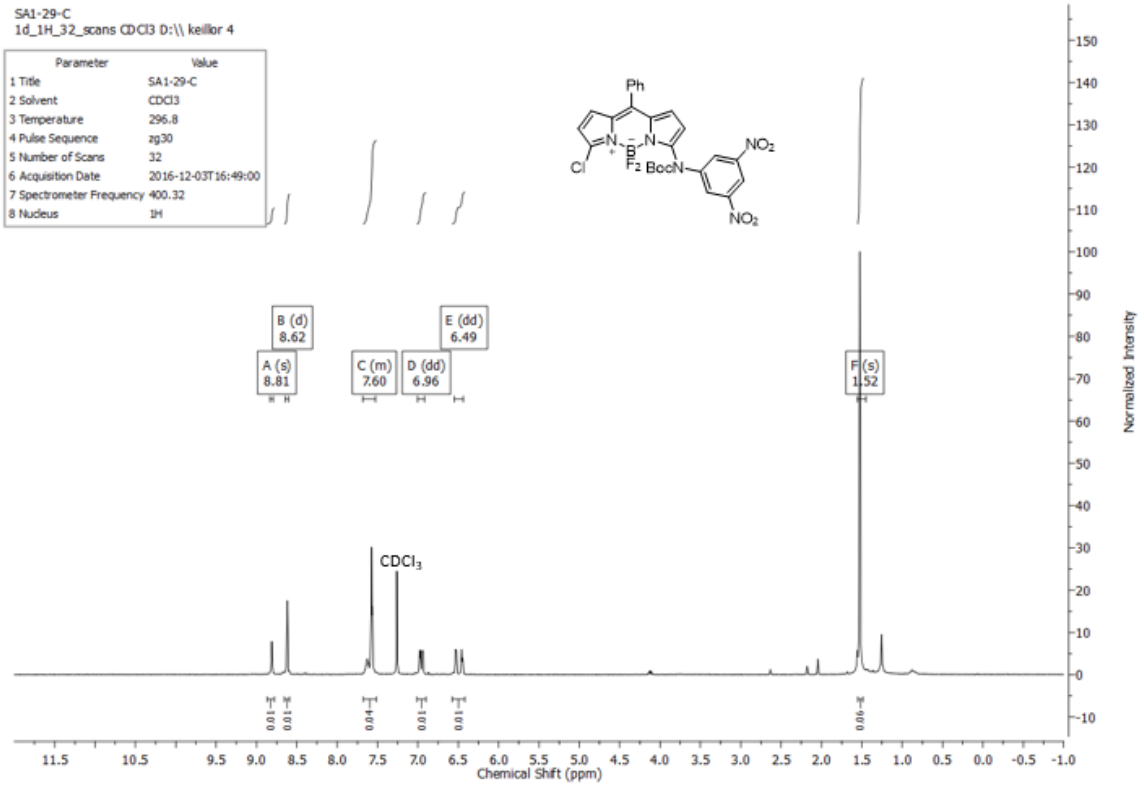
SA1-29-C
1d_1H_32_scans CDCl3 D:\\ keillor 4
Parameter Value
1 Title SA1-29-C
2 Solvent CDCl3
3 Temperature 296.8
4 Pulse Sequence zg30
5 Number of Scans 32
6 Acquisition Date 2016-12-03T16:49:00
7 Spectrometer Frequency 400.32
8 Nucleus 1H
Ph
Cl
BocN
NO2
NO2
B (d) 8.62
A (s) 8.81
C (m) 7.60
D (dd) 6.96
E (dd) 6.49
F (s) 1.52
CDCl3
Chemical Shift (ppm)
Normalized Intensity

Compound **2.4**

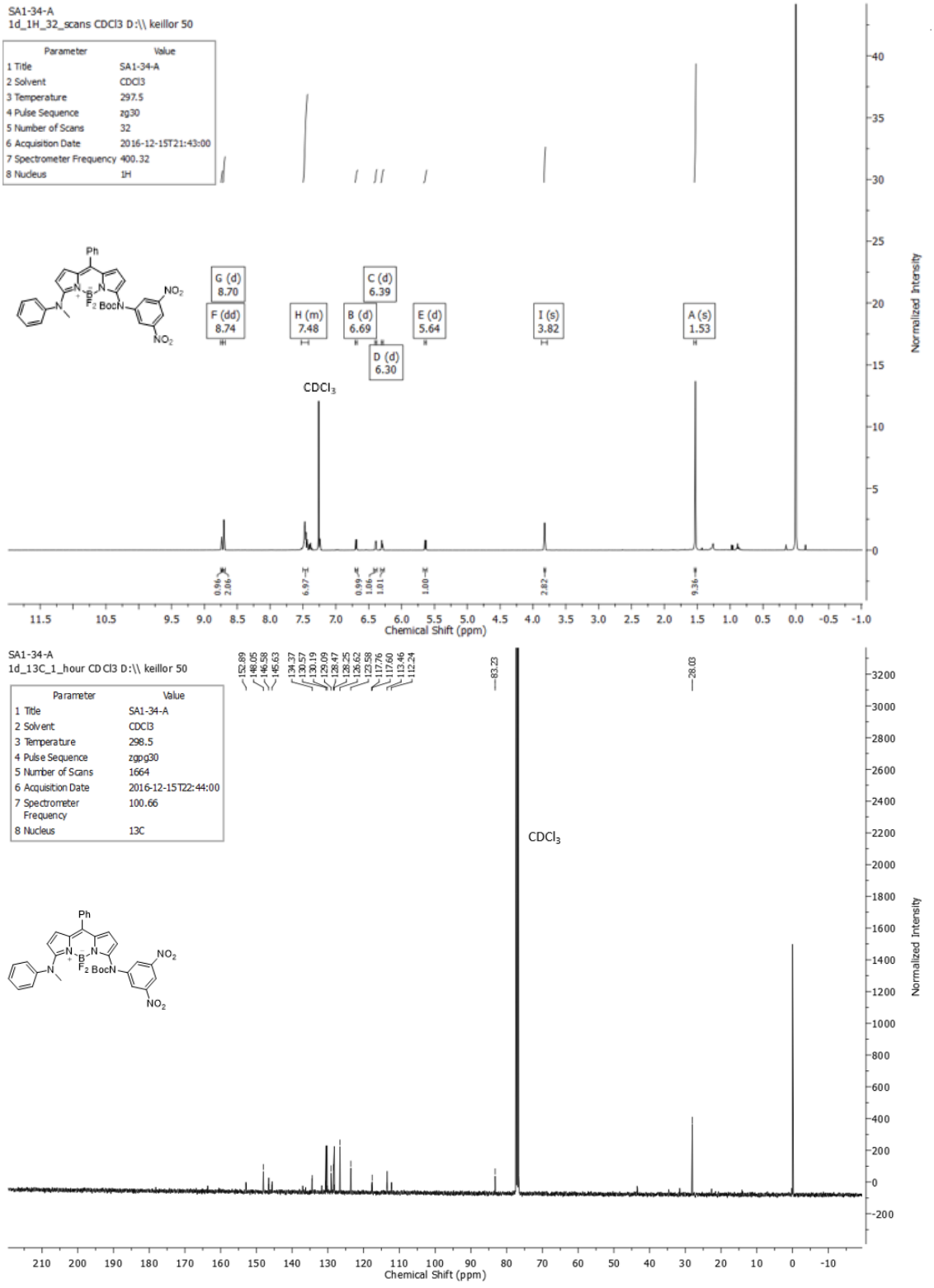
SA1-34-A
1d_1H_32_scans CDCl3 D:\\ keillor 50
Parameter Value
1 Title SA1-34-A
2 Solvent CDCl3
3 Temperature 297.5
4 Pulse Sequence zg30
5 Number of Scans 32
6 Acquisition Date 2016-12-15T21:43:00
7 Spectrometer Frequency 400.32
8 Nucleus 1H
G (d) 8.70
F (dd) 8.74
H (m) 7.48
C (d) 6.39
B (d) 6.69
D (d) 6.30
E (d) 5.64
I (s) 3.82
A (s) 1.53
CDCl3
Chemical Shift (ppm)
Normalized Intensity
SA1-34-A
1d_13C_1_hour CDCl3 D:\\ keillor 50
Parameter Value
1 Title SA1-34-A
2 Solvent CDCl3
3 Temperature 298.5
4 Pulse Sequence zgpg30
5 Number of Scans 1664
6 Acquisition Date 2016-12-15T22:44:00
7 Spectrometer Frequency 100.66
8 Nucleus 13C
152.89
146.05
146.58
145.63
134.37
130.57
130.19
129.09
128.47
128.25
126.62
123.58
117.76
117.60
113.46
112.24
83.23
28.03
CDCl3
Chemical Shift (ppm)
Normalized Intensity

Compound **2.5**

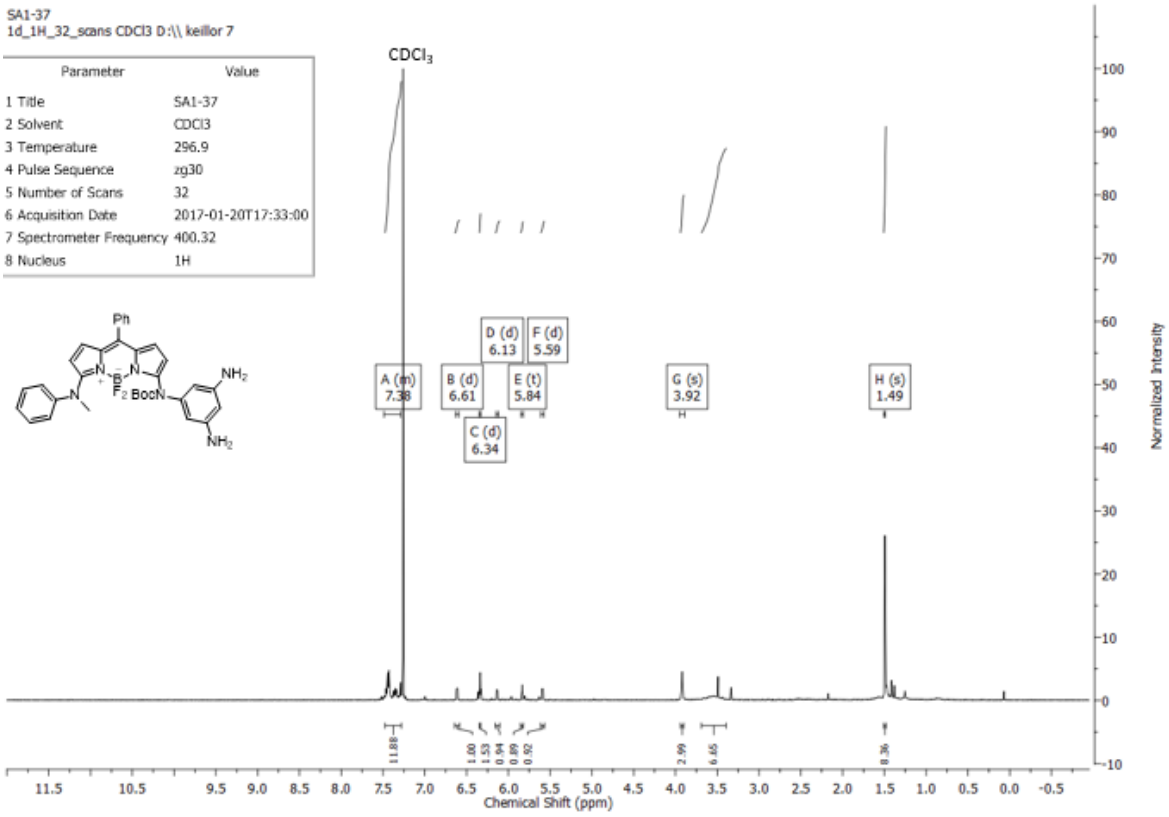
SA1-37
1d_1H_32_scans CDCl3 D:\\ keillor 7
Parameter Value
1 Title SA1-37
2 Solvent CDCl3
3 Temperature 296.9
4 Pulse Sequence zg30
5 Number of Scans 32
6 Acquisition Date 2017-01-20T17:33:00
7 Spectrometer Frequency 400.32
8 Nucleus 1H
CDCl3
A (m) 7.38
B (d) 6.61
C (d) 6.34
D (d) 6.13
E (t) 5.84
F (d) 5.59
G (s) 3.92
H (s) 1.49
Ph
BocN
NH2
NH2
Normalized Intensity
Chemical Shift (ppm)

Compound **2.18**

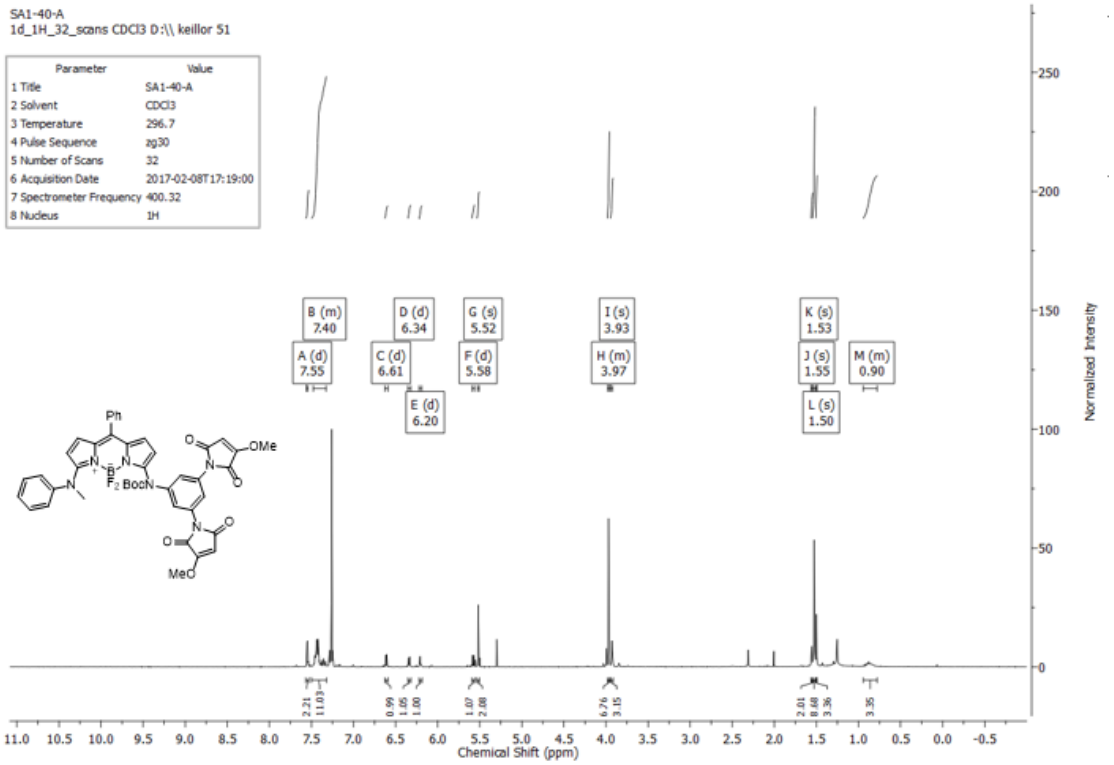

Compound **2.20**

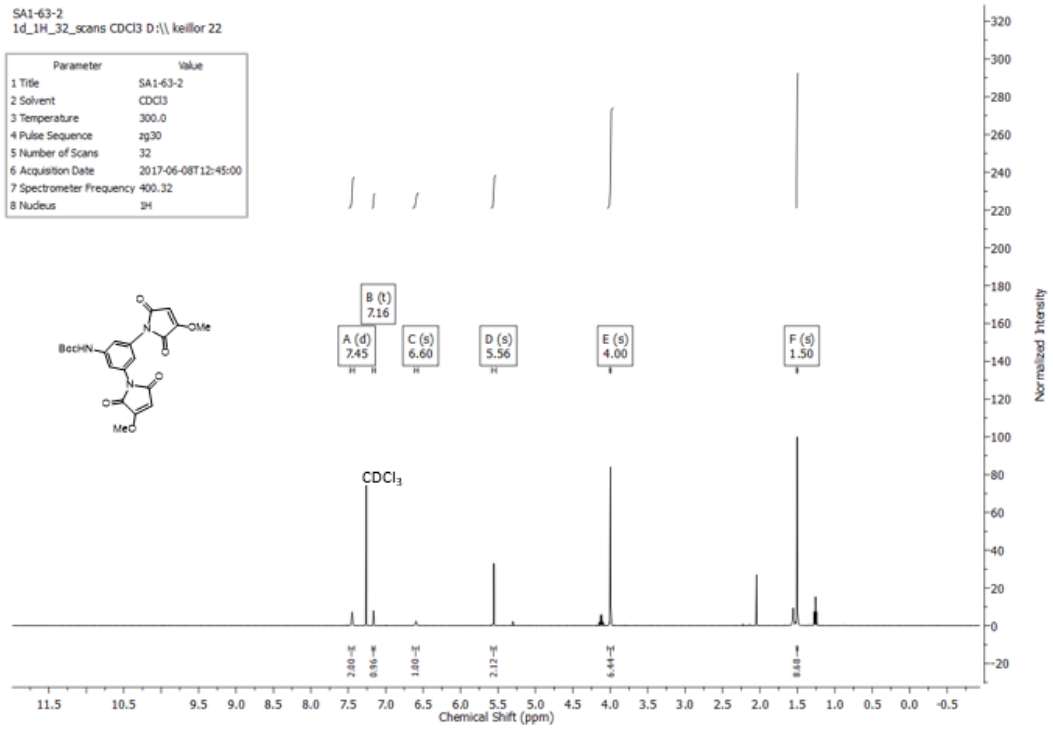

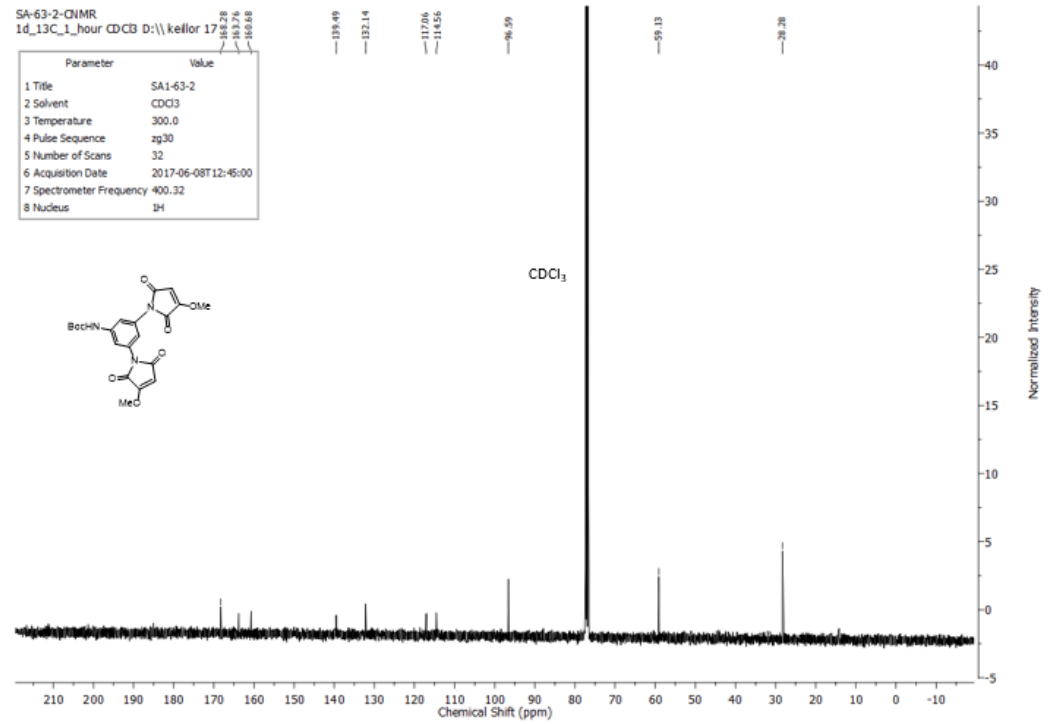

Compound **2.21**

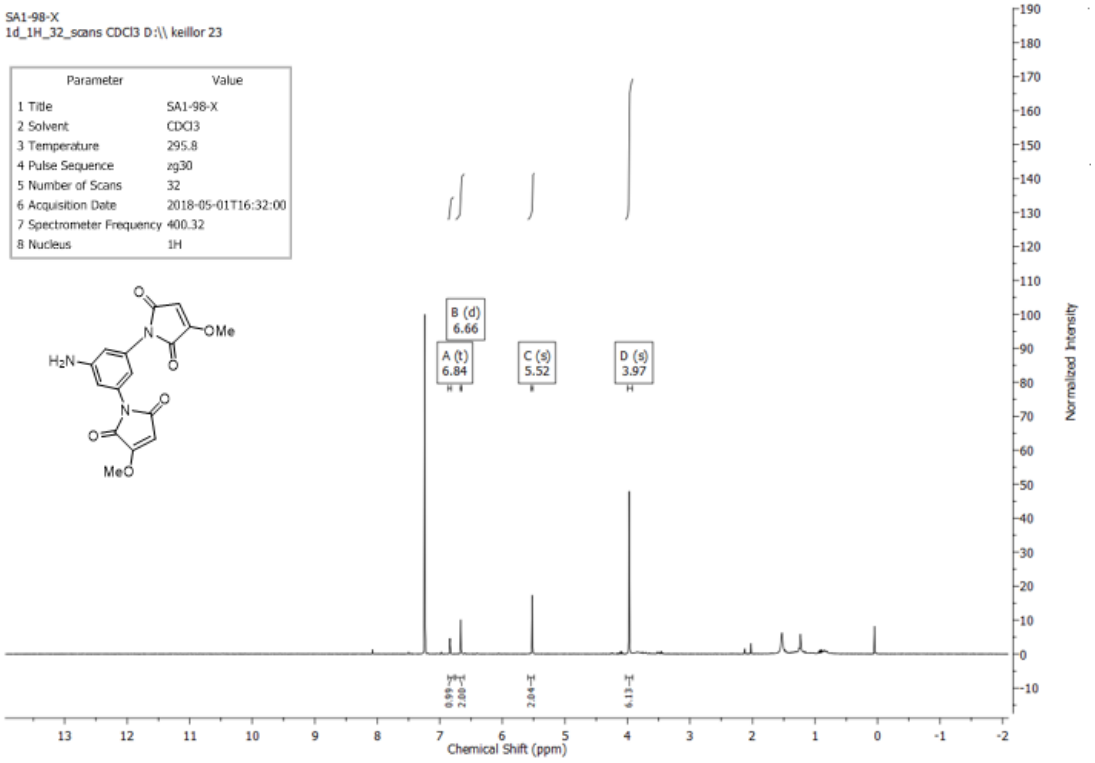

Compound **2.22**

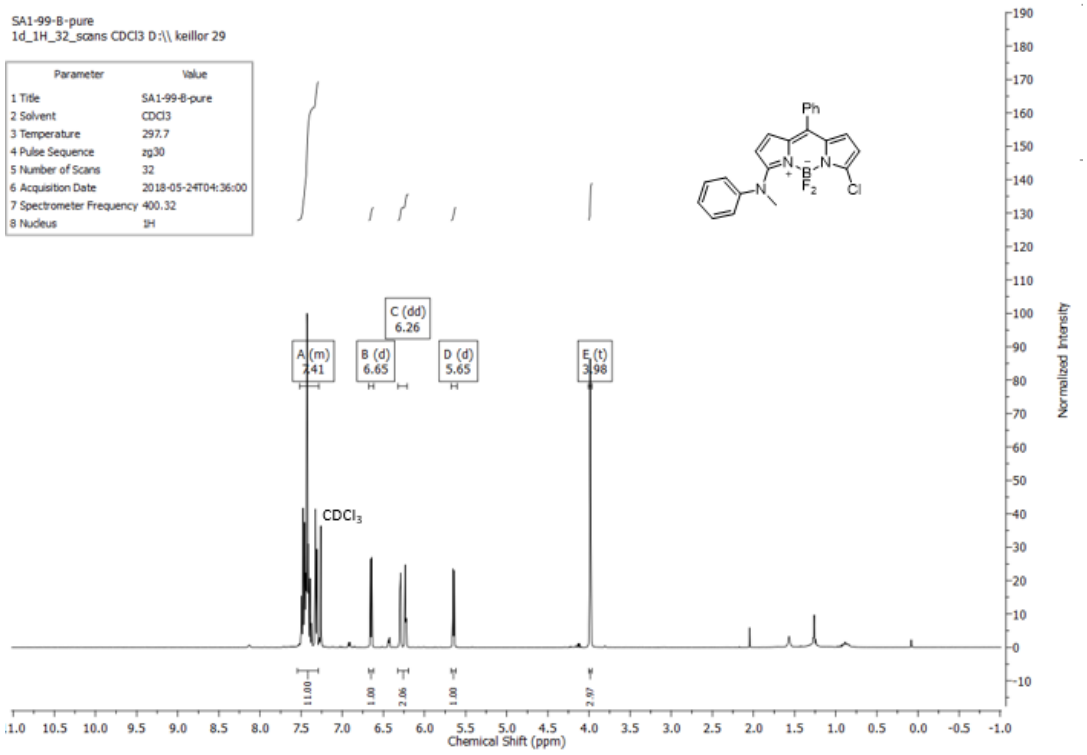

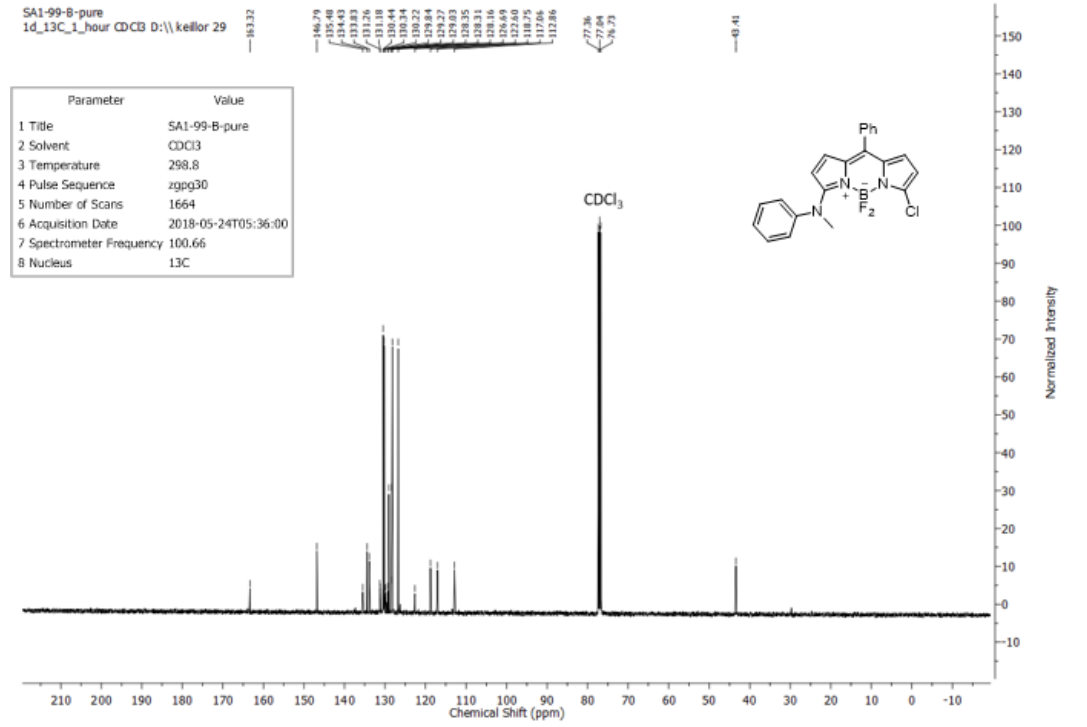

Compound **2.23**

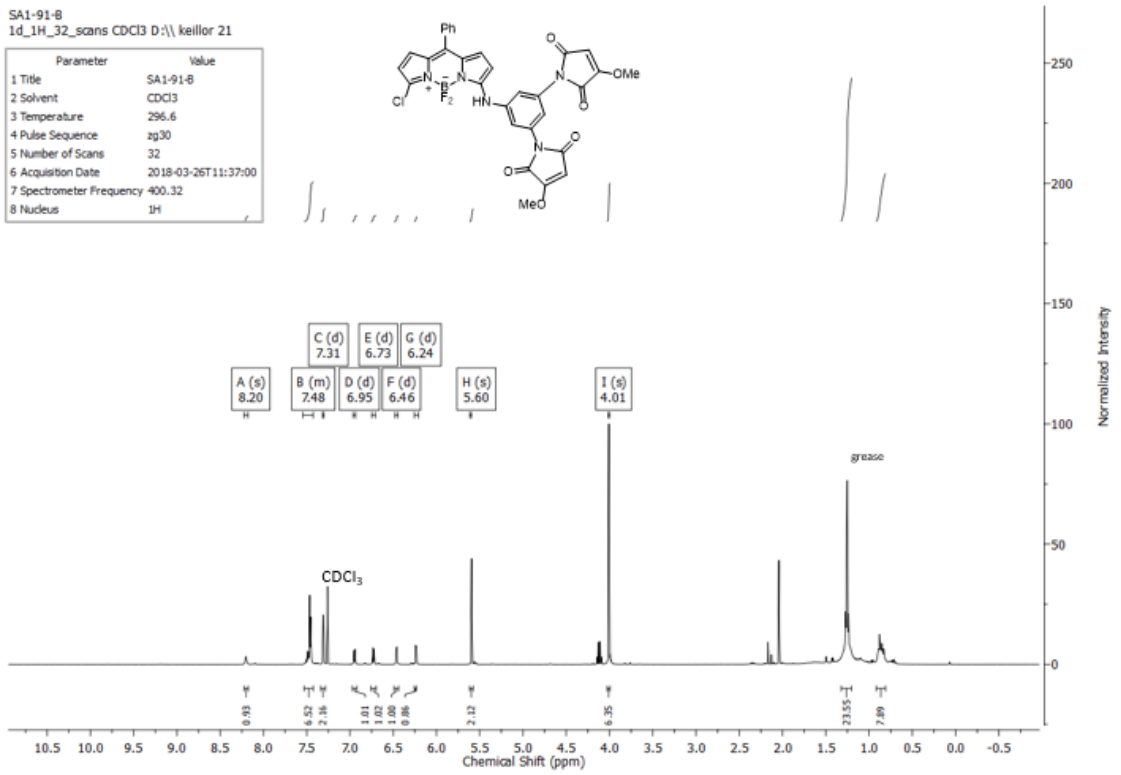
SA1-91-B
1d_1H_32_scans CDCl3 D:\\ keillor 21
Parameter Value
1 Title SA1-91-B
2 Solvent CDCl3
3 Temperature 296.6
4 Pulse Sequence zg30
5 Number of Scans 32
6 Acquisition Date 2018-03-26T11:37:00
7 Spectrometer Frequency 400.32
8 Nucleus 1H
Ph
Cl
HN
OMe
MeO
C (d) 7.31
E (d) 6.73
G (d) 6.24
A (s) 8.20
B (m) 7.48
D (d) 6.95
F (d) 6.46
H (s) 5.60
I (s) 4.01
grease
CDCl3
Normalized Intensity
Chemical Shift (ppm)

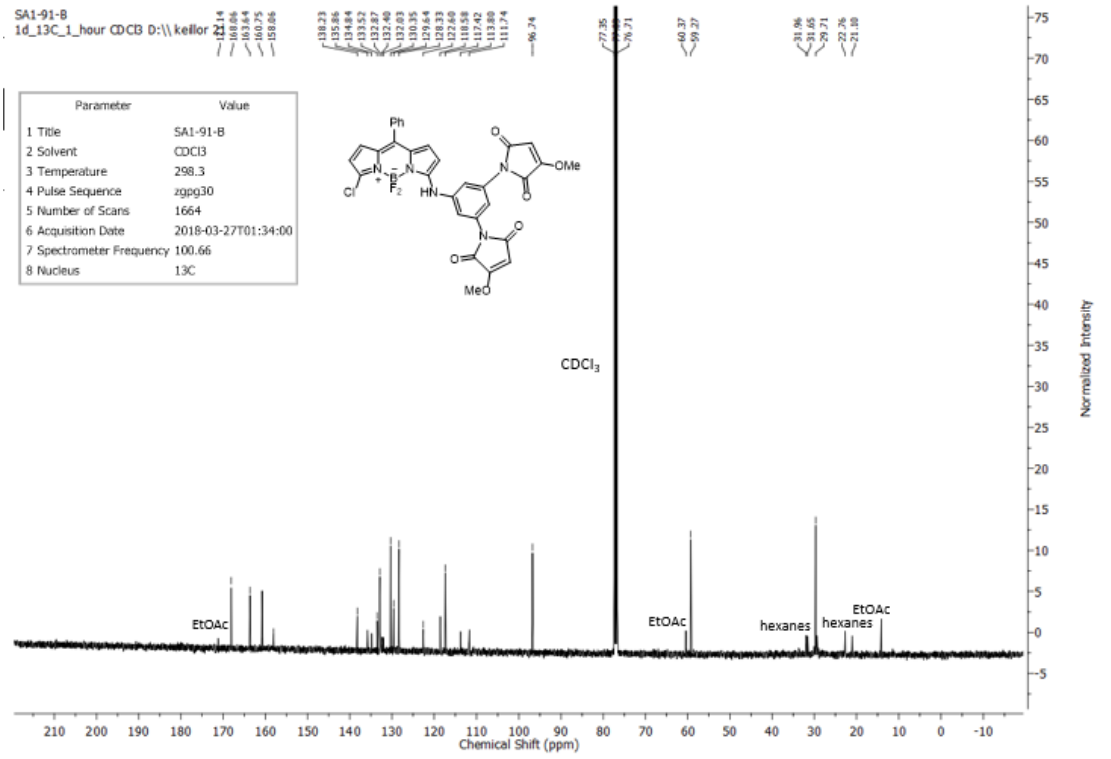
SA1-91-B
1d_13C_1_hour CDCl3 D:\\ keillor 21
Parameter Value
1 Title SA1-91-B
2 Solvent CDCl3
3 Temperature 298.3
4 Pulse Sequence zgpg30
5 Number of Scans 1664
6 Acquisition Date 2018-03-27T01:34:00
7 Spectrometer Frequency 100.66
8 Nucleus 13C
Ph
Cl
HN
OMe
MeO
CDCl3
EtOAc
EtOAc
hexanes
EtOAc
hexanes
Normalized Intensity
Chemical Shift (ppm)

Compound **2.24**

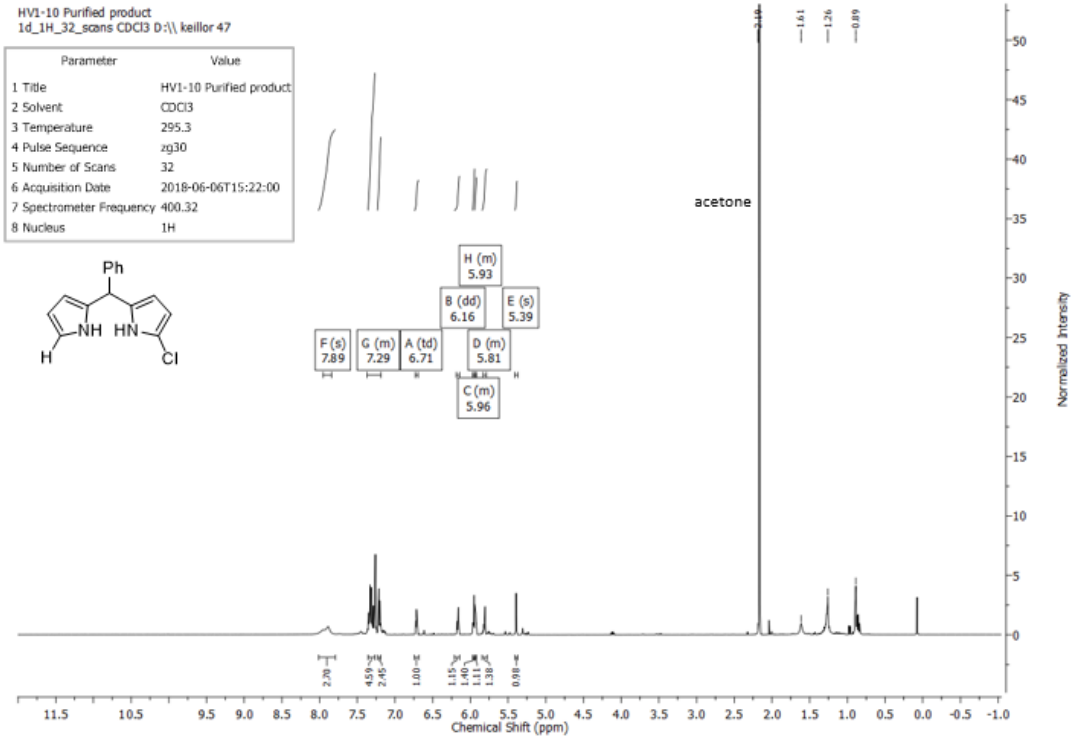

Compound **2.25**

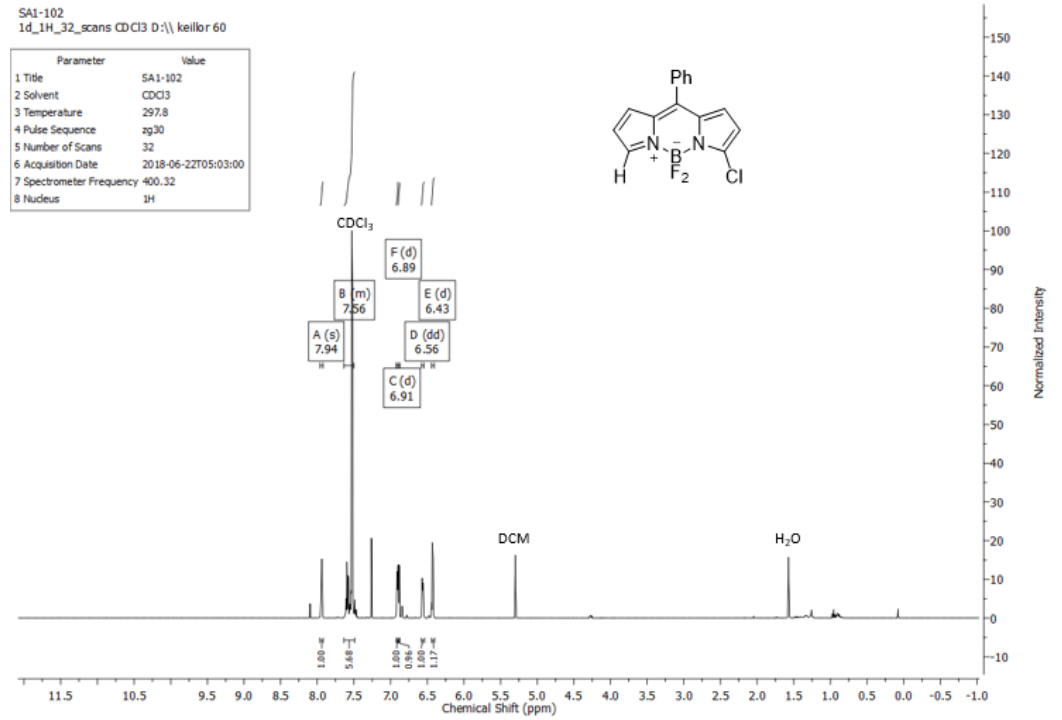

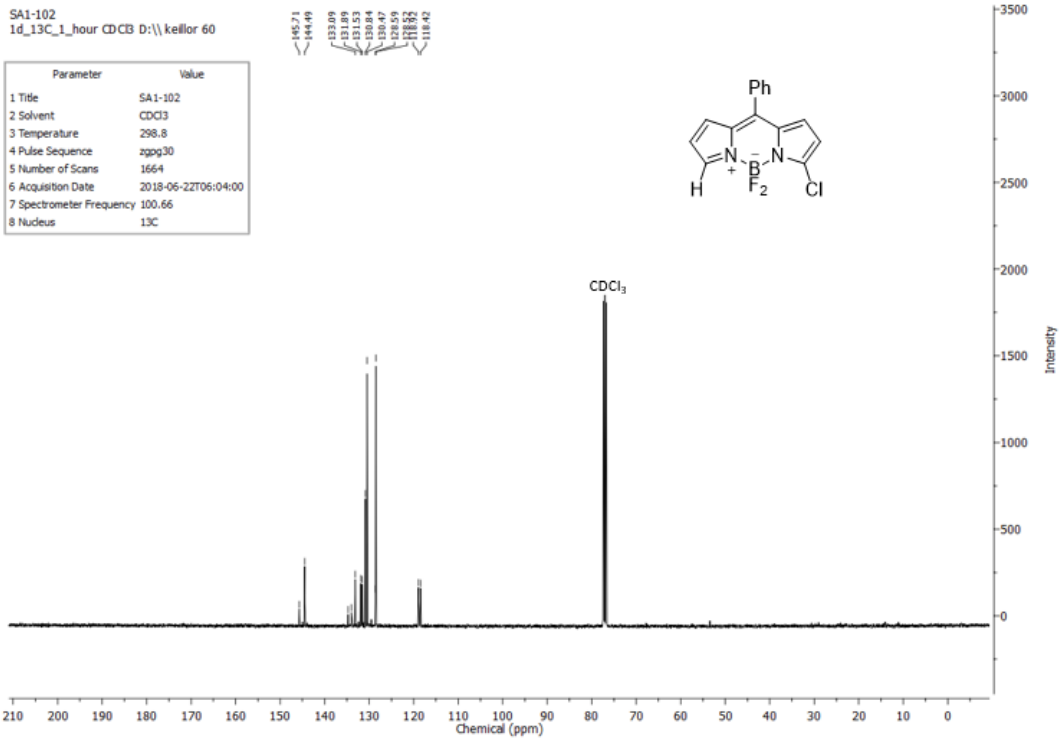

Compound **2.26**

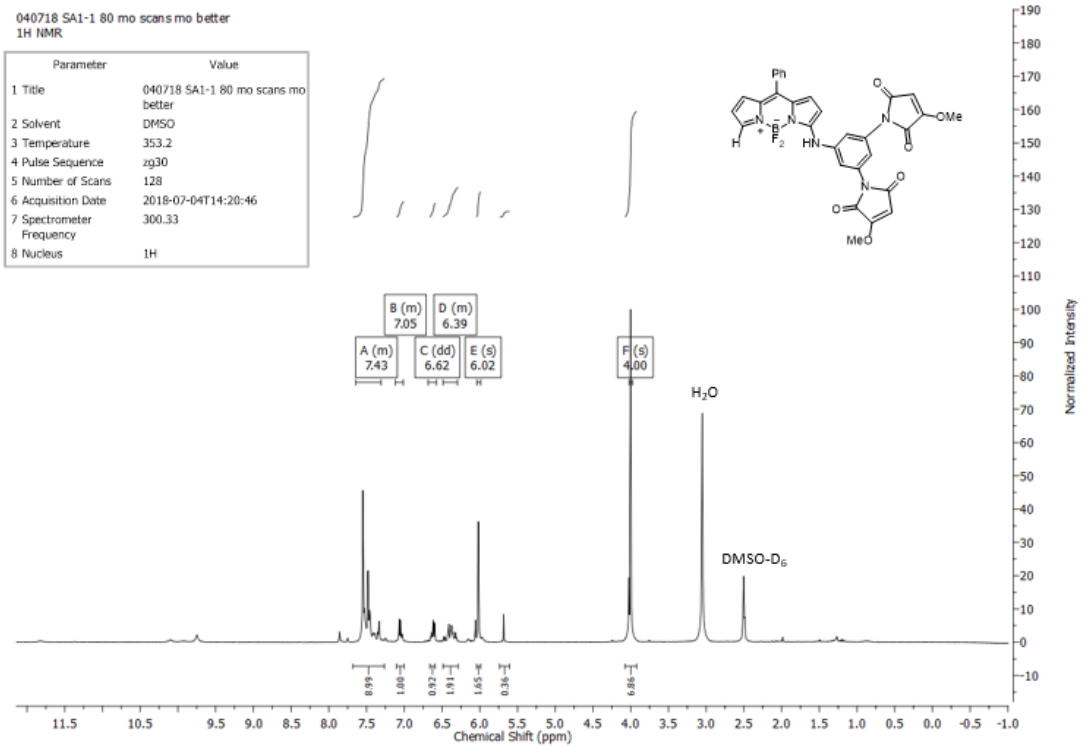

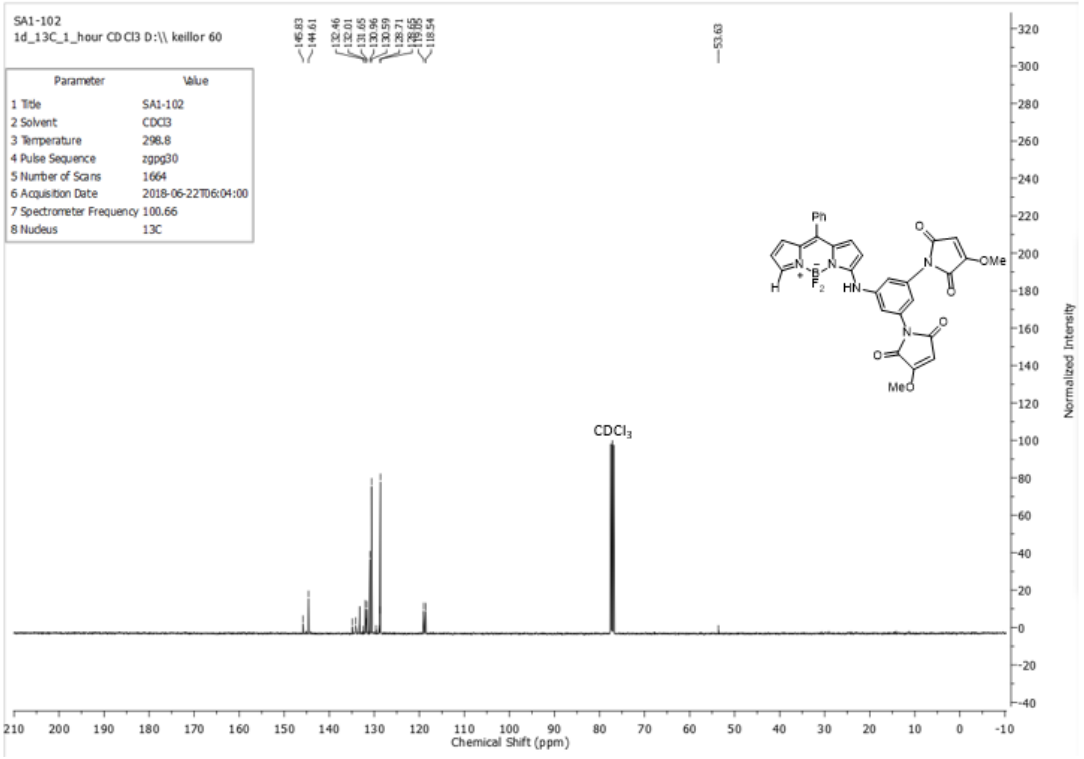

Chapter Three NMR Spectra

Compound **3.1**

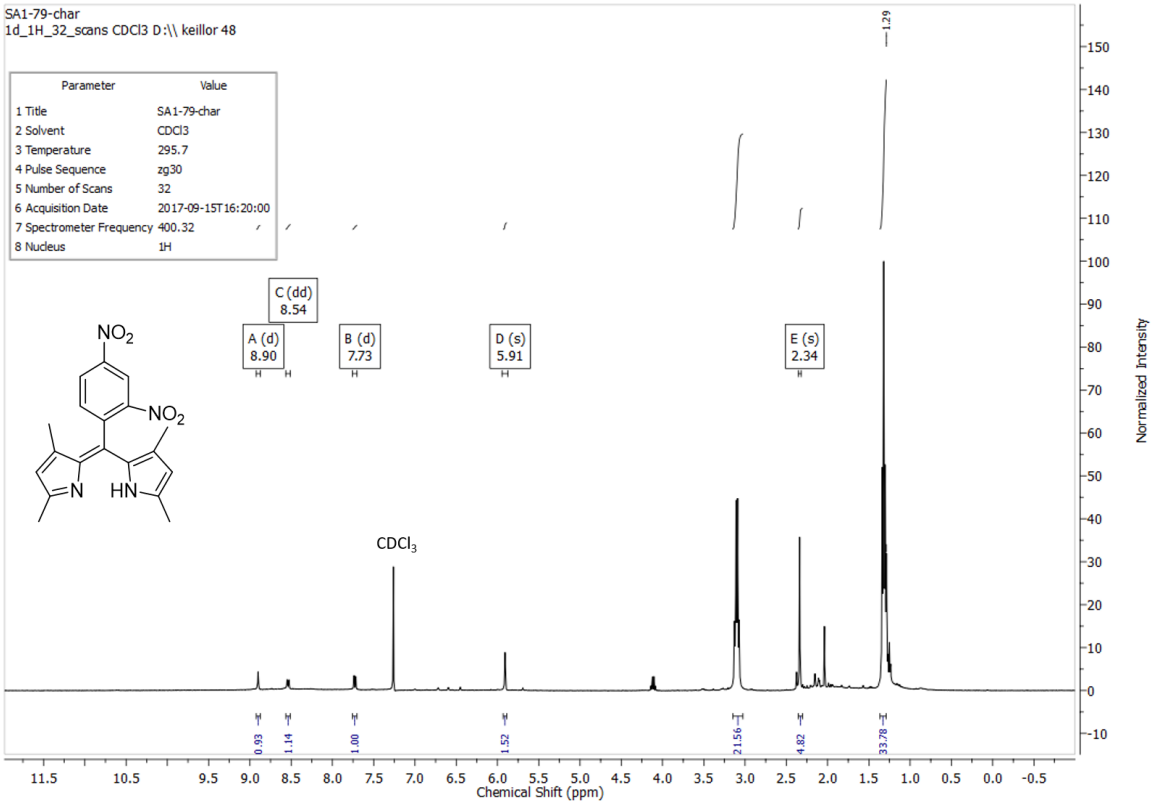

Compound **3.2**

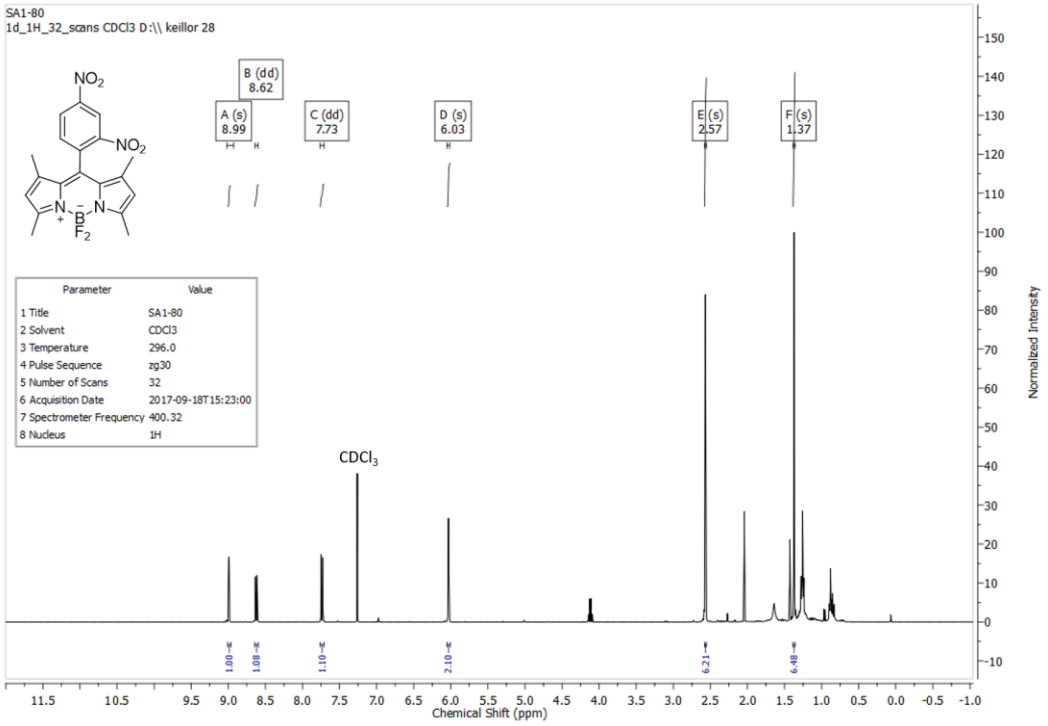
SA1-80
1d_1H_32_scans CDCl3 D:\\ keillor 28
B (dd) 8.62
A (s) 8.99
C (dd) 7.73
D (s) 6.03
E (s) 2.57
F (s) 1.37
Parameter Value
1 Title SA1-80
2 Solvent CDCl3
3 Temperature 296.0
4 Pulse Sequence zg30
5 Number of Scans 32
6 Acquisition Date 2017-09-18T15:23:00
7 Spectrometer Frequency 400.32
8 Nucleus 1H
CDCl3
Chemical Shift (ppm)
Normalized Intensity

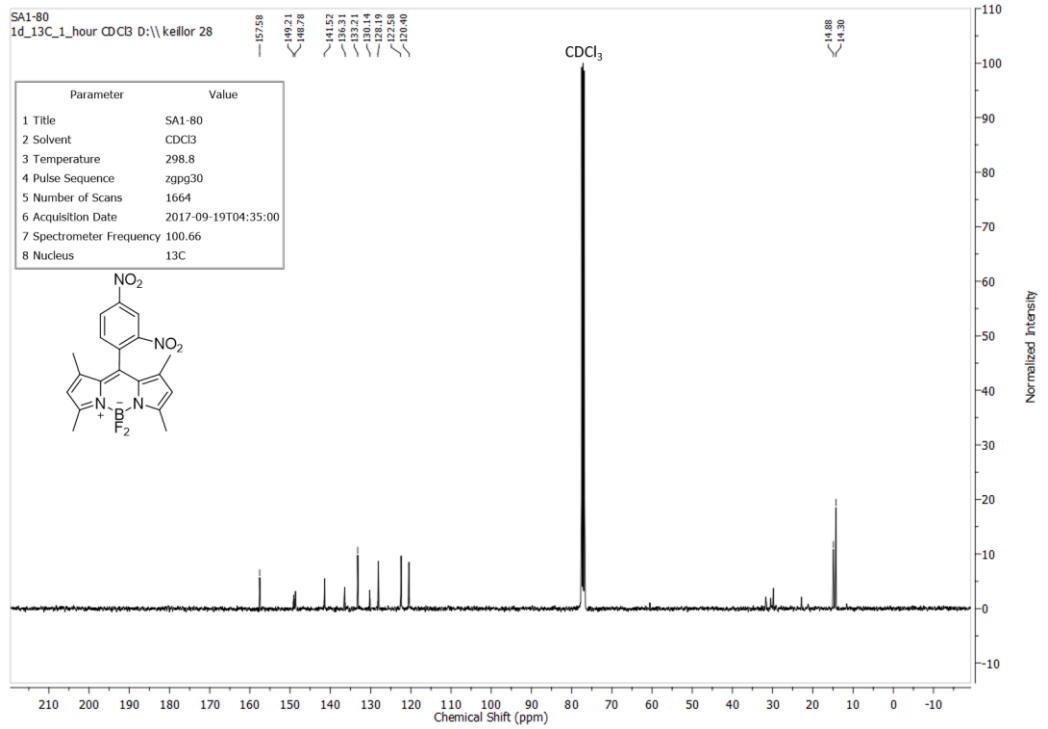
SA1-80
1d_13C_1_hour CDCl3 D:\\ keillor 28
Parameter Value
1 Title SA1-80
2 Solvent CDCl3
3 Temperature 298.8
4 Pulse Sequence zgpg30
5 Number of Scans 1664
6 Acquisition Date 2017-09-19T04:35:00
7 Spectrometer Frequency 100.66
8 Nucleus 13C
CDCl3
Chemical Shift (ppm)
Normalized Intensity

Compound **3.3**

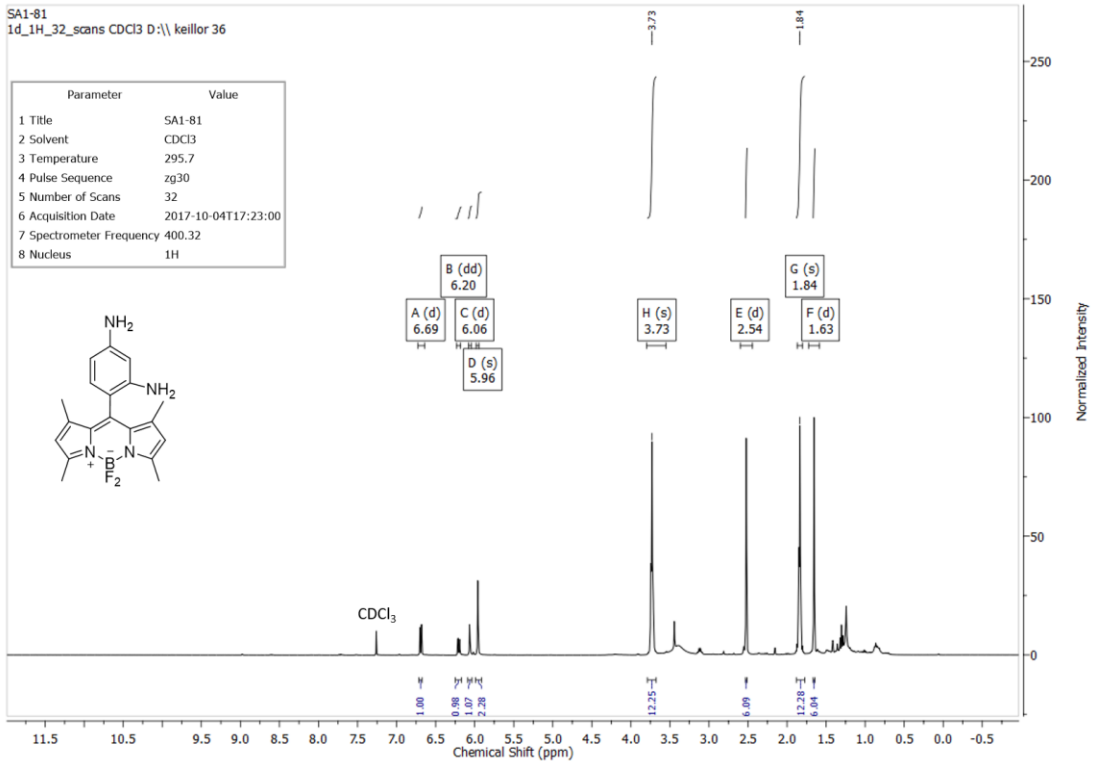
SA1-81
1d_1H_32_scans CDCl3 D:\\ keillor 36
Parameter Value
1 Title SA1-81
2 Solvent CDCl3
3 Temperature 295.7
4 Pulse Sequence zg30
5 Number of Scans 32
6 Acquisition Date 2017-10-04T17:23:00
7 Spectrometer Frequency 400.32
8 Nucleus 1H
A (d) 6.69
B (dd) 6.20
C (d) 6.06
D (s) 5.96
H (s) 3.73
E (d) 2.54
G (s) 1.84
F (d) 1.63
CDCl3
Chemical Shift (ppm)
Normalized Intensity

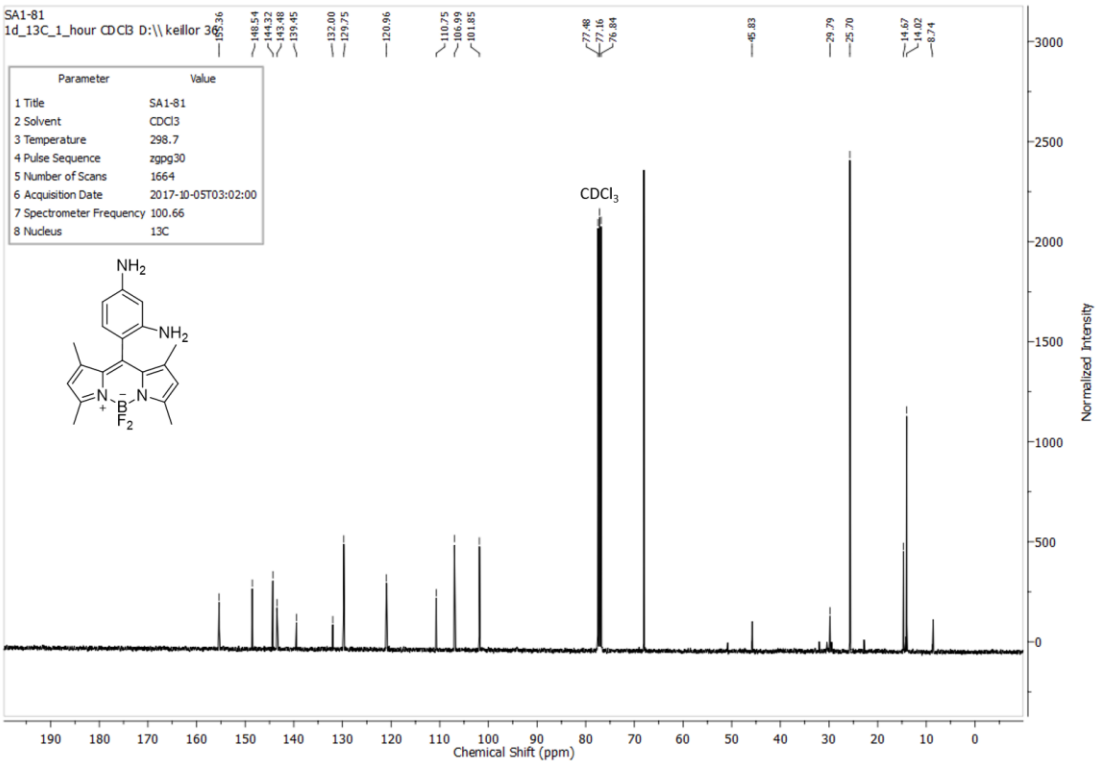
SA1-81
1d_13C_1_hour CDCl3 D:\\ keillor 36
Parameter Value
1 Title SA1-81
2 Solvent CDCl3
3 Temperature 298.7
4 Pulse Sequence zgpg30
5 Number of Scans 1664
6 Acquisition Date 2017-10-05T03:02:00
7 Spectrometer Frequency 100.66
8 Nucleus 13C
CDCl3
Chemical Shift (ppm)
Normalized Intensity

Compound **3.4**

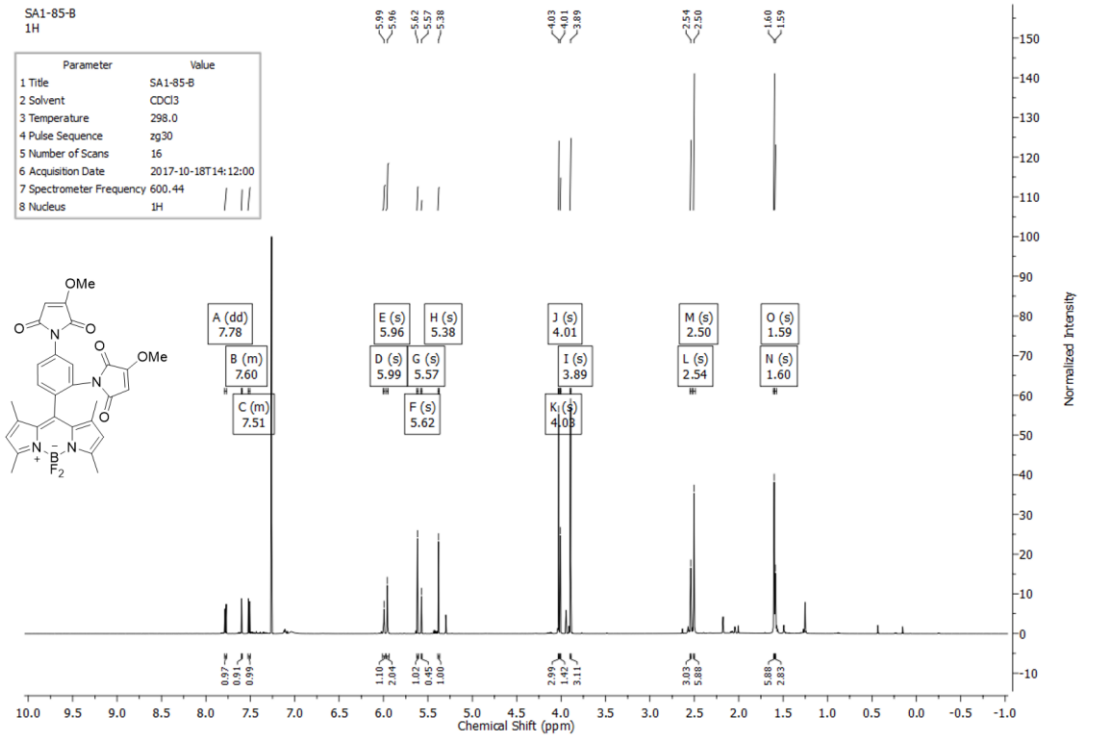
SA1-85-B
1H
Parameter Value
1 Title SA1-85-B
2 Solvent CDCl3
3 Temperature 298.0
4 Pulse Sequence zg30
5 Number of Scans 16
6 Acquisition Date 2017-10-18T14:12:00
7 Spectrometer Frequency 600.44
8 Nucleus 1H
A (dd) 7.78
B (m) 7.60
C (m) 7.51
D (s) 5.99
E (s) 5.96
F (s) 5.62
G (s) 5.57
H (s) 5.38
I (s) 3.89
J (s) 4.01
K (s) 4.03
L (s) 2.54
M (s) 2.50
N (s) 1.60
O (s) 1.59
Chemical Shift (ppm)
Normalized Intensity

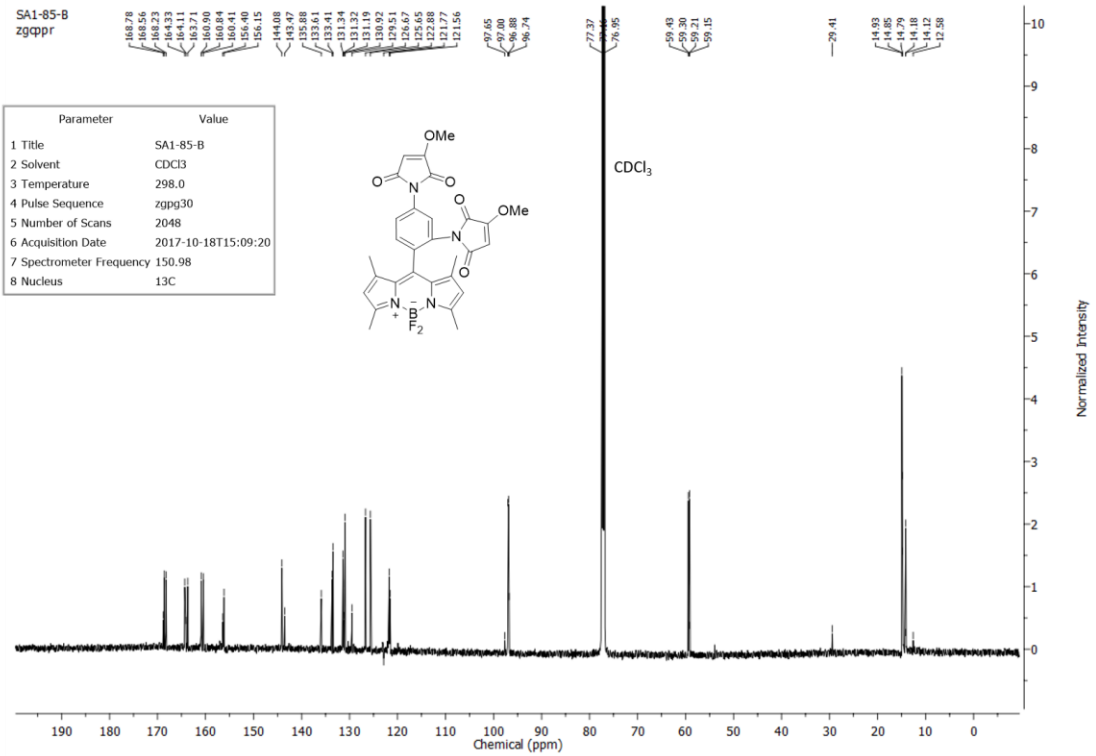
SA1-85-B
zgcppr
Parameter Value
1 Title SA1-85-B
2 Solvent CDCl3
3 Temperature 298.0
4 Pulse Sequence zgpg30
5 Number of Scans 2048
6 Acquisition Date 2017-10-18T15:09:20
7 Spectrometer Frequency 150.98
8 Nucleus 13C
CDCl3
Chemical (ppm)
Normalized Intensity

References

(1) Zhao, J.; Chen, J.; Ma, S.; Liu, Q.; Huang, L.; Chen, X.; Lou, K.; Wang, W. Recent Developments in Multimodality Fluorescence Imaging Probes. *Acta Pharm. Sin. B* **2018**, *8* (3), 320–338.

(2) Lichtman, J. W.; Conchello, J.-A. Fluorescence Microscopy. *Nature Methods*. **2005**, *2* (12), 910–919.

(3) Frigault, M.; Lacoste, J.; Swift, J.; Brown; Claire. Live-Cell Microscopy - Tips and Tools. *J. Cell Sci.* **2009**, *122*, 753–767.

(4) Galbraith, C. G.; Galbraith, J. A. Super-Resolution Microscopy at a Glance. *J. Cell Sci.* **2011**, *124*, 1607–1611.

(5) Specht, E. A.; Braselmann, E.; Palmer, A. E. A Critical and Comparative Review of Fluorescent Tools for Live-Cell Imaging. *Annu. Rev. Physiol*, **2017**, *79*, 93–117.

(6) Tsien, R. Y. The Green Fluorescent Protein, *Annu. Rev. Biochem*, **1998**, *67*, 509–544.

(7) Cong, L.; Ran, F. A.; Cox, D.; Lin, S.; Barretto, R.; Habib, N.; Hsu, P. D.; Wu, X.; Jiang, W.; Marraffini, L. A.; et al. Multiplex Genome Engineering Using CRISPR/Cas Systems. *Science* **2013**, *339* (6121), 819–823.

(8) Boch, J.; Scholze, H.; Schornack, S.; Landgraf, A.; Hahn, S.; Kay, S.; Lahaye, T.; Nickstadt, A.; Bonas, U. Breaking the Code of DNA Binding Specificity of TAL-Type III Effectors. *Science.* **2009**, *326* (5959), 1509–1512.

(9) Day, R. N.; Davidson, M. W.; Edu, R. The Fluorescent Protein Palette: Tools for Cellular Imaging. *Chem. Soc. Rev.* **2009**, *38* (10), 2887–2921.

(10) Los, G. V; Encell, L. P.; Mcdougall, M. G.; Hartzell, D. D.; Karassina, N.; Zimprich, C.; Wood, M. G.; Learish, R.; Friedman Ohana, R.; Urh, M.; et al. HaloTag: A Novel Protein Labeling Technology for Cell Imaging and Protein Analysis. *ACS Chem. Biol.* **2018**, *3* (6), 13.

(11) Keppler, A.; Gendreizig, S.; Gronemeyer, T.; Pick, H.; Vogel, H.; Johnsson, K. A General Method for the Covalent Labeling of Fusion Proteins with Small Molecules in Vivo. *Nat Biotechnol.* **2002**, *21*, 86–89.

(12) Gautier, A.; Juillerat, A.; Heinis, C.; Reis Corrê, I.; Kindermann, M.; Beaufils, F.; Johnsson, K. An Engineered Protein Tag for Multiprotein Labeling in Living Cells. *Chem. Biol.* **2008**, *15*, 128–136.

(13) Miller, L. W.; Cai, Y.; Sheetz, M. P.; Cornish, V. W. In Vivo Protein Labeling with Trimethoprim Conjugates: A Flexible Chemical Tag. *Nat. Methods.* **2005**, *2* (4), 255–257.

(14) Zhang, Y.; Park, K.-Y.; Suazo, K. F.; Distefano, M. D. Recent Progress in Enzymatic Protein Labelling Techniques and Their Applications. *Chem. Soc. Rev.* **2018**.

(15) Wals, K.; Ovaa, H.; Honek, J. F.; Schmeing, M. Unnatural Amino Acid Incorporation in E. Coli: Current and Future Applications in the Design of Therapeutic Proteins. *Front Chem.* **2014**, *2*, 1–12.

(16) Rodriguez, E. A.; Lester, H. A.; Dougherty, D. A. Improved Amber and Opal Suppressor

TRNAs for Incorporation of Unnatural Amino Acids in Vivo. Part 2: Evaluating Suppression Efficiency. *RNA.* **2007**, *13*, 1715–1722.

(17) Spriestersbach, A.; Kubicek, J.; Schäfer, F.; Block, H.; Maertens, B. Purification of His-Tagged Proteins. *Methods Enzymol.* **2015**, *559*, 1–15.

(18) Adams, S. R.; Campbell, R. E.; Gross, L. A.; Martin, B. R.; Walkup, G. K.; Yao, Y.; Llopis, J.; Tsien, R. Y. New Biarsenical Ligands and Tetracysteine Motifs for Protein Labeling in Vitro and in Vivo: Synthesis and Biological Applications. *J. Am. Chem. Soc.* **2002*, 214,*** 6063–6067.

(19) Li, C.; Tebo, A.; Gautier, A.; Li, C.; Tebo, A. G.; Gautier, A. Fluorogenic Labeling Strategies for Biological Imaging. *Int. J. Mol. Sci.* **2017**, *18* (7), 1473.

(20) Ding, F.; Zhan, Y.; Lu, X.; Sun, Y. Recent Advances in Near-Infrared II Fluorophores for Multifunctional Biomedical Imaging. *Chem. Sci.* **2018**, *9*, 4370–4380.

(21) Lukinavičius, G.; Umezawa, K.; Olivier, N.; Honigmann, A.; Yang, G.; Plass, T.; Mueller, V.; Reymond, L.; Corrêa Jr, I. R.; Luo, Z.-G.; et al. A Near-Infrared Fluorophore for Live-Cell Super-Resolution Microscopy of Cellular Proteins. *Nat. Chem.* **2013**, *5* (2), 132–139.

(22) Heim, R.; Cubbit, A. B.; Tsien, R. Y. Improved Green Fluorescence. *Nature.* **1995**, *373*, 663–664.

(23) Giepmans, B. N. G.; Adams, S. R.; Ellisman, M. H.; Tsien, R. Y. The Fluorescent Toolbox for Assessing. *Science.* **2006**, *312*, 217–224.

(24) Griffin, B. A.; Adams, S. R.; Tsien, R. Y. Specific Covalent Labeling of Recombinant

Protein Molecules inside Live Cells. *Science.* **1998**, *281* (5374), 269–272.

(25) Thorn, K. S.; Naber, N.; Matuska, M.; Cooke, R.; Vale, R. D. A Novel Method of Affinity-Purifying Proteins Using a Bis-Arsenical Fluorescein. *Protein Sci.* **2008**, *9* (2), 213–217.

(26) Estévez, J. M.; Somerville, C. FlAsH-Based Live-Cell Fluorescent Imaging of Synthetic Peptides Expressed in *Arabidopsis* and Tobacco. *Biotechniques.* **2006**, *41* (5), 569–574.

(27) Shieh, P.; Hangauer, M. J.; Bertozzi, C. R. Fluorogenic Azidofluoresceins for Biological Imaging. *J. Am. Chem. Soc.* **2012,** *134*, 17428–17431.

(28) Devaraj, N. K.; Hilderbrand, S.; Upadhyay, R.; Mazitschek, R.; Weissleder, R. Bioorthogonal Turn-On Probes for Imaging Small Molecules inside Living Cells. *Angew. Chemie Int. Ed.* **2010**, *49* (16), 2869–2872. .

(29) Mizukami, S.; Watanabe, S.; Hori, Y.; Kikuchi, K. Covalent Protein Labeling Based on Noncatalytic-Lactamase and a Designed FRET Substrate. *J. Am. Chem. Soc.* **2009**, *131*, 5016–5017.

(30) Chen, Y.; Tsao, K.; Keillor, J. W. INVITED REVIEW Fluorogenic Protein Labelling: A Review of Photophysical Quench Mechanisms and Principles of Fluorogen Design. *Can. J. Chem.* **2015**, *93*, 389–398.

(31) Guy, J.; Caron, K.; Phane Dufresne, S.; Michnick, S. W.; Skene, W. G.; Keillor, J. W. Convergent Preparation and Photophysical Characterization of Dimaleimide Dansyl Fluorogens: Elucidation of the Maleimide Fluorescence Quenching Mechanism. *J. Am.*

Chem. Soc. **2007**, *129* (39), 11969–11977.

(32) Chen, Y.; Tsao, K.; Keillor, J. W. Fluorogenic Protein Labelling: A Review of Photophysical Quench Mechanisms and Principles of Fluorogen Design. *Can. J. Chem.* **2015**, *93*, 389–398.

(33) Ueno, T.; Urano, Y.; Setsukinai, K.-I.; Takakusa, H.; Kojima, H.; Kikuchi, K.; Ohkubo, K.; Fukuzumi, S.; Nagano, T. Rational Principles for Modulating Fluorescence Properties of Fluorescein. *J. Am. Chem. Soc.* **2004**, *126*, 14079–14085.

(34) Weller, A. Kinetics of Fluorescence Quenching by Electron and H-Atom Transfer. *Isr. J. Chem.* **1970**, *8* (2), 259–271.

(35) Lincoln, R.; Greene, L. E.; Krumova, K.; Ding, Z.; Cosa, G. Electronic Excited State Redox Properties for BODIPY Dyes Predicted from Hammett Constants: Estimating the Driving Force of Photoinduced Electron Transfer. *J. Phys. Chem. A.* **2014**, *118*, 10622–10630.

(36) Guy, J.; Castonguay, R.; Campos-Reales Pineda, N. B.; Jacquier, V.; Caron, K.; Michnick, S. W.; Keillor, J. W. De Novo Helical Peptides as Target Sequences for a Specific, Fluorogenic Protein Labelling Strategy. *Mol. Biosyst.* **2010**, *6* (6), 976–987.

(37) Phane Girouard, S.; Lè Ne Houle, M.-H.; Grandbois, A.; Keillor, J. W.; Michnick, S. W. Synthesis and Characterization of Dimaleimide Fluorogens Designed for Specific Labeling of Proteins. *J. Am. Chem. Soc.* **2005**, *127*, 559–566.

(38) Marqusee, S.; Robbins, V. H.; Baldwin, R. L. Unusually Stable Helix Formation in Short

Alanine-Based Peptides. *Proc. Natl. Acad. Sci. USA.* **1989**, *86*, 5286–5290.

(39) Merutka, G.; Shalongo, W.; Stellwagen, E. A Model Peptide with Enhanced Helicity. *Biochemistry.* **1991**, 4245–4248.

(40) Strmiskova, M.; Tsao, K.; Keillor, J. W. Rational Design of a Highly Reactive Dicysteine Peptide Tag for Fluorogenic Protein Labelling. *Org. Biomol. Chem.* **2018**, *16* (34), 6332–6340.

(41) Guy, J.; Caron, K.; Dufresne, S.; Michnick, S. W.; Skene, W. G.; Keillor, J. W. Convergent Preparation and Photophysical Characterization of Dimaleimide Dansyl Fluorogens: Elucidation of the Maleimide Fluorescence Quenching Mechanism. *J. Am. Chem. Soc.* **2007**, *129* (39), 11969–11977.

(42) Thao P. Le; Joy E. Rogers; Kelly, L. A. Photoinduced Electron Transfer in Covalently Linked 1,8-Naphthalimide/Viologen Systems. *J. Phys. Chem. A.* **2000**, *104*, 6778–6785.

(43) Caron, K.; Lachapelle, V.; Keillor, J. W. Dramatic Increase of Quench Efficiency in "Spacerless" Dimaleimide Fluorogens. *Org. Biomol. Chem.* **2011**, *9* (1), 185–197.

(44) Chen, Y.; Tsao, K.; De Francesco, É.; Keillor, J. W. Ring Substituent Effects on the Thiol Addition and Hydrolysis Reactions of N-Arylmaleimides. *J. Org. Chem.* **2015**, *80* (24), 12182–12192.

(45) Renault, K.; Fredy, J. W.; Renard, P.-Y.; Sabot, C. Covalent Modification of Biomolecules through Maleimide-Based Labeling Strategies. *Bioconjug. Chem.* **2018**, *29* (8), 2497–2513.

(46) Chen, Y.; Clouthier, C. M.; Tsao, K.; Strmiskova, M.; Lachance, H.; Keillor, J. W. Coumarin-Based Fluorogenic Probes for No-Wash Protein Labeling. *Angew. Chem. Int. Ed.* **2014**, *53* (50), 13785–13788.

(47) Treibs, A.; Kreuzer, F.-H. Difluorboryl-Komplexe von Di- Und Tripyrrylmethenen. *Justus Liebigs Ann. Chem.* **1968**, *718* (1), 208–223.

(48) Boens, N.; Leen, V.; Dehaen, W. Fluorescent Indicators Based on BODIPY. *Chem. Soc. Rev.* **2012**, *41* (3), 1130–1172.

(49) Yu, C.; Wu, Q.; Wang, J.; Wei, Y.; Hao, E.; Jiao, L. Red to Near-Infrared Isoindole BODIPY Fluorophores: Synthesis, Crystal Structures, and Spectroscopic and Electrochemical Properties. *J. Org. Chem.* **2016**, *81*, 3761–3770.

(50) Patalag, L. J.; Jones, P. G.; Werz, D. B. BOIMPYs: Rapid Access to a Family of Red-Emissive Fluorophores and NIR Dyes. *Angew. Chem. Int. Ed.* **2016**, *55* (42), 13340–13344.

(51) Kamkaew, A.; Burgess, K. Aza-BODIPY Dyes with Enhanced Hydrophilicity. *Chem. Commun.* **2015**, *51* (53), 10664–10667.

(52) Matsumoto, T.; Urano, Y.; Shoda, Y.; Kojima, H.; Nagano, T. A Thiol-Reactive Fluorescence Probe Based on Donor-Excited Photoinduced Electron Transfer: Key Role of Ortho Substitution. *Org. Lett.* **2007**, *9* (17), 3375–3377.

(53) Chen, Y.; Tsao, K.; Acton, S. L.; Keillor, J. W. A Green BODIPY-Based, Super-Fluorogenic, Protein-Specific Labelling Agent. *Angew. Chem. Int. Ed.* **2018**, *57* (38),

12390–12394.

(54) Lincoln, R.; Greene, L. E.; Krumova, K.; Ding, Z.; Cosa, G. Electronic Excited State Redox Properties for BODIPY Dyes Predicted from Hammett Constants: Estimating the Driving Force of Photoinduced Electron Transfer. *J. Phys. Chem. A.* **2014**, *118* (45), 10622–10630.

(55) Fan, G.; Yang, L.; Chen, Z. Water-Soluble BODIPY and Aza-BODIPY Dyes: Synthetic Progress and Applications. *Front. Chem. Sci. Eng.* **2014**, *8* (4), 405–417.

(56) Kowada, T.; Maeda, H.; Kikuchi, K. BODIPY-Based Probes for the Fluorescence Imaging of Biomolecules in Living Cells. *Chem. Soc. Rev.* **2015**, *44* (14), 4953–4972.

(57) Boens, N.; Verbelen, B.; Dehaen, W. Postfunctionalization of the BODIPY Core: Synthesis and Spectroscopy. *European J. Org. Chem.* **2015**, *2015* (30), 6577–6595..

(58) Karlsson, J. K. G.; Harriman, A. Origin of the Red-Shifted Optical Spectra Recorded for Aza-BODIPY Dyes. *J. Phys. Chem. A* **2016**, *120* (16), 2537–2546.

(59) Boens, N.; Wang, L.; Leen, V.; Yuan, P.; Verbelen, B.; Dehaen, W.; Van der Auweraer, M.; De Borggraeve, W. D.; Van Meervelt, L.; Jacobs, J.; et al. 8-HaloBODIPYs and Their 8-(C, N, O, S) Substituted Analogues: Solvent Dependent UV–Vis Spectroscopy, Variable Temperature NMR, Crystal Structure Determination, and Quantum Chemical Calculations. *J. Phys. Chem. A.* **2014**, *118* (9), 1576–1594.

(60) Rohand, T.; Baruah, M.; Qin, W.; Boens, N.; Dehaen, W. Functionalisation of Fluorescent BODIPY Dyes by Nucleophilic Substitution. *Chem. Commun.* **2006**, *3*, 266–268.

(61) Gazitú, M.; Tapia, R. A.; Contreras, R.; Campodó Nico, P. R. Mechanistic Pathways of Aromatic Nucleophilic Substitution in Conventional Solvents and Ionic Liquids. *New J. Chem.* **2014**, *38*, 2611.

(62) Chen, Y.; Clouthier, C. M.; Tsao, K.; Strmiskova, M.; Lachance, H.; Keillor, J. W. Coumarin-Based Fluorogenic Probes for No-Wash Protein Labeling. *Angew. Chem. Int. Ed.* **2014**, *53* (50), 13785–13788.

(63) Sahoo, K.; Mhaske, S. B.; Argade, N. P. Facile Routes to Alkoxymaleimides / Maleic Anhydrides. *Synthesis.* **2002**, *3*, 346–349.

(64) Baruah, M.; Qin, W.; Basari, N.; Borggraeve, W. M. De. BODIPY Based Hydroxyaryl Derivatives as Fluorescent pH Probes. *J. Org. Chem.* ***2005***, *70* (10), 4152–4157.

(65) Yu, M.; Wong, J. K. H.; Tang, C.; Turner, P.; Todd, M. H.; Rutledge, P. J. Efficient Deprotection of F-BODIPY Derivatives: Removal of BF_2 using Brønsted Acids. *Beilstein J. Org. Chem.* **2015**, *11*, 37–41.

(66) Pompeo, M.; Farmer, J. L.; Froese, R. D. J.; Organ, M. G. Room-Temperature Amination of Deactivated Aniline and Aryl Halide Partners with Carbonate Base Using a Pd-PEPPSI-IPentCl-o-Picoline Catalyst. *Angew. Chem. Int. Ed.* **2014**, *53* (12), 3223–3226.

(67) Alnoman, R. B.; Stachelek, P.; Knight, J. G.; Harriman, A.; Waddell, P. G. Synthesis of 2-AminoBODIPYs by Palladium Catalysed Amination. *Org. Biomol. Chem.* **2017**, *15* (36), 7643–7653.

(68) Beh, M. H. R.; Douglas, K. I. B.; House, K. T. E.; Murphy, A. C.; Sinclair, J. S. T.;

Thompson, A. Robust Synthesis of F-BODIPYs. *Org. Biomol. Chem.* **2016**, *14* (48), 11473–11479.

(69) Kornberg, R. D.; Lorch, Y. Twenty-Five Years of the Nucleosome, Fundamental Particle of the Eukaryote Chromosome. *Cell.* **1999**, *98* (3), 285–294.

(70) Fulmer, G. R.; Miller, A. J. M.; Sherden, N. H.; Gottlieb, H. E.; Nudelman, A.; Stoltz, B. M.; Bercaw, J. E.; Goldberg, K. I. NMR Chemical Shifts of Trace Impurities: Common Laboratory Solvents, Organics, and Gases in Deuterated Solvents Relevant to the Organometallic Chemist. *Organometallics.* **2010**, *29* (9), 2176–2179.

(71) Lou, Z.; Hou, Y.; Chen, K.; Zhao, J.; Ji, S.; Zhong, F.; Dede, Y.; Dick, B. Different Quenching Effect of Intramolecular Rotation on the Singlet and Triplet Excited States of Bodipy. *J. Phys. Chem. C.* **2017**, *122*, 185–193.

(72) Montero, D.; Tachibana, C.; Rahr Winther, J.; Appenzeller-Herzog, C. Intracellular Glutathione Pools Are Heterogeneously Concentrated. *Redox Biol.* **2013**, *1* (1), 508–513.

(73) Loudet, A.; Burgess, K. BODIPY Dyes and Their Derivatives: Syntheses and Spectroscopic Properties. *Chem. Rev.* **2007**, *107*, 4891-4932.

(74) Leyendekkers, J. V.; Hunter, R. J. Refractive Index of Aqueous Electrolyte Solutions. Extrapolations to Other Temperatures, Pressures, and Wavelengths and to Multicomponent Systems. *J. Chem. Eng. Data.* **1977**, *22* (4), 427–431.

(75) Fan, P.; Hard, T.; Kearns, D. R. A Fluorescence Study of the Binding of Hoechst 33258 and Dapi to Halogenated DNAs. *Photochemistry and Photobiology.* **1990**, *51* (1), 77–86.

(76) Thurlkill, R. L.; Grimsley, G. R.; Scholtz, J. M.; Pace, C. N. PK Values of the Ionizable Groups of Proteins. *Protein Sci.* **2006**, *15* (5), 1214–1218.

(77) Bulaj, G.; Kortemme, T.; Goldenberg, D. Ionization−Reactivity Relationships for Cysteine Thiols in Polypeptides. *Biochemistry.* **1998**, *37*, 8965–8972.

(78) Keillor, J. W.; Brown, R. S. Attack of Zwitterionic Ammonium Thiolates on a Distorted Anilide as a Model for the Acylation of Papain by Amides. A Simple Demonstration of a Bell-Shaped PH/Rate Profile. *Am. Chem. Soc.* **1992**, *114*, 7983–7989.

(79) Bittel, A. M.; Davis, A. M.; Wang, L.; Nederlof, M. A.; Escobedo, J. O.; Strongin, R. M.; Gibbs, S. L. Varied Length Stokes Shift BODIPY-Based Fluorophores for Multicolor Microscopy. *Sci. Rep.* **2018.**

(80) Karlsson, J. K. G.; Harriman, A. Origin of the Red-Shifted Optical Spectra Recorded for Aza-BODIPY Dyes. *J. Phys. Chem. A* **2016**, *120* (16), 2537–2546.